Mechanism of Action of Platinum Anticancer Drugs: from Kinetic to Structural Studies

A Thesis Submitted for the Degree of

Doctor of Philosophy

by

Yu Chen, *M.Sc.*

Department of Chemistry
University of Edinburgh
King's Buildings, West Mains Road
Edinburgh, EH9 3JJ

Sept. 1999

Abstract

Cisplatin, *cis*-[$Pt(NH_3)_2Cl_2$], has been a successful and widely used anticancer drug since the discovery of its activity 30 years ago. Up to now the mechanism of action of this drug is still not well understood. In this thesis, pH dependent platinum-sulfur interactions, the solution structure of a cisplatin DNA GpG intrastrand adduct and the chemistry of a new platinum anticancer drug have been investigated. Using [^1H, ^{15}N] 2D NMR spectroscopy and HPLC, together with ^{15}N-labelled amine ligands, highly pH dependent interconversion between S- and N-bound methionine adducts of $\{Pt(dien)\}^{2+}$ (dien = diethylenetriamine) *via* dien ring-opened intermediates has been observed. The isolated ring-opened intermediate exists as four diastereomers and was surprisingly long-lived. This study suggests a possible role for thioether-sulfur in the transfer and activation of platinum drugs. The NMR solution structure of a DNA 14mer duplex containing a cisplatin 1,2-GpG intrastrand crosslink has been determined by combined NOE measurements, coupling constants and restrained molecular dynamics calculations. Platination at GpG site causes significant bending and unwinding of the DNA duplex. The 3′-side of the DNA duplex is much more bent towards the major groove. Sequence-dependent structural characteristics are discussed and compared with the other reported structures of intrastrand platinated DNA. The 2-picoline (2-methylpyridine) complex, *cis*-[$PtCl_2(NH_3)$(2-Pic)] (**1**), has recently entered clinical trials and is highly active against cisplatin resistant cell-lines. The crystal structure of **1** shows steric hindrance induced by the 2-CH_3 group towards an axial approach to Pt, while its 3-picoline analogue (**2**) is less sterically hindered. ^{15}N labelling of complexes **1** and **2** allowed both the hydrolysis rates and pKa values of the complexes to be determined using 2D [^1H, ^{15}N] NMR spectroscopy. The steric effect of 2-picoline ligand reduces the reactivity of the complex during substitution reactions and the position *cis* to 2-picoline is more affected. The rate constants for reactions between **1** and guanosine 5′-

monophosphate (5′-GMP) were determined *via* 2D NMR studies, and compared with those for reactions with **2**. The reactivity of **1** with thiol ligand of glutathione (GSH) was greatly reduced. Both mono- and bis-GMP adducts were observed in the competitive reactions of **1** with GSH and GMP. Slow rotation about the Pt-N picoline bond and fast rotation about Pt-N7 GMP bonds on the NMR time scale were observed for the bis(GMP) adducts of **1**. These features of **1** may play an important role in its altered spectrum of biological activity compared to cisplatin. Complex **1** forms four stereoisomers in reactions with d(GpG) and a 14mer DNA single strand due to the different orientations of 2-picoline (either towards 5′-G or 3′-G) and slow rotation of Pt-N(2-Pic) bond. These contrast with reactions of **1** with a 14mer DNA duplex, in which only one major stereoisomer was observed. 2D NMR experiments and molecular modelling suggest that favourable steric interactions, H-bonding and van der Waals contact provide the structural basis for this unusually high stereoselectivity. These results give new insights into the effect of ligand design on the nature of platinated DNA lesions.

Dedicated to
my wife
mum and dad

Acknowledgements

I would like to thank Professor Peter J. Sadler for his excellent supervision and enthusiasm. Throughout my three years study, his encouragement and constant interest always gave me great support and motivation. Needless to say I am very grateful to him.

My special thanks go to Dr. Zijian Guo, for his great help and stimulating discussion during my study. His support and friendship to me are invaluable.

I would like to thank all the members of the PJS group, past and present, for their support and wisdom. They are good friends and co-workers. Among them, thanks are especially due to Dr. John A. Parkinson for help with NMR experiments and molecular modelling, Dr. Abraha Habtemariam for his valuable advice both in and out of the chemistry lab and Dr. P. del Socorro Murdoch for assistance with HPLC experiments. Dr. Hongzhe Sun and Ms. Hongyan Li provided me with a lot of help during my first two years of working and living in Edinburgh, and I wish to express my gratitude to them. Dr. Simon Parsons deserves my thanks for his amazing efficiency with X-ray crystal structure determinations.

I am indebted to the Committee of Vice-Chancellors and Principals (CVCP) for an ORS Award and University of Edinburgh for a Research Studentship, which have made my study in Edinburgh possible; also to EC COST programme for giving me the chance and support to attend the workshop meetings, which are very helpful experiences for postgraduate students.

Finally, my sincere thanks go to my wife and parents for their constant support, understanding, encouragement, and patience throughout these years.

Declaration

Except where specific reference is made to other sources, the work contained in this thesis is the original work of the author. It has been composed by the candidate and not been submitted, in whole or in part, for any of other degree.

Yu Chen

Contents

Lists of Figures

Figure 2.2 Plot of $^{1}J(^{195}Pt\text{-}^{15}N)$ *versus* $\delta(^{15}N)$ for Pt-NH_3, Pt-NH_2 and Pt-NH, showing a similar dependence on the *trans* ligand. Data are taken from literature. (Ref. 22, 59-62)

Figure 2.3 The theoretical increase in receptivity (abundance × sensitivity) obtainable by isotope enrichment and inverse ^{1}H detection of ^{13}C, ^{15}N and ^{195}Pt. In practice inverse $^{1}H\text{-}\{^{195}Pt\}$ detection is limited by the broad linewidths of the ^{195}Pt satellites.

Figure 2.4 General appearance of a 2D [^{1}H, ^{15}N] HMQC or HSQC spectrum. The ^{195}Pt satellites are usually more intense for symmetrical Pt species (Pt(IV) rather than Pt(II)).

Figure 3.1. Formation of $[Pt(^{15}N\text{-dien})(^{15}N\text{-L-Met-}S)]^{2+}$ (**2**) by reaction of $[Pt(^{15}N\text{-dien})Cl]^{+}$ (**1**) (5 mM) with ^{15}N-L-MetH in 1:1 molar ratio at 298 K, pH 6.0. The 2D [^{1}H, ^{15}N] HSQC NMR spectrum was recorded after 12 h of reaction. The peaks labeled **2a** and **2b** are assigned to protons on each of the two NH_2 groups, and **2c** to the NH group. ^{195}Pt satellites are labeled with *.

Figure 3.2. A 2D [^{1}H, ^{15}N] HSQC NMR spectrum recorded 12 h after increasing the pH of a solution containing complex (**2**) as $[Pt(^{15}N\text{-dien})(^{15}N\text{-L-Met-}S)]^{2+}$ (Fig. 3.2A) or $[Pt(^{15}N\text{-dien})(^{14}N\text{-L-Met-}S)]^{2+}$ (Fig. 3.2B) from 6.0 to 8.5. Peak assignments: **2a** and **2b**, NH_2 (*trans* to N) of complex (**2**); **3a**, **3b** and **3a´**, NH_2 (*trans* to N) and **3c**, NH (*trans* to N) of $[Pt(^{15}N\text{-dien})(\text{L-Met-}N)]^{+}$ (**3**); **3d**, NH_2 (*trans* to N) of N-bound ^{15}N-L-Met in complex (**3**). The cross-peak for NH (*trans* to S) of complex (**2**) is not observed because of fast exchange with solvent protons on NMR timescale at this pH. Cross-peaks (**3a** - **3d**) exhibit further coupling in the ^{1}H dimension.

Figure 3.3 The 2D [^{1}H, ^{15}N] HSQC NMR spectra recorded 1 h after lowering the pH of solutions containing complexes (**2**) and (**3**) (see Fig. 3.2) containing ^{15}N-labelled L-Met (Fig. 3.3A) or unlabelled L-Met (Fig. 3.3B) from 8.5 to 3.3. The boxed cross-peaks are assignable to the dien-ring-opened intermediate [Pt(^{15}N-dienH-*N,N´*)(L-Met-*S,N*)]$^{2+}$ (**4**). Note the absence of the peaks in box **e** and peak **3d** in Fig. 3.3B (^{14}N-L-MetH used). Peak assignments: **2a** and **2b**, NH_2 *trans* to N with ^{195}Pt satellites (*) and **2c**, NH *trans* to S of complex (**2**); **3a**, **3b** and **3a´**, NH_2 (*trans* to N) and **3c**, NH (*trans* to N) of complex (**3**); **3d**, NH_2 (*trans* to N) of N-bound ^{15}N-L-Met in complex (**3**); boxes **g** and **h** can be tentatively assigned to Pt-NH (*trans* to N) and Pt-NH_2 (*trans* to S) groups of dien in ring-opened intermediate (**4**); box **e**, NH_2 (*trans* to N) of N-bound ^{15}N-L-Met in intermediate (**4**); peak **f,** unassigned.

Figure 3.4 The HPLC chromatograms for the reaction of [Pt(dien)Cl]$^{+}$ (**1**) with L-MetH (5 mM, 1:1, 298 K, pH 6.0, 24 h). (A) 12 h after pH adjustment from 6.0 to 8.5; (B) 0.5 h after lowering pH from pH 8.5 to 3.3; (C) 2 h after pH adjustment from 8.5 to 3.3; (D) 24 h after pH adjustment from 8.5 to 3.3. Peak assignments: **a,** [Pt(dien)(L-Met-*S*)]$^{+}$ (**2**); **b**, [Pt(dien)(L-Met-*N*)]$^{+}$ (**3**); **c,** dien ring-opened intermediate [Pt(dienH-*N,N´*)(L-Met-*S,N*)]$^{2+}$ (**4**); **d** and * are from free L-MetH and the solvent front respectively.

Figure 3.5 The 2D [^{1}H,^{15}N] HSQC NMR spectrum of the HPLC-isolated dien ring-opened complex (**4**) (peak **c** in Fig. 3.4B) at pH 4.0. Only the NH_2 group of L-MetH was ^{15}N-labelled, and the four sets of cross-peaks (peaks **a**, **a´** to **d**, **d´**) can be assigned to the nonequivalent Pt-NH_2 groups in the four diastereoisomers of [Pt(dienH-*N,N´*)(^{15}N-L-Met-*S,N*)]$^{2+}$. All peaks have $^{2}J(NH_a,NH_b)$ of *ca* 12 Hz, while only peaks **a** and **b** have an additional $^{3}J(\alpha CH,NH)$ of *ca* 13 Hz.

Figure 3.6 Part of the 500 MHz ^{1}H NMR spectrum of HPLC isolated dien ring-opened complex (**4**) at pH 4.0 (peak **c**, Fig. 3.4B), showing four singlets from S-CH_3 of diasteroisomers of *S,N*-chelated L-Met.

Figure 4.1 X-ray crystal structures of *cis*-[$PtCl_2(^{15}NH_3)$(2-picoline)] (**1**) and *cis*-[$PtCl_2(^{15}NH_3)$(3-picoline)] (**2**) showing the steric hindrance caused by the 2-methyl group in complex **1**. Colour code: H (white), C (pale green), N (blue), Cl (bright green), Pt (yellow).

Figure 4.2 Intermolecular hydrogen bonding in crystals of (**A**) complex **1**, and (**B**) complex **2**; N–H•••Cl distances for complex **1** range from 2.55 Å to 2.74 Å and for complex **2** from 2.62 Å to 2.81 Å.

Figure 4.3 2D [^{1}H,^{15}N] HSQC NMR spectra of 2 mM aqueous solutions of (**A**) *cis*-[$PtCl_2(^{15}NH_3)$(2-picoline)] (**1**), and (**B**) *cis*-[$PtCl_2(^{15}NH_3)$(3-picoline)] (**2**) after 3 h at 310 K. Peak **a** is assigned to the starting complex, peaks **b**, **c** to the two monoaqua complexes (H_2O *cis* to NH_3 and H_2O *trans* to NH_3, respectively), and peak **d** to the diaqua complex. Time dependence of the concentrations of the dichloro complexes and aqua adducts are shown in (**C**) of **1** and (**D**) of **2**, respectively. Labels: **1** and **2** (■), monoaqua complexes **3a** and **4a** (▲), monoaqua complexes **3b** and **4b** (●), diaqua complexes **5** and **6** (+). The curves are the computer best fits calculated with the rate constants shown in Table 4.3.

Figure 4.4 pH dependence of the ^{1}H NMR chemical shifts of NH_3 in the monoaqua complexes and diaqua complexes: (**A**) complex **1**, and (**B**) complex **2**. The curves represent the computer best fits using the pK_a values listed in Scheme 4.2. Labels:

monoaqua complexes **3a** and **4a** (▲), monoaqua complexes **3b** and **4b** (◆), diaqua complexes **5** and **6** (O).

Figure 5.1 2D [^{1}H, ^{15}N] HSQC NMR spectra from reactions of 2 mol equiv. of 5′-GMP (0.1 M $NaClO_4$, 296 K) with (A) ($^{15}NH_3$)-**1**, pH = 6.85, after 40 h and (B) ($^{15}NH_3$)-**2** pH = 6.55, after 20 h. Peak assignments are given in Table 5.1.

Figure 5.2 Plots of the relative concentrations of species **a** to **h** (based on Pt-NH_3 peak integrals) versus time for the reactions shown in Fig. 5.1. (A) 2-Picoline complex **1**, (B) 3-picoline complex **2**. Peak labels: (**a**) ◆, (**b**) □, (**c**) ▲, (**d**) ×, (**e**) +, (**f**) ■, (**g**) ●, (**h**) Δ. The curves are the computer best fits for the rate constants given in Table 5.2.

Figure 5.3 ^{1}H NMR spectra recorded after 2 h and 1 week of reactions at 296 K of 5′-GMP (2 mol equiv) with (A) complex **1,** and (B) complex **2**. The peaks labelled * are from the aromatic protons of picoline ligands.

Figure 5.4 The temperature dependence of the H8 ^{1}H NMR signals of *cis*-[Pt(NH_3)(2-picoline)(5′-GMP)$_2$]$^{2+}$.

Figure 5.5 2D EXSY spectrum (mixing time = 1 s) for *cis*-[Pt(NH_3)(2-picoline)(5′-GMP)$_2$]$^{2+}$ showing exchange cross-peaks between the two methyl signals, indicative of the slow rotation of coordinated 2-picoline.

Figure 5.6 Two-dimensional [^{1}H, ^{15}N] HSQC NMR spectra for reactions of GSH (1 mol equiv) with (A) complex **1,** and (B) complex **2,** recorded at 296 K, pH 7 (100 mM phosphate buffer) after 3.5 h. Peaks (**1a** to **1c,** and **2a** to **2c**) are assigned according to

Table 5.1; the others are unassigned. Satellites (^{195}Pt) of peaks **1a** and **2a** are labelled with *. Peaks with ^{15}N chemical shifts near -40 ppm are characteristic of NH_3-Pt *trans* to sulfur.

Figure 5.7 Time dependence of the concentrations of the starting complex **1** (■), its monoaquachloro adducts (**1b** + **1c**) (▲), and complex **2** (O), its monoaquachloro adducts (**2b** + **2c**) (×), during reactions with GSH (1:1 molar ratio, pH 7, 296 K).

Figure 5.8 2D [^{1}H, ^{15}N] HSQC NMR spectrum for the competitive reaction of GSH and 5′-GMP with complex **1** (molar ratio: 2:2:1) at 296 K, pH 7.0 (100 mM phosphate buffer) recorded after 14.5 h. Peaks of 5′-GMP adducts (**1d**, **1e**, **1h**) and GSH adducts (**1j**, **1q**) are labelled according to those in Table 5.1 and Table 5.4. Satellites of peak **1a** are labelled with *. The peaks in the dashed box are due to the formation of GSH adducts (^{15}N chemical shifts near -40 ppm are characteristic of NH_3-Pt *trans* to sulfur), but no specific assignments were made. Peak **1r** is tentatively assigned to an adduct with one GMP and one GSH ligand in the *cis* position (NH_3-Pt *trans* to N7).

Figure 5.9 Schematic representations of the possible isomers in a C_2-symmetrical *cis*-PtA_2G_2 complex and their interconversion. Arrows represent an N7-bound G as shown on the right side of the Figure.

Figure 5.10 Diastereomers of *cis*-[Pt($^{15}NH_3$)(2-picoline)(5′-GMP-*N7*)$_2$]$^{2+}$. The arrows (➞) represent 5′-GMP molecules, with the head of the arrow denoting H8.

Figure 6.1 HPLC chromatograms for the reaction of *cis*-$[Pt(NH_3)_2(H_2O)_2]^{2+}$ with DNA 14-mer single strand **I** (100 μM, 1:1.2 molar ratio, 298K). (A) one week after incubation; (B) re-injection of purified sample corresponding to "bound" fraction in A, the unplatinated single strand with retention time *ca.* 7 min has disappeared.

Figure 6.2 2D [^{1}H, ^{15}N] NMR spectrum recorded at 298 K of (A) the HPLC purified platinated G*G* 14-mer single strand **I***; (B) platinated 14-mer DNA duplex **III*** formed by annealing the purified G*G* single strand **I*** with its complementary CC strand **II** (0.1 M $NaClO_4$, pH 6.0, 9 mM phosphate buffer, 90% H_2O/10% D_2O). Only one pair of cross-peaks was observed in each spectrum which suggests that the purity of the platinated single strand and duplex samples is high.

Figure 6.3 Contour plot of the 2D NOESY spectrum (300 ms mixing time, 99.9% D_2O, 278 K) of **III*** showing the aromatic H8/H6/H2 to H1′/H5 region. The sequential NOESY walks are shown in (A) for the platinated G*G* top strand **I***, and (B) for the unplatinated CC bottom strand **II** present in the duplex **III***.

Figure 6.4 A contour plot of 300 ms NOESY spectrum of DNA duplex **III*** at 278 K showing the H2′/H2′′/thymidine Me-to-aromatic region NOE connectivities.

Figure 6.5 A contour plot of the 150 ms NOESY spectrum of DNA duplex **III*** recorded in 90% H_2O/10% D_2O at 278 K showing the imino-to-imino region. A sequential walk was made between the imino protons involved in Watson-Crick hydrogen bonding in the platinated 14-mer DNA duplex, which is only interrupted at G7* site. The imino protons of the two base-pairs at each of the 5′ and 3′ ends are not observed. The 1D ^{1}H spectrum of the same region is plotted on the top.

Figure 6.6 Temperature dependent 1D ^{1}H spectrum of DNA duplex **III*** in the imino proton region showing the appearance of G7* imino proton at low temperature. Assignments are indicated on the top of the peaks.

Figure 6.7 Simulated (A) and observed (B) cross-peaks for A14 H1′-to-H2′ and H2′′in 2D DQF-COSY spectra of DNA duplex **III***. The simulation was carried out using SPHINX and LINSHA programs, The simulation indicates the presence of only the C3′-endo conformation for A14 deoxyribose.

Figure 6.8 Standard A- and B-form 14-mer DNA duplexes built in Sybyl 6.3 and used as starting models for structural calculations. Colour code: C (white), H (cyan), N (blue), O (red), P (orange).

Figure 6.9 A capped stick model of the rMD calculated 14-mer DNA duplex **III***, where the G_7*G_8* site is modified by *cis*-$\{Pt(NH_3)_2\}^{2+}$. Colour code: C (white), H (cyan), N (blue), O (red), P (orange), Pt (purple).

Figure 6.10 Helical axes calculated by the program CURVES for the final structure.

Figure 6.11 Extended view of the central four base pairs $T_6G^*_7G^*_8T_9/A_{23}C_{22}C_{21}A_{20}$ of the platinated 14-mer DNA duplex **III***. The duplex is unwound and the base pairs are destacked at the G*G* site. Colour code: C (white), H (cyan), N (blue), O (red), P (orange), Pt (purple).

Figure 6.12 Graphic plots of the variation of the minor groove width with the base pair step. The minor groove width of standard A- and B-forms of DNA are plotted with dashed lines for comparison. (•) for the platinated 14-mer DNA duplex.

Figure 6.13 Superimposed 10 structures calculated from A-1 and B-1 with randomly assigned initial atom velocities (five each), showing the flexibility of the 5′ and 3′-ends. Colour code: C (white), N (blue), O (red), P (orange), Pt (purple).

Figure 7.1 The 2D [^{1}H, ^{15}N] HSQC NMR spectrum recorded after 1 week of reaction of *cis*-[$PtCl_2(^{15}NH_3)$(2-Pic)] **1** with d(GpG) dimer at (A) 298 K (1 mM, 1:1 molar ratio, 100 mM $NaClO_4$, pH 6.0, 9 mM phosphate buffer, 90% H_2O/10% D_2O). The two pairs of peaks are shown in two dotted boxes and their relative intensities are 2:2:3:3 (from left to right). (B) 338 K, one pair of peaks becomes closer and the other pair has merged.

Figure 7.2 The 2D [^{1}H, ^{15}N] HSQC NMR spectrum of reaction of *cis*-[$PtCl_2(^{15}NH_3)$(2-Pic)] **1** (1 mol equiv.) with 14-mer DNA duplex **III** at 298 K (1 mM, 100 mM $NaClO_4$, pH 6.0, 9 mM phosphate buffer, 90% H_2O/10% D_2O) recorded after (A) 15 hours. Peak assignments: **a** is the starting complex **1**; **b** and **c** are the two monoaqua species (in dashed boxes for intensity comparison with those in hydrolysis experiment in Chapter 4); **d** is the final major adduct; those intermediates unassigned are labelled as *. (B) Recorded after 1 week. The integral percentages of the major peak and the two minor peaks are indicated.

Figure 7.3 ^{1}H NMR spectrum recorded after (A) 0.5 h and (B) 1 week of reaction of *cis*-[$PtCl_2(^{15}NH_3)$(2-Pic)] **1** (1 mol equiv.) with 14-mer DNA duplex **III** at 298 K for the same sample in Fig. 7.2. The assignments of peaks in (B) are listed in Table 7.1. The broad peak for T6 H2′ at 0.43 ppm is scaled up on top.

Figure 7.4 Expansion of the aromatic region of the 200 ms 2D NOESY NMR spectrum for the same sample of platinated DNA duplex as used for Fig. 7.2 in 99.9% D_2O. Assignments are shown on the right-hand side (Pic refers to the 2-methylpyridine ligand), and the dashed line shows the connectivity from Pic-H6 to G7 H8 and G7 H8 to G8 H8.

Figure 7.5 Slices taken through the 2D NOESY spectrum at the chemical shifts of (a) 2-picoline H6, (b) T6 H2′ and (c) T6 CH_3, showing NOE connectivities to other protons. Detailed peak assignments and NOE information are listed in Tables 7.1 and 7.2, respectively.

Figure 7.6 2D DQFCOSY NMR spectrum for the same sample as Fig. 7.2 in 99.9% D_2O. The assignments of protons on picoline ring are shown on the right-hand side (Pic refers to the 2-methylpyridine ligand), and the dashed lines show connectivities between Pic-H6, H5, H4 and H3.

Figure 7.7 Stereoview of four molecular models for the G*G* adduct of duplex **III**: 2-picoline *trans* to G8 (3′-G) with the 2-methyl group orientated either (A) towards the phosphate backbone (**Methyl-Out**) or (B) towards the centre of the major groove (**Methyl-In**); 2-picoline *trans* to 5′-G also with either (C) **Methyl-Out** or (D) **Methyl-In** orientations.

Figure 7.8 (A) Space-filling model of *cis*-{$Pt(NH_3)$(2-Pic)}-d(ATACAT**G***G*TACATA)·d(TATGTACCATGTAT), with *cis*-$\{Pt(NH_3)(2\text{-Pic})\}^{2+}$ shown in green. The perfect fit and alignment of the 2-picoline ligand along the major groove can be seen. (B) Close-up view of the Pt binding site showing NOE connectivities (yellow dashed lines, listed in Table 7.2) between 2-picoline and DNA. H-bonding between Pt-NH_3 and O6 of G8 is shown as a yellow dotted line. Colour code: C (white), H (cyan), N (blue), O (red), P (orange), Pt (purple).

List of Schemes

List of Tables

Publications:

1) [H-1, N-15] nuclear magnetic resonance studies of $[Pt(dien)Cl]^+$ (dien= diethylenetriamine): Hydrolysis and reactions with nucleotides

Zijian Guo, **Yu Chen**, Erle Zang, Peter J. Sadler

J. Chem. Soc., Dalton Trans., 1997, 4107-4111.

2) Stereospecific and kinetic control over the hydrolysis of a sterically hindered platinum picoline anticancer complex

Yu Chen, Zijian Guo, Simon Parsons, Peter J. Sadler

Chem. Eur. J., 1998, *4*, 672-676.

3) Interconversion between S- and N-bound L-methionine adducts of $Pt(dien)^{2+}$ (dien= diethylenetriamine) *via* dien ring-opened intermediates

Yu Chen, Zijian Guo, Piedad del Socorro Murdoch, Erle Zang, Peter J. Sadler

J. Chem. Soc., Dalton Trans., 1998, 1503-1508.

4) Kinetic control of reactions of a sterically-hindered platinum picoline anticancer complex with guanosine 5′-monophosphate and glutathione

Yu Chen, Zijian Guo, John A. Parkinson, Peter J. Sadler

J. Chem. Soc., Dalton Trans., 1998, 3577-3585.

5) A new platinum anticancer drug forms a highly stereoselective adduct with duplex DNA

Yu Chen, John A. Parkinson, Zijian Guo, Tom Brown, Peter J. Sadler

Angew. Chem. Int. Ed. 1999, *38*, 2060-2063.

6) ^{195}Pt and ^{15}N NMR spectroscopic studies of cisplatin reactions with biomolecules

Yu Chen, Zijian Guo and Peter J. Sadler

in '***Cisplatin-Chemistry and Biochemistry of a Leading Anticancer Drug***',

Ed. B. Lippert, WILEY-VCH, Basel, 1999, pp.293-318.

Abbreviations:

cis-Pt:	*cis*-$[PtCl_2(NH_3)_2]$, *cis*-DDP
COSY:	2D correlation spectroscopy
dien:	Diethylenetriamine
DQF:	Double-quantum filtered
EXSY:	2D exchange spectroscopy
Glutathione:	γ-L-Glu-L-Cys-Gly
GMP:	Guanosine 5´-monophosphate
GSH:	Glutathione
HMG:	High mobility group
HMQC, HSQC:	Heteronuclear multiple-quantum (or single quantum) coherence
HPLC:	High performance liquid chromatography
hSRY:	Sex determining factor in humans
ICL:	Interstrand cross-link
LEF-1:	Lymphoid enhancer binding protein
L-HMet:	L-methionine
MT:	Metallothionein
NMR:	Nuclear magnetic resonance
NOESY:	2D nuclear Overhauser effect spectroscopy
NOE:	Nuclear Overhauser effect
Pic:	Picoline, methyl-pyridine
rMD:	Restrained molecular dynamics
RMSD:	root-mean-square deviation
SSRY-1:	Structure specific recognition protein
UV:	Ultraviolet spectroscopy
WATERGATE:	Water suppression by gradient-tailored excitation

Chapter 1

Platinum Anticancer Drugs

1.1 Cisplatin

The compound *cis*-$[PtCl_2(NH_3)_2]$, clinically known as 'cisplatin' (often abbreviated as *cis*-Pt), was discovered to be cytostatically active and became a very effective antitumour drug in the 1960's.[1] It is one of the most widely used and successful drug in cancer chemotherapy. It is highly effective in the treatment of a number of tumours, e.g. testicular and ovarian cancer. In combination therapy with other drugs, cisplatin is also used to treat cervical, bladder and head/neck tumours.[2] it has become well known that cisplatin reacts with cellular components such as DNA and proteins.[3,4] A key reaction step in the mechanism of action appears to be the binding of the *cis*-$\{Pt(NH_3)_2\}^{2+}$ unit to cellular DNA at two neighbouring guanine bases, and more specifically at N7 position.[5]

Despite the successful therapeutic use of *cis*-Pt, it still suffers from serious side effects which include: (1) poor solubility in saline, (2) severe toxicity (e.g. nausea, ear damage, vomiting, loss of sensation in hands and kidney toxicity), (3) the development of resistance.[6,7] Also, the applicability of *cis*-Pt is still limited to a narrow range of tumours. These raise the importance of understanding the mechanism of anticancer activity of cisplatin and lead to the search for new generations of Pt drugs which can circumvent those problems.

1.2 Development of New Platinum Drugs

Derivatives belonging to the *cis*-$[PtX_2(amine)_2]$ structural class (X = leaving anionic group; amine = any primary or secondary amine), show similar or improved biological activity compared with cisplatin. Among them, the second-generation platinum drug carboplatin, $[Pt(1,1\text{-cyclobutanedicarboxylato})(NH_3)_2]$, has been in routine clinical use and has less toxic side-effects than cisplatin. Both cisplatin and its closely related analogue carboplatin lead to high levels of resistance in various tumours.

Three major mechanisms have been proposed for cisplatin resistance in vivo.[8] First, the reduced intracellular concentrations of the drug due to either blocking uptake or increasing efflux. Second, the increased inactivation of the drug through reaction with intracellular ligands such as glutathione and metallothionein. Finally, the increased removal of drug-DNA adducts by cell-based repair systems including nucleotide excision repair.

In order to reduce the spontaneous drug resistance developed in certain tumours and at the same time achieve a similar level of effectiveness, a third-generation serious of drugs containing different amines has evolved during the last decade. They include platinum(IV) pro-drugs (e.g. JM216, Fig. 1.1) that have potential to be administered orally.[9] It is still not very clear whether or not such compounds are reduced before binding to the DNA, although most evidence suggest that the formation of Pt(IV)-DNA adducts is too slow to account for the activity.[10]

One strategy to overcome cisplatin resistance has been to use sterically hindered carbocyclic amines, these include DWA2114R, oxaliplatin and most recently ZD0473 (or AMD473), shown in Fig. 1.1. The bulky ligands in these complexes may prevent recognition and inhibit nucleotide excision repair even though they form similar adducts to those of cisplatin.[11,12] DWA2114R is currently in phase III clinical trials. The chiral ligand used in this compound provides the interesting observation that the *R*-isomer is not toxic while the *S*-isomer is. The activity of a chiral platinum drug may provide insight into the stereo requirements of adduct formation or possibly the intermolecular interactions that occur following DNA binding. Oxaliplatin has been in clinical trials since 1986, both in combination therapy and as a single agent drug for the treatment of colorectal cancer.[12,13] It is active in cisplatin resistant ovarian cancer, and was the first cisplatin derivative to be approved in France for the treatment of advanced colorectal cancer. ZD0473 is a newly reported anticancer active drug, which is now in phase I clinical trials in UK.[14]

Compared with cisplatin, this new drug is both oral and i. v. active and shows diminished cross-resistance to cisplatin in three different cell lines with acquired cisplatin resistance.[15] It also lacks nephrotoxicity. The steric hindrance of the 2-methyl pyridine ligand appears to play an important role during the substitution reactions,[16,17] and highly stereoselective formation of G*G* adduct with DNA duplex may be recognised differently by excision repair system.[18]

Until now, most of the potential drugs have two amines in a *cis* geometry (symmetric, asymmetric, chelating or not), and the presence of at least one N-H group on the amine, as well as leaving groups with a weaker *trans* effect than the amine. These characters were found to be necessary in structure-activity relationships for platinum compounds. By applying careful variations in: (a) the chosen amine ligand on platinum (chelating or not, hydrogen-bond donor, steric effects, bioactive carrier groups, possible side arms for secondary DNA interactions), and (b) the selected leaving groups at platinum (non-toxic, optimal ligand-exchange kinetics, possibility of acting as a pro-drug), more new drugs can be expected.[19]

Besides the 'classical' platinum compounds, completely different structural classes of platinum antitumour drugs have also been reported. The recently reported dinuclear and trinuclear platinum-amine compounds (e.g. BBR3464, Fig. 1.1) appear to be able to form very different types of DNA lesions to those of cisplatin.[20] The activity of these compounds depends on the chain length of backbone.[21] The elevated activity level in cisplatin-resistant cells and in some cases the different activity spectrum, suggest that these compounds have a potentially different mechanism to that proposed for mononuclear cisplatin derivatives. The trinuclear platinum complex is now in phase I clinical trials in the USA. *Trans*-[$PtCl_2$(*E*-imino ether)$_2$] complex (*trans-EE*) (imino ether = $HN{=}C(OCH_3)CH_3$) is another reported anticancer active complex.[22] Compared with its *cis* isomer (*cis-EE*), the *trans-EE* is not only more cytotoxic but also endowed with significant antitumor activity, which implies a new

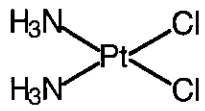

cisplatin

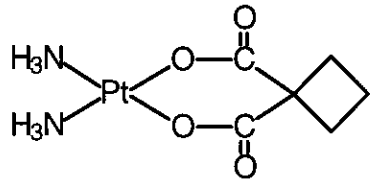

carboplatin

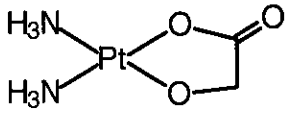

254-S

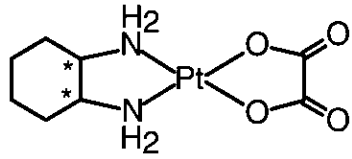

oxaliplatin

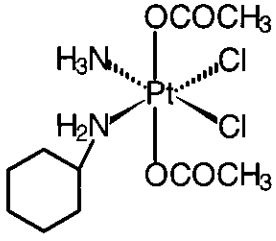

JM-216

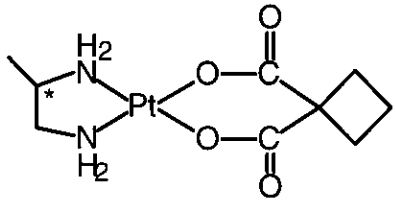

NK 121

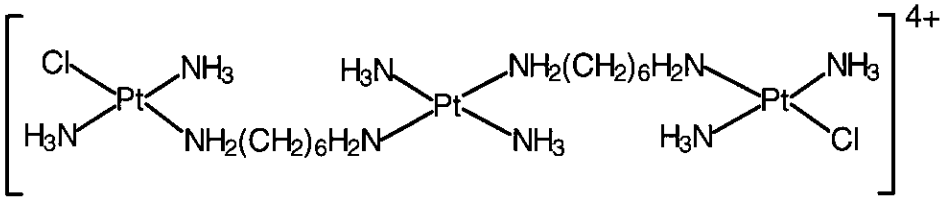

BBR-3464

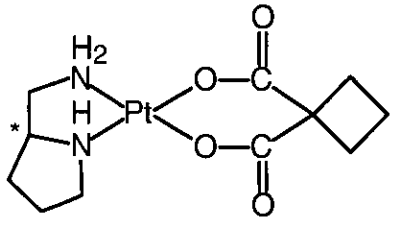

DWA2114R

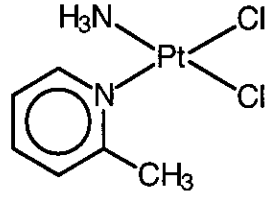

ZD0473

Figure 1.1 Some clinically used Pt drugs and some compounds which are in different stages of clinical trials.

mechanism for the activity of *trans* platinum complexes.

From the platination complexes which have been investigated so far, it is clear that the relationship between structure and activity is extremely complex. Many factors that can influence activity have to be taken into account, for instance, reactions prior to cell uptake, the rate and mechanism of cell uptake, deactivation prior to DNA binding, the rate of DNA binding, the adduct profile that results, and the repair and removal of the DNA adducts. Those factors all have the potential to profoundly influence the activity of the complex, and each factor can also differ substantially between one tumour type to another. Simple unifying structure-activity rules are only likely to be indicative of classes of compounds that act by similar mechanisms. However, it is still generally true that compounds adhering to the structure-activity rules can be expected to be active.[23]

Overall, new structures (to increase activity, overcome the above-mentioned problems of resistance and reduce toxicity) and improved sequence selectivity (to avoid mutagenic side effects) of platinum drugs may result in better treatment of tumours that are not sensitive enough to cisplatin. Some of the first, second and third generation of platinum compounds clinically used or on trial are shown in Fig. 1.1.

1.3 Mechanism of Action of Cisplatin

After administration, either by injection or infusion, *cis*-Pt circulates in the blood. Because of the relatively high concentration of chloride ions in blood (100 mM), the hydrolysis of *cis*-Pt is inhibited and it remains almost unchanged before entering both normal and tumour cells. The mechanism of how cisplatin enters cells still remains under-defined. Existing data suggest that cisplatin enters cells *via* transmembrane channels, though these data are also consistent with high-capacity facilitated transport.[24] Once inside the cell, *cis*-Pt hydrolyses to give active forms of aqua-species such as *cis*-$[PtCl(NH_3)_2(H_2O)]^+$ and *cis*-$[Pt(NH_3)_2(H_2O)_2]^{2+}$ because of

the much lower chloride ion concentration (about 4 mM). Hydrolysis is known to be the rate-limiting step in the binding of cisplatin to DNA.[25]

In theory, a large variety of biological molecules could be the potential targets for platinum compounds, including DNA, RNA and proteins. From the Hard-Soft Acid-Base theory, S-donor ligands in proteins would bind strongly and generate the most stable bonds. Binding to lone pairs of nitrogen atoms can also be very strong. These types of binding would involve amino acid side chains of proteins from cysteine, methionine, histidine and the solvent-exposed N7 atoms of adenine and guanine in double-stranded DNA. Usually, interactions of platinum antitumor complexes with S-containing biomolecules are thought to have an overall negative effect on antitumor activity. Such interactions can be responsible for the inactivation of Pt(II) species, development of resistance and toxic side effects such as nephrotoxicity. But recent studies have shown that sulfur ligands, especially thioether from methionine or perhaps oxidised glutathione, could also play a key role in the transfer of Pt to the nucleic acids.[26,27]

The antitumour activity of cisplatin depends on its ability to modify the structure of the DNA of cancer cells. Approximately 1% of the intracellular cisplatin reacts with genomic DNA and yields a variety of mono-adducts and intra- and inter-strand crosslinks. The most electron-donating sites in duplex DNA are known to be guanine residues located adjacent to a second guanine residue.[28,29] For all third-generation platinum anticancer agents, guanine-N7 position appears to be the preferred binding site. Therefore it is not surprising that the major DNA lesions both *in vitro* and *in vivo* are intrastrand d(GpG) crosslinks. Besides GG intrastrand crosslinks (70%), the other major DNA adducts of cisplatin are intrastrand AG (but not GA) crosslinks (15%), the remainder being minor 1,3-intrastrand and interstrand crosslinks involving two non-neighbouring guanines.[30] Platination of DNA by *trans*-DDP was found to give the following adducts after digestion: dG-Pt-dC (50%), dG-

Pt-dG (40%), dG-Pt-dA (10%).[31] As expected, *trans*-DDP does not form intrastrand chelates between adjacent nucleotides. From the genetic effects of DNA adducts formed by *cis*-DDP, the G*G* adduct is the most genotoxic of the three major *cis*-$\{Pt(NH_3)_2\}^{2+}$ intrastrand crosslinks, which collectively account for ~95% of the adducts formed by *cis*-DDP. Although highly toxic, the G*G* adduct is ~4-5 fold less mutagenic than the A*G* adduct. Since the mutagenic properties are important factors which may lead to the development of second tumours, drugs with a high ratio of toxicity to mutagenicity are desirable. Therefore platinum drugs should be designed to maximize the occurrence of the G*G* adduct and minimize the frequency of the more mutagenic A*G* adduct.[32]

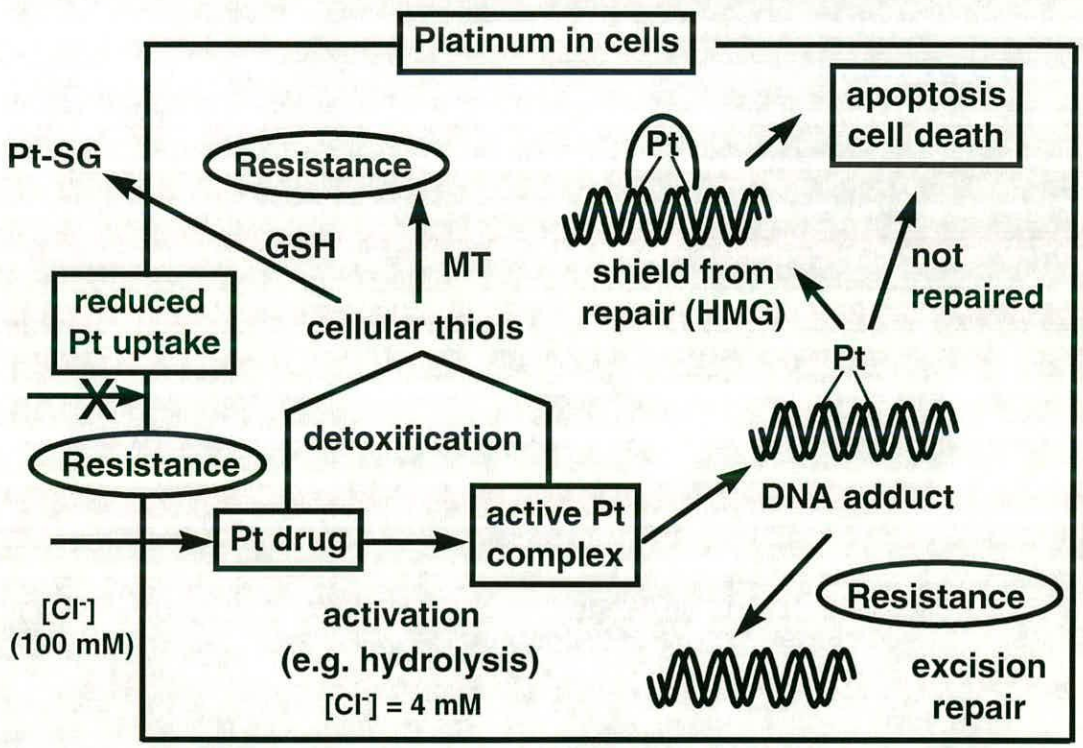

Figure 1.2 Schematic representation of reactions of cisplatin in the cell. (based on Ref. 33)

The fate of cells following cisplatin exposure depends on both the extent of damage induced and on the cellular response to damage. One potentially important way in which cisplatin may kill cells is by induction of apoptosis. Apoptosis is a ubiquitous, genetically regulated mechanism of active cell death that is conserved in multicellular organisms. Considerable evidence indicates that cisplatin can kill cells by apoptosis.[34,35] Proteins that specifically recognise cisplatin induced DNA damage have been found, such as HMG proteins. Through binding to cisplatin-DNA adducts, HMG proteins could either protect cisplatin adducts from recognition by DNA repair enzymes or trigger apoptosis.[36] A schematic and somewhat hypothetical picture for the multi-step transport and reaction of *cis*-Pt in cell is illustrated in Fig. 1.2.

1.4 Reactions with Amino Acids and Nucleotides.

Pt(II) being a "soft" metal ion is known to have a very high affinity for "soft" ligand atoms such as sulfur. Sulfur-containing ligands, e.g. glutathione (GSH), N-acetyl-L-cysteine, have been investigated as rescue agents for the removal of Pt from the body. The thioether L-methionine (L-HMet) is thought to play an important role in the metabolism of cisplatin, and one of the few characterised metabolites of cisplatin is [Pt(L-Met)$_2$] which has been isolated from urine.[37] [Pt(L-Met)$_2$] exists as

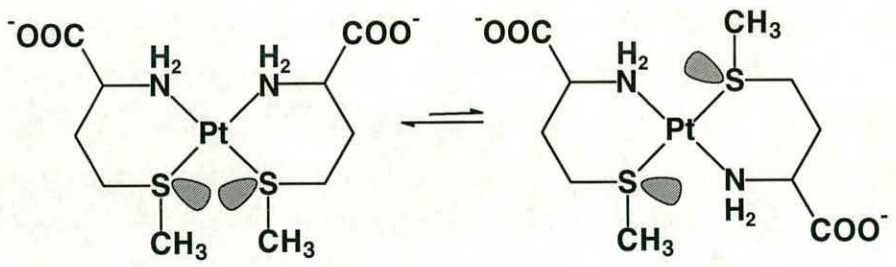

Cis ***Trans***

a mixture of *cis* and *trans* isomers in aqueous solution.[38,39] At neutral pH, the isomers interconvert extremely slowly (half-lives of 22.4 h and 3.2 h for the *cis* and *trans*

isomers, respectively, at 310 K) with the *cis* isomer predominating at equilibrium (10:1, $K = 7.0$).

The S-containing tripeptide glutathione (γ-Glu-Cys-Gly) is present in cells at millimolar concentrations. The formation of Pt:GSH complexes may play an

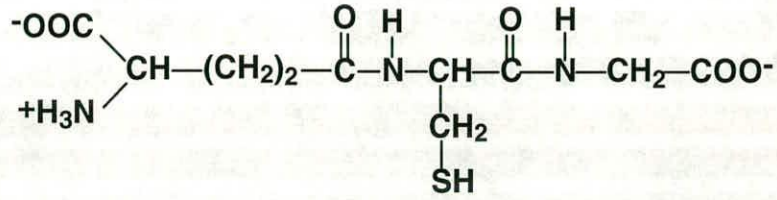

Glutathione (GSH)

important role in the biological activity of platinum complexes. GS-Pt complexes can be pumped out of cells through an ATP-dependent process.[40] During the reaction of *cis*-$[PtCl_2(^{15}NH_3)_2]$ with GSH, the mono-substituted complex *cis*-$[PtCl(SG)(^{15}NH_3)_2]$ is formed first, but several other species containing a $^{15}NH_3$-Pt-S linkages are present within a few minutes.[41] Release of $^{15}NH_3$ ligands has been observed and no coordinated $^{15}NH_3$ is contained in the final product, which is consistent with a high-molecular mass polymer with a 1:2 Pt:GSH stoichiometry. A product containing a dinuclear Pt_2S_2 four-membered ring has been observed from reactions of *cis*-$[Pt(NH_3)_2(H_2O)_2]^{2+}$ with GSH.[42] Glutathione can also affect macrochelate ring closure of *cis*- and *trans*-DDP monofunctional adducts on DNA.[43] Compared with cisplatin, the reaction between GSH and *trans*-DDP monofunctional adducts more rapidly leads to the formation of sulfur-bound, glutathione-trapped monofunctional adducts. Glutathione does not appear to react with *cis*- or *trans*-DDP bifunctional adducts. These results are consistent with proposals that the biological inactivity of

trans-DDP may arise from selective trapping of monofunctional adducts before they ring-close to form bifunctional lesions.

MT is a low-molecular weight protein rich in cysteine (~30%) and thought to be responsible for cisplatin detoxification. The tetrapeptide Boc-Cys(SMe)-Ser-Ala-Cys(SMe)-$CONH_2$ (CSAC) has been used as a model for metallothionein (MT) for reactions of MT with *cis*-DDP and *trans*-DDP.[44] The reaction with cisplatin forms a mixture of different diastereoisomers and polymeric species, with NH_3 liberation due to the strong *trans*-effect of sulfur. *Trans*-DDP, on the other hand, forms a 2:1 complex coordinated to the -S-CH_3 groups and no ammonia release is observed.

Therapeutic nucleophilic agents for cisplatin, such as Na(ddtc) (sodium diethyldithiocarbamate) and thiourea, can help to remove Pt from certain proteins so as to relieve toxicity.[45] The mechanism may be based on the relatively easy reversal of Pt binding to methionine side chains. In contrast, nephrotoxicity, thought to be caused by formation of Pt-cysteine adducts (Pt(II) thiolate bonds), cannot be reversed by Na(ddtc) and thiourea.

The pH-dependent S,O- versus S,N-chelation in the reaction of *cis*-$[Pt(NH_3)_2(H_2O)_2]^{2+}$ with S-methyl-L-cysteine (mecysH) and L-methionine has been studied by Appleton *et al.*[46] The chelate products $[Pt(NH_3)_2(mecys\text{-}S,N)]^+$ and $[Pt(NH_3)_2(met\text{-}S,N)]^+$ were observed at pH values near 5. In strongly acidic conditions (pH $\leq$ 0.5), the initial product from the reaction with mecysH is $[Pt(NH_3)_2(mecysH\text{-}S,O)]$ which slowly converts to the S,N-chelate. A similar reaction sequence occurs with methionine, but *cis*-$[Pt(NH_3)_2(metH\text{-}S)_2]^{2+}$ is also formed in competition with the *S,O*- chelate.

Intramolecular migration of the model fragment $\{Pt(dien)\}^{2+}$ from sulfur to imidazole-N^1 in histidylmethionine (his-metH) has been investigated by HPLC and NMR methods.[47] Under acidic conditions, the dominant Pt complex is [Pt(dien)(his-metH-*S*)]$^{2+}$, while the imidazole N1-bound complex, [Pt(dien)(his-metH-*N1*)]$^{2+}$ becomes the major species at pH values higher than 6.1. The dinuclear intermediate [Pt(dien)(his-metH-*N1*,*S*)]$^{2+}$ was observed during the slow isomerization.

Although the kinetic reactivity of sulfur is high, the Pt-thioether bond is labile in the presence of other nucleophiles.[48] This could provide a novel pathway for DNA platination. The competitive binding of Met, His, 5′-GMP, 5′-AMP, 5′-TMP and 5′-CMP to $\{Pt(dien)Cl\}^+$ in aqueous solution show that 5′-GMP selectively displaces S-bound Met. Initially only L-Met coordinates to Pt with little GMP coordination, but in the later stages of the reaction coordinated L-Met is displaced by N7 of GMP.[48,49] It is notable that thioethers such as L-Met react with Pt(II) amines faster than thiols such as GSH, and reactions of thiols tend to be irreversible.[50] Intramolecular migration of $\{Pt(dien)\}^{2+}$ from S to guanosine-N7 in S-guanosyl-L-homocysteine has been observed by van Boom *et al.*[51] Novel intermediates including *cis*-[Pt(GMP-*N7*)(Met-*S*)($^{15}NH_3$)$_2$]$^{2+}$ and *cis*-[Pt(GMP-*N7*)(Met-*S*,*N*)($^{15}NH_3$)]$^+$ (N7 *trans* to S) have been detected and characterised in the reaction of cisplatin with 5′-GMP in the presence of L-Met.[52] Ammonia release was observed during the formation of intermediates. Monodentate S-bound L-HMet can coordinate to Pt reversibly, whereas S,N-chelated L-Met is much more inert. Interestingly the reaction of 5′-GMP with cisplatin is faster in the presence of L-Met than in the absence.

Highly stable monofunctional adducts are formed during reactions of monodentate S-bound N-acetyl-L-methionine complexes $[Pt(en)(MeCO\text{-}Met\text{-}S)Cl]^+$ and $[Pt(en)(MeCO\text{-}Met\text{-}S)_2]^{2+}$ (MeCO-Met = N-acetyl-L-methionine) with 5′-GMP and GpG.[53] Such adducts formed by methionine and its derivatives could play a role in the trapping of monofunctional adducts of platinum anticancer drugs with DNA *in vivo*.

The lower side-effects and toxicity of carboplatin $[Pt(NH_3)_2(CBDCA\text{-}O,O')]$ (H_2CBDCA: cyclobutane-1,1-dicarboxylic acid) compared with cisplatin, can be attributed to its lower reactivity caused by the presence of the chelating CBDCA ligand. It could be a pro-drug for cisplatin but the rate of hydrolysis is very slow (half-life in water > 4.4 years). A ring-opened carboplatin adduct containing monodentate CBDCA can be detected during reactions of carboplatin with 5′-GMP.[54] The fast reactions of carboplatin with 5′-GMP compared with nitrate, phosphate and Cl^- suggest that direct attack of nucleotides on carboplatin may be of importance in the mechanism of action of this drug.[54] Ring-opened adducts of carboplatin can form not only from reactions with nucleotides, but also by the attack of sulfur amino acids.[55] Reactions with thioether ligands are much more rapid compared with thiols. Surprisingly very stable ring-opened species such as $[Pt(CBDCA\text{-}O)(NH_3)_2(L\text{-}HMet\text{-}S)]$ are formed, which has a half-life for Met-*S*, *N* closure of 28 h at 310 K. A similar species was detected as a major metabolite in the urine of animals treated with carboplatin.[56] Such an intermediate could also play a role in the biological activity of this drug.

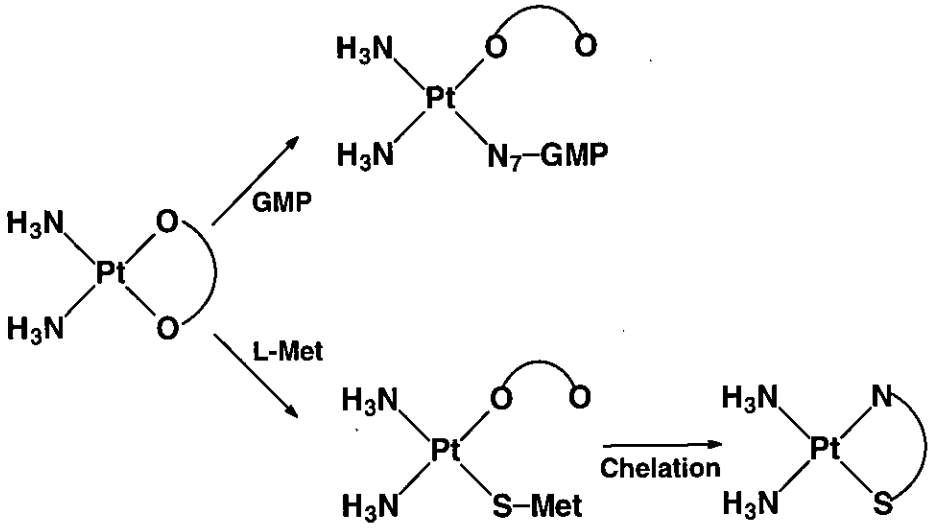

Scheme 1.1 Reactions of 5′-GMP and L-Met with carboplatin.

1.5. Kinetic Studies of Reactions of Cisplatin with GG Single Strand and Duplex DNA

Recently there has been much interest in investigating the mechanism of formation of d(GpG) intra- or inter-strand crosslinks on either DNA single strands or duplexes. Such interest is important because the lifetimes of the various species along the pathways may determine their biological significance. For example, intermediates may live long enough to be recognised by repair systems, and monofunctional adducts en route to d(GpG) chelates may themselves distort the structure of DNA.[57,58] Chottard et al. have identified individual monofunctional adducts during reactions of *cis*-$[Pt(NH_3)_2(H_2O)_2]^{2+}$ with single and double-stranded DNA at pH 4.4.[59,60] They found that the 5′-G is platinated fasted than 3′-G, but the 3′-G monofunctional adduct chelates faster. The differences were increased in duplexes compared to single strands and were sequence-dependent. By observing ^{1}H and ^{15}N NMR resonances of Pt-$^{15}NH_3$ groups,[61] Sadler et al. reported the first direct comparison of the kinetics of platination of defined single- and double-stranded DNA with cisplatin.[62] The rate of platination of one of the GG residues was faster by a

factor of *ca.* 4 for both the single GG strand and duplex, and the monofunctional adduct that formed faster on the duplex (probably 3′G) also ring-closed faster by about an order of magnitude. One of the monofunctional adducts on the duplex (5′G) had a surprisingly long life-time (5 days at 298K).[63] In contrast, there was little difference between the rates of ring closure of the two monofunctional adducts on the GG single strand. GG platination gave rise to an equilibrium between two major forms (kinked or bent) of the GG chelate. Double platination on adjacent nucleobases has been reported to occur at high-salt conditions.[64] The intrastrand cross-link could compete with the second metal coordination.

Using 2D [^{1}H, ^{15}N] HSQC NMR spectroscopy, rates of platination of AG and GA containing double-stranded DNA have been compared.[65] It was concluded that the bifunctional intrastrand adduct profile observed when cisplatin binds to DNA is substantially controlled by the rate of formation of monofunctional adducts at the different X-purine-purine-X sequences. Monofunctional binding of cisplatin to the GpA sequence is approximately an order of magnitude slower than binding to either GpG or ApG sequences. A slow rate of closure also contributes to the nonformation of the bifunctional GpA adduct. Kinetic studies of GG versus AG platination on hairpin-stabilised duplex oligonucleotides were also carried out using HPLC methods.[66]

1.6 Structural Studies of Platinated DNA Duplexes

Significant distortion of the DNA structure upon platination was indicated in the early studies of cisplatin binding to nucleobases and nucleotides. The crystal structures of [$Pt(NH_3)_2${d(pGpG)}][67,68] and [$Pt(NH_3)_2${d(CpGpG)}][69] gave evidence of the structural changes upon cisplatin adduct formation. The *cis*-diammine-platinum(II) moiety binds to the N7 atoms of the two guanine rings, which are orientated in a head-to-head manner and destacked, the dihedral angle between the

purine base planes being 81°.[67] Using two-dimensional NMR methods, Den Hartog *et al.* reported the first solution structure of cisplatin chelated to two neighbouring guanines.[70]

Recently a number of high-resolution structure determinations have been obtained for the major cisplatin adduct on duplex DNA[71-76] as well as minor adducts.[77,78,79] The high resolution (2.6 Å) X-ray crystal structure of an intrastrand G*pG* platinated DNA duplex d(CCU^{Br}CTG*G*TCTCC)·(GGAGACCAGAGG) has been reported,[72] where U^{Br} is a 5-bromo-U heavy atom derivative of the native DNA sequence used for phasing. The triclinic unit cell contained two independent molecules which allowed two different but very similar structures of the platinated duplex (molecules A and B) to be obtained. There are several interesting features revealed from the analysis of this X-ray structure of the cisplatin-modified dodecamer duplex. The duplexes are bent towards the major groove with the bend locus near the site of platination. Two different bending angles were observed: one is ~39° similar to that reported from gel electrophoresis studies, and the other is ~55°. The bend is due in large part to a very shallow roll of 26° towards the major groove of the platinated G*G*, which results in considerable strain at the Pt-N7 bonds. The Pt atom lies 1 Å out of the plane of the guanine rings. Duplex formation and crystal packing preclude more complete destacking of the bases, and base pairing is retained throughout much of the helix. The duplex contains an A-form/B-form junction situated just to the 3′ side of the platinum adduct, with the first 8 base pairs (bp) to the 5′-side of the platinum site exhibiting A-form DNA parameters. This A-B fusion, which is only observed in the crystal structure of the platinated duplex, is thought most likely to be due to crystal packing. A projection of the DNA structure, based on the X-ray coordinates, is shown in Fig. 1.3.

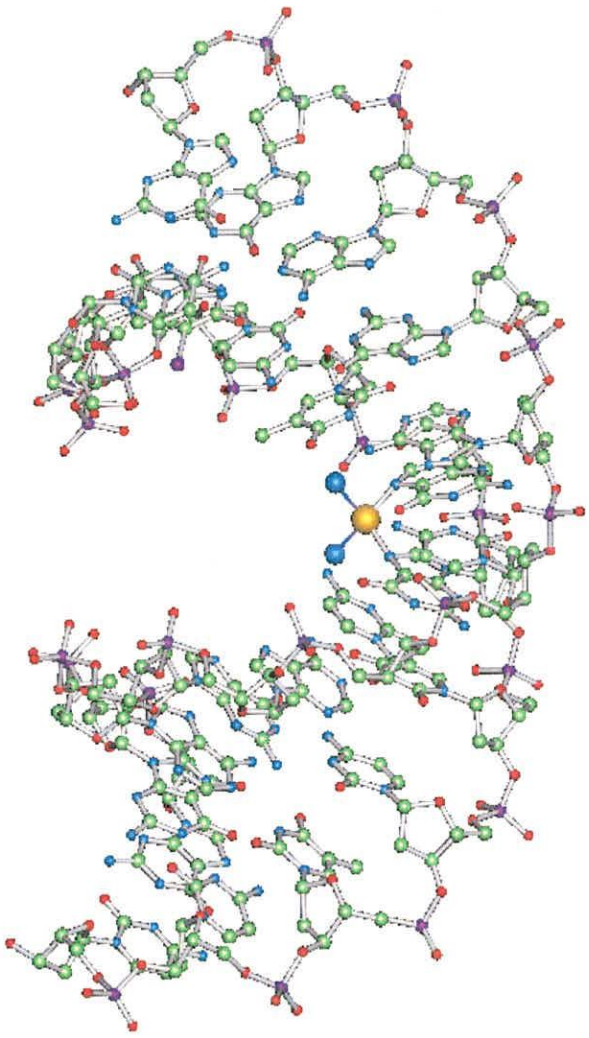

Figure 1.3 The structure of the GpG platinated DNA duplex d(CCTCTG*G*TCTCC)/d(GGAGACCAGAGG) as determined by X-ray diffraction.[72] Colour code: C (green), N (blue), O (red), P (purple), Pt (yellow).

The solution structure of the cisplatin-modified DNA dodecamer was also determined by high-resolution 2D NMR spectroscopy and restrained Molecular Dynamics (rMD) refinement by the same group, in order to find out the effect of crystal packing on the structural features.[74] The sequence of the DNA dodecamer d(CCTCTG*G*TCTCC)·d(GGAGACCAGAGG) is the same as the one used in crystal structural studies. There is a significant bend of 78° toward the major groove

resulting largely from the 49° guanine-guanine roll at the site of platination. These features are much more exaggerated than those observed in the X-ray crystal structure, probably due to the absence of the crystal packing forces. The larger roll between guanine bases relieves the strain imposed on the Pt-N7 guanine bonds, but still the Pt atom is displaced from each base plane by ~0.8 Å. A common property of the solution and crystal structures is the widening and flattening of the minor groove opposite the platinum adduct, affording geometric parameters resembling those found in A-form DNA. The unwinding of the helix at the site of the platination is 25°. Although considerably distorted from B-form DNA, the solution structure of the platinated duplex has predominately B-type sugar puckers (S conformation). Only the 5′-platinated guanosine (G6*) has its deoxyribose ring in the C3′-endo conformation, and the remaining 23 ring sugar puckers exist in the C2′-endo or closely related C3′-exo conformation.

With the normal NMR NOESY methods, usually it is possible only to observe NOE connectivities between protons < 5 Å apart. This small distance limitation presents difficulties for determination of the global features of DNA duplexes, for example bend angles or long range unwinding, although the local geometry of DNA helices can be resolved to high resolution. Recently a spin-labelled platinum compound *cis*-[Pt(NH_3)(4-amino-TEMPO)Cl] has been used in studies of the solution structure of a platinated-DNA.[75] This compound binds to the GpG site of DNA in a similar manner to cisplatin, with the label nestling rigidly in the major groove of the duplex. The use of this spin-labelled platinum compound allows the detection of long-range electron-proton distances for use in restrained molecular dynamics. The structure of the reduced diamagnetic duplex d(CTCTCGGTCTC)·d(GAGACCGAGAG) was determined by using conventional 2D NMR methods and distance-restrained molecular dynamics, and then further refined by applying 99 additional long-range (< 20 Å) electron-proton distance constraints. Refinements of

Table 1.1 Major structural parameters for G*G* platinated DNA structures.

Complex	dodecamer[72]	dodecamer[74]	octamer[73]	undecamer[75]
method	X-ray[a]	NMR[a]	NMR[a]	NMR[b]
	crystal	solution	solution	solution
DNA form	A/B junction	primarily B	primarily B	primarily B
Minor groove width(Å)	9.5-11.0	9.4-12.5	4.5-7.8	9.0-12.0
depth (Å)	3.0	1.4	3.2	2.1
P-P distance (Å)	5.5	6.9	6.8	6.8
Roll at G*G* bases (°)	26	49	42	59
Pt atom displacement	1.3 Å, 5′	0.8 Å, 5′	1.0 Å, 5′	0.5 Å, 5′
from guanine ring	0.8 Å, 3′	0.8 Å, 3′	0.8 Å, 3′	0.65 Å, 3′
Average helix twist (°)	32	25	25	26
DNA bend (°)	39 and 55[c]	78	58	~81

[a] *cis*-$[Pt(NH_3)_2Cl_2]$ was used in the study.

[b] Spin-labelled compound *cis*-$[Pt(NH_3)$(4-amino-TEMPO)ClI] was used in this study, which provided long-distance constraints for rMD.

[c] Two independent molecules.

the structure with either conventional interproton or a combination of the electron-proton and interproton restraints afforded the same local but different global structures. The final refined structure has a bend angle of ~81°, even larger than that observed for the dodecamer in solution. From the result of this study, it appears that the use of paramagnetic constraints is especially important in defining the ends of a duplex structure. These are usually poorly determined by NMR because of the intermolecular motion and a lack of the full complement of interproton NOEs for these base pairs.

The solution structure of another *cis*-$[Pt(NH_3)_2]^{2+}$ platinated duplex DNA d(CCTG*G*TCC)·d(GGACCAGG) containing the G*G* intrastrand cross-link was also reported.[73] Interestingly, the G*G* intrastrand crosslink adduct slowly converted into a more stable interstrand didentate adduct (between G4 and G9) promoted by the presence of the nucleophilic chloride ion. This phenomenon is not observed in the other structural studies with longer sequences and may be due to its strained Pt-N7 bonds in this very short length and less stable platinated DNA structure.

Structural studies of cisplatin-DNA adducts are not only focused on the major intrastrand G*G* adduct, but also on the other minor adducts which can also play an important role in the anticancer activity of this drug. The intrastrand AG crosslink is the second major adduct formed by cisplatin with DNA, which accounts for ~20% of the total adducts. For cancer patients, a correlation exists between the level of intrastrand GG and AG crosslinks in leukocyte DNA and their response to cisplatin therapy.[80] The solution structure of a nonanucleotide duplex crosslinked by cisplatin at an ApG sequence has been solved recently by means of NMR and molecular modeling.[79] It showed that the nucleotide was kinked towards the major groove in a way similar to the G*G* adduct. The major difference was at the position of the thymine complementary to the platinated adenine A*. It remained stacked on its 5´-neighbour, corresponding to the "E-model", whereas in the G*G* adduct, the cytosine facing the 5´-G was found to oscillate between the 5´-branch ("model E", stacking on 5´ side) and 3´-branch ("model C", stacking on 3´ side).

An early study of the minor adduct 1,3-intrastrand GTG cross-link by gel electrophoresis experiments revealed that the DNA duplex is bent by ~35° and unwound by 23°.[81] The solutional structure of a 13-mer duplex was determined recently by NMR spectroscopy and rMD.[82] The 1,3-intrastrand cross-link does not distort the global helical structure to the extent observed in the 1,2-intrastrand

adducts but significantly disrupts local base pairing and stacking at the 5′-side of the adduct.

The interstrand cross-link (ICL) represents a small fraction (~5%) of the adducts formed by cisplatin on duplex DNA. Formation of a cisplatin ICL is usually easy at a GpC step[83] and is expected to cause significant distortion of B-form DNA due to the long (>7 Å) distance between the two bind sites of G-N7. The structures of two different duplexes containing the cisplatin interstrand cross-link have been determined by NMR and rMD.[77,78] In both models, the double-helix is bent and unwound but with significantly different angle values. Extensive unwinding caused by the ICL adduct produces a local left-handed helix geometry about the platinum atom resembling that of Z-DNA. In both cases, some of the forces which may be necessary for stabilizing unusual platinum-DNA structures have been observed: base stacking, unconventional hydrogen bonding, and electrostatic interactions. The X-ray crystal structure of a DNA duplex containing a cisplatin interstrand cross-link has been solved at 1.63 Å resolution.[84] The double-helix is bent by 47° and unwound by 70°. The crystals are stabilized by intermolecular contacts involving two cytosines extruded from the double-helix, one of which makes a triplet with a terminal G·C pair. The platinum residue is embedded into a cage of nine water molecules linked to the cross-linked guanines, to the two ammine groups, and to the phosphate backbone through other water molecules. The presence of the cage of water molecules around the lesion could interfere with the lability of the cross-link under physiological conditions,[85] and might be relevant for the mechanism of recognition of the ICL by proteins.

Structural analogues of *cis*-DDP do not show a greatly altered spectrum of clinical efficacy in comparison to the parent drug. [86] With respect to DNA binding, they are also very similar. The alteration of the DNA binding mode in comparison to *cis*-DDP could possibly give alternative antitumour activity. On the basis of this

hypothesis, a new class of dinuclear platinum complexes has been developed. These compounds are of special interest because they show high activity *in vitro* and *in vivo* against tumour cell lines which are resistant to *cis*-DDP.[87,88] The DNA-binding properties of dinuclear platinum complexes are affected by changing the diamine chain length and the coordination spheres.[89,90] Structures with dinuclear platinum compounds coordinated to dinucleotides have been reported,[91] and it has been shown that intrastrand chelation to neighbouring guanines is still possible. But with a self-complementary octanucleotide,[92] it was found that only a 1,2-interstrand adduct formed. The dinuclear platinum-amine unit lies in the minor groove of the dumbell DNA.

1.7 Recognition of Platinated DNA by Cellular Proteins.

The specific mechanisms that trigger apoptosis in response to cisplatin have not been defined. Such mechanisms logically must include ways to detect damage as well as to determine whether damage is sufficiently severe to be lethal. Much attention has recently focused on identification and characterisation of proteins that recognise cisplatin induced DNA damage.[93] At least two such types of proteins have now been identified: mismatch repair proteins and high mobility group (HMG) proteins.[36]

Mismatch repair is a post-replication repair system that corrects unpaired or mispaired nucleotides. Mismatch repair deficiency predisposes cells to genomic instability and also confers tolerance to damage induced by certain alkylating agents in some model systems.[94,95] In one of these model systems, loss of mismatch repair was accompanied by loss of p53 function, which could disrupt cell cycle and apoptosis regulation and contribute to further genomic instability.[96] One recent preliminary report shows that some cell lines with mismatch repair defects may also

be less proficient at nucleotide excision repair, which is the primary mechanism by which Pt-DNA adducts are repaired.[97]

Mismatch repair proteins recognise but do not remove cisplatin-DNA adducts. It is hypothesised that mismatch repair proteins attempt to insert the 'correct' base on the non-damaged strand opposite to the adduct. Establishment of such a 'futile' repair cycle might then generate a signal triggering apoptosis. According to this hypothesis, loss of mismatch repair proteins confers resistance through failure to recognise and initiate apoptosis in the response to DNA damage. Resistant cells thus acquire the ability to tolerate damage that would otherwise be lethal.

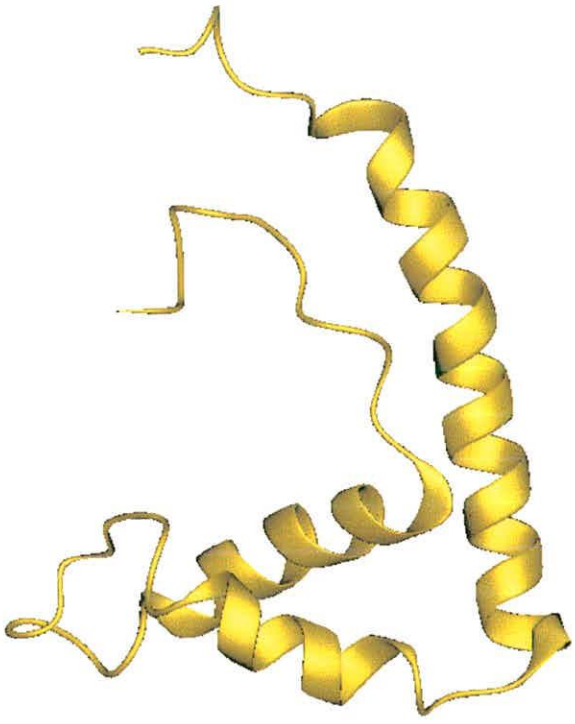

Figure 1.4 Structure of HMG1 domain B as determined by 2D NMR spectroscopy.[103,104]

The HMG domain is a DNA-binding motif composed of approximately 80 amino acids. It was first identified in the high mobility group protein 1 (HMG1), so named because of its rapid mobility on polyacrylamide electrophoresis gels. The HMG1 domain (box) is shared in most of the DNA-binding proteins. The HMG domain proteins are divided into two subfamilies based upon their ability to bind DNA in a structure-specific versus a sequence-specific manner. This includes the structure-specific HMG1 and HMG2 proteins and the sequence-specific HMG-domain proteins LEF-1 and hSRY. The HMG proteins are a multifunctional family of small non-histone chromatin-associated proteins, which recognise distorted DNA structure.[98-101] These chromosomal proteins found in higher eukaryotes are believed to play a role in transcription, cell differentiation, and assembly of chromatin structure.[102] HMG1 is a 25-kDa protein with two HMG domains (A and B) and an acidic tail. Both HMG1-A and B domains specifically recognise locally bent and unwound DNA, with similar binding affinities ($K_d \sim 10^{-9}$ M). The solution structures for the two HMG1 domains show similar secondary structures which consist of three α-helices arranged in a distorted L-shape providing a concave surface for DNA binding, as shown in Fig. 1.4.[103,104] Other HMG family proteins include human structure specific recognition protein (SSRP-1) and the ribosomal RNA (rRNA) transcription factor hUBF.

Lymphoid enhancer binding protein 1, LEF-1, contains one HMG domain. It contacts AT base pairs primarily in the minor groove; replacement of AT with IC base pairs, which are identical in the minor groove but differ in the major groove, has no effect on binding.[105] LEF-1 activates transcription both by bending DNA, a property of its HMG domain, and by interacting with other proteins.[106] Another HMG-domain protein is hSRY, the sex determining factor in humans. HSRY binds to four-way junctions as well as to AACAAAG and related sequences.[107,108] Much

like LEF-1, SRY binds to DNA in the minor groove, bends it, and activates transcription.

The HMG proteins bind to the most abundant DNA adducts of the anticancer drug cisplatin, especially the 1,2-d(GpG) and 1,2-d(ApG) intrastrand cross-links but not the 1,3-d(GpTpG) intrastrand cross-links or adducts made by *trans*-DDP or $[Pt(dien)Cl]^+$. The kinked, unwound, platinated DNA provides a basis for recognition and binding, but these processes are hindered if the formation of the platinum-induced DNA lesion is accompanied by a local denaturation or an increased flexibility of the duplex around the adduct.[109] It is interesting to note that the DNA interstrand cross-links induced by cisplatin are efficiently bound to HMG1 protein or cleaved by T4 endonuclease VII, but that the same type of lesion made by transplatin is not.[33,110,111] A recent study of HMG-1 binding to cisplatin GG adducts has shown that the DNA sequence around the platinated site is an important factor in determining the binding strength.[112] DNA having A/T flanking G*G* sequences is bound preferentially by both proteins. HMG-1A bound more tightly than HMG-1B to any of the platinated DNAs, with typically a 10- to 100-fold lower K_d values. SSRP1 binds specifically to cisplatin-DNA intrastrand adducts.[113] A recently reported study showed that hUBF binds cisplatin d(GpG) intrastrand adduct with extraordinarily high binding affinity (K_d ~ 60 pM), which is likely due to additive contributions from multiple HMG domains participating in the binding.[114]

Not only do HMG-domain proteins recognise and bind pre-bent DNA, but they can further bend and distort the helix on binding.[115] This study indicated that the role of the HMG1 may be one of structural distortion, bending DNA for nucleosome packaging, or for transcription mediation, facilitating binding of transcription factors to pre-bent DNA. The molecular basis for sequence-specific DNA recognition by the HMG domains of LEF-1 and SRY has been determined by NMR.[116-118] The unwound and bent DNA duplex conformation in both of these complexes resembles very

closely the structure of DNA containing a *cis*-DDP d(GpG) intrastrand adduct. The sequence-specific interaction between DNA and the HMG box of LEF-1 or SRY occurs exclusively in the minor groove.

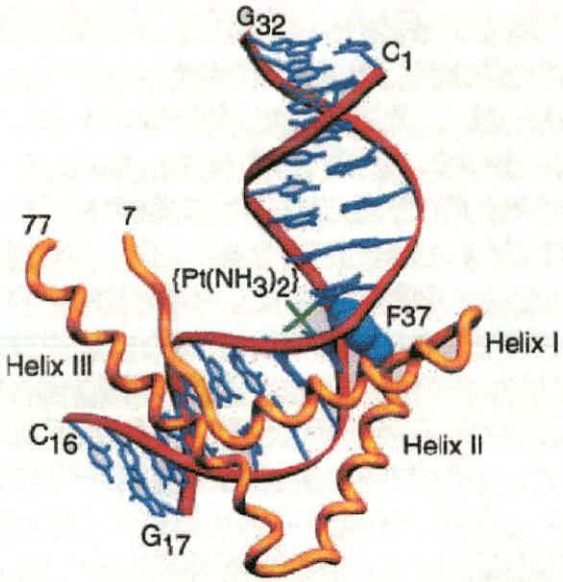

Figure 1.5 The X-ray structure of the complex between the non-sequence-specific domain A of HMG and cisplatin-modified DNA.[119] The protein backbone is shown in yellow, the intercalating Phe37 residue as van der Waals spheres, and the DNA in red and blue with the *cis*-[$Pt(NH_3)_2${d(GpG)-N7(G_8)-N7(G_9)}] intrastrand adduct in green. Numbers indicate the first (N terminus) and last (C terminus) ordered residues of the protein in the crystal structure.

An X-ray crystal structure of HMG1 domain A bound to a 16-base pair DNA fragment containing the major cisplatin-DNA 1,2-d(GpG) intrastrand cross-link was solved to 2.5 Å resolution recently.[119] The HMG-1A protein binds to the widened minor groove of DNA duplex with its concave surface. The DNA is strongly kinked at a hydrophobic notch created at the Pt-DNA crosslink and protein binding extends exclusively to the 3′ side of the platinated strand, covers five basepair steps. Residue

Phe37 is intercalated into this hydrophobic crevice and stacked onto the platinated G9 base at a distance of 3.5 Å. Binding of the domain is dramatically reduced in a mutant in which alanine is substituted for phenylalanine at this position. The binding site observed in this crystal structure differs from that in the structures of sequence-specific HMG domains, which bind to the bend locus near the centre of the protein-binding site.[117,118] A further examination of sequence alignments reveals nearly all chromatin-associated HMG-domain proteins (structure-specific) have a hydrophobic residue at position 37 that can serve as a bending wedge, while those sequence-specific HMG domains found in transcription factors have a polar residue at the same position which would allow sequence-specific hydrogen-bond formation.

There are several ways in which the binding of HMG proteins to cisplatin-DNA adducts might affect the biological activity of cisplatin.[120,121] One of the hypotheses is that the HMG-domain proteins may block the cisplatin-DNA adducts from recognition by the repair apparatus, thereby enhancing the cytotoxic properties of the drug. The blocking of excision-repair of cisplatin-DNA adducts has been observed both in human cell extracts and in yeast cells. By repairing the damage on DNA caused by cisplatin binding, the cell might increase the probability of its survival. The second possibility is that the HMG-domain proteins may themselves be part of the excision repair apparatus of the cell, by recognising the damage created by the cisplatin adducts. The third possibility is that the cisplatin titrates or "hijacks" the protein away from its natural binding sites. Assuming that the hijacked protein is in some manner vital to the tumour cell, its diversion could sensitise the cells to cisplatin.[122]

One critical regulator of apoptosis is the tumour suppressor protein p53.[123] It plays a central role in the regulation of cellular growth and is a potent transcription factor activated in response to a variety of DNA damaging agents including irradiation or anticancer drugs, leading to cell cycle arrest at the G1/S phase

checkpoint or to induction of apoptosis.[124] Disruption of this pathway occurs in a wide variety of human cancers and correlates with the development of the tumorogenic mutants that are defective in DNA binding and consequently cannot activate transcription. Sequence-specific DNA binding and transactivation are the key activities that control the biological function of p53. One crystallographic structure of a p53 DNA binding domain binding to target DNA has been reported.[125] Wild-type p53 binds to DNA as a tetramer on the outside of the DNA loop, and causes DNA bending and twisting.[126] Recent experiments provide evidence that inactivation of the p53 DNA binding domain GSEs (genetic suppressor elements) can confer resistance to cisplatin.[127]

There are about 200 to 300 human genes transcriptionally activated by p53. The effects of p53 are complex and difficult to study in isolation. Much more work needs to be done in order to clarify the precise role of p53 as a determinant of cisplatin sensitivity.

1.8 References

[1] J. Reedijk, *Inorg. Chim. Acta*, **1992**, *198-200*, 873.

[2] C. F. J. Barnard, *Plat. Met. Rev.*, **1989**, *33*, 162.

[3] E. L. M. Lempers, J. Reedijk, *Adv. Inorg. Chem.* **1991**, *37*, 175.

[4] W. I. Sundquist, S. J. Lippard, *Coord. Chem. Rev.* **1990**, *100*, 293.

[5] M. J. Bloemink and J. Reedijk, *Metal ions Biol. Sys.*, **1996**, *32*, 641.

[6] C. F. J. Barnard, *Plat. Met. Rev.* **1989**, *33*, 162.

[7] W. J. F. Van der Vijgh, *Clin. Pharmacokin.* **1991**, *21*, 242.

[8] D. P. Gately, S. B. Howell, *Brit. J. Cancer* **1993**, *67*, 1171.

[9] C. M. Giandomenico, M. J. Abrams, B. A. Murrer, J. F. Vollano, M. I. Rheinheimer, S. B. Wyer, G. E. Bossard, J. D. Higgins III, *Inorg. Chem.* **1995**, *34*, 1015.

[10] O. Novakova, O. Vrana, V. Kiseleva and V. Brabec, *Eur. J. Biochem.* **1995**, *228*, 616.

[11] T. Matsumoto, K. Endoch, K. Akamatsu, K. Kamisango, H. Mitsui, K. Koizumi, K. Morikawa, M. Koizumi, T. Matsuno, *Br. J. Cancer* **1991**, *64*, 41.

[12] E. Cvitkovic, *Br. J. Cancer* **1998**, *77* (S4), 8.

[13] H. Bleiberg, *Br. J. Cancer* **1998**, *77* (S4), 1.

[14] F. I. Raynaud, F. E. Boxall, P. M. Goddard, M. Valenti, M. Jones, B. A. Murrer, M. Abrams, L. R. Kelland, *Clin. Cancer Res.* **1997**, *3*, 2063.

[15] J. Holford, S. Y. Sharp, B. A. Murrer, M. Abrams, L. R. Kelland, *Br. J. Cancer* **1998**, *77*, 366.

[16] Y. Chen, Z. Guo, S. J. Parsons, P. J. Sadler, *Chem. Eur. J.* **1998**, *4*, 672.

[17] Y. Chen, Z. Guo, J. A. Parkinson, P. J. Sadler, *J. Chem. Soc. Dalton Trans.* **1998**, 3577.

[18] Y. Chen, J. A. Parkinson, Z. Guo, P. J. Sadler, *Angew. Chem. Int. Ed. Engl.* **1999**, *38*, 2060.

[19] J. Reedijk, *Chem. Comm.* **1996**, 801.

[20] N. Farrell, *Comments Inorg. Chem.* **1995**, *16*, 373.

[21] A. J. Kraker, J. D. Hoeschele, W. L. Elliott, H. D. H. Showalter, A. D. Sercel, N. P. Farrell, *J. Med. Chem.* **1992**, *35*, 4526.

[22] M. Coluccia, A. Nassi, F. Loseto, A. Boccarelli, M. A. Mariggio, D. Giordano, F. P. Intini, P. Caputo, G. Natile, *J. Med. Chem.* **1993**, *36*, 510.

[23] T. W. Hambley, *Coord. Chem. Rev.* **1997**, *166*, 181.

[24] D. P. Gately, S. B. Howell, *Br. J. Cancer*, **1993**, *67*, 1171.

[25] N. P. Johnson, J. D. Hoeschele, R. O. Rahn, *Chem. Biol. Interactions*, **1980**, *30*, 151.

[26] S. S. G. E. van Boom, J. Reedijk, *J. Chem. Soc. Chem. Commun.* **1993**, 1397.

[27] K. J. Barnham, M. I. Djuran, P. del S. Murdoch, P. J. Sadler, *J. Chem. Soc. Chem. Commun.* **1994**, 721.

[28] A. Pullman, C. Zakrzewska, D. Perahia, *Int. J. Quantum Chem.* **1979**, *16*, 395; A. Pullman, B. Pullman, *Q. Rev. Biophys.* **1981**, *14*, 289.

[29] I. Saito, M. Takayama, H. Sugiyama, K. Nakatani, A. Tsuchida, M. Yamamoto, *J. Am. Chem. Soc.* **1995**, *117*, 6406.

[30] A. M. J. Fichtinger-Schepman, J. L. van der Veer, J. H. J. den Hartog, P. H. M. Lohman, J. Reedijk, *Biochemistry* **1985**, *24*, 707.

[31] A. Eastman, M. M. Jennerwein, D. L. Nagel, *Chem.-Biol. Interact.* **1988**, *67*, 71.

[32] K. J. Yarema, S. J. Lippard and J. M. Essigmann, *Nucleic Acids Res.* **1995**, *23*, 4066.

[33] Z. Guo, P. J. Sadler, *Adv. Inorg. Chem.* **1999**, in press.

[34] D. E. Evans, C. Dive, *Cancer. Res.* **1993**, *53*, 2133.

[35] A. Eastman, *Cancer Cells* **1990**, *2*, 275.

[36] R. P. Perez, *Eur. J. Cancer* **1998**, *34*, 1535.

[37] C. M. Riley, L. A. Sternson, A. J. Repta, S. A. Slyter, *Anal. Biochem.* **1983**, *130*, 203.

[38] R. E. Norman, J. D. Ranford, P. J. Sadler, *Inorg. Chem.* **1992**, *31*, 877.

[39] P. del S. Murdoch, J. D. Ranford, P. J. Sadler, S. J. Berners-Price, *Inorg. Chem.* **1993**, *32*, 2249.

[40] I. Toshihisa, A.-O. Francis, *J. Biol. Chem.* **1993**, *268*, 20116.

[41] S. J. Berners-Price, P. W. Kuchel, *J. Inorg. Biochem.* **1990**, *38*, 305.

[42] T. G. Appleton, J. W. Connor, J. R. Hall, P. D. Prenzler, *Inorg. Chem.* **1989**, *28*, 2030.

[43]T. G. Appleton, J. R. Hall, S. F. Ralph, *Aust. J. Chem.* **1986**, *39*, 1347.

[44] N. Hadjiliadis, N. Ferderigos, J. Butour, H. Marzarguil, G. Gasmi, J. Laussac, *Inorg. Chem.* **1994**, *33*, 5057.

[45] E. L. M. Lempers, J. Reedijk, *Inorg. Chem.* **1990**, *29*, 217.

[46] T. G. Appleton, J. W. Connor, J. R. Hall, *Inorg. Chem.* **1988**, *27*, 130.

[47] C. D. W. Fröhling, W. S. Sheldrick, *Chem. Commun.*, **1997**, 1737.

[48] K. J. Barnham, M. I. Djuran, P. del S. Murdoch, P. J. Sadler, *J. Chem. Soc. Chem. Commun.* **1994**, 721.

[49] S. S. G. E. van Boom, B. W. Chen, J. M. Teuben, J. Reedijk, *Inorg. Chem.* **1999**, *38*, 1450.

[50] M. I. Djuran, E. L. M. Lempers, J. Reedijk, *Inorg. Chem.* **1991**, *30*, 2648.

[51] S. S. G. E. van Boom, J. Reedijk, *J. Chem. Soc., Chem. Commun.* **1993**, 1397.

[52] K. J. Barnham, M. I. Djuran, P. del. S. Murdoch, J. D. Ranford, P. J. Sadler, *J. Chem. Soc. Dalton Trans.* **1995**, 3721.

[53] K. J. Barnham, Z. Guo, P. J. Sadler, *J. Chem. Soc. Dalton Trans.* **1996**, 2867.

[54] U. Frey, J. D. Ranford, P. J. Sadler, *Inorg. Chem.* **1993**, *32*, 1333.

[55] K. J. Barnham, M. J. Djuran, P. del S. Murdoch, J. D. Ranford, P. J. Sadler *Inorg. Chem.* **1996**, *35*, 1065.

[56] K. J. Barnham, U. Frey, P. del S. Murdoch, J. D. Ranford, P. J. Sadler, *J. Am. Chem. Soc.* **1994**, *116*, 11175.

[57] C. J. van Garderen, H. van den Elst, J. H. van Boom, J. Reedijk, *J. Am. Chem. Soc.* **1989**, *111*, 4123-4125.

[58] V. Brabec, J. Reedijk, M. Leng, *Biochemistry* **1992**, *31*, 12397.

[59] F. Gonnet, J. Kozelka, J. C. Chottard, *Angew. Chem. Int. Ed.* **1992**, *31*, 1483.

[60] F. Reeder, F. Gonnet, J. Kozelka, J. C. Chottard, *J. Inorg. Biochem.* **1995**, *59*, 155; *Chem. Eur. J.* **1996**, *2*, 1068.

[61] S. J. Berners-Price, U. Frey, J. D. Ranford, P. J. Sadler, *J. Am. Chem. Soc.* **1993**, *115*, 8649.

[62] S. J. Berners-Price, K. J. Barnham, U. Frey and P. J. Sadler, *Chem. Eur. J.* **1996**, *2*, 187.

[63] F. Reeder, Z. Guo, P. del S. Murdoch, A. Corazza, T. W. Hambley, S. J. Berners-Price, J.-C. Chottard, P. J. Sadler, *Eur. J. Biochem.* **1997**, *249*, 370.

[64] F. Reeder, J. Kozelka, and J. C. Chottard, *Inorg. Chem.* **1996**, *35*, 1413.

[65] M. S. Davies, S. J. Berners-Price, T. W. Hambley, *J. Am. Chem. Soc.* **1998**, *120*, 11380.

[66] F. Legendre, Jirí Kozelka, J. -C. Chottard, *Inorg. Chem.* **1998**, *37*, 3964.

[67] S. E. Sherman, D. Gibson, A. H. -J. Wang, S. J. Lippard, *Science* **1985**, *230*, 412.

[68] S. E. Sherman, D. Gibson, A. H. -J. Wang, S. J. Lippard, *J. Am. Chem. Soc.* **1988**, *110*, 7368.

[69] G. Admiraal, J. L. van der Veer, R. A. G. de Graaf, J. H. J. den Hartog, J. Reedijk, *J. Am. Chem. Soc.* **1987**, *109*, 592.

[70] J. H. J. den Hartog, C. Altona, J. H. van Boom, G. A. van der Marel, C. A. G. Haasnoot and J. Reedijk, *J. Biomol. Struct. Dyn.* **1985**, *2*, 1137.

[71] P. M. Takahara, A. C. Rosenzweig, C. A. Frederick, S. J. Lippard, *Nature* **1995**, *377*, 649.

[72] P. M. Takahara, C. A. Frederick, S. J. Lippard, *J. Am. Chem. Soc.* **1996**, *118*, 12309.

[73] D. Yang, S. S. G. E. van Boom, J. Reedijk, J. H. van Boom, A. H. -J. Wang, *Biochemistry* **1995**, *34*, 12912.

[74] A. Gelasco, S. J. Lippard, *Biochemistry* **1998**, *37*, 9230.

[75] S. U. Dunham, S. U. Dunham, C. J. Turner, S. J. Lippard, *J. Am. Chem. Soc.* **1998**, *120*, 5395.

[76] S. S. G. E. van Boom, D. Yang, J. Reedijk, G. A. van der Marel, A. H. -J. Wang, *Biochemistry* **1996**, *13*, 989.

[77] H. Huang, L. Zhu, B. R. Reid, G. P. Drobny, P. B. Hopkins, *Science* **1995**, *270*, 1842.

[78] F. Paquet, C. Perez, M. Leng, G. Lancelot, J. -M. Malinge, *J. Biomol. Struct. Dyn.* **1996**, *14*, 67.

[79] M. -H. Fouchet, E. Guittet, J. A. H. Cognet, J. Kozelka, C. Gauthier, M. Le Bret, K. Zimmermann, J. -C. Chottard, *J. Biol. Inorg. Chem.* **1997**, *2*, 83.

[80] E. Reed, R. F. Ozols, R. Tarone, S. T. Yuspa, M. C. Poirier, *Proc. Natl. Acad. Sci. USA*, **1987**, *84*, 5024.

[81] S. F. Bellon, J. H. Coleman, S. J. Lippard, *Biochemistry* **1991**, *30*, 8026.

[82] C. J. van Garderen, L. P. A. van Houte, *Eur. J. Biochem.* **1994**, *225*, 1169.

[83] M. A. Lemaire, A. Schwartz, A. R. Rahmouni, M. Leng, *Proc. Natl. Acad. Sci. USA*, **1991**, *88*, 1982.

[84] F. Coste, J. -M. Malinge, L. Serre, W. Shepard, M. Roth, M. Leng, C. Zelwer, *Nucleic Acid Res.* **1999**, *27*, 1837.

[85] C. Pérez, M. Leng, J. M. Malinge, *Nucleic Acid Res.* **1997**, *25*, 896.

[86] M. C. Christian, *Semin. Oncol.* **1992**, *19*, 720.

[87] N. Farrell, Y. Qu, M. P. Hacker, *J. Med. Chem.* **1990**, *33*, 2179.

[88] N. Farrell, *Cancer Invest.* **1993**, *11*, 578.

[89] N. Farrell, Y. Qu, L. Feng, B. van Houten, *Biochemistry* **1990**, *29*, 9522.

[90] J. D. Roberts, B. van Houten, Y. Qu, N. Farrell, *Nucleic Acids Res.* **1989**, *17*, 9719.

[91] M. J. Bloemink, J. Reedijk, N. Farrell, Y. Qu and A. I. Stetsenko, *J. Chem. Soc., Chem. Commun.* **1992**, 1002.

[92] D. Yang, S. S. G. E. van Boon, J. Reedijk, J. H. van Boom, N. Farrell and A. H. J. Wang, *Nature Struct. Biol.* **1995**, *2*, 577.

[93] G. Chu, *J. Biol. Chem.* **1994**, *269*, 787.

[94] P. Karran, M. Bignami, *BioEssays*, **1994**, *16*, 833.

[95] R. Fishel, R. D. Kolodner, *Curr. Opin. Genet. Dev.* **1995**, *5*, 382.

[96] D. A. Anthoney, A. J. McIlwrath, W. M. Gallagher, A. R. M. Edlin, R. Brown, *Cancer Res.* **1996**, *56*, 1374.

[97] K. V. Ferry, D. Fink, S. W. Johnson, T. C. Hamilton, S. B. Howell, *Proc. Am. Assoc. Cancer Res.* **1997**, *38* (abstract), 359.

[98] P. M. Pil and S. J. Lippard, *Science* **1992**, *256*, 234.

[99] R. Visse, A. J. van Gool, G. F. Moolenaar, M. de Ruiter, and P. van de Putte, *Biochemistry* **1994**, *33*, 1804.

[100] M. M. Mca'nulty and S. J. Lippard, *Nucleic Acids and Molecular Biology* **1995**, Vol.9, 264.

[101] V. Wunderlich, M. Bottger, *J. Cancer Res. Clin. Oncol.* **1997**, *123*, 133.

[102] R. Grosschedl, K. Giese, J. Pagel, *Trends Genet.* **1994**, *10*, 94.

[103] C. H. Hardman, R. W. Broadhurst, A. R. C. Raine, K. D. Grasser, J. O. Thomas, E. D. Laue, *Biochemistry* **1995**, *34*, 16596.

[104] H. M. Weir, P. J. Kraulis, C. S. Hill, A. R. C. Raine, E. D. Laue, J. O. Thomas, *EMBO. J.* **1993**, *12*, 1311.

[105] K. Giese, J. Cox, R. Grosschedl, *Cell* **1992**, *69*, 185.

[106] K. Giese, R. Grosschedl, *EMBO J.* **1993**, *12*, 4667.

[107] S. Ferrari, V. R. Harley, A. Pontiggia, P. N. Goodfellow, R. Lovell-Badge, M. E. Bianchi, *EMBO J.* **1992**, *11*, 4497.

[108] K. Giese, J. Pagel, R. Grosschedl, *Proc. Natl. Acad, Sci. USA*, **1994**, *91*, 3368-3372.

[109] J. Kasparkova, V. Brabec, *Biochemistry* **1995**, *34*, 12379.

[110] M. A. Lemaire, A. Schwartz, A.R. Rahmouni, M. Leng, *Proc. Natl. Acad. Sci. USA*, **1991**, *88*, 1982.

[111] V. Brabec, M. Sip, M. Leng, *Biochemistry* **1993**, *32*, 11676.

[112] S. U. Dunham, S. J. Lippard, *Biochemistry* **1997**, *36*, 11428.

[113] D. J. Slamon, W. Godolphin, L. A. Jones, *Science*, **1989**, *244*, 707.

[114] X. Zhai, H. Beckmann, H.-M. Jantzen, J. M. Essigmann, *Biochemistry*, **1998**, *37*, 16307.

[115] P. M. Pil, C. S. Chow, S. J. Lippard, *Proc. Natl. Acad. Sci. USA*, **1993**, *90*, 9465.

[116] M. H. Werner, M. E. Bianchi, A. M. Gronenborn, G. M. Clore, *Biochemistry* **1995**, *34*, 11998.

[117] M. H. Werner, J. R. Huth, A. M. Gronenborn, G. M. Clore, *Cell* **1995**, *81*, 705.

[118] J. J. Love, X. Li, D. A. Case, K. Giese, R. Grosschedl, P. E. Wright, *Nature* **1995**, *376*, 791.

[119] U. -M. Ohndorf, M. A. Rould, Q. He, C. O. Pabo, S. J. Lippard, *Nature* **1999**, *399*, 708.

[120] B. A. Donahue, M. Augot, S. F. Bellon, D. K. Treiber, J. F. Toney, S. J. Lippard, J. M. Essigmann, *Biochemistry* **1990**, *29*, 5872.

[121] E. R. Jamieson, S. J. Lippard, *Chem. Rev.* **1999**, *99*, 2467.

[122] M. M. McA'Nulty, S. J. Lippard, in *Nucleic Acids and Molecular Biology*, ed. by F. Eckstein and D. M. J. Lilley, Springer-Verlag, Berlin, **1995**, *9*, 264.

[123] W. El-Diery, T. Tokino, V. E. Velculescu, *Cell* **1993**, *75*, 817.

[124] A. J. Levine, *Cell*, **1997**, *88*, 323.

[125] Y. J. Cho, S. Gorina, P. D. Jeffrey, N. P. Pavletich, *Science*, **1994**, *265*, 346.

[126] A. K. Nagaich, V. B. Zhurkin, S. R. Durell, R. L. Jernigan, E. Appella, R. E. Harrington, *Proc. Natl. Acad. Sci. USA*, **1999**, *96*, 1875.

[127] W. M. Gallagher, M. Cairney, B. Schott, I. B. Roninson, R. Brown, *Oncogene* **1997**, *14*, 185.

Chapter 2

Theory of Experimental Methods

2.1 NMR Spectroscopy

2.1.1 ^{195}Pt and ^{15}N NMR Spectroscopy

A) ^{195}Pt NMR[1,2,3] ^{195}Pt is a reasonably sensitive nucleus for NMR detection, with natural abundance of 33.8%, nuclear spin quantum number I = ½, and a receptivity relative to ^{1}H of 3.4×10^{-3}. The limit of detection (*ca.* 10 mM) precludes detection of natural abundance ^{195}Pt signals in physiological fluids. The receptivity can be improved by a factor of three by isotopic enrichment of ^{195}Pt (> 95%). The spin-lattice relaxation time (T_1) for ^{195}Pt is usually in the range of 0.3 to 1.3 s.

The ^{195}Pt chemical shift range is very large, about 15,000 ppm (usually in the range from -600 to 9000 ppm relative to $[PtCl_6]^{2-}$), and often allows easy differentiation between Pt(II) and Pt(IV), which tend to have chemical shifts at the high-field and low-field ends of the range, respectively. The ^{195}Pt chemical shift in monomeric complexes is sensitive primarily to the set of bound donor atoms, see Table 2.1. Some caution is required in searching for peaks, because the shifts of Pt(IV) halides alone span 12000 ppm. Also, usually there are ^{195}Pt chemical shift differences between geometrical isomers and between diastereomers (chiral ligands). For ^{15}N-enriched ligands, the splitting pattern in the ^{195}Pt spectrum indicates the number of non-equivalent ^{15}N atoms coordinated. These characteristics of the ^{195}Pt chemical shift can be utilized in the detection of different intermediates formed during the reactions of platinum complexes with biomolecules. Sometimes even isotopomers are distinguishable: the ^{195}Pt isotope shift difference for ^{195}Pt-$^{35/37}$Cl is 0.17 ppm and for ^{195}Pt-$^{79/81}$Br is 0.03 ppm.[4] Therefore in principle it is possible to count the number of Cl and Br ligands bonded to Pt *via* the isotope splitting pattern. In practice it is difficult to resolve because of line broadening, which is usually due to either relaxation mechanisms or poor temperature control of the sample. The latter is a problem because of strong temperature dependence of ^{195}Pt NMR resonances (0.5 to 1.1 ppm K^{-1}).

Table 2.1 ^{195}Pt NMR chemical shifts of *cis*-Pt adducts with different donor atoms.

Cis-Pt Complexes	$\delta(^{195}Pt)$ range (ppm) [a]	Ref.
cis-$[PtCl_2(NH_3)_2]$	-2149	5
cis-$[Pt(NH_3)_2(O)_2]$	-1460 to -1598	6, 7
cis-$[PtCl(NH_3)_2(O)]$	-1806 to -1841	6
cis-$[Pt(NH_3)_2(N)(O)]$	-2067 to -2147	7
cis-$[PtCl(NH_3)_2(N)]$	-2297 to -2369	5, 8, 9
cis-$[Pt(NH_3)_2(N)_2]$	-2434 to -2660	5, 6, 7
cis-$[Pt(NH_3)_2(S)(O)]$	-2618 to -2800	10, 11
cis-$[Pt(NH_3)_2(S)(N)]$	-2800 to -3218	10, 11
cis-$[Pt(NH_3)_2(S)_2]$	-3200 to -3685	10, 11

[a] Relative to Na_2PtCl_6.

The quadrupolar effects of natural abundance ^{14}N (i.e. 99.6% ^{14}N, $I = 1$) from ammines which coordinate to Pt can broaden the ^{195}Pt resonances. Such quadrupolar effects of ^{14}N have the beneficial effects of shortening the ^{195}Pt relaxation times and allowing rapid pulsing without saturation effects. ^{195}Pt-^{14}N couplings in ^{195}Pt NMR spectra are usually better resolved at higher temperature, because of the decreased quadrupolar relaxation rate of ^{14}N due to the decrease in correlation time. Even in the absence of ^{14}N ligands, ^{195}Pt resonances can still be very broad owing to chemical shift anisotropy (CSA) relaxation, which can be the dominant relaxation mechanism for platinum complexes at high magnetic field strength. Similarly, ^{195}Pt satellites in ^{15}N and ^{1}H spectra of Pt(II) complexes are often broadened beyond detection owing to CSA relaxation of ^{195}Pt.[12] The linewidths of ^{195}Pt satellites of ^{1}H NMR resonances are dependent on the spin-lattice relaxation time of ^{195}Pt:

$$\Delta\nu_{1/2}(H) = [\pi T_2^*(H)]^{-1} + [2\pi T_1(Pt)]^{-1}$$

where $[\pi T_2^*(H)]^{-1}$ is the natural linewidth plus the contribution from magnetic inhomogeneity broadening (measurable from the linewidth of the centre peak). The contribution to ^{195}Pt T_1 relaxation from CSA is given by:

$$[T_1(Pt)]^{-1}(CSA) = (6/7)\times[T_2(Pt)]^{-1}(CSA) = (2/15)\times\gamma_{Pt}^2\times B_0^2\times\Delta\sigma^2\times\tau_c$$

In general, ^{195}Pt satellites (and ^{195}Pt resonances) are sharper in Pt(IV) complexes which are six coordinate and hence more symmetrical (smaller anisotropy $\Delta\sigma$) and are broader at higher fields of measurement (B_0) and in larger molecules (longer correlation time τ_c).

B) ^{15}N NMR

^{14}N NMR spectroscopy can be useful for ammine and amine complexes, but ^{14}N is a quadrupolar nucleus, and quadrupolar relaxation is dominant when the environment of ^{14}N has a low symmetry. This can lead to very broad lines and a consequent reduction in sensitivity. On the other hand, short relaxation times also have the advantage of allowing rapid pulsing so that a large number of transients can be acquired. Thus it is possible to follow reactions of cisplatin in blood plasma and cell culture media at millimolar drug concentrations and to detect ammine release.[13]

By using ^{15}N-substituted ammine complexes, the broadening of ^{195}Pt signals caused by the quadrupolar effects of ^{14}N can be avoided. Both ^{15}N NMR chemical shifts and $^1J(^{195}Pt\text{-}^{15}N)$ coupling constants are sensitive to the nature of the *trans* ligand in Pt ammine and amine complexes, which can provide useful information for identifying the ligands in the coordination spheres of both Pt(II) and Pt(IV) complexes. Typical ^{15}N and ^{1}H shift ranges for Pt^{II}-NH, Pt^{II}-NH_2 and Pt^{II}-NH_3 and $^1J(^{195}Pt\text{-}^{15}N)$ values are shown in Figure 2.1 and Figure 2.2, respectively. In general, ligands with high *trans* influences give rise to smaller ^{195}Pt-^{15}N coupling constants (S < I < Br < Cl < H_2O) and cause a low-field shift of the ^{15}N resonance. The dominant

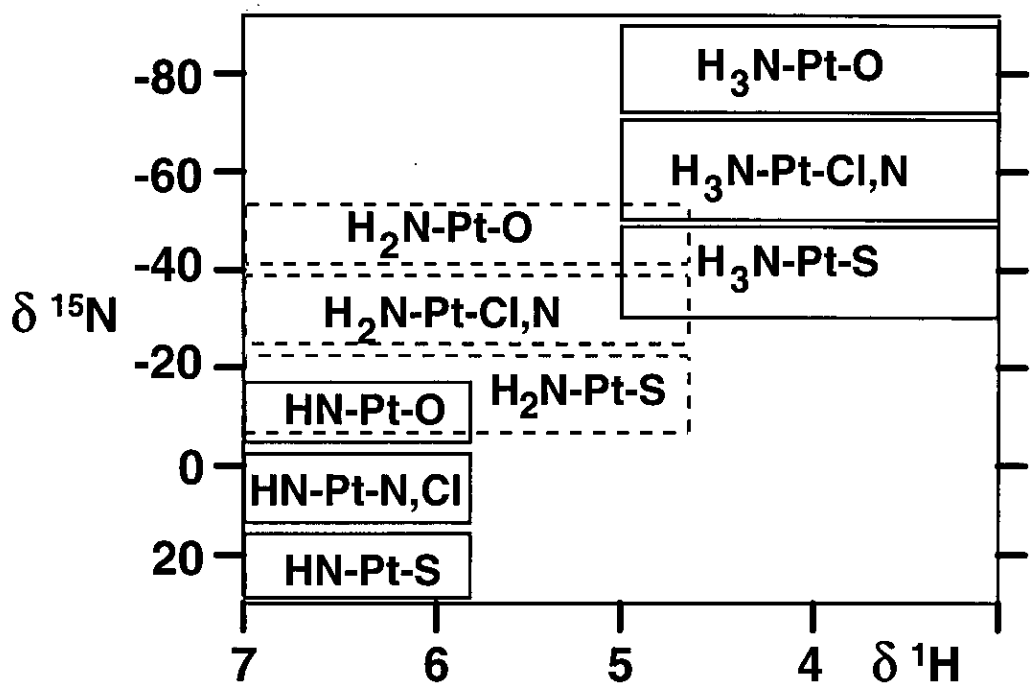

Figure 2.1 Variation of ^{1}H and ^{15}N NMR chemical shifts with the *trans* ligand in Pt^{II}-NH, Pt^{II}-NH_2 and Pt^{II}-NH_3 complexes.[14-20] The ^{15}N chemical shifts of NH_2-Pt and NH-Pt are mainly based on ring-closed $\{Pt(en)\}^{2+}$ and $\{Pt(dien)\}^{2+}$ complexes.

contribution to one-bond coupling constants between ^{195}Pt and ^{15}N is usually interpreted in terms of the Fermi contact interaction involving Pt 6s and N 2s orbitals.[21] The usefulness of $^{1}J(^{195}Pt\text{-}^{15}N)$ values is limited by the difficulty in determining them for larger molecules especially at high observation frequencies on account of the dominance of relaxation *via* chemical shift anisotropy. The $^{1}J(^{195}Pt\text{-}^{15}N)$ values for Pt(IV) are smaller by a factor of about 1.5 (in theory based on the change in hybridization from dsp^2 to d^2sp^3) to 1.2 (in practice) and are 1.4 ($\gamma^{15}N/\gamma^{14}N$) larger than $^{1}J(^{195}Pt\text{-}^{14}N)$ values.

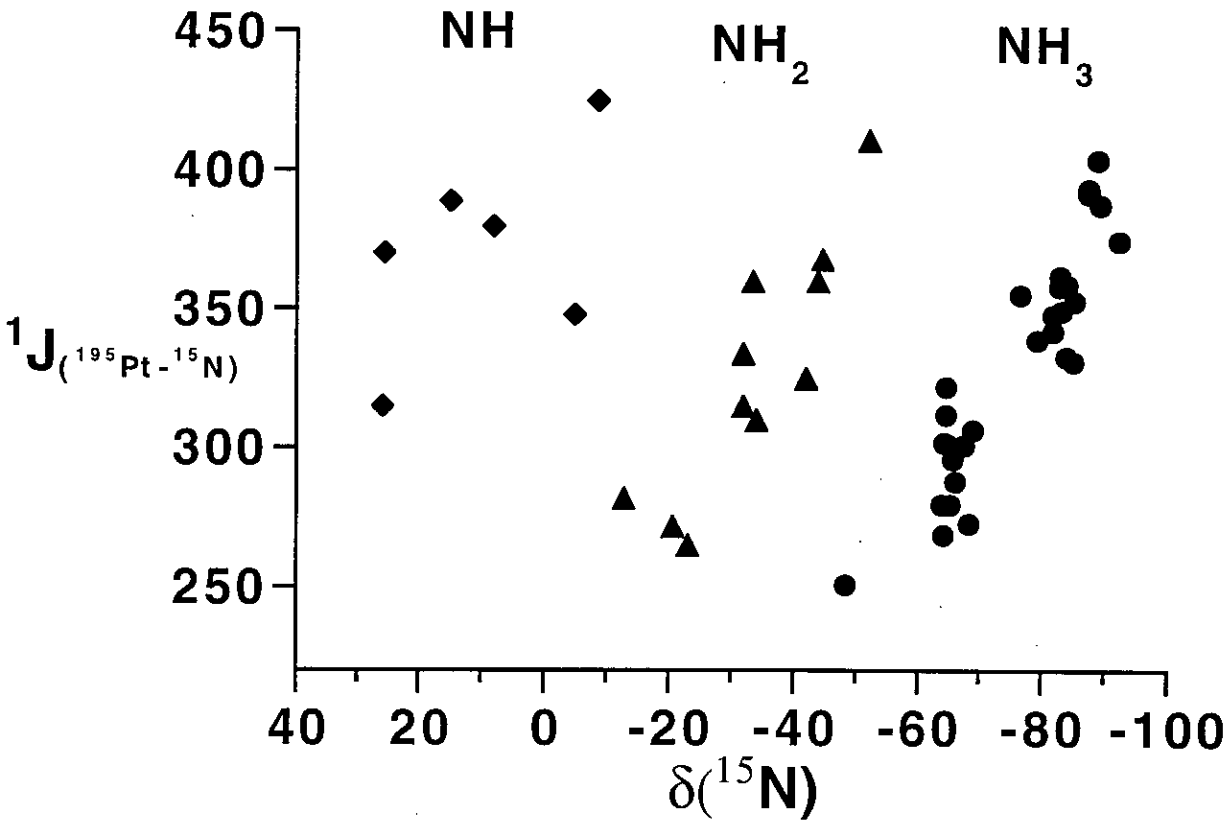

Figure 2.2 Plot of $^{1}J(^{195}Pt\text{-}^{15}N)$ *versus* $\delta(^{15}N)$ for Pt-NH_3, Pt-NH_2 and Pt-NH, showing a similar dependence on the *trans* ligand. Data are taken from literature.[22,59-62]

The low receptivity of ^{15}N (3.85×10^{-6} relative to ^{1}H) limits to some extent its usefulness for directly-detected ^{15}N NMR studies of Pt ammine and amine complexes. However, the sensitivity of detection can be improved by ^{15}N isotopic enrichment combined with enhancement by polarization transfer from ^{1}H (*e.g.* ^{15}N-{^{1}H} DEPT and INEPT pulse sequences). The maximum enhancement in ^{15}N signal intensity achievable *via* polarization transfer is only 9.8 ($\gamma H/\gamma N$), which means that

inverse (^{1}H-detected) ^{15}N methods are usually preferred due to the superior enhancement for ^{15}N-detection (*vide infra*). The repetition time of the pulse sequence is governed by the ^{1}H rather than the longer ^{15}N spin-lattice relaxation time (T_1), which is an additional advantage because it allows more rapid pulsing. For example, ^{15}N-{^{1}H} DEPT sequences enable detection of rapidly-changing intermediates in the reaction of ^{15}N-cisplatin with glutathione,[23] and also ammine release following reaction of ^{15}N-cisplatin with intracellular components in intact red blood cells at concentrations as low as 1 mM.[23] Direct ^{15}N-{^{1}H} DEPT/INEPT methods can be of value in situations where ^{1}H NMR resonances are very broad.

C) Inverse Detection Methods

The sensitivity of ^{15}N can be greatly improved by the use of inverse detection methods (^{1}H-detected ^{15}N) , by a theoretical maximum of 306 $\{(|\gamma H|/|\gamma N|)^{5/2}\}$ with respect to directly detected ^{15}N, such that signals can be detected in aqueous solutions at concentrations of physiological relevance (5 μM), Figure 2.3. ^{1}H-detected inverse methods are applicable to any system which contains a ^{15}N atom with a measurable spin-spin coupling to ^{1}H (i.e. $^1J(^{15}N, ^1H)$ in ammine, primary and secondary amines, but not tertiary amines although a longer range coupling can sometimes be utilised). In practice the best applications are for those systems with large one-bond couplings (e.g. *ca.* 73 Hz for $^{15}NH_3$). Besides the high sensitivity, inverse detection also brings a simplification of complicated spectra because it detects only those protons directly attached to the labelled ^{15}N atoms in the sample. This is very important for investigations of ^{1}H NMR spectra of body fluids or cell culture media which consist of thousands of overlapping resonances.

Although ^{1}H NMR resonances can be detected from NH protons with ^{14}N present in natural abundance (99.6%), they are often broad because of the

quadrupolar relaxation of ^{14}N ($I = 1$). It is also necessary to work in H_2O (as opposed to D_2O), since NH protons in platinum ammine and amine complexes usually

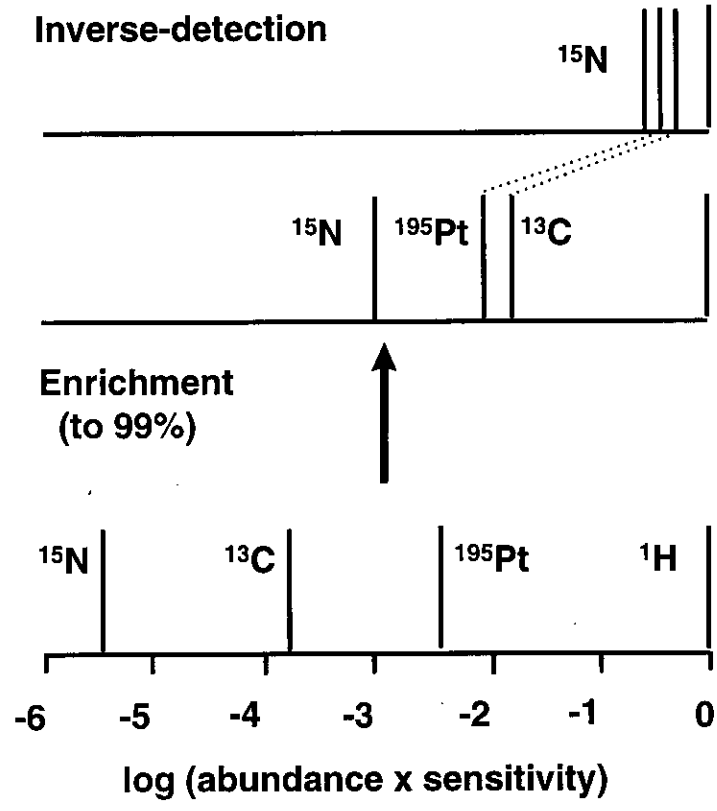

Figure 2.3 The theoretical increase in receptivity (abundance × sensitivity) obtainable by isotope enrichment and inverse ^1H detection of ^{13}C, ^{15}N and ^{195}Pt. In practice inverse ^1H-{^{195}Pt} detection is limited by the broad linewidths of the ^{195}Pt satellites.

exchange with deuterium within minutes. The exchange of NH protons with solvent is much faster for Pt(IV) than for Pt(II) complexes at neutral pH, since, for example, NH_3 ligands on Pt(IV) have lower pK_a values. Introduction of ^{15}N by synthetic labelling usually gives rise to a sharp ^1H NMR doublet for a Pt-^{15}NH group in H_2O together with (CSA-broadened) ^{195}Pt satellites. The resonances move progressively to lower field on changing from Pt-NH_3 to Pt-NH_2 and to Pt-NH, see Figure 2.1. Both

^{15}N and ^{1}H NMR resonances for Pt(IV)-^{15}NH are to lower field than those for Pt(II). Pt(IV) anticancer complexes can be studied by the ^{1}H-{^{15}N} NMR if NH exchange is slowed down by lowering the pH or by other means.

2.1.2 Heteronuclear Multiple (single)-quantum Correlation

In biological NMR, the heteronuclear experiments of interest are those which identify the chemical shifts of protons and X-nuclei that are directly coupled. One obvious use of this correction information is to allow assignments already made for one nuclear species to be transferred to the other. A more important but less obvious use is in overcoming problems caused by overlap in the proton spectrum: in the heteronuclear 2D spectrum the proton resonances are spread out according to the shifts of the heteronuclei to which they are coupled.

The heteronuclear multiple-quantum (and single quantum) coherence (HMQC and HSQC) technique belongs to the family of indirect (or inverse) detection techniques. An important feature of the experiment is that the proton magnetisation which is detected during t_2 originated as proton magnetisation at the start of the sequence. The main advantage of this technique is the enhanced sensitivity, a theoretical maximum of $[|\gamma_H|/|\gamma_X|]^{5/2}$ (306 for ^{15}N) with respect to direct detection, and relatively short repetition time according to the T_1 of the protons and not of the X-nuclei.[24] Therefore it is possible to detect species at concentrations of physiological relevance (mM or even μM) in D_2O or aqueous solution (90% H_2O/10% D_2O) where labile NH protons can be observed. By means of selective labelling ^{15}N, this technique can also simplify a complicated spectrum in which only those protons directly attached to ^{15}N atoms are detected. The basic HMQC and HSQC pulse sequences are shown in Scheme 2.1.

The Pt-^{15}NH protons can be detected selectively by the use of [^{1}H, ^{15}N] single (or multiple) quantum coherence (HSQC and HMQC) pulse sequences. A 1D ^{1}H

spectrum containing only resonances from Pt-^{15}NH species is obtained by acquiring only the first increment in a two-dimensional experiment; resonances for CH and OH (including water) are eliminated. This is particularly useful in studies of body fluids

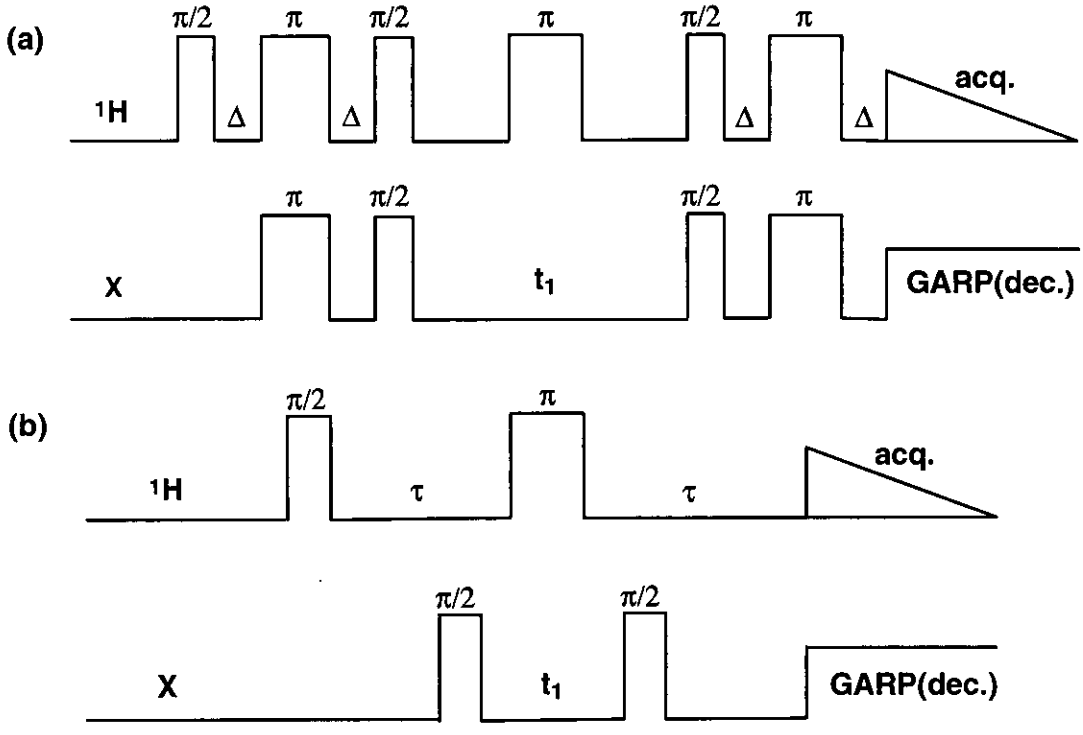

Scheme 2.1 Basic HSQC (a) and HMQC (b) pulse sequences. The delays Δ and τ are ¼J and ½J respectively, where J is the one-bond HX coupling constant. Other modifications are usually needed to improve the suppression and to detect resonances close to the water signal including presaturation (+SCUBA) and WATERGATE (**WATER** suppression by **GrA**dient-**T**ailored **E**xcitation).

or cell culture media, where only the signals from platinum complexes are detected and thousands of other overlapping ^{1}H resonances are filtered out. If ^{15}N decoupling is employed during acquisition (e.g. the GARP method), then each type of Pt-NH resonance appears as a singlet, sometimes together with broadened ^{195}Pt satellites. In practice the water resonance is so intense that it is usually necessary to use additional solvent suppression techniques (e.g. presaturation). The addition of an H_2O T_2

relaxation agent (e.g. 0.5 M $(NH_4)_2SO_4$) can also be helpful to detect NH peaks very close to the H_2O peak. A large improvement in water suppression is achieved by the

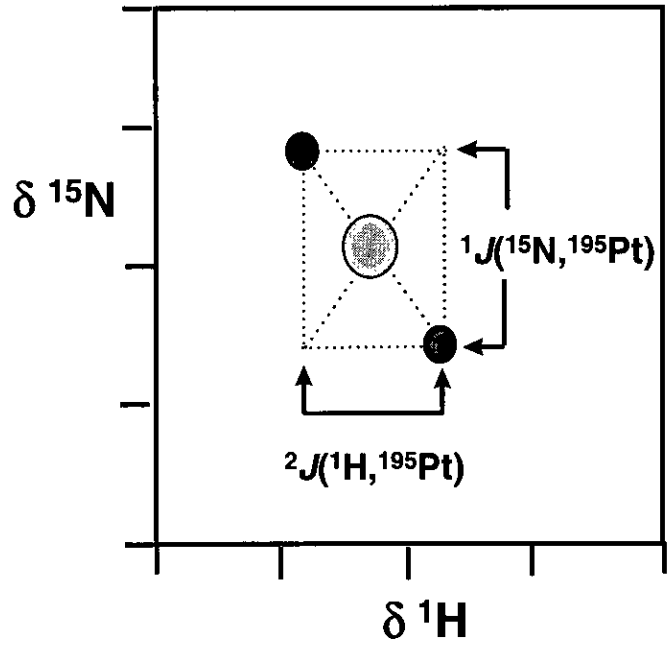

Figure 2.4 General appearance of a 2D [^{1}H, ^{15}N] HMQC or HSQC spectrum. The ^{195}Pt satellites are usually more intense for symmetrical Pt species (Pt(IV) rather than Pt(II)).

use of pulsed field gradients for coherence selection, for example, by use of the HSQC sequences of Stonehouse et al.[25] We have been able to detect NH peaks within a few Hz of the water resonance at concentrations as low as about 10 μM without the need for additional solvent suppression techniques.

The combined detection of ^{1}H and ^{15}N in a 2D inverse NMR experiment is especially powerful, since both the ^{15}N NMR chemical shift (Figure 2.1) and the one-bond coupling constant $^1J(^1H\text{-}^{15}N)$ (Figure 2.2) are diagnostic of the *trans* ligand. As shown in Figure 2.4, the ^{195}Pt satellites (when not broadened beyond detection by the effects of CSA relaxation) in a 2D [^{1}H, ^{15}N] spectrum appear as diagonal peaks which correspond to the $^2J(^{195}Pt\text{-}^1H)$ coupling constant in the $F_2(^1H)$ dimension and

to the $^{1}J(^{195}Pt\text{-}^{15}N)$ coupling in the $F_1(^{15}N)$ dimension. Pt(II) and Pt(IV) ammine and amine complexes can be distinguished by the combination of ^{1}H and ^{15}N chemical shifts.

2.1.3 2D DQF-COSY and NOESY Spectrum

COSY (correlated spectroscopy) is a two-dimensional homonuclear (H, H)-correlated NMR experiment which yields NMR spectra in which ^{1}H chemical shifts along both frequency axes are correlated with each other.[26,27] It is the standard 2D experiment that can be used to identify pairs of protons that have a scalar spin-spin coupling connectivities. There are two inherent drawbacks that limit its usefulness with macromolecules: one is that the fine-structure components that make up each cross-peak appear in antiphase; the other is that the diagonal peaks and the cross-peaks are 90° out of phase in both dimensions. These gives poor sensitivity and extremely harsh weighting functions must be used to give spectra with usable lineshapes which in turn gives a further reduction in sensitivity.

More favourable lineshapes can be obtained by using the double-quantum filtered COSY sequence (DQF-COSY),[28] shown in Scheme 2.2a. In this experiment the diagonal peaks and the cross-peaks all show the same antiphase absorption mode fine-structure. Although the double-quantum filtering attenuates the signals to some extent this is more than offset by the gain resulting from not having to use resolution enhancement to impose acceptable lineshapes on the peaks, this experiment still suffers from poor sensitivity.

The **NOESY** experiment[29,30] is often used to identify pairs of protons that are undergoing cross-relaxation, i.e. protons that would show an NOE in 1D experiments. The characteristic feature of the NOESY pulse sequence (shown in Scheme 2.2b) is the mixing time τ. The cross-peaks are generated by magnetisation transfer that takes place during the mixing time so the length of this delay must be

chosen according to the rate of the transfer process. In contrast to the COSY experiment, both cross-peaks and diagonal peaks in NOESY spectra can be obtained with absorption-mode lineshapes. The experiments are therefore eminently suitable for studying macromolecules. If presaturation is used in a NOESY experiment it is usually also necessary to irradiate the solvent during the mixing time. A complicated factor is that the NOESY pulse sequence cannot distinguish between magnetisation transfer caused by cross-relaxation and magnetisation transfer by chemical exchange. In macromolecules, both give cross-peaks of the same sign as the diagonal.

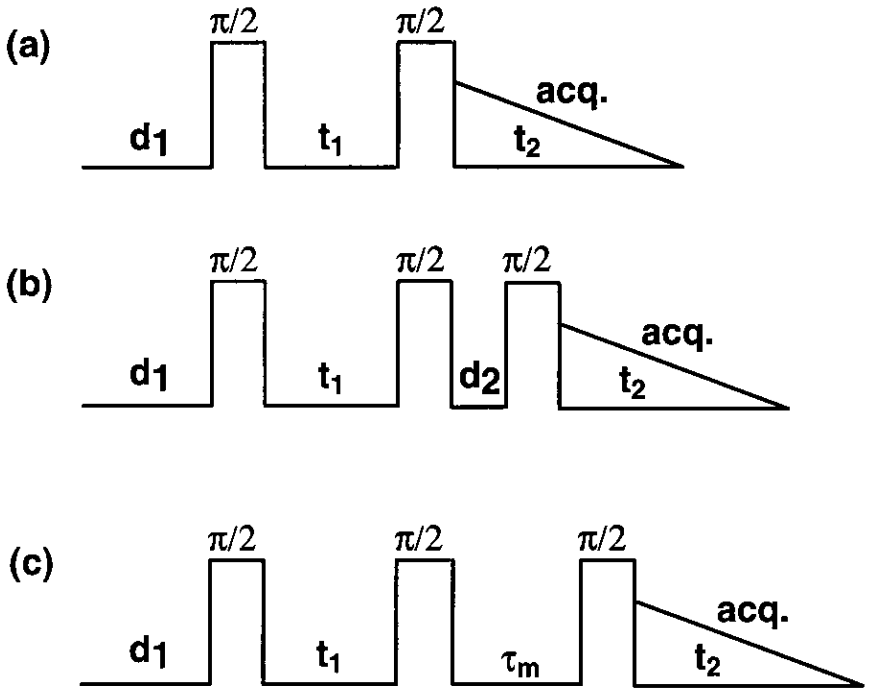

Scheme 2.2 Pulse sequence for two-dimensional (a) COSY; (b) DQF-COSY and (c) NOESY, τ_m is the mixing time.

2.1.4 Dynamic NMR Spectroscopy

Dynamic NMR spectroscopy is very useful in studying reactions with rate constants in the range 10^{-1} to 10^{3} s^{-1}, which is too slow for optical spectroscopic methods but too fast for investigation by classical methods. From the temperature

dependence of the resonance lines, the rate constants and activation parameters can be obtained.[31] A complete line-shape analysis can allow determination of the precise rate constants of the exchange process, but in studying an exchange process it is often not necessary to go through a complete line-shape analysis to obtain the information needed.

If the coalescence temperature T_c at which the two signals just coalesce was detected, the rate constant k_c is given by:

$$k_c = 2.22\ \Delta\nu$$

Here $\Delta\nu$ is the separation in Hz between the two signals in the absence of exchange. It is determined experimentally from spectra recorded at temperatures which are as far below the coalescence temperature as possible. This equation is only valid provided that: 1) the dynamic process occuring is first-order kinetically, 2) the two singlets have equal intensities, 3) the exchanging nuclei are not coupled to each other. An important fact of k_c is that it is determined by the magnitude of $\Delta\nu$, which is in turn proportional to the resonance frequency. Thus T_c is not a constant, but depends on the observing frequency.

From the Eyring equation, the free enthalpy of activation $\Delta G_c^{\ddagger}$ at T_c can be determined:

$$\Delta G_c^{\ddagger} = 19.14\, T_c\, (10.32 + \log \frac{T_c}{k_c})\ \mathrm{J\ mol^{-1}}$$

The NOESY pulse sequence used to investigate dynamic processes such as chemical exchange is called 2D **EXSY** NMR spectroscopy.[32,33] The two experiments are both formally and practically identical. This technique has several advantages over conventional 1D techniques (e.g. saturation transfer, selective excitation and lineshape analysis etc.). The first is the ability to study exchange networks involving n sites, thus all the dynamic data can be determined by a single 2D EXSY experiment. The second advantage is the ability to study partially overlapped spectra, where 1D selective excitation (saturation transfer) experiment is not possible. Finally

a 2D spectrum becomes clear (for multi-site exchange) if the dynamic processes are monitored as a function of mixing time (τ_m).

For quantitative analysis, a 2D EXSY spectrum can be treated according to the Bloch-McConnell equations:

$$M = M^\circ \exp(Rt_m) \qquad \text{(Eq. 2.1)}$$

where M is the matrix comprising the peak volumes of the 2D spectrum, R is a matrix of dimensions equal to the number of sites between which exchange is occurring, containing all the exchange rate constants and spin-lattice relaxation rates, and t_m is the mixing time. The integral intensity I_{ij} of the 2D absorption peak at ω_i, ω_j is given by:

$$I_{ij}(t_m) = M_j^\circ \exp(-Rt_m)_{ij} \qquad \text{(Eq. 2.2)}$$

For the simplest case of first-order two-site exchange with equal populations ($M_A = M_B = M$, $k_{+1} = k_{-1} = k$) and equal relation rates ($R_A = R_B = R$), then:

Diagonal peaks: $I_{AA} = I_{BB} = \frac{1}{2}\{[1 + \exp(-2kt_m)]\exp(-t_mR)\}$ (Eq. 2.3)

Cross-peaks: $I_{AB} = I_{BA} = \frac{1}{2}\{[1 - \exp(-2kt_m)]\exp(-t_mR)\}$ (Eq. 2.4)

In this simple two-site exchange system, the exchange rate can be determined from the initial rate of build-up of cross-peak intensity at short mixing times

$$(\delta I_{AB}/\delta t_m)_i = M^\circ k \qquad \text{(Eq. 2.5)}$$

or directly from the ratio of the cross and diagonal peak intensities at short mixing times:

$$\frac{I_{AA}}{I_{AB}} = \frac{1 + \exp(-2kt_m)}{1 - \exp(-2kt_m)} = \frac{(1 - kt_m)}{kt_m} \qquad \text{(Eq. 2.6)}$$

Equation (2.6) can also be extended to N-site exchange, and a dynamic matrix is needed to extract the dynamic data.[34,35]

2.1.5 The Process of Generating an NMR Structure.[36]

Four stages are necessary to generate an NMR-based structure for a double-helical nucleic acid fragment. These stages are intricately overlapped with each other. The first phase includes the generation of proton homonuclear 2D NMR spectra sufficient to provide spectral assignments for as many of the exchangeable and non-exchangeable protons as possible. In most cases, it includes several 2D NOESY spectra with different mixing times in H_2O and D_2O, DQF-COSY and TOCSY experiments.

The second stage of the process is to extract accurate intensities of 2D NOE cross-peaks and convert them into distances *via* computational tools using iterative **Complete Relaxation Matrix Analysis**, which can simulate spin-diffusion effects. The programme **MARDIGRAS**[37] was used in my work. It is important here to determine realistic error bounds consistent with the quality of the experimental data. Deoxyribose coupling constants can be extracted from DQF-COSY directly or indirectly and subsequently utilised to generate torsion angles to define the sugar pucker. By comparing the computer simulated and the experimental fine-structure of cross-peaks in 2D DQF-COSY spectra, individual J-couplings can be deduced and subsequently the conformation analysis of sugar pucker (C2′ or C3′-endo) can be carried out. The computer programmes used to do this are called **SPHINX** and **LINSHA**.[38] SPHINX generates a data file from the simulation, and LINSHA calculates the shape of the peaks resulting from SPHINX. It takes into account line-widths, digital resolution in both dimensions and other acquisition and processing parameters.

In the next stage, the NMR-derived restraint information is used to search conformational space for a single structure that is most compatible with all restraints. Various computing tools are available for determining the nucleic acid structures from NMR constraints. In this work, the **restrained Molecular Dynamics** (rMD) approach was used. Molecular motion is simulated starting from an initial model

structure (both A- and B-form DNA). The search for the final structure is guided through minimisation of a composite energy function that comprises the empirical force-field parameters to maintain proper stereochemistry and a penalty term for noncompliance with the NMR-derived restraints. Fine tuning parameters of the rMD is needed for the convergence of final structures calculated from different starting models such as A- and B-forms of DNA. Sometimes a theoretical 2D NOESY spectrum calculated from the final structure is needed to compare with the experimental data.

A detailed structural analysis constitutes the final stage of the refinement process. For this the programme **CURVES**[39] was used. It is important to understand that typical rMD structures depend on both the restraints and the force field, which means that some structural features are sensitive to the balance of those two major features. Analysis and validation of NMR-based rMD structures and their properties should be rigorously in accord with all experimental data.

2.2 High Performance Liquid Chromatography (HPLC)[40]

HPLC is one of the fastest developing analytical techniques. It has arisen from the theories of liquid chromatography (LC) and instrumentation that were originally developed for gas chromatography(GC). The mixture to be analysed is dissolved in a suitable solvent, introduced ("injected") at one end of the column, and carried through the column by a continuous flow of the same solvent ("mobile phase"). The separation takes place in the column, which contains "sorptive" particles of large surface area. These particles are referred to as the "stationary phase". Injected sample components interact reversibly with the stationary phase in a continuous manner. If a component of the mixture (a solute) is absorbed weakly onto the surface of the solid stationary phase it will travel down the column faster than another solute that is more strongly absorbed. The mobile phase (also called the

eluant) is pumped through the column bed of the tightly packed chromatographic particles using a solvent delivery system ("pump"). With the selection of the proper mobile phase and column packing material, a separation of different components can be achieved. As the sample components emerge from the column, a suitable detector is used to monitor and transmit a signal to a recording device. The chromatogram is a record of the detector response as a function of time and indicates the presence of the components as "peaks".

Besides the classical liquid-solid chromatography mentioned above, there are other sorption mechanisms that can be used for separation, depending on whether a liquid or a solid is chosen as the stationary phase, or the kind of solid used. Liquid-Liquid chromatography uses a liquid stationary phase coated on to a finely divided inert solid support. Separation is due to differences in the partition coefficients of solutes between the stationary liquid and the liquid mobile phase. In normal phase LC, the stationary phase is polar while the mobile phase is composed of nonpolar solvents. The situation is opposite for reverse-phase LC, in which the mobile phase is more polar than the stationary phase. Solutes are eluted according to polarity with both techniques. With reverse phase, most polar first and with normal phase least polar first, and the retention times of solutes can be changed by changing the polarity of the stationary phase or (more easily) the mobile phase. In ion-exchange chromatography, the stationary phase is an ion exchange resin, and separations are based on attractive ionic forces between solute ions and the exchange sites on the resin. Separations are made using a polar mobile phase, usually water containing salts or small amount of alcohol, and a stationary phase containing either acidic or basic fixed sites. And finally in size-exclusion chromatography, the separation depends on differences in size and shape, more precisely the hydrodynamic volume, of the molecules in a sample. The larger molecules do not enter the pores of the column particles and are excluded more quickly.

In analytical HPLC, the mobile phase is normally pumped through the column at a flow rate of 1-5 ml/min. If the composition of the mobile phase is constant, the method is called "isocratic" elution. The composition of the mobile phase can be a binary, ternary or quaternary solvent mixture. Alternatively, the composition of the mobile phase can be made to change in a predetermined way during the separation, a technique called "gradient" elution. Modern solvent delivery systems allow the selection of a wide range of gradient profiles and variation of the time over which the gradient is delivered. Besides the shape and time of the gradient, other factors including compatibility of the two solvents with the detector, and miscibility with the sample solution, have to be considered.

Some of the important concepts defining the quality of a chromatographic separation are listed below.

Capacity factor k´, where

$$k' = \frac{\text{amount of solute in the stationary phase}}{\text{amount of solute in the mobile phase}} = \frac{(t_R - t_0)}{t_0} = \frac{(V_R - V_0)}{V_0}$$

t_R and t_0 are the retention time of solute retained on the column and unretained which travelling as the mobile phase. k' can also be simply described as the ratio of the elution volume of the component, V_R, to the void volume of the column, V_0.

Selectivity of the column is the ability to discriminate between the two components. It is expressed in terms of a "separation factor" α:

$$\alpha = \frac{k'_2}{k'_1} = \frac{t_{R2} - t_0}{t_{R1} - t_0} = \frac{(V_2 - V_0)}{(V_1 - V_0)}.$$

Efficiency of the column, which can be measured using quantities of plate number (N) and plate height (H):

$$N = 16\left(\frac{t_R}{w}\right)^2, H = \frac{L}{N}$$

t_R is the retention time of the component, w is the peak width, L and N are the length and plate number of the column, and H is the plate height.

The *resolution* of the separation can be defined as

$$Rs = 0.25\left(\frac{\alpha-1}{\alpha}\right)\left(\frac{\bar{k}}{1+\bar{k}}\right)N^{1/2}$$

where $\bar{k}$ is the average capacity factor for the two peaks, and N is the average plate number.

2.3. UV Absorption Spectroscopy [41]

The combination of purine and pyrimidine bases in nucleic acids results in strong ultraviolet absorption in the range of 240-280 nm. It is modulated by the stereochemistry and conformational influences of the ribose-phosphate backbone which is essentially transparent to light of that wavelength.

The absorbance at a wavelength λ (A_λ) is a measure of the relative intensity of a beam of light before ($I_\lambda°$) and after (I_λ) it passes through a solution containing the absorbing molecule: $A_\lambda = \log(I_\lambda°/I_\lambda) = \varepsilon_\lambda cl$, where c is the concentration (M), l is the pathlength of the cell (cm), and ε_λ is the extinction coefficient ($cm^{-1}M^{-1}$) Oligonucleotides exhibit a strong UV absorption maximum, λ_{max}, at about 260 nm and a molar extinction coefficient, ε, of the order of 10^4 ($M^{-1}\cdot cm^{-1}$). The absorption arises almost entirely from π-π* electronic transitions in the purine and pyrimidine components. The intensity and exact position of the λ_{max} is a function of both the base composition of the nucleic acid and the state of the base-pairing interactions present, the salt concentration of the solution, and its pH. Most importantly, base-base stacking results in decrease in ε known as hypochromicity. This arises from dipole-dipole interactions that depend on the three-dimensional structure of an oligonucleotide and ranges in magnitude from 1-11% for deoxyribonucleoside phosphates to 30% for most helical polynucleotides.

UV absorption is a sensitive and convenient way to monitor the 'melting behaviour' of DNA and RNA. The method depends on the difference in extinction coefficient between double stranded and single stranded DNA. When the UV

absorption of a nucleic acid sample is measured as a function of temperature, the resulting plot is known as a melting curve. The midpoint of the increase in absorbance with increasing temperature is known as the melting temperature, T_m. This is dependent on the base-composition of the sample, the salt concentration of its solution, and even the types of counter-ion present. The melting temperature is reduced at lower salt concentration because cations can stabilise the DNA duplex. Divalent cations such as Mg^{2+} are much more effect in stabilising duplexes.[41] Such melting is a co-operative phenomenon and the observed melting curves become progressively steeper with increasing length of the oligonucleotides.

2.4 References

[1] F. M. Macdonald, P. J. Sadler, *^{195}Pt NMR spectroscopy: applications to the study of anticancer drugs, in 'Biochemical mechanisms of platinum anticancer drugs'*, Eds. D. C. H. McBrien and T. R. Slater, IRL Press Ltd., Oxford, 1986, pp. 361-381.

[2] S. J. Berners-Price, P. J. Sadler, *Cood. Chem. Rev.* **1996**, *151*, 1.

[3] K. J. Barnham, S. J. Berners-Price, Z. Guo, P. del S. Murdoch, P. J. Sadler, NMR Spectroscopy of Platinum Drugs: From DNA to Body Fluids, in *'Platinum and Other Metal Coordination Compounds in Cancer Chemotherapy 2'*, Ed. H. M. Pinedo, J. H. Schornagel, Plenum Press, New York, 1996, pp. 1-16.

[4] I. M. Ismail, S. J. S. Kerrison, P. J. Sadler, *J. Chem. Soc. Chem. Commun.* **1980**, 1261.

[5] D. P. Bancroft, C. A. Lepre, S. J. Lippard, *J. Am. Chem. Soc.* **1990**, *112*, 6860.

[6] T. G. Appleton, J. R. Hall, S. F. Ralph, *Aust. J. Chem.* **1986**, *39*, 1347.

[7] T. G. Appleton, J. R. Hall, S. F. Ralph, *Inorg. Chem.* **1985**, *24*, 673.

[8] G. M. Clore, A. M. Gronenborn, *J. Am. Chem. Soc.* **1982**, *104*, 1369.

[9] S. K. Miller, L. G. Marzilli, *Inorg. Chem.* **1985**, *24*, 2421.

[10] T. G. Appleton, J. R. Hall, S. F. Ralph, *Inorg. Chem.* **1985**, *24*, 4685.

[11] T. G. Appleton, J. W. Connor, J. R. Hall, *Inorg. Chem.* **1988**, *27*, 130.

[12] I. M. Ismail, S. J. S. Kerrison, P. J. Sadler, *Polyhedron*, **1982**, *57*, 1.

[13] R. E. Norman, P. J. Sadler, *Inorg. Chem.* **1988**, *27*, 3583.

[14] K. J. Barnham, M. I. Djuran, P. del. S. Murdoch, J. D. Ranford, P. J. Sadler, *J. Chem. Soc. Dalton Trans.* **1995**, 3721.

[15] K. J. Barnham, M. J. Djuran, P. del S. Murdoch, J. D. Ranford, P. J. Sadler *Inorg. Chem.* **1996**, *35*, 1065.

[16] S. J. Berners-Price, J. D. Ranford, P. J. Sadler, *Inorg. Chem.* **1994**, *33*, 5842.

[17] Z. Guo, T. W. Hambley, P. del. S. Murdoch, P. J. Sadler, U. Frey, *J. Chem. Soc. Dalton Trans.* **1997**, *4*, 469.

[18] Y. Chen, Z. Guo, P. del S. Murdoch, E. Zang, P. J. Sadler, *J. Chem. Soc, Dalton Trans.* **1998**, 1503.

[19] K. J. Barnham, Z. Guo, P. J. Sadler, *J. Chem. Soc. Dalton Trans.* **1996**, 2867.

[20] A. I. Ivanov, J. Christodoulou, J. A. Parkinson, K. J. Barnham, A. Tucker, J. Woodrow, P. J. Sadler, *J. Biol. Chem.* **1998**, *273*, 14721.

[21] P. S. Pregosin, H. Omura, L. M. Venanzi, *J. Am. Chem. Soc.* **1973**, *95*, 2047.

[22] T. G. Appleton, J. R. Hall, S. F. Ralph, C. S. M. Thompson, *Inorg. Chem.* **1989**, *28*, 1989.

[23] S. J. Berners-Price, P. W. Kuchel, *J. Inorg. Biochem.* **1990**, *38*, 327.

[24] L. Müller, *J. Am. Chem. Soc.* **1979**, *101*, 4481; A. Bax, R. G. Griffey, B. L. Hawkins, *J. Magn. Reson.* **1983**, *55*, 301; D. H. Live, D. G. Davis, W. C. Agosta, D. Cowburn, *J. Am. Chem. Soc.* **1984**, *106*, 6104.

[25] J. Stonehouse, G. L. Shaw, J. Keeler, E. D. Laue, *J. Magn. Reson.* **1994** A, *107*, 178.

[26] W. P. Aue, E. Bartholdi, R. R. Ernst, *J. Chem. Phys.*, **1976**, *64*, 2229.

[27] K. Nagayama, A. Kumar, K. Wüthrich, R. R. Ernst, *J. Magn. Reson.*, **1980**, *40*, 321.

[28] M. Rance, O. W. Sorensen, G. Bodenhausen, G. Wagner, R. R. Ernst, K. Wüthrich, *Biochem. Biophys. Res. Commun.*, **1983**, *117*, 479.

[29] J. Jeener, B. H. Meier, P. Bachmann, R. R. Ernst, *J. Chem. Phys.* **1979**, *71*, 4546.

[30] A. Kumar, R. R. Ernst, K. Wüthrich, *Biochem. Biophys. Res. Commun.*, **1980**, *95*, 1.

[31] H. Friebolin, *Basic One- and Two- Dimensional NMR Spectroscopy*, VCH, Weinheim, **1991**.

[32] R. R. Ernst, G. Bodenhausen, A. Wokaun, in "*Principles of nuclear magnetic resonance in one and two dimensions*", Chapter 9, Clarendon Press, Oxford, **1987**.

[33] L. Y. Lian, G. C. K. Roberts, in "*NMR of Macromolecules – A Practical Approach*" (Edited by G. C. K. Roberts), Chapter 6, IRL press, Oxford, **1993**.

[34] K. G. Orrell, V. Sik, D. Stephson, *Prog. NMR spectros.* **1990**, *22*, 121.

[35] K. G. Orrell, V. Sik, *Ann. Rep. NMR spectros.* **1993**, *27*, 104.

[36] U. Schmitz, T. L. James, *Methods in Technology*, **1995**, *261*, 3.

[37] M. Gochin, T. L. James, *Biochemistry*, **1990**, *29*, 11172. M. Gochin, T. L. James, *Biochemistry*, **1990**, *29*, 11161. B. A. Borgias, T. L. James, *J. Magn. Reson.* **1990**, *87*, 475.

[38] K. Weisz, R. H. Shafer, W. Egan, T. L. James, *Biochemistry*, **1992**, *31*, 7477.

[39] G. Ravishanker, S. Swaminathan, D. L. Beveridge, R. Lavery, H. Sklenar, *J. Biomol. Struct. Dyn.* **1989**, *6*, 669.

[40] S. Lindsay, "*High performance liquid chromatography*", second edition, John Wiley & Sons, **1992**.

[41] G. M. Blackburn, M. J. Gait, in "*Nucleic Acids in Chemistry and Biology*", second edition, Oxford University Press, **1996**, pp446-447.

Chapter 3

Interconversion between S-bound and N-bound L-methionine Adducts of {Pt(dien)}$^{2+}$ (dien=diethylenetriamine) *via* dien Ring-opened Intermediates

3.1 Abstract

The reaction between $[Pt(^{15}N\text{-dien})Cl]^+$ (**1**) and L-methionine (L-MetH, H_3N^+-$CH(CH_2CH_2SCH_3)$-COO^-) has been studied using $[^1H,^{15}N]$ 2D NMR spectroscopy and HPLC, together with ^{15}N-labelled amine ligands. The complex [Pt(dien)(L-MetH-*S*)]$^{2+}$ (**2**) was dominant at neutral pH and converted partially and reversibly to [Pt(dien)(L-Met-*N*)]$^+$ (**3**) at pH > 8. When the pH was lowered from 8 to 3, the dien ring-opened intermediate [Pt(dienH-*N,N'*)(L-Met-*S,N*)]$^{2+}$ (**4**) was formed which converted slowly into complex (**2**). Complex (**4**) was separated by HPLC and characterized by NMR spectroscopy as a mixture of 4 diastereomers (due to chiral centres at S and NH) present in a 2:2:1:1 molar ratio. This isolated intermediate had a surprisingly long lifetime (days) in 0.55 M $(NH_4)H_2PO_4$ (pH 4.0).

3.2 Introduction

Sulfur-containing biomolecules may react in vivo with platinum antitumor compounds. Possible such reactive biomolecules are cysteine, methionine, glutathione, and metallothionein and other proteins. These reactions could be responsible for inactivation, resistance and toxicity of platinum drugs.[1]

Methionine (L-MetH) is an important amino acid which is involved in the metabolism of platinum drugs, and platinum bis-methionine complexes have been identified as metabolites in the urine of patients undergoing cisplatin *cis*-$[Pt(NH_3)_2Cl_2]$ therapy.[2] The complex [Pt(L-Met-*S,N*)$_2$] exists in aqueous solution as a mixture of *cis* and *trans*-isomers which undergo slow interconversion, with the *cis* isomer predominating at equilibrium (*K*: 7.0),[3] but these are unreactive species which can be considered to be a detoxified form of Pt. However, a recent *in vivo* experiment has demonstrated that cisplatin incubated with methionine has reduced nephrotoxicity while the cytotoxicity against cancer cells is maintained.[4] Methionine and its derivatives can form stable ring-opened complexes with carboplatin and its

analogues.[5] Since carboplatin itself reacts with nucleobases very slowly, it is conceivable that a methionine-containing peptide or protein may play an important role in transport or activation of carboplatin and in the transfer of Pt onto DNA. S-bound methionine can be displaced by N7 of the DNA base guanine,[6,7] and L-methionine can increase the rate of reaction of guanosine 5′-monophosphate with cisplatin at pH 7.[8]

Methionine is able to coordinate to Pt(II) in a very versatile manner in aqueous solution. A simple system of L-methionine and $K_2[PtCl_4]$ in molar ratio 2:1 generates over 10 platinum species.[9] Thioether sulfur, amino nitrogen and carboxylate oxygen[10] are all capable of binding to Pt(II). The favored binding site is sulfur, and S,N-chelation is a common binding mode. In methionine-containing peptides, coordination of the amide N is also possible.[11,12]

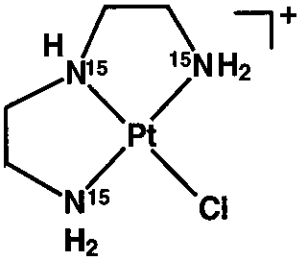

Platinum-dien chelate rings are considered to be both thermodynamically more stable and kinetically more inert compared with cisplatin, and reactions of $[Pt(dien)Cl]^+$ are often studied as models of the first binding step of cisplatin.[13,14] The binding of $[Pt(dien)Cl]^+$ is capable of distorting DNA structure[15] and inducing local DNA denaturation.[16] It has been shown that $[Pt(dien)Cl]^+$ binds to homocysteine or methionine through the thioether sulfur,[17] and S-bound thioethers can be displaced from Pt(II) intra-[7,11] or inter-molecularly[6] by nitrogen (N7) from guanine at physiological pH.[18] Guanine is known to be a major target for DNA platination by anticancer drugs.[1] An intramolecular migration of $\{[Pt(dien)]\}^{2+}$ from sulfur to

imidazole-N1 in the dipeptide histidylmethionine at pH > 6 has also been reported recently.[19]

In this work, I have sought to gain further insight into sulfur-nitrogen migration by 2D [^{1}H,^{15}N] HSQC NMR spectroscopic and HPLC studies of reactions of [Pt(dien)Cl]$^{+}$ with L-methionine *via* the use of ^{15}N-labelled dien and L-MetH.

3.3 Experimental

Materials and Methods

L-Methionine (L-MetH) and ^{15}N-labelled L-MetH (99% ^{15}N) were purchased from Sigma. ^{15}N-labelled diethylenetriamine (^{15}N-dien) and [Pt(^{15}N-dien)Cl]Cl were prepared according to the reported procedures.[20,21] All other chemicals were purchased from Aldrich.

NMR spectroscopy

NMR spectra were recorded at 298 K on Bruker DMX500 (^{1}H 500.13 MHz; ^{15}N 50.7 MHz), using 5-mm NMR tubes. The chemical shift references were as follows: ^{1}H, dioxane (internal, 3.743 ppm), ^{15}N (external, 1 M $^{15}NH_4Cl$ in 1.5 M HCl). For ^{1}H NMR, typical acquisition conditions for 1D spectra were as follows: 45-60^{o} pulses, 16-32 K data points, 2-3 s relaxation delay, collection of 32-128 transients, final digital resolution of 0.2–1 Hz/pt. 2D [^{1}H,^{15}N] HSQC NMR spectra (optimized for ^{1}J(N, H) = 72 Hz) were recorded using the sequence of Stonehouse et al.[22] The ^{15}N-spins were decoupled by irradiation with the GARP-1 sequence during acquisition. Water suppression was achieved by pulsed-field gradients. Typically, 8 scans were acquired for each of 128 increments of t_1 and the final resolution was 4 Hz/point for the F2 dimension and 8 Hz/point for the F1 dimension. For the HPLC separated sample, 256 acquisitions were used per t_1 period and the final resolution was 2 Hz/point for the F2 dimension and 1 Hz/point for the F1 dimension.

HPLC

The following equipment was used: Gilson 305 pumps, Gilson 806 manometric module, LKB 2141 variable wavelength monitor, and Rheodyne sample injector. Analytical separations were carried out at 298 K on a Nucleosil (100-5SA) cation-exchange column by injecting aliquots of the reaction mixture at various pH and time intervals with detection at 210 nm. A solution of $(NH_4)H_2PO_4$ solution (0.55 M, pH 4.0) was used as eluent. The data were analyzed using Dynamax Method Manager Software. The HPLC separation was carried out with the help of Dr. P. del S. Murdoch.

pH measurements

The pH values of the solutions were adjusted with $HClO_4$ (1 M) or NaOH (1 M) and determined using a Corning 240 pH meter equipped with an Aldrich micro combination electrode, calibrated with Aldrich buffer solutions at pH 4, 7 and 10.

NMR sample preparation

All the NMR samples (except that separated by HPLC) were in $90\%H_2O/10\%D_2O$ (0.6 ml), and contained 0.1 M $NaClO_4$ to maintain a constant ionic strength. Buffer was not used in order to avoid possible interference with the reactions. The reactions of [Pt(^{15}N-dien)Cl]Cl (5 mM) with L-MetH (^{15}N or ^{14}N) were conducted at a 1:1 molar ratio at constant temperature.

3.4 Results

First the substitution of the chloride ligand of $[Pt(^{15}N\text{-dien})Cl]^+$ (**1**) by the S of L-MetH at pH 6 was studied. The effect on the product of increasing the pH to 8 was then investigated, followed by lowering the pH to 3. All of the reactions were studied

by both NMR and HPLC. For 2D [^{1}H,^{15}N] NMR, both ^{15}N-labelled or unlabelled dien and L-MetH were used, and some HPLC-separated fractions of ^{15}N-labelled L-MetH were examined by 2D [^{1}H,^{15}N] NMR. As summarized recently, the ^{15}N chemical shifts of Pt-NH of Pt-^{15}N-dien complexes are usually diagnostic of the *trans* ligands.[23] For an Pt-NH *trans* to an oxygen donor, the ^{15}N chemical shift is *ca* -10 ppm, for an Pt-NH *trans* to nitrogen or chloride, the ^{15}N shift is *ca* 10 ppm, and *trans* to sulfur about 30 ppm. For Pt-NH_2 of amine, the ^{15}N chemical shifts are as follows: *trans* to O, -40 to -50 ppm; *trans* to N, Cl, -25 to -35 ppm; *trans* to S, -5 to -15 ppm. In this study, the above information has been used to assign the ligands *trans* to the amine groups.

1) NMR spectroscopy

Reaction of [Pt(dien)Cl]$^{+}$ with L-MetH at pH 6 followed by pH adjustment to 8.5

The reaction of ^{15}N-labelled complex (**1**) (5 mM) with ^{15}N-L-MetH in a 1:1 molar ratio at pH 6.0 and 298 K was followed by 2D [^{1}H,^{15}N] NMR for a period of 12 h. After 30 minutes of incubation, three new cross-peaks at 5.75, 5.58/-30.29 ppm (peaks **2a** and **2b,** Fig 3.1) and 6.97/26.36 ppm (peak **2c,** Fig 3.1) were present in the spectrum in addition to three cross-peaks of the starting complex (**1**). The new cross-peaks increased in intensity with time, while the cross-peaks for complex (**1**) decreased in intensity. After 10 h, only peaks **2a, 2b** and **2c** were observable. Fig. 3.1 shows a 2D [^{1}H,^{15}N] NMR spectrum recorded 12 h after incubation. Peaks **2a** and **2b** have ^{15}N chemical shifts similar to those for Pt-NH_2 of complex (**1**), in which two pairs of non-equivalent ^{1}H were observed, and can be assigned to the protons of the two *trans* Pt-NH_2 groups. Peak **2c** has a ^{15}N-chemical shift in the region expected for Pt-NH *trans* to a sulfur. Therefore the cross-peaks **2a, 2b** and **2c** can be assigned to the S-bound L-MetH adduct [Pt(^{15}N-dien)(^{15}N-L-MetH-*S*)]$^{2+}$ (**2**). The 2D NMR

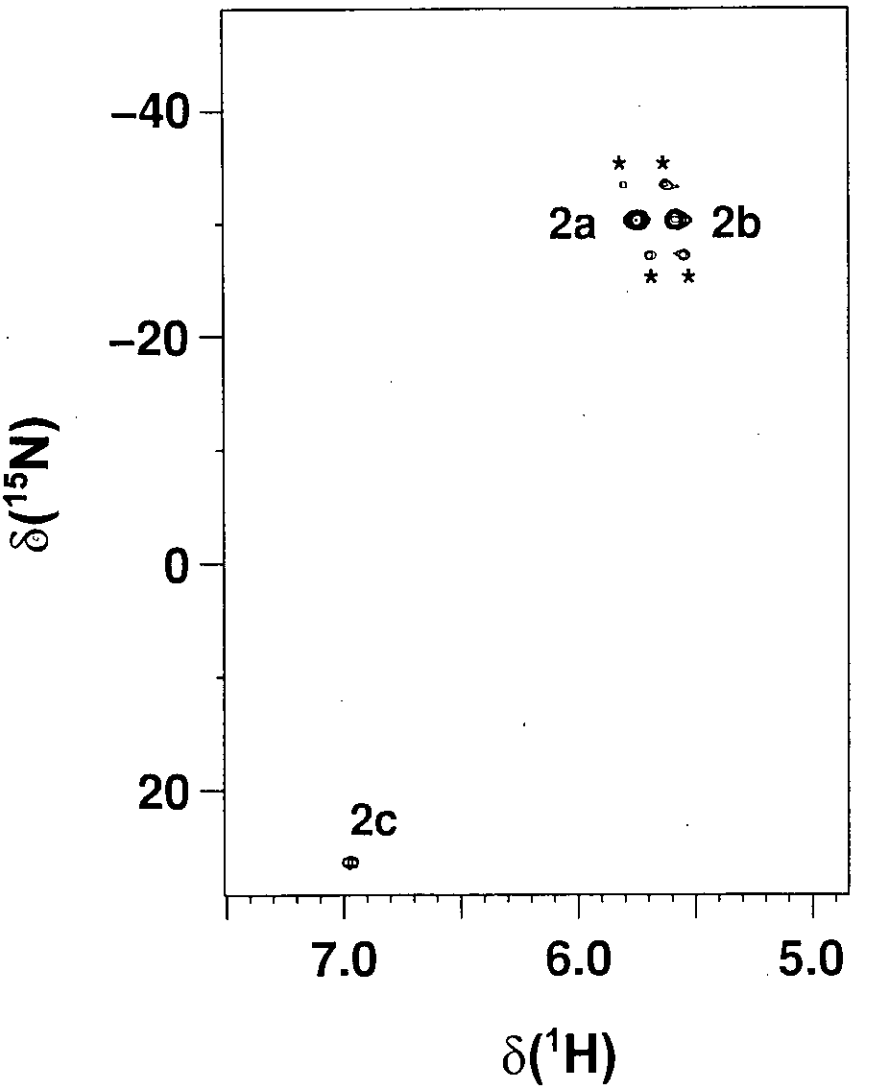

Figure 3.1. Formation of [Pt(^{15}N-dien)(^{15}N-L-Met-*S*)]$^{2+}$ (**2**) by reaction of [Pt(^{15}N-dien)Cl]$^{+}$ (**1**) (5 mM) with ^{15}N-L-MetH in 1:1 molar ratio at 298 K, pH 6.0. The 2D [^{1}H, ^{15}N] HSQC NMR spectrum was recorded after 12 h of reaction. The peaks labeled **2a** and **2b** are assigned to protons on each of the two NH_2 groups, and **2c** to the NH group. ^{195}Pt satellites are labeled with *.

Table 3.1 ^{1}H and ^{15}N chemical shifts of $\{Pt(dien)\}^{2+}$ and $\{Pt(dienH\text{-}N,N')\}^{3+}$ complexes. The spectra were recorded during the reaction of ^{15}N-labelled complex (**1**) with ^{15}N-labelled L-methionine at 298 K.

Compound	pH	^{15}N-dien ($^{1}H/^{15}N$) [a]		^{15}N-L-Met ($^{1}H/^{15}N$) [a]
		NH (*trans* to)	NH_2 (*trans* to)	(NH_2 *trans* to N)
$[Pt(^{15}N\text{-dien})Cl]^{+}$ (**1**)	6.0	6.69/7.68 (Cl)	5.29, 5.08/-34.20 (N)	
$[Pt(^{15}N\text{-dien})(^{15}N\text{-L-MetH-}S)]^{2+}$ (**2**)	6.0	6.97/26.36 (S)	5.75, 5.58/-30.29 (N)	
$[Pt(^{15}N\text{-dien})(^{15}N\text{-L-Met-}N)]^{+}$ (**3**)	8.5	6.46/6.76 (N)	5.42/-32.40 (N)	4.89/-36.76
			5.02/-32.40 (N)	
			5.25/-32.83 (N)	
$[Pt(^{15}N\text{-dienH-}N,N')(^{15}N\text{-L-Met-}S,N)]^{2+}$ [b] (**4**)	3.3			
R, R-		6.71/-13.18 (N)	5.39/-10.17; 5.74/-10.17 (S)	5.00/-46.01; 5.81/-46.01 [d]
R, S-		6.59/-12.48 (N)	5.33/-9.32; 5.62/-9.32 [c] (S)	4.94/-46.37; 5.85/-46.37 [d]
S, R-		6.66/-14.06 (N)	5.48/-9.82; 5.78/-9.82 (S)	5.18/-46.59; 5.82/-46.59 [d]
S, S-		6.57/-12.80 (N)	5.59/-10.10 [c] (S)	5.11/-46.77; 5.97/-46.77 [d]

[a] Some cross-peaks are multiplets but no detailed analysis was attempted due to the resolution limitation of the 2D spectra (4 Hz per data point in ^{1}H dimension). [b] The assignment of peaks to individual diastereoisomers is arbitrary, and the pairing of the cross-peaks is based on the peak intensities. [c] Overlapped. [d] These cross-peaks are better resolved in the HPLC purified (**4**), as shown in Fig. 5, and the minor differences in $\delta(^{1}H)$ (*ca* 0.1 ppm) and $\delta(^{15}N)$ (*ca* 0.3 ppm) compared to the values in Table 2 may be due to the different ionic strengths and pH values of the samples.

spectrum of the solution was recorded again after 7 d at 298 K, and peaks for complex (**2**) were unchanged.

The pH of the above solution was raised from 6.0 to 8.5, and the time dependence of the resultant [^{1}H, ^{15}N] 2D NMR spectrum investigated for a period of 24 h. The cross-peaks assigned to complex (**2**) gradually decreased in intensity, whilst five new cross-peaks appeared with ^{1}H, ^{15}N chemical shifts of 5.42/-32.40 (peak **3a** in Figure 3.2A) 5.25/-32.83 (**3b**), 5.02/-32.40 (**3a´**), 4.89/-36.76 (**3d**) and 6.46/6.76 (**3c**) ppm. Figure 3.2A shows the spectrum recorded 12 h after the pH adjustment, by which time equilibrium had been reached. Each peak contained fine structure which can be assigned to NH_AH_B and NH-CH_2 coupling (7 to 11 Hz) but this was not further analyzed. Cross-peaks **3a**, **3a´** and **3b** have ^{15}N chemical shifts in the region expected for Pt-NH_2 groups *trans* to N or Cl, and peak **3c** has a ^{15}N chemical shift characteristic of Pt-NH *trans* to N or Cl. The new peaks have ^{1}H, ^{15}N chemical shifts different from complex (**1**), Table 3.1, and Cl^- can be ruled out as the ligand *trans* to Pt-NH. Peaks **3a** and **3a´** have the same ^{15}N-chemical shifts, and the relative areas of peaks **3a** : **3b** : **3a´** are 1:2:1, therefore **3a** and **3a´** can reasonably be assigned to two non-equivalent protons on one NH_2 group of dien, and peak **3b** to the other NH_2 group with coincident ^{1}H shifts.

Peak **3d** also has a ^{15}N chemical shift in the region of Pt-NH_2 groups *trans* to N or Cl, and when the above reaction was repeated using ^{15}N-labelled complex (**1**) but unlabelled L-MetH, peak **3d** disappeared (Figure 3.2B) showing that this arises from a coordinated NH_2 group of L-Met. Therefore peaks **3a** - **3c** can be assigned to the Pt-NH_2 and Pt-NH groups of a dien ligand and the observed peaks are consistent with the formation of [Pt(^{15}N-dien)(^{15}N-L-Met-*N*)]$^+$ (**3**) at pH 8.5, Table 3.1. Curiously cross-peak **2c** (Fig. 3.1), assigned to Pt-NH group of the S-bound L-MetH complex (**2**), became broader with time and disappeared from the 2D spectrum 5 h after pH adjustment to 8.5.

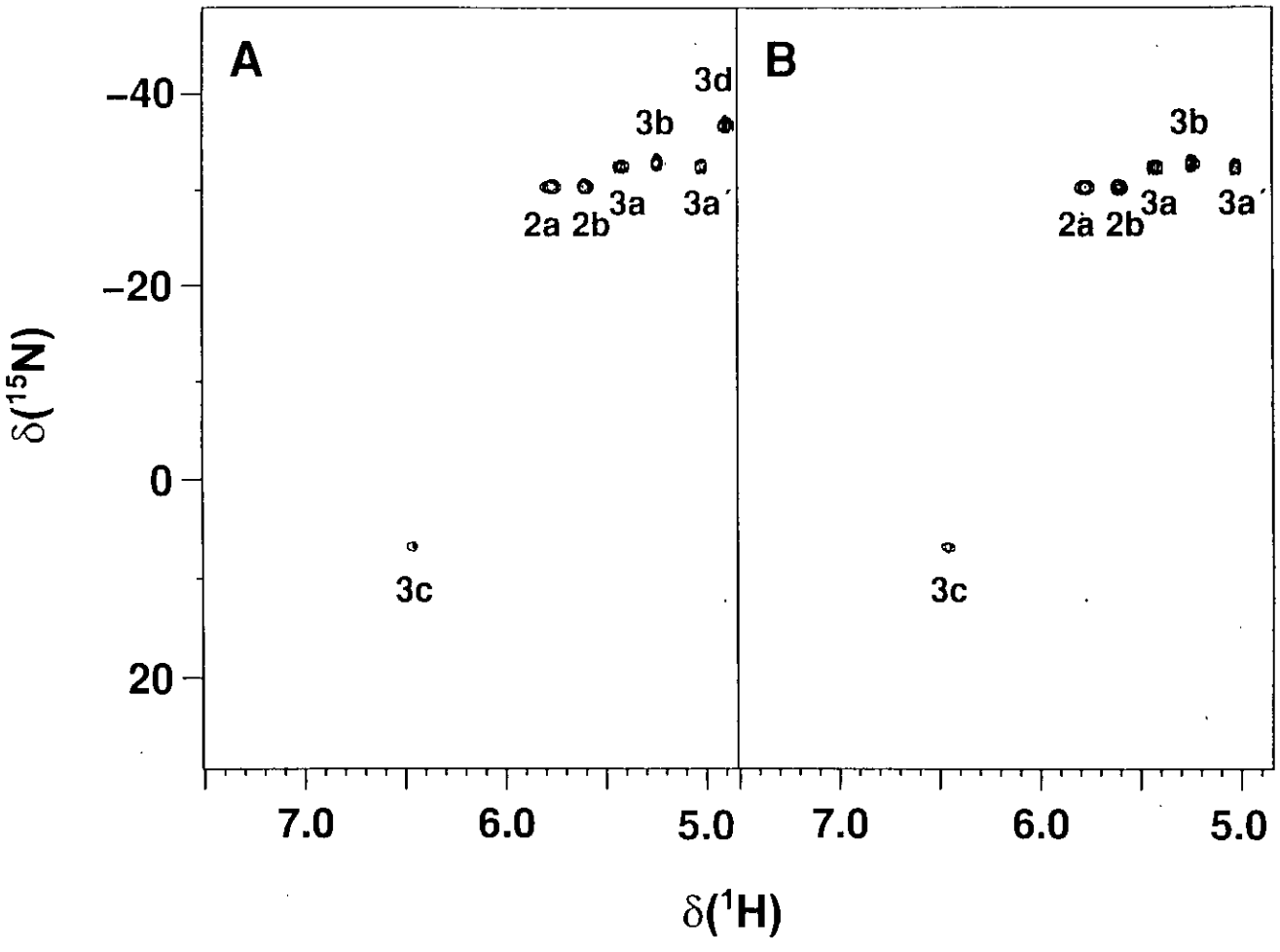

Figure 3.2 A 2D [^{1}H, ^{15}N] HSQC NMR spectrum recorded 12 h after increasing the pH of a solution containing complex (**2**) as [Pt(^{15}N-dien)(^{15}N-L-Met-*S*)]$^{2+}$ (A) or [Pt(^{15}N-dien)(^{14}N-L-Met-*S*)]$^{2+}$ (B) from 6.0 to 8.5. Peak assignments: **2a** and **2b**, NH_2 (*trans* to N) of complex (**2**); **3a**, **3b** and **3a´**, NH_2 (*trans* to N) and **3c**, NH (*trans* to N) of [Pt(^{15}N-dien)(L-Met-*N*)]$^{+}$ (**3**); **3d**, NH_2 (*trans* to N) of N-bound ^{15}N-L-Met in complex (**3**). The cross-peak for NH (*trans* to S) of complex (**2**) is not observed because of fast exchange with solvent protons on NMR timescale at this pH. Cross-peaks (**3a** - **3d**) exhibit further coupling in the ^{1}H dimension.

Effect of pH decrease from 8.5 to 3.3

The pH of the above solution containing an equilibrium mixture of complexes (**2**) and (**3**) (labelled with both ^{15}N-dien and ^{15}N-L-MetH) was lowered from 8.5 to 3.3 and the time dependence of the 2D spectrum was followed for 24 h at 298 K. During the first hour, peak **2c** reappeared (Pt-NH of complex (**2**), slowing down of NH exchange rate at low pH) and new cross-peaks appeared in the ^{1}H/^{15}N regions from 5.99 to 4.91/-46.01 to -46.77 ppm, 6.71 to 6.57/-13.18 to -12.80 ppm, and 5.80 to 5.32/-10.22 to -9.32 ppm (boxes **e**, **g**, and **h**, respectively, in Figure 3.3A), and peaks for complexes (**2**) and (**3**) (**2a**, **2b**, and **3a** to **3d**) were still observable, with the same ^{1}H and ^{15}N chemical shifts as at the higher pH (Fig. 3.2A). The cross-peaks in boxes **e**, **g**, and **h** each corresponded to a total of four different ^{15}N chemical shifts (Table 3.1) with intensity ratio of ca 2:2:1:1. All these new cross-peaks decreased in intensity with time and eventually disappeared after 10 h, whereas the cross-peaks for complex (**2**) increased in intensity with time, whilst those for complex (**3**) decreased in intensity but were still just visible after 24 h. A cross-peak at 7.81/17.68 ppm, which has similar ^{1}H and ^{15}N chemical shifts to those of the NH_3^+ group for free ^{15}N-L-MetH, was initially observed, but disappeared within 1 h after the pH adjustment.

This reaction was reinvestigated using ^{15}N-labelled complex (**1**) but unlabelled L-MetH. In this case, cross-peak **3d** and those in box **e** of Fig. 3.3A were not observed, Figure 3.3B. Therefore these cross-peaks must be due to the coordination of $^{15}NH_2$ of L-methionine.

No new 2D cross-peaks were observed when the pH of a solution containing complex (**2**) (^{15}N-dien and ^{15}N-labelled L-Met) was adjusted directly from 6 to 3, without initially being raised to pH 8.5.

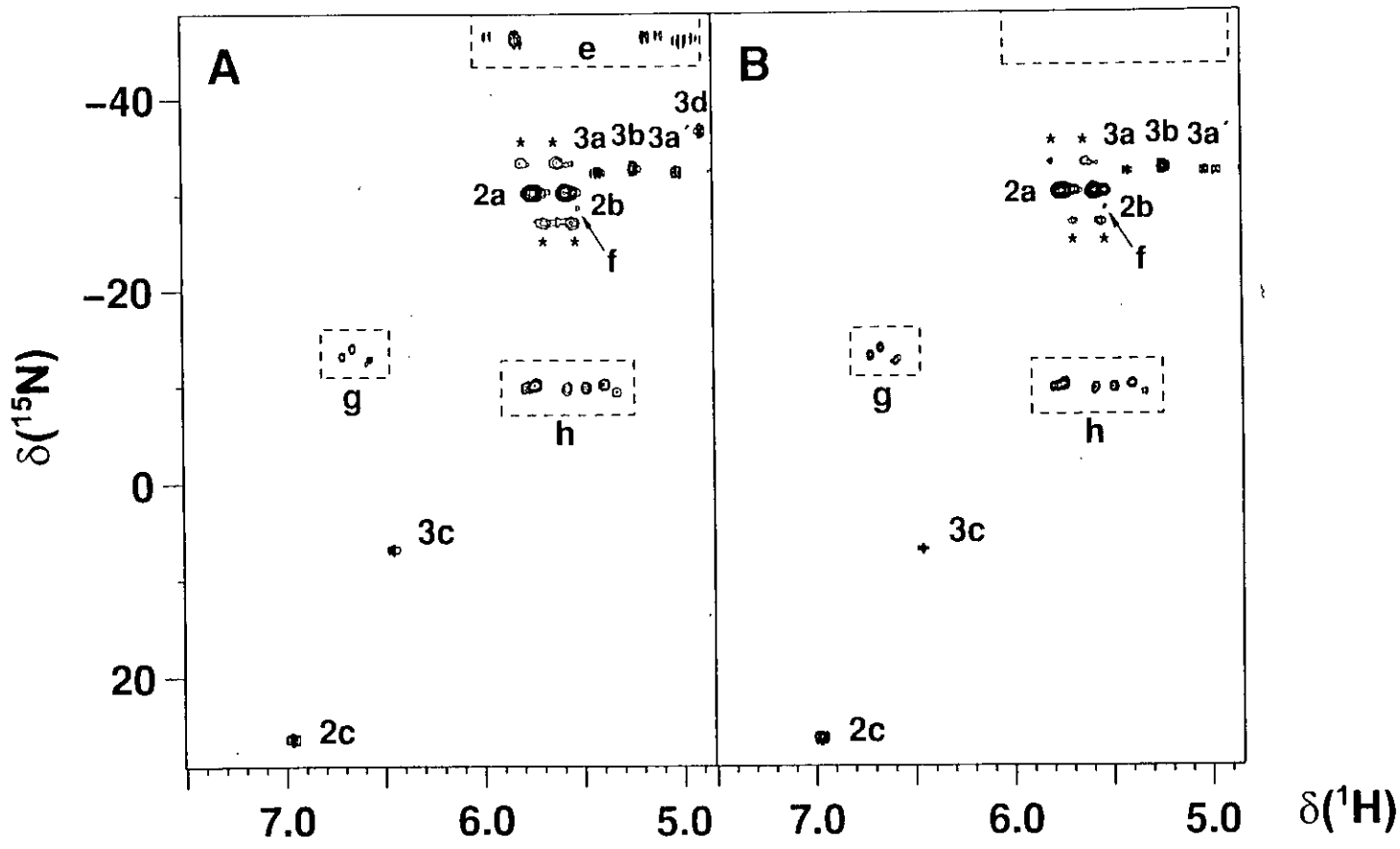

Figure 3.3 The 2D [^{1}H, ^{15}N] HSQC NMR spectra recorded 1 h after lowering the pH of solutions containing complexes (**2**) and (**3**) (see Fig. 3.2) containing ^{15}N-labelled L-Met (A) or unlabelled L-Met (B) from 8.5 to 3.3. The boxed cross-peaks are assignable to the dien-ring-opened intermediate [Pt(^{15}N-dienH-*N,N´*)(L-Met-*S,N*)]$^{2+}$ (**4**). Note the absence of the peaks in box **e** and peak **3d** in Fig. 3.3B (^{14}N-L-MetH used). Peak assignments: **2a** and **2b**, NH_2 *trans* to N with ^{195}Pt satellites (*) and **2c**, NH *trans* to S of complex (**2**); **3a**, **3b** and **3a´**, NH_2 (*trans* to N) and **3c**, NH (*trans* to N) of complex (**3**); **3d**, NH_2 (*trans* to N) of N-bound ^{15}N-L-Met in complex (**3**); boxes **g** and **h** can be tentatively assigned to Pt-NH (*trans* to N) and Pt-NH_2 (*trans* to S) groups of dien in ring-opened intermediate (**4**); box **e**, NH_2 (*trans* to N) of N-bound ^{15}N-L-Met in intermediate (**4**); peak **f,** unassigned.

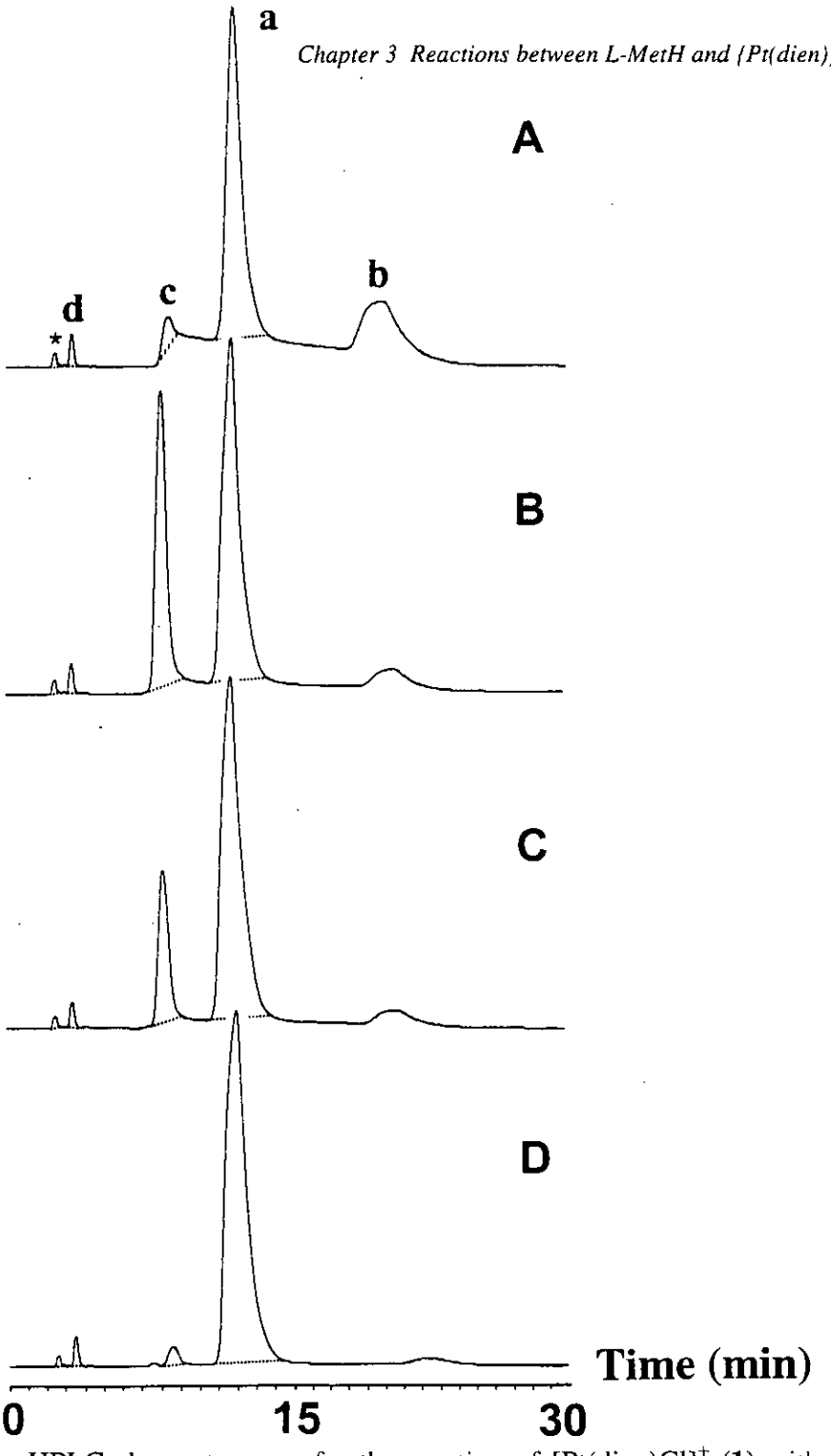

Figure 3.4 The HPLC chromatograms for the reaction of $[Pt(dien)Cl]^+$ (**1**) with L-MetH (5 mM, 1:1, 298 K, pH 6.0, 24 h). (A) 12 h after pH adjustment from 6.0 to 8.5; (B) 0.5 h after lowering pH from pH 8.5 to 3.3; (C) 2 h after pH adjustment from 8.5 to 3.3; (D) 24 h after pH adjustment from 8.5 to 3.3. Peak assignments: **a,** $[Pt(dien)(L\text{-}Met\text{-}S)]^+$ (**2**); **b**, $[Pt(dien)(L\text{-}Met\text{-}N)]^+$ (**3**); **c,** dien ring-opened intermediate $[Pt(dienH\text{-}N,N')(L\text{-}Met\text{-}S,N)]^{2+}$ (**4**); **d** and * are from free L-MetH and the solvent front respectively.

2) HPLC

Reactions of unlabelled $[Pt(dien)Cl]^+$ (**1**) with ^{15}N-L-MetH were also followed by HPLC at different pH values. Several eluents were tested and 0.55 M $(NH_4)H_2PO_4$, pH 4.0 was found to provide the optimum separation of reactants and products present in the solutions and was used in all the HPLC work.

The HPLC chromatogram from the reaction of complex (**1**) with ^{15}N-L-MetH (5 mM, 1:1) pH 6.0, 298 K for 24 h, showed only one major peak with retention time of *ca* 12.0 min. After the pH of the solution was raised to 8.5 and left for 12 h, the HPLC chromatogram showed a new broad peak with elution time of *ca* 20.0 min (peak **b**) as well as a strong peak with retention time of *ca* 12.0 min (peak **a**, Figure 3.4A). The pH of the solution was then lowered from 8.5 to 3.3 and the HPLC chromatogram was followed with time for a period of 24 h. Within the first hour, a new peak (**c**) with retention time of 8.2 min appeared and reached its maximum intensity (Fig. 3.4B), and then decreased in intensity along with peak **b** (Fig. 3.4C). After 24 h peaks **b** and **c** had almost disappeared (Fig. 3.4D).

The fraction corresponding to peak **b** (Fig. 3.4) from the reaction at pH 8.5 was collected. When this was re-chromatographed after standing for 3 days at 298 K, the chromatogram showed only peaks **c** and **a** (3:1 ratio). This change can be explained by the decrease in the pH of the collected fraction to 4.0 (that of the 0.55 M $(NH_4)H_2PO_4$ eluent). Under these conditions peak **c** was very long-lived, and even detectable after several weeks.

3) Characterization of intermediate detected during pH adjustment from 8.5 to 3.3

Attempts were made to separate the intermediate and characterize it further by NMR methods. Unlabelled complex (**1**) and ^{15}N-L-MetH (10 mM, 1:1) were incubated for 24 h at pH 6 to allow formation of complex (**2**). The pH of the solution was then

adjusted to 8.5, and after 12 h was lowered to 3.3. The fraction corresponding to the intermediate of peak **c** in the HPLC chromatogram of Fig. 3.4 was collected 30 min after pH adjustment, and lyophilized. The lyophilized sample was re-dissolved in 0.6 ml of 90%H_2O-10%D_2O, which gave rise to a solution of pH *ca* 4.0 because of the presence of $(NH_4)H_2PO_4$. The resulting 2D [^1H, ^{15}N] HSQC NMR spectrum is shown in Fig. 3.5, and appears to contain 6 doublets (**a´**, **d´**, **c**, **d**, and **b´** overlapped with **c´**), and 2 triplets (**a** and **b**) corresponding to four ^{15}N chemical shifts, Table 3.2. The splittings (13-14 Hz) can be assigned to $^2J(NH_a,NH_b)$ and $^3J(\alpha CH,NH)$ couplings involving coordinated ^{15}N-L-Met. The relative intensities of cross-peaks **c**:**d** and **a**:**b** is *ca.* 2:1. The chemical shifts and relative intensities of these cross-peaks in Fig. 3.5 are nearly the same as those in box **e** of Fig. 3.3 (δ ^{15}N between -46 to -47 ppm, Table 3.2). The peaks in boxes **g** and **h** (Fig. 3.3A) for complex (**4**) are not observed in this experiment because the dien ligand is not ^{15}N-labelled. The ^1H NMR spectrum of this sample contained four singlets with shifts of 2.641, 2.635, 2.579, 2.567 ppm assignable to coordinated SCH_3 groups of L-Met ligands (Fig. 3.6). These had relative areas of 2:2:1:1. The ^1H NMR spectrum of the solution was recorded again after 3 days at 298 K, and no changes were observed.

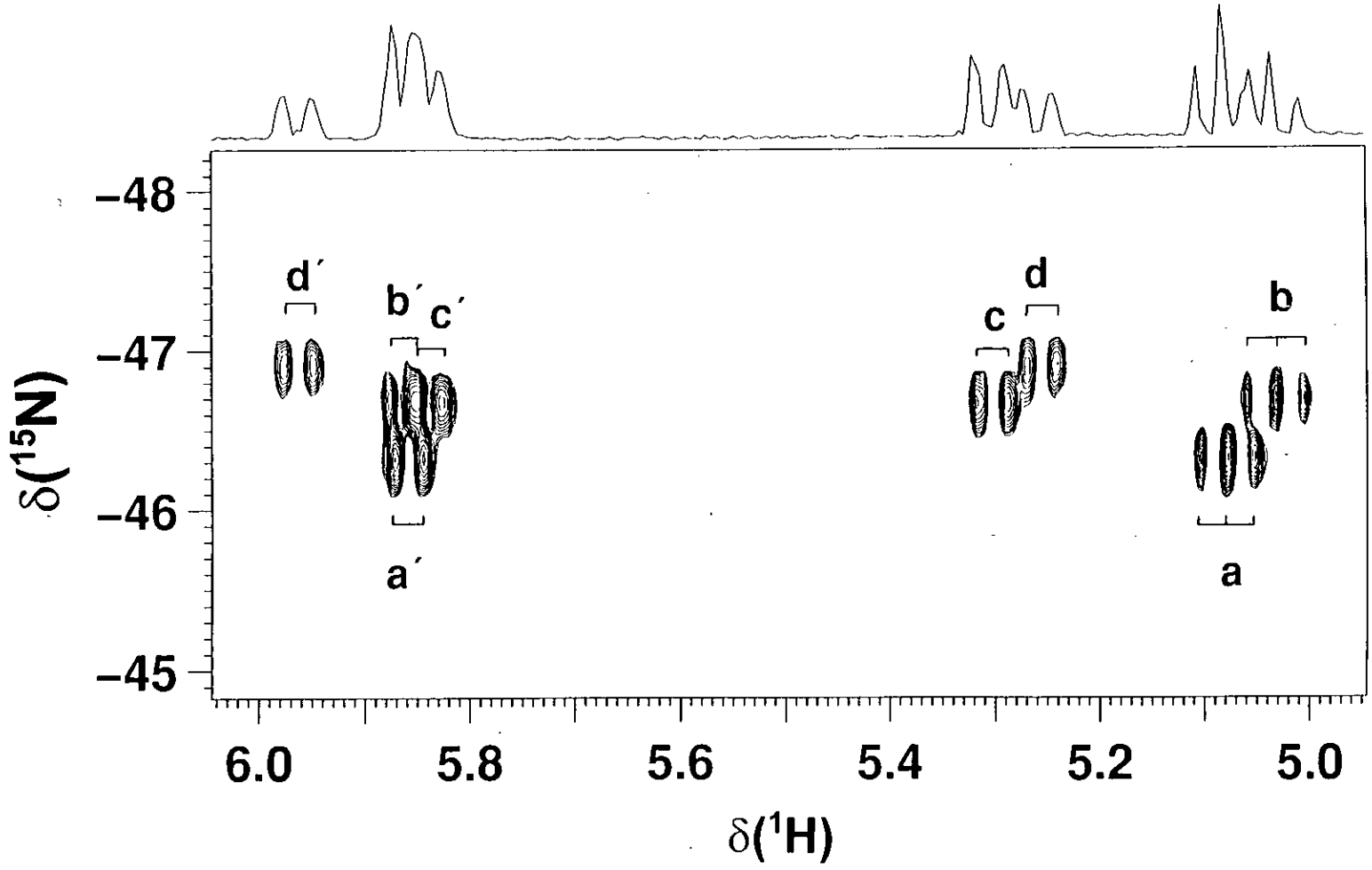

Figure 3.5 The 2D [^{1}H,^{15}N] HSQC NMR spectrum of the HPLC-isolated dien ring-opened complex (**4**) (peak **c** in Fig. 3.4B) at pH 4.0. Only the NH_2 group of L-MetH was ^{15}N-labelled, and the four sets of cross-peaks (peaks **a**, **a´** to **d**, **d´**) can be assigned to the nonequivalent Pt-NH_2 groups in the four diastereoisomers of [Pt(dienH-*N,N´*)(^{15}N-L-Met-*S,N*)]$^{2+}$. All peaks have $^{2}J(NH_a,NH_b)$ of *ca* 12 Hz, while only peaks **a** and **b** have an additional $^{3}J(\alpha CH,NH)$ of *ca* 13 Hz.

Table 3.2 ^{1}H and ^{15}N chemical shifts of HPLC separated complex (**4**) [Pt(dienH-*N,N´*)(^{15}N-L-Met-*S,N*)]$^{2+}$ (pH 4.0, 298 K).

Diastereomer [a]	SCH_3 δ (^{1}H)	Peak	δ ($^{1}H/^{15}N$) (NH_2 *trans* to N)
R, R	2.641	**a**	5.08/-46.32 (t)
		a´	5.86/-46.32 (d)
R, S	2.579	**b**	5.03/-46.70 (t)
		b´	5.86/-46.70 (d)
S, R	2.635	**c**	5.31/-46.68 (d)
		c´	5.84/-46.68 (d)
S, S	2.567	**d**	5.26/-46.92 (d)
		d´	5.97/-46.92 (d)

[a] The assignment of peaks to individual diastereomers is arbitrary, and the pairing of the SCH_3 signals with $^{15}NH_2$ cross-peaks is based on the peak intensities. The upfield cross-peaks for *R, R*- and *R, S*-diastereomers appeared as triplets due to ^{3}J(αCH,NH) (*ca* 13 Hz) as well as $^{2}J(NH_a,NH_b)$ (*ca* 12 Hz) , whilst only $^{2}J(NH_a,NH_b)$ splittings (*ca* 12 Hz) were observable for all other signals.

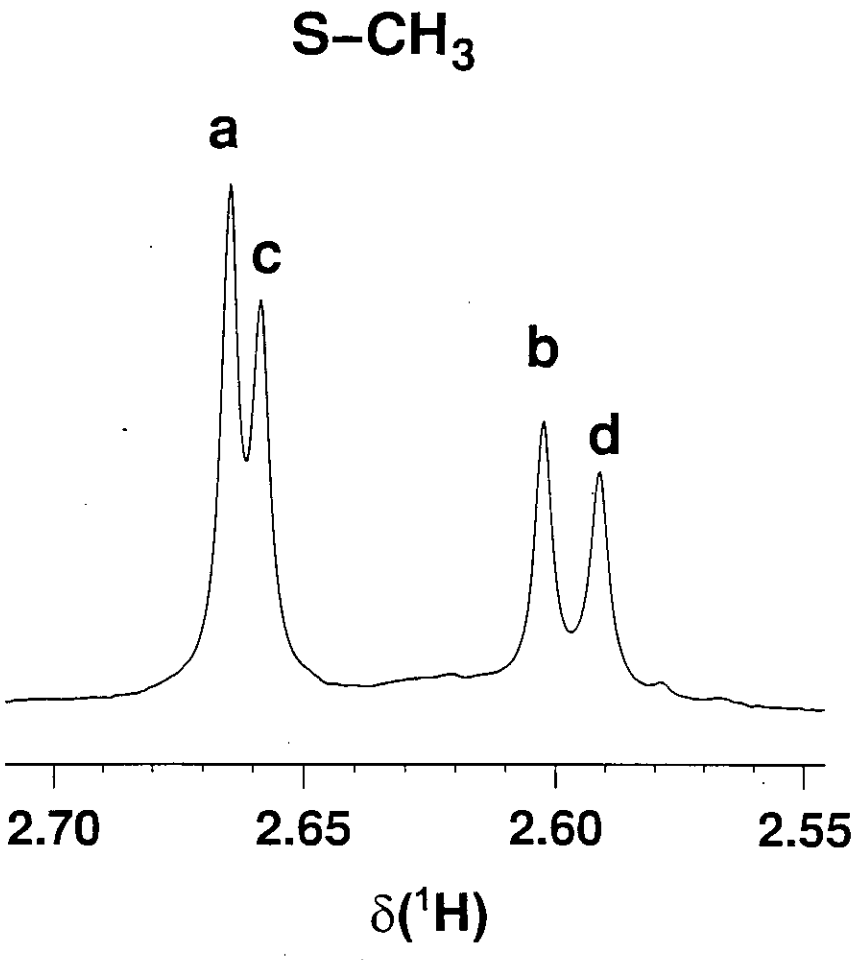

Figure 3.6 Part of the 500 MHz ^{1}H NMR spectrum of HPLC isolated dien ring-opened complex (**4**) at pH 4.0 (peak **c**, Fig. 3.4B), showing four singlets from S-CH_3 of diasteroisomers of *S,N*-chelated L-Met.

3.5 Discussion

Competition between sulfur and nitrogen ligands in coordination to platinum(II) is currently attracting attention because this could provide new routes for DNA platination *via* a protein fragment. Thioether S can bind reversibly to Pt(II), and at physiological pH, it can be replaced by a N donor from N7 of guanine.[6,7,17] It can also be replaced by N1 of imidazole from His at pH > 6.[19] In this work, the mode of binding of L-MetH to {Pt(dien)}$^{2+}$ at a variety of pH values has been investigated.

S- and N-bound [Pt(dien)(L-Met)] complexes

The NMR data show unambiguously that at pH 6, initial binding of L-MetH to $[Pt(dien)Cl]^+$ (**1**) takes place *via* Cl^- displacement with S which has a high affinity for Pt(II). Correspondingly, in the HPLC experiment at this pH, only one major peak (peak **a**, Fig. 3.4) was observed for the product. When the pH of $[Pt(dien)(L\text{-}Met\text{-}S)]^+$ (**2**) was adjusted to 8.5, the deprotonated amino group (pK_a 9.28 for free L-MetH[24]) from L-Met slowly displaces S to form the thermodynamically-favored product $[Pt(dien)(L\text{-}Met\text{-}N)]^{2+}$ (**3**).

The two Pt-NH_2 groups of complex (**3**) have different ^{15}N chemical shifts and the two ^1H NMR peaks for one of the two Pt-NH_2 groups are well separated (*ca* 0.4 ppm), which may be a consequence of H-bonding with the carboxylate group of N-bound L-methionine at both pH 8.5 and 3.3 (Scheme 3.1). Since methionine is asymmetric, they in theory will all have different chemical shifts.

2) Identification of Intermediate (complex 4)

Lowering the pH of a solution containing the N-bound complex (**3**) from pH 8.5 to 3.3 gave rise to peaks for intermediates both in 2D [^1H, ^{15}N] NMR spectra and in HPLC chromatograms. By using ^{15}N-labelled L-MetH in comparison with unlabelled L-MetH (Fig. 3.3A, B), the coordination of NH_2 of L-Met in the intermediate was confirmed and ^{15}N-chemical shifts of the cross-peaks (box **e**, Fig. 3.3A) are comparable to those of *trans*-$[Pt(^{15}N\text{-}L\text{-}Met\text{-}S,N)_2]$ (for which the NH_2-Pt-NH_2 groups gave rise to cross-peaks at -41 to -43 ppm).[3] Cross-peaks in box **h** (NH_2 *trans* to S) in Fig. 3.3 can be assigned to Pt-NH_2 (^{15}N-dien) groups of the intermediate. Therefore, it seems likely that a major intermediate observed after pH adjustment from 8.5 to 3.3 is a complex with *S,N*-chelated L-Met and a chelate-ring-opened dien ligand, $[Pt(^{15}N\text{-}dienH\text{-}N,N')(^{15}N\text{-}L\text{-}Met\text{-}S,N)]^{2+}$. Cross-peaks in box **g** (Fig. 3.3) can be tentatively assigned to NH *trans* to a nitrogen ligand for the Pt-NH of $[Pt(^{15}N\text{-}$

dienH-*N,N'*)(^{15}N-L-Met-*S,N*)]$^{2+}$. For bis-chelated dien ligand, a Pt-NH group *trans* to N would be expected to have an ^{15}N chemical shift of *ca* 10 ppm,[23] in the present case the ^{15}NH shifts of [Pt(^{15}N-dienH-*N,N'*)(^{15}N-L-Met-*S,N*)]$^{2+}$ appears to be shifted to high field by 20 ppm, an effect which is presumably caused by the ring-opening. The appearance and disappearance of peak **c** observed in HPLC chromatogram after pH adjustment from 8.5 to 3.3 are consistent with those cross-peaks observed in the NMR experiments (Fig. 3.3), and therefore can be assigned to the same ring-opened species.

Due to the presence of chiral NH and S centers in [Pt(dienH-*N,N'*)(L-Met-*S,N*)]$^{2+}$ (**4**), four diastereomers would be expected: *R,R*; *R,S*; *S,R*; *S,S* (omitting *S* centre at αC for L-methionine) . The *R, S* inversion at the chiral SCH_3 center in *S,N*-chelated L-Met is usually slow on the NMR time scale; for example the energy barrier of such inversion in [Pt(L-Met-*S,N*)Cl_2] has been estimated to be of 74.6 kJ mol^{-1}.[9] Therefore as shown in Fig. 3.3, the four sets of cross-peaks in box **e**, **g** and **h** can be assigned to the four diastereomers. Similarly, four SCH_3 singlets were observed in the ^{1}H NMR spectrum of HPLC purified intermediate (Fig. 3.6). The relative area of the four sets of cross-peaks in boxes **e**, **g** and **h**, and the four SCH_3 singlets, is about 2:2:1:1. This can be attributed to the predominance of one of the two configurations at chiral S. A 2:1 ratio has been observed previously for *R, S* diastereomers of *N,S*-chelated methionine[10] and methionine-containing dipeptide[12] complexes of Pt(II).

The four different ^{15}N chemical shifts of cross-peaks in the 2D [^{1}H,^{15}N] spectrum of the HPLC-purified intermediate (Fig. 3.5) are also consistent with the presence of four diastereoisomers. Each pair of cross-peaks has the same ^{15}N chemical shift, but very different ^{1}H chemical shifts (Δδ, 0.5-0.8 ppm). This suggests that one of the two NH_2 protons of chelated ^{15}N-L-Met in complex (**4**) is strongly involved in H-bonding, perhaps with the deprotonated carboxylate group, which

forms a strained five-membered ring. Alternatively, the ring conformation may allow the dien NH_3^+ group to interact with the CO_2^- group of coordinated L-Met, and, in so doing, may influence the ^1H chemical shifts of the NH_2 groups. For comparison the ^1H chemical shift differences for the ^1H resonances of the NH_2 in *trans*-[Pt(^{15}N-L-Met-*S,N*)$_2$] are only *ca* 0.3-0.4 ppm.[3]

The $^2J(NH_a,NH_b)$ values for cross-peaks observed in the 2D [^1H,^{15}N] HSQC NMR spectrum (Fig. 3.5) are comparable to those values reported for *trans*-[Pt(^{15}N-L-Met-*S,N*)$_2$] (*ca* 12 Hz).[3] ^3J(αCH,NH) (*ca* 13 Hz) splittings were also observed for cross-peaks (**a** and **b**), which implies that envelope conformations may be adopted for the six-membered-ring in two of the four isomers. The other two isomers may adopt flattened boat conformations for which ^3J(αCH,NH) tends to be small, and therefore perhaps not observable. This is the case for *trans*-[Pt(^{15}N-L-Met-*S,N*)$_2$]: several Pt-NH_2 peaks have ^3J(αCH,NH) values of 9-14 Hz, whilst other peaks have no detectable couplings.[3]

After pH adjustment from 8.5 to 3.3, the free nucleophilic S atom of (**3**) could attack the apical position of platinum, leading to labilization of Pt-NH_2 bond and the formation of dien ring-opened S, N-chelate [Pt(dienH-*N,N'*)(L-Met-*S,N*)]$^{2+}$ (**4**) with S *trans* to NH_2 of dien. Complex (**4**) may convert to (**2**) either *via* isomerization to (**5**) (S *trans* to NH of dien) or involving pseudorotation of a five-coordinate intermediate by an associative mechanism.[25] The unassigned cross-peaks which are in very low intensity in Fig. 3.3 could possibly be due to complex (**5**). Proton transfer from the free NH_3^+ group of ring-opened dien in complex (**5**) to the more basic methionine amino group could rapidly give complex (**2**). The fact that no dien ring-opened intermediate was observed when the pH of complex (**2**) was adjusted directly from 6 to 3, shows that dien chelate ring-opening requires displacement of dien NH_2 by S.

Very few examples of chelate ring-opened dien platinum complexes have been reported in the literature. The only crystal structure of a ring-opened dien complex is that for [Pt(dienH-*N,N'*)Cl]Cl_2, obtained from a strongly acidic solution (1 M HCl).[26] Ring-opening of Pt-dien ring has been reported in the presence of excess of diethyldithiocarbamate and thiourea,[27,28] and the complex [Pt(dienH-*N,N'*)(Guo-N7)(thiourea-*S*)]$^{2+}$ has been isolated by HPLC at pH < 2.0.[28] Ring-opened ethylenediamine Pt complexes with the di- and tripeptide Gly-HMet and Gly-Met-HGly have been detected at pH 2.4, and such a ring-opened complex containing Met-HHis has also been identified at pH 9.6.[12,29]

The present work appears to provide the first example of an HPLC-isolated and NMR-characterized Pt-dien ring-opened complex. Complex (**4**) is very long-lived (weeks) in the presence of high concentrations of $(NH_4)H_2PO_4$, which suggests that the phosphate group may form strong H-bonds with the dangling NH_3^+ of dien and stabilize the dien ring-opened form.

Reedijk et al. [30] have observed a pH dependent Pt migration from S to N while studying the reaction between (**1**) and S-adenosyl-L-homocysteine. When they adjusted the pH from 11 to 4, the N-bound Pt complex gave rise to *ca* 20% of 'side products' which could not be characterized. These could also be due to the formation of dien ring-opened adducts.

Taken together, these results show that significant migration of {Pt(dien)} from S-bound to N-bound L-Met occurs at pH values above 8, while N-bound L-Met transfers to S-bound L-Met at pH 3 *via* dien ring-opening intermediates, long-lived isomers in which L-Met S is *trans* to coordinated dien NH_2. The process is summarized in Scheme 3.1.

Scheme 3.1 {Pt(dien)}$^{2+}$ migration from S-bound to N-bound L-Met and dien ring-opening *via S,N*-chelation of L-Met.

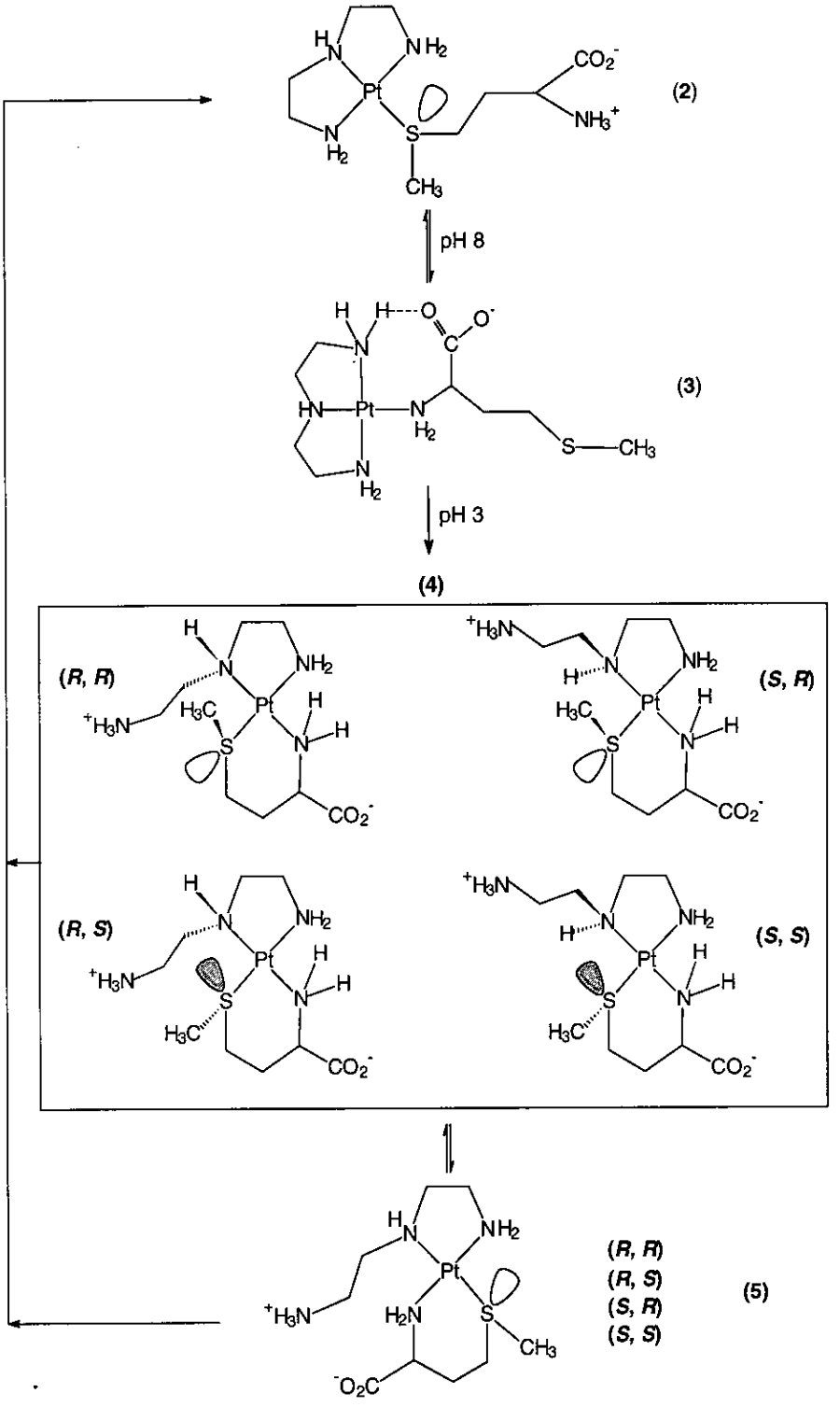

3.6 Conclusion

This work has shown that at neutral pH $[Pt(dien)Cl]^{+}$ (**1**) forms predominantly an S-bound L-Met complex (**2**). Complex (**2**) reversibly converted to the N-bound complex (**3**) at pH 8.5. The adjustment of pH from 8.5 to 3.3 gave rise to formation of the dien ring-opened intermediate $[Pt(dienH\text{-}N,N')(L\text{-}Met\text{-}S,N)]^{2+}$ (**4**) with NH trans to L-Met NH_2, which converted slowly into complex (**2**), the only stable adduct at pH 3.3. Complex (**4**) exists as a mixture of four diastereomers with molar ratio of 2:2:1:1 due to the chiral S centre of L-Met and chiral NH of dien. The two NH_2 protons of L-Met in each of the four diasteromers of complex (**4**) exhibit remarkably different ^{1}H NMR shifts.

3.7 References

[1] J. Reedijk, *Chem. Commun.*, **1996**, 801.

[2] C. M. Riley, L. A. Sternson, A. J. Repta, S. A. Slyter, *Anal. Biochem.*, **1983**, *130*, 203.

[3] P. del S. Murdoch, J. Ranford, P. J. Sadler and S. J. Berners-Price, *Inorg. Chem.* **1993**, *32*, 2249.

[4] P. M. Deegan, I. S. Pratt and M. P. Ryan, *Toxicol.*, **1994**, *89*, 1.

[5] K. J. Barnham, U. Frey, P. del S. Murdoch, J. D. Ranford, P. J. Sadler and D. R. Newell, *J. Am. Chem. Soc.*, **1994**, *116*, 11175.

[6] K. J. Barnham, M. I. Djuran, P. del S. Murdoch and P. J. Sadler, *J. Chem. Soc., Chem. Commun.* **1994**, 721.

[7] J. M. Teuben, S. S. G. E. van Boom, J. Reedijk, *J. Chem. Soc., Dalton Trans.*, **1997**, 3979.

[8] K. J. Barnham, M. I. Djuran, P. del. S. Murdoch, J. D. Ranford, P. J. Sadler, *J. Chem. Soc., Dalton Trans.*, **1995**, 3721.

[9] R. E. Norman, J. D. Ranford and P. J. Sadler, *Inorg. Chem.*, **1992**, *31*, 2249.

[10] T. G. Appleton, J. W. Connor and J. R. Hall, *Inorg. Chem.*, **1988**, *27*, 130.

[11] Z. Guo, T. W. Hambley, P. del S. Murdoch, P. J. Sadler, U. Frey, *J. Chem. Soc., Dalton Trans.* **1996**, 469.

[12] A. F. M. Siebert, W. S. Sheldrick, *J. Chem. Soc., Dalton Trans.* **1997**, 385.

[13] M. I. Djuran, E. L. M. Lempers, J. Reedijk, *Inorg. Chem.* **1991**, *30*, 2648.

[14] P. del S. Murdoch, Z. Guo, J. A. Parkinson, P. J. Sadler, *J. Biol. Inorg. Chem.* **1999**, *4*, 32.

[15] V. Brabec, J. Reedijk, M. Leng, *Biochemistry* **1992**, *31*, 12397.

[16] V. Brabec, V. Boudny, Z. Balcarová, *Biochemistry* **1994**, *33*, 1316.

[17] S. S. G. E. van Boom, J. Reedijk, *J. Chem. Soc., Chem. Commun.* **1993**, 1397.

[18] S. S. G. E. van Boom, B. W. Chen, J. M. Teuben, J. Reedijk, *Inorg. Chem.* **1999**, *38*, 1450.

[19] C. D. W. Fröhling and W. S. Sheldrick, *Chem. Commun.*, **1997**, 1737.

[20] E. Zang and P. J. Sadler, *Synthetic Commun.*, **1997**, *27*, 3145.

[21] Z. Guo, P. J. Sadler, E. Zang, *Chem. Commun.*, **1997**, 27.

[22] J. Stonehouse, G. L. Shaw, J. Keeler and E. D. Laue, *J. Magn. Res. Ser A*, **1994**, *107*, 174.

[23] Z. Guo, Y. Chen, E. Zang and P. J. Sadler, *J. Chem. Soc., Dalton Trans.*, **1997**, 4107.

[24] R. M. C. Dawson, D. C. Elliott, W. H. Elliott, K. M. Jones, *Data for Biochem. Res.*, Oxford Science Publications, third edition, 1993.

[25] M. Mikola, K. D. Klika, A. Hakala, J. Arpalahti, *Inorg. Chem.* **1999**, *38*, 571.

[26] G. Mahal and R. van Eldik, *Inorg. Chim. Acta*, **1987**, *132*, 165.

[27] E. L. M. Lempers and J. Reedijk, *Inorg. Chem.*, **1990**, *29*, 217.

[28] M. Mikola, J. Vihanto and J. Arpalahti, *J. Chem. Soc., Chem. Commun.*, **1995**, 1759.

[29] C. D. W. Fröhling and W. S. Sheldrick, *J. Chem. Soc., Dalton. Trans.*, **1997**, 4411.

[30] E. L. M. Lempers and J. Reedijk, *Inorg. Chem.*, **1990**, *29*, 1880.

Chapter 4

Stereospecific and Kinetic Control over Hydrolysis of a Sterically Hindered Platinum Picoline Anticancer Complex

4.1 Abstract

cis-[$PtCl_2(NH_3)$(2-picoline)] (**1**) (ZD0473) is a recently reported anticancer active complex. Hydrolysis may be an important step in its intracellular activation and interaction with DNA. In this chapter, [^1H, ^{15}N] 2D NMR spectroscopy is used to determine the hydrolysis rates for each chloride ligand of this complex and its 3-picoline analogue **2**. The pK_a values of the aqua and diaqua ligands as well as the X-ray crystal structures of **1** and **2** are reported. For the 3-picoline complex **2** the rate of hydrolysis of Cl^- *trans* to NH_3 (k_{1b} = 1.0 × 10^{-4} s^{-1}, I = 0.1 M, 310 K) is similar to that of cisplatin, but slower for Cl^- *trans* to 3-picoline (k_{1a} = 4.5 × 10^{-5} s^{-1}). Both of the first hydrolysis rates for the 2-picoline complex **1** are slower than those of **2**, but in contrast to **2**, the hydrolysis of Cl^- *trans* to NH_3 (*cis* to 2-picoline) is slower (k_{1b} = 2.2 × 10^{-5} s^{-1}) than for Cl^- *trans* to 2-picoline (k_{1a} = 3.2 × 10^{-5} s^{-1}). The crystal structure of **2** revealed that the pyridine ring is tilted by 49° with respect to the Pt square plane, whereas in **1** the ring is almost perpendicular (103°). This introduces steric hindrance by the CH_3 group towards an axial approach to Pt from above, leading to a destabilisation of the expected trigonal-bipyramidal transition state, an effect well-known in substitution reaction of Pt(II) complexes. The pK_a values for the monoaqua adducts of **1** (6.13 and 6.49) and **2** (5.98 and 6.26 for H_2O *trans* to picoline and NH_3, respectively) and for the diaqua adducts (5.22, 7.16 for **1** and 5.07, 6.94 for **2**) are >0.3 units lower than for cisplatin. The slowness of the hydrolysis, combined with the dominance of (inert) hydroxo species, is expected to contribute to a greatly reduced reactivity of the sterically-hindered 2-picoline complex under intracellular conditions.

4.2 Introduction

Cisplatin is one of the most widely used anticancer drug in the world. It is extraordinarily effective against certain cancers, for example, testicular and ovarian

cancer and is increasingly used against cervical, bladder and head/neck tumours. Due to the acquired drug resistance in treatment of certain cancers and severe normal tissue toxicity of cisplatin, there is a need for new agents which do not exhibit cross-resistance and are less toxic.[1] Most active platinum compounds have the general formula *cis*-[$PtAm_2X_2$], where Am is an am(m)ine ligand with at least one NH group and X is a moderately strongly-bound anionic leaving group such as chloride.[2] Derivatives belonging to this structural class show similar or slightly improved biological activity. Recently there has been interest in pyridine complexes.[3,4,5] The presence of planar pyridine ligands, as in *cis* or *trans*-[$PtCl_2$(pyridine)$_2$] complexes, can reduce the rates of DNA binding compared with *cis* and *trans*-DDP,[6] and by changing the nature or position of substituents on the pyridine ligands, different binding affinities for DNA can be achieved.[4]

The 2-picoline (2-methylpyridine) complex *cis*-[$PtCl_2(NH_3)$(2-picoline)] (**1**) (ZD0473, former name AMD473), is a newly-reported anticancer complex which is now in phase I clinical trials in UK.[7,8] It has been developed at the Institute of Cancer Research, in collaboration with Johnson Matthey Technology Centre/AnorMED. ZD0473 is reported to possess activity against cisplatin-resistant cell lines, and against an acquired cisplatin-resistant subline of a human ovarian carcinoma xenograph, by injection and oral administration.[9] It showed significantly reduced cross-resistance to cisplatin in a panel of three cell lines with known acquired platinum drug resistance mechanisms: reduced accumulation, increased cytoplasmic detoxification by cellular thiols or increased DNA repair/tolerance of platinum-DNA adducts.[10] The toxicity of ZD0473 is also greatly reduced, with no renal toxicity observed.

Once dissolved in water, the labile chloride ions of cisplatin are slowly replaced by water molecules in a stepwise manner: first forming monoaqua species and then further hydrolysis to form diaqua species. The relative amounts of all these

hydrolysis species vary as a function of pH and (externally added) chloride concentration. The mechanism of action of cisplatin is believed to involve activation *via* hydrolysis inside cells where the Cl^- concentration is much lower (*ca.* 4 mM) than outside cells (*ca.* 100 mM). Hydrolysis is the rate limiting step in the reaction of *cis*-Pt with DNA. Since water is a far better leaving group than chloride and hydroxide, it is very important to determine the hydrolysis rates and pK_a values of the hydrolysis adducts.

Various methods have been used before to determine the hydrolysis rates and pK_a values of Pt(II) complexes, those include conductivity, spectrophotometry, HPLC, Cl^- ion titration, Cl^- ion specific electrode, H^+ ion titration and capillary electrophoresis.[11-13] Detailed kinetic studies of the hydrolysis of cisplatin have been carried out by Miller and House.[13] Using ^{15}N and ^{195}Pt NMR spectroscopy, accurate pK_a values for hydrolysis species of cisplatin were reported. [14,15] 2D [^1H, ^{15}N] HSQC spectroscopy is a very powerful tool in accurate and rapid measurement of hydrolysis rates and pK_a values at low concentrations (mM), if the ammine groups of platinum complex are ^{15}N labelled.[14]

Few chemical studies of ZD0473 have been reported although it appears to hydrolyse, form interstrand DNA cross-links and bind to plasma proteins much more slowly than cisplatin.[8,16] In this work, complex **1** has been labelled with ^{15}N and 2D [^1H, ^{15}N] HSQC spectroscopy were used to compare its hydrolysis behaviour with that of the isomeric 3-picoline derivative **2**, since hydrolysis is likely to be an important initial activation step for this drug. The pK_a values for the mono- and diaqua complexes have also been determined since hydroxo ligands on Pt(II) are usually inert compared to aqua ligands. The data reveal notable differences between the chemistry of the sterically-hindered picoline complex and that of cisplatin.

4.3 Experimental

Chemicals and preparation of complexes: 2- and 3-Picoline were purchased from Aldrich. *Cis*-$[PtCl_2(^{15}NH_3)_2]$ was prepared according to a reported procedure.[17] Complexes **1** and **2** were prepared by a similar procedure to that described in the literature for natural abundance, mixed ligand ammine/amine Pt(II) complexes.[18]

pH Measurements: These were performed using a Corning 145 pH meter equipped with an Aldrich micro combination electrode calibrated with Aldrich buffer solutions of pH 4, 7 and 10. The values of pH were adjusted with 1 M $HClO_4$ or NaOH as appropriate.

X-ray Crystallography: Crystals of complexes **1** ($^{15}NH_3$) and **2** ($^{14}NH_3$) were obtained by the slow evaporation of aqueous solutions containing excess KCl. Data for **1** and **2** were collected on Stadi-4 diffractometers equipped with an Oxford Cryosystems low-temperature device. Scan models were both ω–θ. Complex **2** crystallised as fine, delicate needles, which tended to form co-axially aligned clumps and exhibited broad diffraction profiles. For these reasons, $Cu_{K\alpha}$ radiation was used for its intensity advantage over $Mo_{K\alpha}$ radiation. The structures were refined by full-matrix least-squares against F^2 (SHELXL1). H-atoms were placed in calculated positions: the CH_3 and NH_3 were modelled as rotating rigid groups. All non-H atoms were refined anisotropically. Data collection and structure determination were carried out by Dr. S. Parsons.

Crystal data for the two structures are listed in Table 4.1, and selected bond lengths and angles are given in Table 4.2. Crystallographic data (excluding structure factors) for the structures reported in this paper have been deposited with the Cambridge Crystallographic Data Centre as supplementary publication no. CCDC-100573.

Table 4.1 X-ray crystal structure data for complexes **1** and **2**.

	1	**2**
Empirical formula	$C_6H_{10}Cl_2N^{15}NPt$	$C_6H_{10}Cl_2N_2Pt$
M_r	377.1	376.1
color	yellow	yellow
crystal size (mm)	$0.47 \times 0.39 \times 0.25$	$0.43 \times 0.08 \times 0.08$
crystal shape	block	needle
crystal system	monoclinic	orthorhombic
space group	$P2_1/c$	$Pbca$
a (Å)	9.859 (2)	12.287(8)
b (Å)	8.910 (2)	7.318(8)
c (Å)	11.197 (2)	20.801(14)
β (°)	102.684 (15)	90
V (Å^3)	959.6 (3)	1871(3)
Z	4	8
λ (Å)	0.71073	1.54178
T (K)	220(2)	220(2)
ρ_{calcd} (g cm^{-3})	2.604	2.420
μ_{calcd} (mm^{-1})	15.119 ($Mo_{K\alpha}$)	30.166 ($Cu_{K\alpha}$)
F(000)	688	1240
2θ range (°)	5.9-50	8.5-140
abs. Correction ($T_{min/max}$)	ψ-scans (0.0033/0.0175)	Shelxa (0.0263/0.4036)
refl. Collected	3725	4662
unique refl.	1688 (R_{int}=0.0358)	1672 (R_{int}=0.0560)
refl. Used	1684	1670
parameters	102	101
$R1$ ($F_0>4\sigma(F_0)$) [a]	0.0355	0.0437
$wR2$ (all data) [b]	0.0903	0.1183
$g1$; $g2$ [c]	0.0596; 0.0000	0.0746; 0.0000
resid. Elec. Density (eÅ^{-3})	+1.52/-1.16	+1.56/-2.72

[a] $R1 = \Sigma(||F_0|-|F_c||)/\Sigma|F_0|$. [b] $wR2 = \{\Sigma[w(F_0^2-F_c^2)^2]/\Sigma[w(F_0^2)^2]\}^{1/2}$.
[c] $w = 1/[\sigma^2(F_0^2)+(g1\times P)^2+g2\times P]$; $P = (F_0^2+2F_c^2)/3$.

Table 4.2 Selected bond lengths (Å) and angles (°) for complexes **1** and **2**.

	1	**2**
Pt-N(1)	2.017(8)	2.008(8)
Pt-N(2)	2.030(8)	2.039(9)
Pt-Cl(1)	2.299(2)	2.296(3)
Pt-Cl(2)	2.322(2)	2.309(3)
N(1)-Pt-N(2)	90.5(3)	90.5(4)
N(1)-Pt-Cl(1)	177.6(2)	177.3(3)
N(2)-Pt-Cl(1)	87.3(2)	86.8(3)
N(1)-Pt-Cl(2)	89.5(2)	90.9(2)
N(2)-Pt-Cl(2)	176.1(3)	178.6(3)
Cl(1)-Pt-Cl(2)	92.70(8)	91.72(10)

NMR Spectroscopy: NMR spectra were recorded on a Bruker DMX500 instrument using 5 mm tubes. All the samples were recorded in 90% H_2O/10% D_2O (0.6 ml), and containing 0.1 M $NaClO_4$ to maintain a constant ionic strength. The chemical shifts are reported relative to sodium trimethylsilyl-[d_4]propanoate (through internal dioxane at 3.743 ppm) for ^1H, and 1 M $^{15}NH_4Cl$ in 1.5 M HCl for ^{15}N (external). Typical acquisition conditions for ^1H spectra were: 45-60° pulses, 2.5 s relaxation delay, 64-256 transients, final digital resolution 0.2 Hz per point. When necessary the water resonance was suppressed by presaturation, or by means of the WATERGATE pulsed-field-gradient sequence.[19]

Both 1D ^{15}N-edited ^1H NMR spectra and 2D [^1H, ^{15}N] HSQC spectra (optimized for $^1J(N,H)$ = 72 Hz) were recorded by using the sequence of Stonehouse *et. al.*[20] The ^{15}N-spins were decoupled by irradiating with the GARP-1 sequence during acquisition.

Data Analysis: For the kinetic analysis of NMR data, the appropriate differential equations were integrated numerically, and the rate constants were determined by a nonlinear optimisation procedure using the programme SCIENTIST (Version 2.01, MicroMath Inc.). The errors represent one standard deviation. Equilibrium constants were calculated from the equilibrium concentrations of species determined by integration of the 2D NMR spectra. The analysis was carried out with the help of Dr. Zijian Guo.

For first-order rate reactions: $A \rightarrow B + C$. Let the initial concentration of A be a mol·dm^{-3}. If after a time t, x mol·dm^{-3} of A has reacted, the remaining concentration of A is $a - x$, and x mol·dm^{-3} of B or C has been formed. The rate of formation of B or C is thus dx/dt. For a first-order reaction this rate is proportional to the instantaneous concentration of A, so that[21]

$$\frac{dx}{dt} = A' = k_1(a - x)$$

For second-order rate equations: $A + B \rightarrow C + D$. Let the initial concentrations at $t = 0$ be a mol·dm^{-3} of A and b mol·dm^{-3} of B. After a time t, x mol·dm^{-3} of A, and of B, will have reacted, forming x mol·dm^{-3} of C and of D. If a second-order rate is followed, then

$$\frac{dx}{dt} = A' = B' = k_2(a - x)(b - x)$$

For the hydrolysis reaction:

$$[Pt(NH_3)(Picoline)Cl_2] + H_2O \rightleftharpoons [Pt(NH_3)(Picoline)(H_2O)Cl]^+ + Cl^-$$

The forward reaction is considered as first order because of the large excess of water, while the back reaction is a second order reaction. For the hydrolysis reaction (scheme 4.1), if at time t, the concentrations of species a, b, c and d are A, B, C and D, respectively, then the corresponding reaction rates are:

$$A' = -k_{1a}\cdot A - k_{1b}\cdot A + k'_{1a}\cdot B\cdot(B+C+D) + k'_{1b}\cdot C\cdot(B+C+D)$$

$$B' = k_{1a}\cdot A - k_{2a}\cdot B + k'_{2a}\cdot D\cdot(B+C+D) - k'_{1a}\cdot B\cdot(B+C+D)$$

$$C' = k_{1b}\cdot A - k_{2b}\cdot C + k'_{2b}\cdot D\cdot(B+C+D) - k'_{1b}\cdot C\cdot(B+C+D)$$

$$D' = k_{2a}\cdot B + k_{2b}\cdot C - k'_{2a}\cdot D\cdot(B+C+D) - k'_{2b}\cdot D\cdot(B+C+D)$$

The above model equations were used in least squares fitting of the NMR data (the change of concentration of each species with time), with a set of initial parameters chosen to perform the simulations.

Scheme 4.1

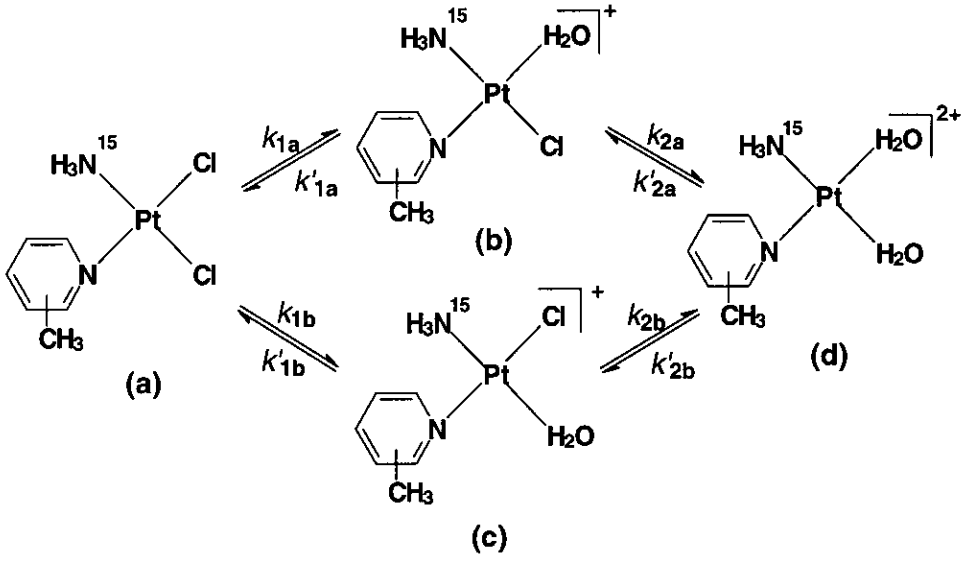

Titration curves were fitted to the Henderson-Hasselbalch equation using the KaleidaGraph numerical analysis programme (Synergy Software, Reading, PA, USA) on a Macintosh computer. The equation is as follows:

$$\delta_{obs} = \{\delta_+[H^+]^n + \delta_0 K_a^n\}/\{[H^+]^n + K_a^n\}$$

where δ_{obs} = observed chemical shift; δ_+ and δ_0 = limiting chemical shift of fully protonated and deprotonated chemical shift, respectively; n = Hill coefficient and K = dissociation constant.

4.4 Results and Discussion

Synthesis of ^{15}N labelled complexes 1 and 2: A solution of *cis*-[Pt($^{15}NH_3$)$_2$Cl$_2$] (100 mg, 0.33 mmol) and tetraethylammoniumchloride·xH_2O (0.065 mg) in

dimethylacetamide (20 ml) was heated to 100 ± 2°C for 6 h. A slow stream of nitrogen was bubbled through the reaction mixture during this period. After the reaction, the orange solution was cooled to room temperature. Ethyl acetate/hexane (90 ml, 1:1 *v/v*) was added and the cloudy reaction mixture was left in the freezer over night at -10°C. A clear, colourless solution and a thick, orange oil was produced after this procedure. The clear solution was discarded and the oil was dissolved in 8ml water. The amminetrichloroplatinate $[Pt(^{15}NH_3)Cl_3]^-$ was used directly in the following reactions.

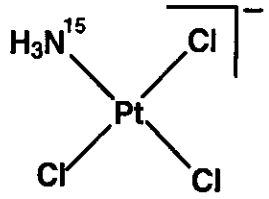

To the solution of amminetrichloroplatinate, KI (166 mg, 0.99 mmol) was added. The reaction mixture was stirred at room temperature for about 10 min to give $[Pt(^{15}NH_3)I_3]^-$, then 32 µl of 2-picoline was added. The reaction mixture was stirred at room temperature for two hours and the yellow precipitate *cis*-$[PtI_2(^{15}NH_3)$(2-picoline)], was collected, washed with cold water and air-dried. Yield: 70.5 mg (37.8%).

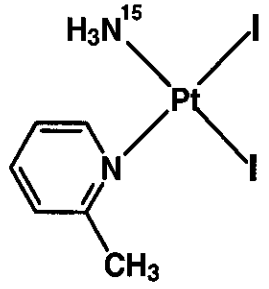

Cis-$[PtI_2(^{15}NH_3)$(2-picoline)] (70.5 mg, 1.26×10^{-4} mmol) was suspended in water (10 ml) with $AgNO_3$ (41.8 mg) and stirred in the dark for about 20 hours. The yellow/green precipitate was removed by filtration and the remaining *cis*-$[Pt(^{15}NH_3)$(2-picoline)$(H_2O)_2]^{2+}$ was stirred with an excess KCl for about 2 hours.

The yellow precipitate *cis*-[$PtCl_2(^{15}NH_3)$(2-picoline)] was collected by filtration and washed with cold water. Yield: 35 mg (27%).

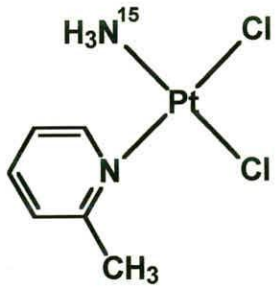

Element analysis calculated for $C_6H_{10}Cl_2N^{15}NPt$: C, 19.1%; H, 2.65%; N, 7.69%. Found: C, 19.28%; H, 2.97%; N, 7.57%. ^{1}H NMR: δ = 8.87 (d, J = 8 Hz, 1H, H-6), 7.81 (m, 1H, H-4), 7.49 (d, J = 8 Hz, 1H, H-3), 7.32 (m, 1H, H-5), 3.13 (s, 3H, CH_3).

Complex **2**, *cis*-[$PtCl_2(^{15}NH_3)$(3-picoline)], was prepared in the same way. The result of element analysis was: C, 18.82%; H, 2.70%; N, 7.31%. ^{1}H NMR: δ = 8.62 (s, 1H, H-2), 8.54 (d, J = 6 Hz, 1H, H-6), 7.77 (d, J = 9 Hz, 1H, H-4), 7.37 (m, 1H, H-5), 2.35 (s, 3H, CH_3).

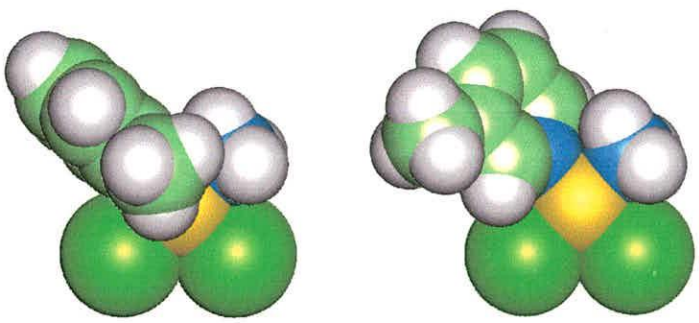

1 **2**

Figure 4.1 X-ray crystal structures of complexes **1** and **2** showing the steric hindrance caused by the 2-methyl group in complex **1**. Colour code: H (white), C (pale green), N (blue), Cl (bright green), Pt (yellow).

X-ray crystal structures: Both ^{15}N-labeled and unlabelled complexes **1** and **2** were prepared, and pale yellow crystals for X-ray analysis were obtained after slowly cooling the filtrate. As can be seen in Figure 4.1, both complexes have a square-planar configuration with angles close to the ideal values of 90° and 180°. In complex **1**, the Pt-Cl(2) bond *trans* to NH_3 is slightly longer (2.322(2) Å) than normal, while the Pt-Cl(1) bond distance (2.299(2) Å) is within the normal range. In complex **2** both Pt-Cl bond lengths (2.296(3) Å, 2.309(3) Å) are close to the expected values. The Pt-N(1) bond lengths in both complexes **1** (2.017(8) Å) and **2** (2.008(8) Å) are comparable to those of *cis*-$[Pt(Py)_2Cl_2]$ (2.01 and 2.04 Å).[22] The most notable feature of the structures is the orientation of the picoline ring with respect to the Pt square-plane. The 3-picoline ligand is tilted by 48.9°, whereas the 2-picoline ligand is almost perpendicular (102.7°) to the plane, so that the 2-methyl group lies directly over the square-plane (H_3C···Pt: 3.224 Å). The space-filling model (Figure 4.1) demonstrates that this introduces steric hindrance to an axial approach to Pt from above. The steric effect leads to a slight twisting of the $[PtN_2Cl_2]$ square plane, with a mean deviation of the atoms from the plane of 0.0406 Å, which is an order of magnitude higher than that for complex **2**.

There are strong intermolecular hydrogen-bonds involved in the crystal packing of both complexes (Figure 4.2). For complex **1,** the three H atoms of the NH_3 ligand are H-bonded to four Cl ligands from two neighbouring molecules, while for complex **2,** H-bonds of similar strength are formed only to three of the four Cl ligands. Such intermolecular H-bonds are common in chloro Pt(II) am(m)ine complexes.[23,24] A very weak graphitic-type of interaction between the picoline groups of neighbouring molecules of **1** may also be present. In complex **1,** layers containing Cl···H-N H-bonding interactions alternate with layers containing picoline groups. In

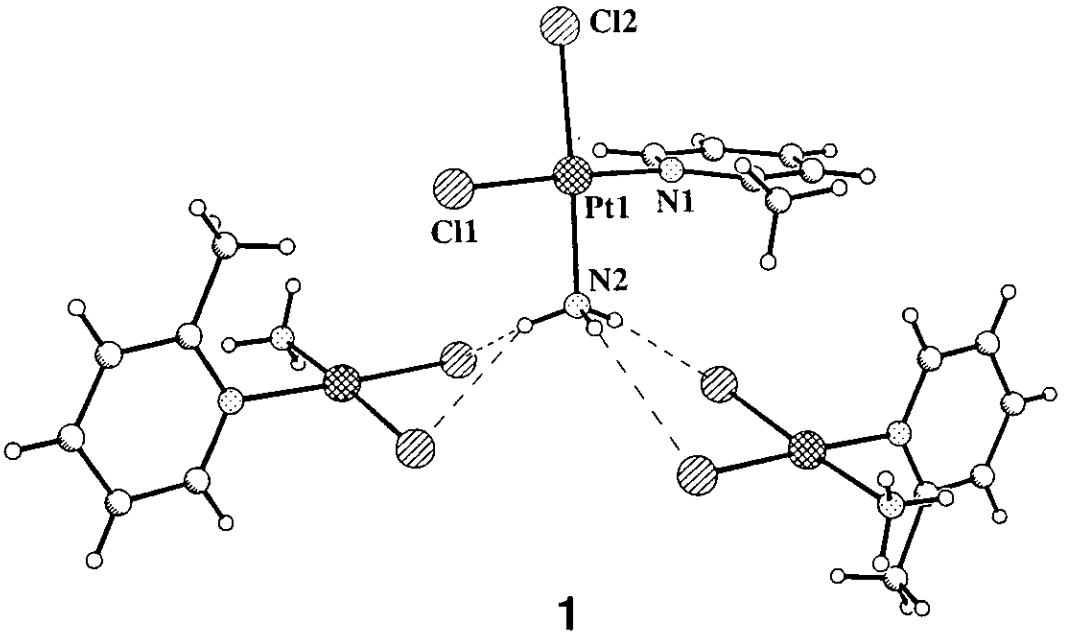

1

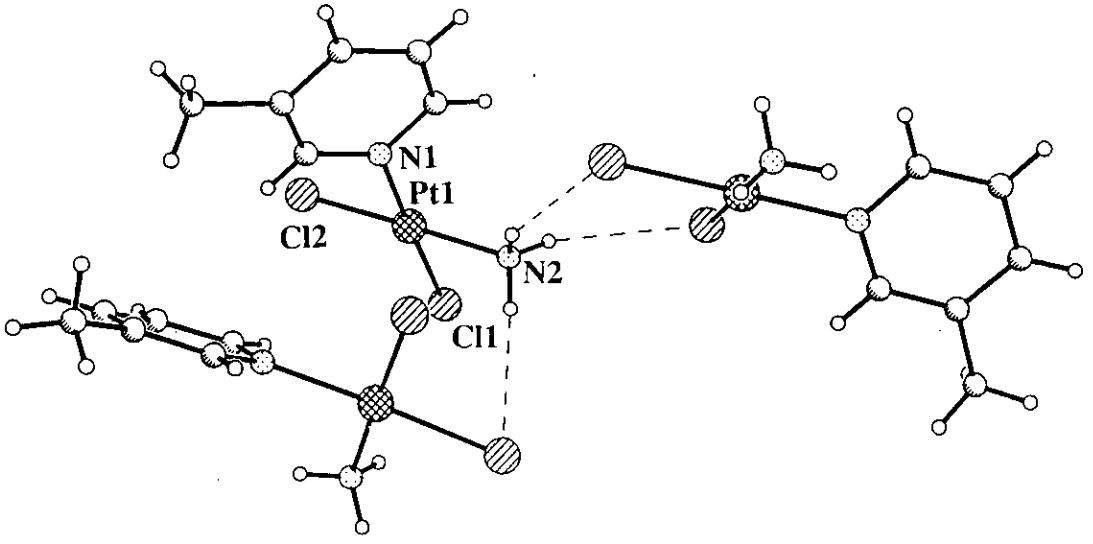

2

Figure 4.2 Intermolecular hydrogen bonding in crystals of (**A**) complex **1**, and (**B**) complex **2**; N–H• • •Cl distances for complex **1** range from 2.55 Å to 2.74 Å and for complex **2** from 2.62 Å to 2.81 Å.

complex **2**, the molecules themselves form layers, with H-bonds both within and between layers.

Hydrolysis: The [^{1}H, ^{15}N] 2D NMR spectra of $^{15}NH_3$-labelled **1** and **2** in aqueous solutions containing 0.1 M $NaClO_4$ were each monitored for a period of over 20 h at 310 K. Initially a single cross-peak was observed at 4.15/-66.52 ppm assignable to the dichloro complex **1**. After 1 h, two additional cross-peaks with similar intensities were detected at 4.40/-64.41 ppm and 4.32/-87.25 ppm. The former peak is consistent with an assignment to complex **3a**, with an ^{15}N shift diagnostic of ^{15}N *trans* to N or Cl,[25] and the latter to **3b** with ^{15}N *trans* to O, Scheme 4.2. Both peaks increased in intensity for several hours, while the peak for **1** decreased in intensity. After about 2.5 h, a fourth cross-peak appeared at 4.41/-82.91 ppm. This was assigned to the diaqua complex **5** (Figure 4.3A); however, even after 20 h, this accounted for only <10% of the total $^{15}NH_3$-Pt species present.

For the 3-picoline complex **2**, the time-dependence of the [^{1}H, ^{15}N] 2D NMR spectrum was similar to that of complex **1**, except that the cross-peak **c** (Figure 4.3B) assignable to one of the two monoaqua complexes was more intense than the other. The ^{15}N chemical shifts for the peaks of the 3-picoline complexes are shifted slightly to lower field with respect to those of the 2-picoline adducts. However, the ^{1}H chemical shifts are very similar. The time-dependence of the concentrations of species detected during hydrolysis of complexes **1** and **2** is shown in Figures 4.3C and 3D. The assignments of the peaks for the aqua complexes were confirmed by pH titrations, Figure 4.4, and these allowed the determination of pK_a value for each monoaqua complex as well as two pK_a values for each diaqua complex, Scheme 4.2.

The NMR data allow the determination of the hydrolysis rates for each individual chloride ligand in the initial complexes **1** and **2,** and in the monoaqua complexes **3a, b** and **4a, b** (Table 4.3). It is notable that the hydrolysis rates of the

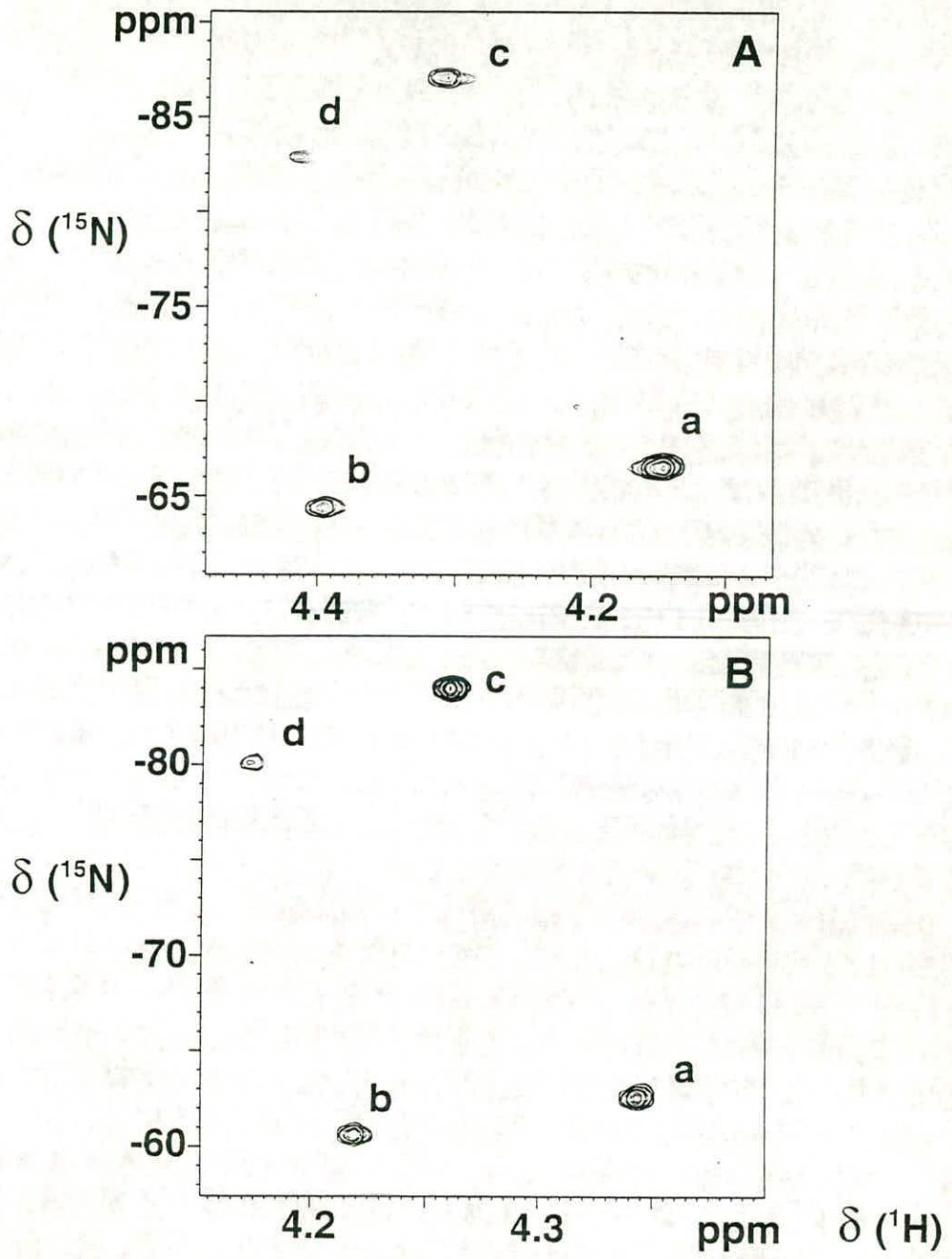

Figure 4.3 2D [^{1}H,^{15}N] HSQC NMR spectra of 2 mM aqueous solutions of (**A**) *cis*-[$PtCl_2$($^{15}NH_3$)(2-picoline)] (**1**), and (**B**) *cis*-[$PtCl_2$($^{15}NH_3$)(3-picoline)] (**2**) after 3 h at 310 K. Peak **a** is assigned to the starting complex, peaks **b**, **c** to the two monoaqua complexes (H_2O *cis* to NH_3 and H_2O *trans* to NH_3, respectively), and peak **d** to the diaqua complex. Time dependence of the concentrations of the dichloro complexes and aqua adducts are shown in (**C**) of **1** and (**D**) of **2**, respectively. Labels: **1** and **2** (■), monoaqua complexes **3a** and **4a** (▲), monoaqua complexes **3b** and **4b** (●), diaqua complexes **5** and **6** (+). The curves are the computer best fits calculated with the rate constants shown in Table 4.3.

Figure 4.3 (C) and (D)

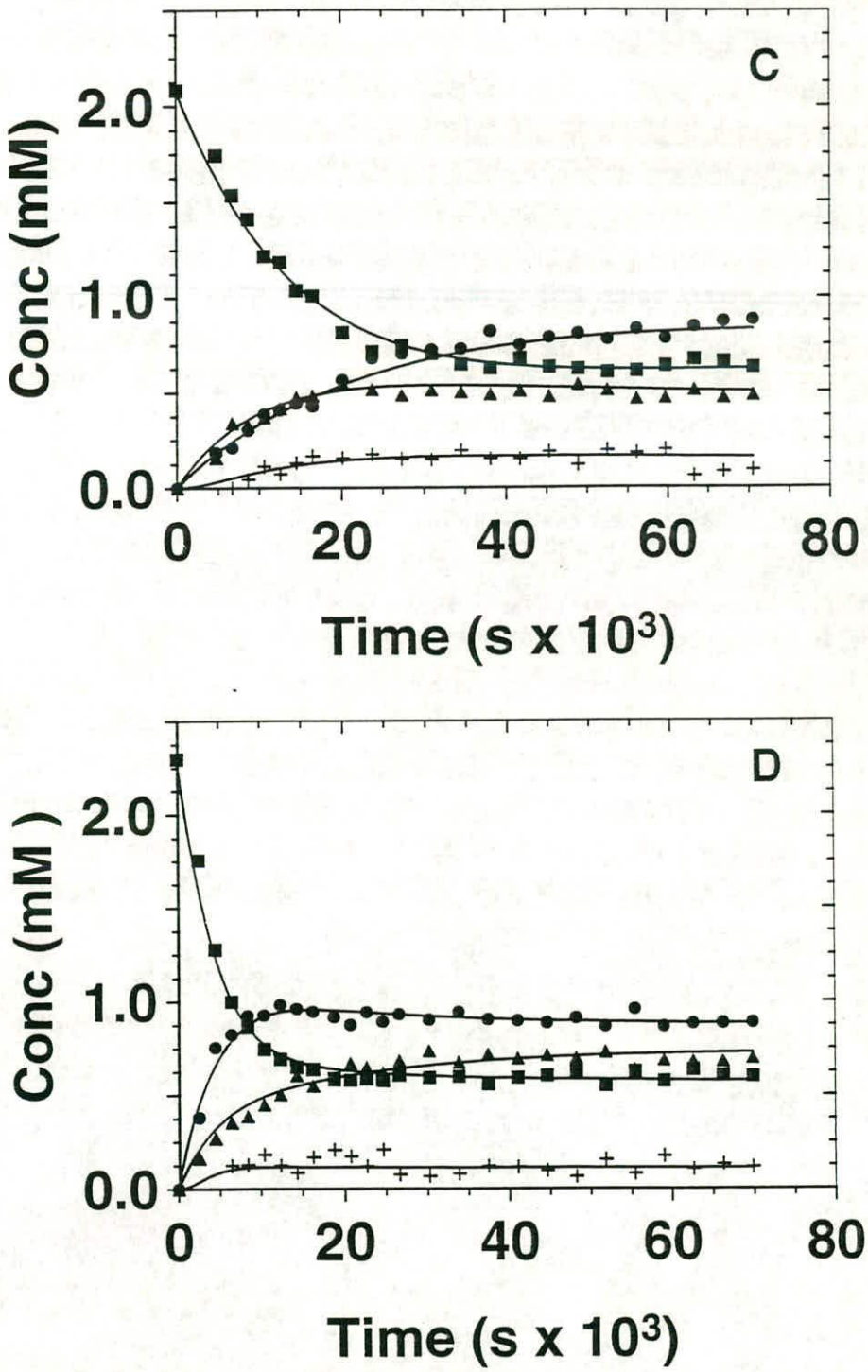

Scheme 4.2. Comparison of half-lives for hydrolysis (310 K) and pK_a values (298 K) of platinum-picoline complexes (0.1 M $NaClO_4$).

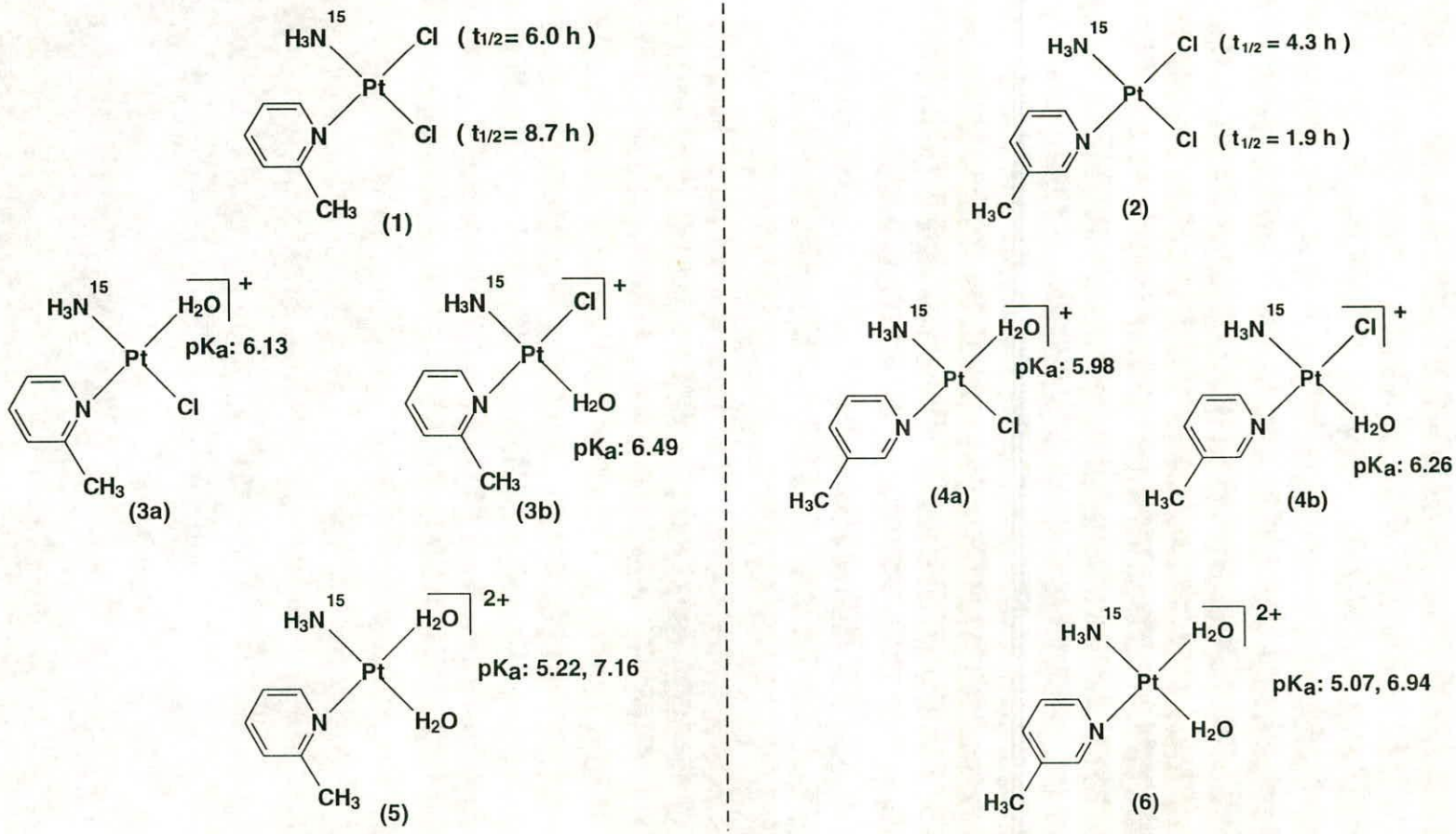

Table 4.3 Rate and equilibrium constants for the hydrolysis of the platinum-picoline complexes **1** (pH = 4.6) and **2** (pH = 4.4) at 310 K (0.1 M $NaClO_4$). Data reported for cisplatin under related conditions (308 K, 0.32 M KNO_3) are listed for comparison.

Compounds	Rate constants [a] ($\times 10^{-6}$ s^{-1})	Equilibrium constants [b] ($\times 10^{-4}$ M)
1 2-picoline	k_{1a}: 31.9 ± 1.5 k_{1b}: 22.1 ± 1.4 k_{2a}: 73 ± 14 k_{2b}: 3.5 ± 2.5	K_{1a}: 12.1 K_{1b}: 21.4 K_{2a}: 4.8 K_{2b}: 2.7
2 3-picoline	k_{1a}: 44.7 ± 1.9 k_{1b}: 103 ± 4 k_{2a}: 35.0 ± 1.7 k_{2b}: 78 ± 60	K_{1a}: 23.2 K_{1b}: 28.0 K_{2a}: 2.8 K_{2b}: 2.3
cisplatin[c]	k_1: 75.9	K_1: 43.7

[a]: The errors in the rates for the second hydrolysis step are large because the fitting process is relatively insensitive to the rate of the back reaction. Hence these constants are not discussed in the text.

[b]: Constants correspond to kinetic steps indicated, *i.e.*, K_{1a} to equilibrium between **1** (or **2**) and **3a** (or **4a**), *etc.*

[c]: Ref 18.

two Cl^- ligands of complex **1** are both slower than those for complex **2** (Table 4.3). The Cl^- ligand *trans* to NH_3 in complex **1** hydrolyses about four times more slowly than that in the unhindered complex **2**. In complex **2,** the Cl^- ligand *trans* to NH_3 hydrolyses about twice as fast as that *trans* to 3-picoline. This might be expected from the higher *trans* influence of NH_3 (pK_a=9.29) versus 3-picoline (pK_a=6.0).[26] However, for complex **1**, the situation is reversed: hydrolysis is faster for the Cl^- ligand *trans* to 2-picoline (pK_a=6.1).[26] All the first step hydrolysis rates determined here are slower than that of cisplatin ($t_{1/2}$: 1.75 h at 310 K).[13]

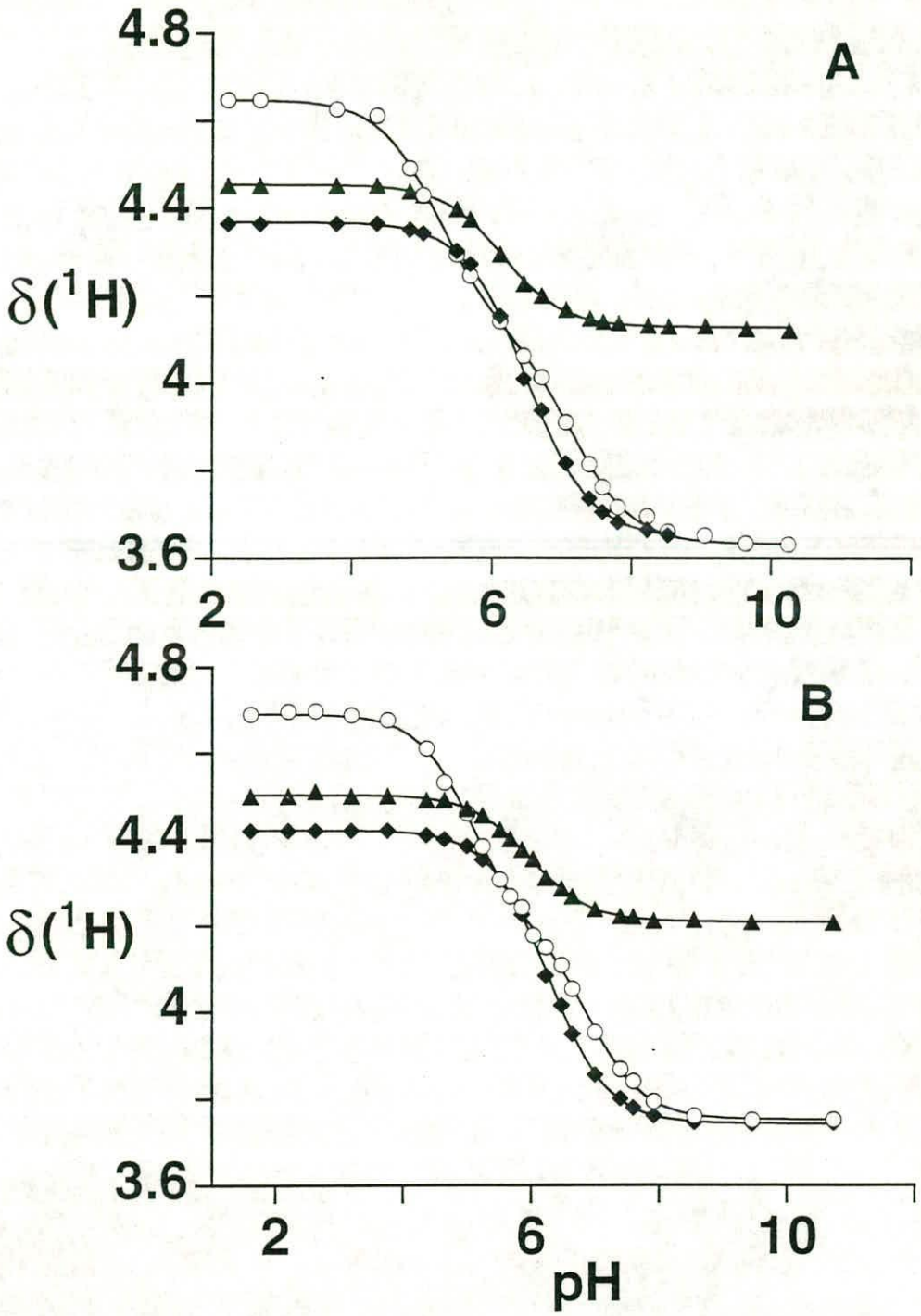

Figure 4.4 pH dependence of the ^1H NMR chemical shifts of NH_3 in the monoaqua complexes and diaqua complexes: (**A**) complex **1**, and (**B**) complex **2**. The curves represent the computer best fits using the pK_a values listed in Scheme 4.2. Labels: monoaqua complexes **3a** and **4a** (▲), monoaqua complexes **3b** and **4b** (◆), diaqua complexes **5** and **6** (O).

Axial steric interactions have long been known to decrease the rate of substitution reactions of square-planar complexes.[27,28] For example, the rate of reaction of 2-picoline with $[AuCl_4]^-$ is about 9 times slower than with 3-picoline, but 10 times faster than with 2,6-dimethylpyridine which blocks both axial sites. In the complexes *cis*-$[Pt(PEt_3)_2(R)Br]$, the rate of displacement of Br^- by MeOH decreases dramatically as the steric hindrance by the aryl ligand R, which is *cis* to the leaving group, increases: Ph ≈ *p*-MeC_6H_4 >> *o*-MeC_6H_4 > *o*-EtC_6H_4 > 2,4,6-$Me_3C_6H_2$.[29] In an associative mechanism with a trigonal-bipyramidal transition state, the ligands *cis* to the leaving group become axial to the trigonal plane in the 5-coordinate transition state, and interact with the entering and leaving groups at a 90°, so that the steric effect is more prominent on the ligand in the position *cis* to the bulky ligand.

pK_a values: A change of the methyl group from the 2- to the 3-position only has a small effect on the pK_a values of the aqua ligands, lowering them by *ca.* 0.2 units (Scheme 4.2). The pK_a values for both the monoaqua and diaqua adducts of the 2-picoline and 3-picoline complexes are >0.3 units lower than that of cisplatin. This means that although the sterically-hindered 2-picoline complex **1** will exist predominately (about 70%) as a dichloro adduct under extracellular conditions (0.1 M Cl^-, pH 7.4), under intracellular conditions (4 mM Cl^-, pH 7.4), the hydroxo/chloro and dihydroxo adducts of **1** will predominate (>70%), whereas for cisplatin the dichloro, chloro/aqua and chloro/hydroxo are present in about equal proportions (about 30% each).[30] The slowness of the hydrolysis steps of complex **1** (Table 4.3) coupled with the dominance of (inert) hydroxo species would both be expected to contribute to its greatly reduced reactivity under intracellular conditions.

4.5 Conclusions

The Cl^- ligand *cis* to 2-picoline (*trans* to NH_3) in the complex *cis*-[$PtCl_2(NH_3)$(2-picoline)] (**1**) hydrolyses about 4 times more slowly than that in cisplatin ($t_{1/2}$: 8.7 h at 310 K, compared with 1.8 h for cisplatin), and both Cl^- ligands of **1** hydrolyse more slowly than the 3-picoline analogue **2**. X-ray crystallography has confirmed the steric hindrance introduced by the 2-methyl group of the picoline ligand in **1**, which has the effect of destabilising the expected trigonal-bipyramidal transition state, an effect well-known in substitution reaction of square planar Pt(II) complexes.[27] The pK_a values of the monoaqua and diaqua adducts of both **1** and **2** are >0.3 units lower than those similar cisplatin adducts. This, combined with slower hydrolysis (Table 4.3), is likely to result in a reduced intracellular activity of complex **1** compared to cisplatin and may contribute to its high activity against cisplatin-resistant cell lines. Studies of reactions of complexes **1** and **2** with guanosine 5′-monophosphate (5′-GMP) were also made, which is reported in the next chapter, and have established that hydrolysis is the rate-limiting step for both complexes **1** and **2**. The formation of the bis-GMP adduct of complex **1** is about twice as slow as that for complex **2**, which is consistent with the brief report that complex **1** forms DNA cross-links extremely slowly.[8] Further NMR studies should allow a detailed insight to be gained into the effect of steric hindrance on the formation of DNA adducts.

4.6 References

[1] *Platinum and Other Metal Coordiantion Compounds in Cancer Chemotherapy* 2, (Eds.: H.M. Pinedo, J.H. Schornagel), Plenum Press, New York, **1996**.

[2] J. Reedijk, *Chem. Comm.*, **1996**, 801.

[3] M. Vanbeusichem, N. Farrell, *Inorg. Chem.*, **1992**, *31*, 634.

[4] M. Cusumano, M. L. Di Pietro, A. Giannetto, *Chem. Commun.*, **1996**, 2527.

[5] L. S. Hollis, W. I. Sundquist, J. N. Burstyn, W. J. Heigerbernays, S. F. Bellon, K. J. Ahmed, A. R. Amundsen, E. W. Stern, S. J. Lippard, *Cancer Res.* **1991**, *51*, 1866.

[6] Y. Zou, B. Van Houten, N. Farrell, *Biochemistry*, **1993**, *32*, 9632.

[7] B. A. Murrer, *Eur. Patent Appl.* EP 0 727 430 A1, Bulletin 34, **1996**.

[8] F. Raynaud, F. Boxall, P. Goddard, M. Valenti, M. Jones, B. A. Murrer, M. Abrams, L. R. Kelland, *Clin. Cancer Res.* **1997**, *3*, 2063.

[9] J. Holford, S. Y. Sharp, B. A. Murrer, M. Abrams, L. R. Kelland, *Br. J. Cancer* **1998**, *77*, 366.

[10] L. R. Kelland, G. Abel, M. J. McKeage, M. Jones, P. M. Goddard, M. Valenti, B. A. Murrer, K. R. Harrap, *Cancer Res.* **1993**, *53*, 2581.

[11] J. R. Perumareddi, A. W. Adamson, J. Phys. Chem. 1978, 72, 414.

[12] R. N. Bose, R. D. Cornelius, R. E. Viola, *J. Am. Chem. Soc.* **1986**, *108*, 4403.

[13] S. E. Miller, D. A. House, *Inorg. Chim. Acta*, **1989**, *161*, 131; S. E. Miller, D. A. House, *Inorg. Chim. Acta*, **1989**, *166*, 189; S. E. Miller, D. A. House, *Inorg. Chim. Acta*, **1990**, *173*, 53; S. E. Miller, D. A. House, *Inorg. Chim. Acta*, **1991**, *187*, 125; S. E. Miller, K. J. Gerard, D. A. House, *Inorg. Chim. Acta*, **1991**, *190*, 135.

[14] S. J. Berners-Price, T. A. Frenkiel, U. Frey, J. D. Ranford, P. J. Sadler, *J. Chem. Soc., Chem. Commun.* **1992**, 789.

[15] T. G. Appleton, J. R. Hall, S. F. Ralph, C. S. M. Thompson, *Inorg. Chem.* **1989**, *28*, 1989.

[16] J. Holford, F. Raynaud, B. Murrer, K. Grimaldi, J. A. Hartley, M. Abrams, L. R. Kelland, *Anti-Cancer Drug Design*, **1998**, *13*, 1.

[17] S. J. S. Kerrison, P. J. Sadler, *J. Chem. Soc., Chem. Commun.*, **1977**, 861.

[18] S. J. Barton, K. J. Barnham, A. Habtemariam, P. J. Sadler, R. E. Sue. *Inorg. Chim. Acta*, **1998**, *273*, 8.

[19] M. Piotto, V. Saudek, V. Sklenar, *J. Biomol. NMR,* **1992**, *2*, 661.

[20] J. Stonehouse, G. L. Shaw, J. Keeler, E. D. Laue, *J. Magn. Reson. Ser. A,* **1994**, *107*, 178.

[21] W. J. Moore, in "Physical Chemistry", fifth edition, Longman Group Limited, 1981.

[22] P. Colamarino, P. L. Orioli, *J. Chem. Soc. Dalton Trans,* **1975**, 1656.

[23] G. H. W. Milburn, M. R. Truter, *J. Chem. Soc. (A)*, **1966**, 1609.

[24] E. G. Talman, W. Brüning, J. Reedijk, A. L. Spek, N. Veldman, *Inorg. Chem.*, **1997**, *36*, 854.

[25] S. J. Berners-Price, P. J. Sadler, *Coord. Chem. Rev.*, **1996**, *151*, 1.

[26] G. Pettit, L. D. Pettit, *IUPAC Stability Constants Database*, IUPAC and Academic Software, Otley, United Kingdom, **1993**.

[27] F. Basolo, J. Chatt, H. B. Gray, R. G. Pearson, B. L. Shaw, *J. Chem. Soc.*, **1961**, 2207.

[28] L. Cattalini, F. Guidi, M. L. Tobe, *J. Chem. Soc. Dalton Trans,* **1993**, *2*, 233.

[29] R. Romeo, D. Minniti, M. Trozzi, *Inorg. Chem.* **1976**, *15*, 1134.

[30] A. F. LeRoy, R. T. Lutz and R. L. Dedrick, *Cancer Treatment Rep.*, **1979**, *63*, 59.

Chapter 5

Kinetic Control of Reactions of a Sterically-hindered Platinum Picoline Anticancer Complex with Guanosine 5´-monophosphate and Glutathione

5.1 Abstract

Kinetic studies (296 K, 0.1 M $NaClO_4$, pH 6-7) of reactions of the anticancer complex *cis*-[$PtCl_2(NH_3)$(2-picoline)] (**1**) (ZD0473) with guanosine 5′-monophosphate (5′-GMP) and the tripeptide glutathione (GSH) using 2D [^1H, ^{15}N] HSQC NMR spectroscopy are reported, and compared to reactions of the isomeric complex *cis*-[$PtCl_2(NH_3)$(3-picoline)] (**2**). Reactions with 5′-GMP followed two pathways with either hydrolysis *trans* to NH_3 or picoline as the first step, with subsequent formation of Cl/GMP and H_2O/GMP intermediates, and *cis*-[$Pt(^{15}NH_3)$(picoline)(5′-GMP-*N7*)$_2$]$^{2+}$ as the final product. Eight rate constants were determined for each starting Pt complex **1** and **2**. The rates of ligand substitution (Cl^- by H_2O and H_2O by 5′-GMP) *cis* to 2-picoline were 2-12 times slower than the same ligand substitution *cis* to 3-picoline. This was also the case for ligand substitution *trans* to 2-picoline (2-3 times slower), except that when 5′-GMP was present as the *cis* ligand (second stage of substitution) the rate of substitution was enhanced for the 2-picoline complex. Slow rotation about the Pt-N picoline bond (0.62 s^{-1}) and fast rotation about Pt-N7 GMP bonds on the NMR time scale were observed at 296 K for the bisGMP adduct of complex **1**, while these were both fast for the analogous adduct of complex **2**. Reactions of GSH with **1** were *ca* 3 times slower than those with **2**, and appeared to proceed *via* aquated intermediates with initial substitution *trans* to 2-picoline for **1** and *trans* to NH_3 for **2**, but no kinetic analyses were attempted due to the complexity of the reactions. Both mono- and bis-GMP adducts were observed during competitive reactions of GSH and 5′-GMP with complex **1** (molar ratio: 2:2:1) at pH 7, 296 K. These features of the chemistry of **1** may play an important role in its altered spectrum of biological activity compared to cisplatin.

5.2 Introduction

Cisplatin, *cis*-$[PtCl_2(NH_3)_2]$, is a widely-used anticancer drug. Because of its serious toxic side-effects and the spontaneous development of drug resistance in tumours, there is a need for new drugs which circumvent these drawbacks. Investigations have been made of the activity of many other platinum complexes, most of which belong to the structural class *cis*-$[PtAm_2X_2]$ (X = anionic leaving group; Am = ammonia, primary or secondary amine).[1] An exception is the 2-picoline (2-methylpyridine) complex *cis*-$[PtCl_2(NH_3)$(2-picoline)] (**1**) (ZD0473), which is currently in phase I clinical trials.[2,3] It possesses activity against cisplatin-resistant cell lines and against an acquired cisplatin-resistant subline of a human ovarian carcinoma xenograph both by injection and by oral administration.[2] It appears to circumvent thiol-mediated resistance mechanisms whilst still maintaining the ability to form cytotoxic lesions with DNA.[3,4]

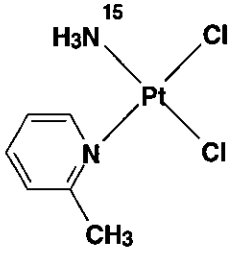

(1)

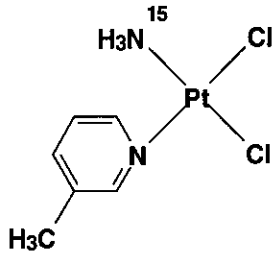

(2)

In order to gain an understanding of the chemical reactivity of this complex, investigation has been made with its X-ray crystal structure and hydrolysis behaviour in comparison with the isomeric 3-picoline complex *cis*-$[PtCl_2(NH_3)$(3-picoline)] (**2**).[5] The most notable feature of the structures is the orientation of the picoline ring with respect to the Pt square-plane. The 2-picoline ligand is almost perpendicular (103°) such that the 2-methyl group lies directly over the square-plane, while the 3-picoline ligand is tilted by 49°. This steric effect plays an important role in determining the hydrolysis rates of the Cl^- ligands. For complex **2,** the rate of hydrolysis of Cl^- *trans* to NH_3 is similar to that of cisplatin ($t_{1/2}$ = 1.75 h, 310 K),[6] while for complex **1** the rate of hydrolysis for the Cl^- ligand *trans* to NH_3 (*cis* to 2-picoline) is about 5 times slower ($t_{1/2}$ = 8.7 h). The slow hydrolysis of **1** can be

attributed to the axial steric hindrance provided by the 2-methyl group. Complex **1** appears to form interstrand DNA cross-links and to bind to plasma proteins much more slowly than cisplatin.[7]

Besides steric effects, electronic factors may also play a role in determining the reactivity of pyridine complexes. For example the presence of planar pyridine ligands in *cis*- or *trans*-[$PtCl_2$(pyridine)$_2$] complexes can reduce the rates of DNA binding compared to ammine complexes.[8] DNA platination is a key event in the mechanism of action of platinum anticancer drugs, and the major adduct formed by attack of cisplatin on DNA is the intrastrand cross-link between N7 atoms of two adjacent guanine (G) residues.[1] In a DNA duplex helix, GN(7) is not involved in *Watson-Crick* base pairing and is exposed in the major groove.

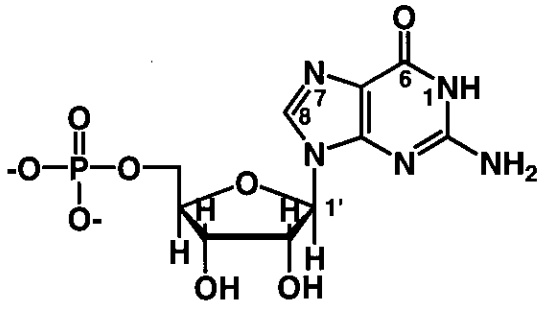

5′-GMP

Guanosine 5′-monophosphate has been widely used to model Pt-DNA interactions. There are several possible metal-binding sites on 5′-GMP, which include: the five nitrogen atoms (each of which has a formal lone pair of electrons) and the carbonyl oxygen atom (in the case of guanine). However N(7) is the preferred binding site because it has a 'directed', sp^2-hybridized lone pair and the site is less sterically crowded. In typical *cis*-PtA_2G_2 adducts, the appearance of one time-averaged set of signals in the ^{1}H-NMR spectrum indicates that rotation about the Pt-N(7) bond is fast on the NMR time scale.[9] However, bulky ligands (A_2) can slow the

rotation about the Pt-N(7) bond, permitting the observation of rotamers which are evident from the appearance of multiple sets of ^{1}H-NMR signals.[10,11]

Besides nucleotides, platinum can also interact with many other biomolecules, especially those containing methionine and cysteine residues. Glutathione (GSH), a cysteine-containing tripeptide (γ-L-Glu-L-Cys-Gly), is the predominant intracellular

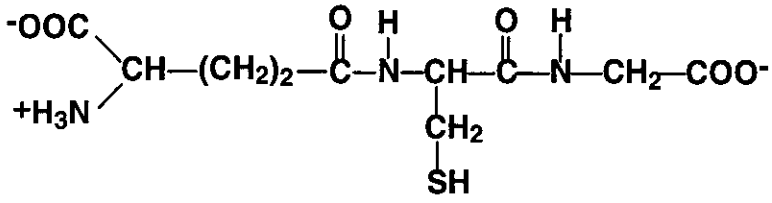

Glutathione (GSH)

thiol with concentrations typically ranging from 0.5 to 10 mM. It has a variety of physiologically important functions in cellular defence and metabolism, and also interacts with a wide range of drugs. GSH can quench DNA-platinum monoadducts before their conversion to cytotoxic DNA cross-links,[12] or it may form complexes with cisplatin, thereby reducing the amount of intracellular cisplatin available for interaction with DNA.[13] Reactions of thiols with Pt complexes are considered to be responsible for drug inactivation and the development of drug resistance.[14] The cytotoxicity of cisplatin has been shown to be enhanced by depletion of cellular GSH in some tumour cells. GSH is over-expressed in cisplatin-resistant cells and the Pt-GS adducts can be pumped out of cells through a novel ATP dependent *GS-X* pump.[15,16] At physiological pH, Pt(II) complexes usually show a kinetic preference for the thiols cysteine and glutathione over 5′-GMP, even in the presence of excess nucleotide.[17]

In this work, the reactions of complex **1** and the less-hindered isomeric complex **2** with 5′-GMP and glutathione (GSH) have been investigated by both 1D

^{1}H and 2D [^{1}H, ^{15}N] HSQC NMR spectroscopy, in order to study the influence of both steric and electronic effects on reactions of potential biological importance.

5.3 Experimental

Materials

2-, 3-Picoline and GSH were purchased from Aldrich. The sodium salt of 5′-GMP was obtained from Sigma. *Cis*-[$PtCl_2(^{15}NH_3)_2$] was prepared according to the reported procedure.[18] ^{15}N labelled complexes **1** and **2** were prepared from *cis*-[$PtCl_2(^{15}NH_3)_2$] as described in Chapter 4. The *cis*-[$Pt(NH_3)$(2-picoline)$(H_2O)_2]^{2+}$ was prepared in situ by addition of slightly less than 2 mol equiv of $AgNO_3$ to an aqueous solution of complex **1**. The solution was stirred in dark for 24 hours and followed by removal of the AgCl precipitate using centrifuge.

NMR spectroscopy

NMR spectra were recorded on a Bruker DMX500 NMR spectrometer operating at 500.13 MHz using a TBI probehead. All data processing, including the integration routines described below, was carried out using XWIN-NMR version 1.3 (Bruker Spectrospin Ltd.). The chemical shift references were as follows: dioxane (internal, 3.767 ppm) for ^{1}H, and 1 M $^{15}NH_4Cl$ in 1.5 M HCl for ^{15}N (external). All spectra were recorded at 296 K unless otherwise stated. Typical acquisition conditions for ^{1}H spectra were: 45-60° pulses, 2.5 s relaxation delay, 64-256 transients, final digital resolution 0.2 Hz per point. The water resonance was suppressed by presaturation, or *via* the WATERGATE pulsed-field-gradient sequence.[19] 2D [^{1}H, ^{15}N] HSQC NMR spectra (optimised for $^{1}J_{(NH)}$ = 72 Hz) were recorded by using the sequence of Stonehouse *et. al.*[20] The ^{15}N-spins were decoupled by irradiating with the GARP-1 decoupling sequence during acquisition. The 2D exchange experiment was performed using phase-sensitive nuclear Overhauser effect spectroscopy (NOESY)

with a mixing time 1 s, at 296 K. Rates were calculated using the program D2DNMR kindly supplied by Dr. K.G. Orrell.[21] Inputs for each calculation consisted of volume integrals from diagonal- and cross-peaks together with population estimates based on 1D ^{1}H NMR spectra.

All samples were in 90%H_2O/10%D_2O (0.6 ml). The reactions of complexes **1** or **2** (3 mM) with 5′-GMP were conducted at a 1:2 molar ratio. Samples contained 0.1 M $NaClO_4$ to maintain a constant ionic strength. Buffer was not used in the reactions of complexes **1** and **2** with 5′-GMP in order to avoid possible interference with the reactions, and the pH values were adjusted to 6.85 and 6.55 (for complexes **1** and **2**, respectively) at the beginning of the reaction. The pH value for the reaction of *cis*-$[Pt(NH_3)(2\text{-picoline})(H_2O)_2]^{2+}$ with 5′-GMP (1:2) was adjusted to 6.47. In the reactions of complex **1** or **2** with GSH (3 mM, 1:1 molar ratio), 100 mM phosphate buffer (pH = 7) was used. Competitive reactions between 5′-GMP and GSH with complexes **1** or **2** (2 mM) were carried out at 2:2:1 molar ratios, with 100 mM phosphate buffer present to maintain neutral pH. After mixing, argon was bubbled through the solution to minimise GSH oxidation and the NMR samples were carefully sealed.

pH measurements

These were made using a Corning 145 pH meter equipped with an Aldrich micro combination electrode calibrated with Aldrich buffer solutions of pH 4, 7 and 10. Values of pH were adjusted with 1 M $HClO_4$ or NaOH as appropriate.

Kinetic measurements

For kinetic analysis of NMR spectra, peak volumes were measured and the relative concentrations of each species were calculated at each time point. The appropriate differential equations were integrated numerically, and the rate constants were

determined by a non-linear optimization procedure using the program SCIENTIST (version 2.01, MicroMath Inc.). The errors represent one standard deviation.

For reaction of complexes **1** or **2** with 5′-GMP (shown in Scheme 5.1), and assuming that at time *t*, the concentrations of species a, b, c, d, e, f, g, h are A, B, C, D, E, F, G and H, respectively. Then the corresponding reaction rates are:

$A' = -k_1 \cdot A - k_2 \cdot A + k'_1 \cdot B \cdot (B+C+D+E+2F+2G+2H) + k'_2 \cdot C \cdot (B+C+D+E+2F+2G+2H)$

$B' = k_1 \cdot A - k_3 \cdot B \cdot (2A_0-D-E-F-G-2H) - k'_1 \cdot B \cdot (B+C+D+E+2F+2G+2H)$

$C' = k_2 \cdot A - k_4 \cdot C \cdot (2A_0-D-E-F-G-2H) - k'_2 \cdot C \cdot (B+C+D+E+2F+2G+2H)$

$D' = k_3 \cdot B \cdot (2A_0-D-E-F-G-2H) - k_5 \cdot D + k'_5 \cdot F \cdot (B+C+D+E+2F+2G+2H)$

$E' = k_4 \cdot C \cdot (2A_0-D-E-F-G-2H) - k_6 \cdot E + k'_6 \cdot G \cdot (B+C+D+E+2F+2G+2H)$

$F' = k_5 \cdot D - k_7 \cdot F \cdot (2A_0-D-E-F-G-2H) - k'_5 \cdot F \cdot (B+C+D+E+2F+2G+2H)$

$G' = k_6 \cdot E - k_8 \cdot G \cdot (2A_0-D-E-F-G-2H) - k'_6 \cdot G \cdot (B+C+D+E+2F+2G+2H)$

$H' = k_7 \cdot F \cdot (2A_0-D-E-F-G-2H) + k_8 \cdot G \cdot (2A_0-D-E-F-G-2H)$

A_0 is the starting concentration of complex **1** or **2**, and k'_1, k'_2, k'_5, k'_6 are the rate constants for back reactions corresponding to k_1, k_2, k_5 and k_6 (Scheme 5.1).

5.4 Results

Labelling the ammine ligand with ^{15}N allowed investigation of the specificity and rates of substitution of the chloride ligands in complexes **1** and **2** by 5′-GMP and GSH to be made for the first time using 2D [^1H, ^{15}N] NMR spectroscopy. The ^{15}N chemical shift is diagnostic of the coordinating atom of the ligand in the position *trans* to the ammine.[22] For an ammine ligand *trans* to an oxygen donor in a Pt(II) complex, the ^{15}N shift lies between -75 and -90 ppm, for an ammine *trans* to nitrogen/chloride, between -55 and -70 ppm, and for ammine *trans* to sulfur, between -40 and -50 ppm.

Reactions of complexes 1 and 2 with 5′-GMP

Scheme 5.1

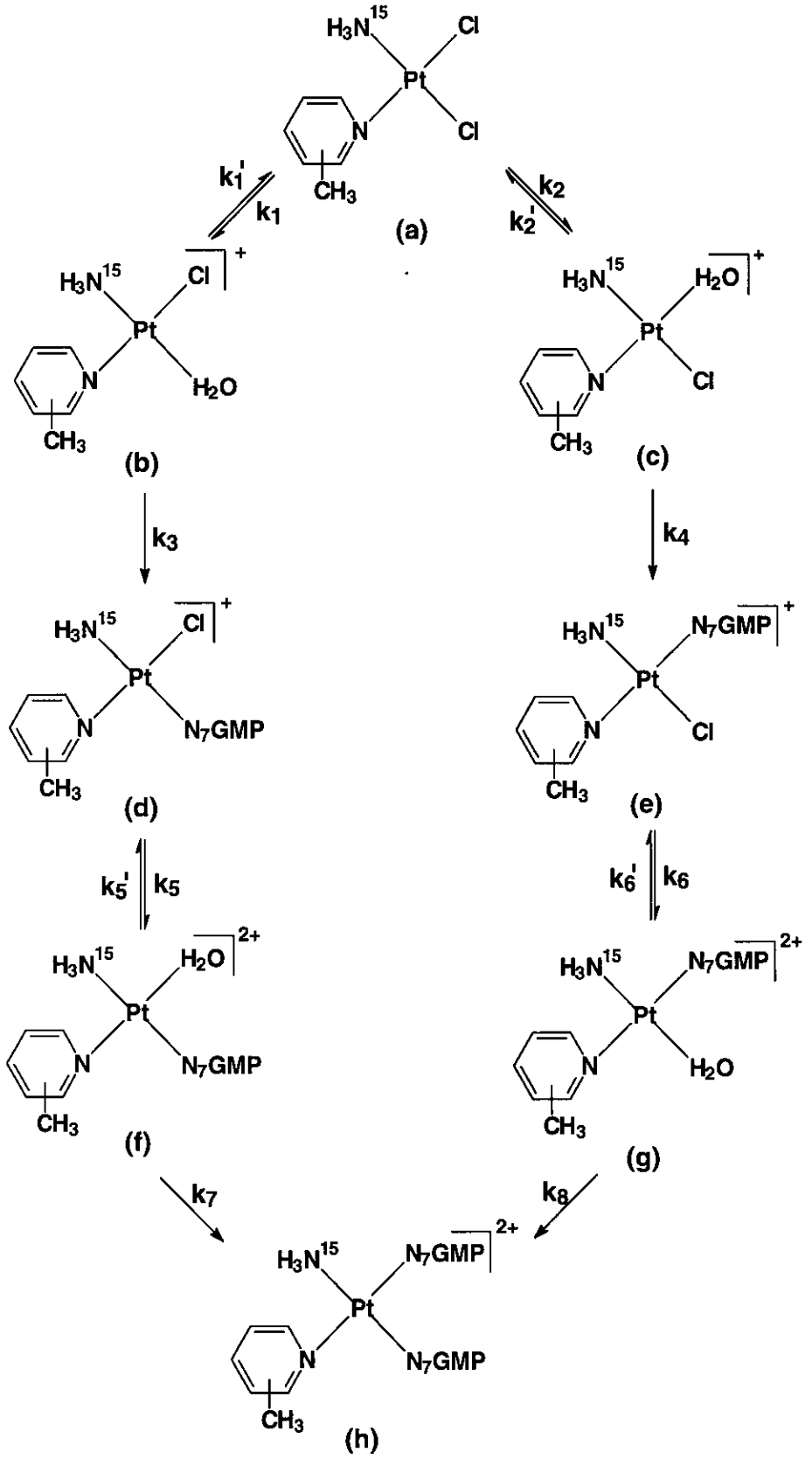
H3N15
Cl
Pt
N
CH3
(a)
k1'
k1
k2
k2'
H2O
(b)
(c)
k3
k4
N7GMP
(d)
(e)
k5'
k5
k6'
k6
2+
(f)
(g)
k7
k8
(h)

Both 1D ^{1}H and 2D [^{1}H, ^{15}N] HSQC NMR spectroscopy were used to monitor the reactions between complex **1** or **2** (3 mM) and 5′-GMP in a 1:2 molar ratio at 296 K and pH 6.85 or 6.55, respectively. 2D [^{1}H, ^{15}N] HSQC NMR spectra recorded 40 h after mixing for complex **1** and 20 h for complex **2** are shown in Figures 5.1A and 5.1B, respectively. For the 3-picoline complex **2**, the peak assignable to **2** at 4.26/-62.68 ppm (peak **2a**) was accompanied by two new peaks (**2b** and **2c**) with chemical shifts of 4.12/-79.62 and 4.33/-61.31 ppm after one hour. The ^{15}N shift of former peak is typical of NH_3 *trans* to O and is consistent with assignment to $[PtCl(^{15}NH_3)(3\text{-picoline})(H_2O)]^+$ (**2b**),[5] and the latter peak to the aqua complex **2c** with $^{15}NH_3$ *trans* to Cl, Table 5.1 (for the structures of complexes, see Scheme 5.1). The intensity of the cross-peak from the monoaqua complex **2b**, in which the H_2O is *trans* to NH_3, is much stronger than that of complex **2c** with H_2O *trans* to 3-picoline. After 2 h, two other new peaks (**2d** and **2e**) appeared at 4.27/-64.21 and 4.53/-60.81 ppm, which are both in the region of $^{15}NH_3$ *trans* to N or Cl. By comparing the intensities of these two peaks with those for the two monoaqua species (**2b**, **2c**), the stronger cross-peak **2d** can be assigned to $[PtCl(^{15}NH_3)(3\text{-picoline})(5'\text{-GMP-}N7)]^+$ (**2d,** GMP *trans* to NH_3), and cross-peak **2e** to $[PtCl(^{15}NH_3)(3\text{-picoline})(5'\text{-GMP-}N7)]^+$ (**2e,** GMP *trans* to 3-picoline). These two peaks reached a maximum intensity after 5 to 6 h and then gradually decreased in intensity. Cross-peaks **2f** at 4.44/-60.93 (NH_3 *trans* to N) and **2g** at 4.47/-75.92 ppm (NH_3 *trans* to O) differ greatly in intensity, comparable to the difference observed for cross-peaks **2d** and **2e** (Fig. 5.1B). Therefore, cross-peak **2f** is assignable to $[Pt(^{15}NH_3)(3\text{-picoline})(5'\text{-GMP-}N7)(H_2O)]^{2+}$ (GMP *trans* to NH_3) (**2f**), and cross-peak **2g** to $[Pt(^{15}NH_3)(3\text{-picoline})(5'\text{-GMP-}N7)(H_2O)]^{2+}$ (GMP *trans* to 3-picoline) (**2g**). Cross-peak **2h** at 4.63/-62.60 ppm, which was observable from soon after the beginning of the

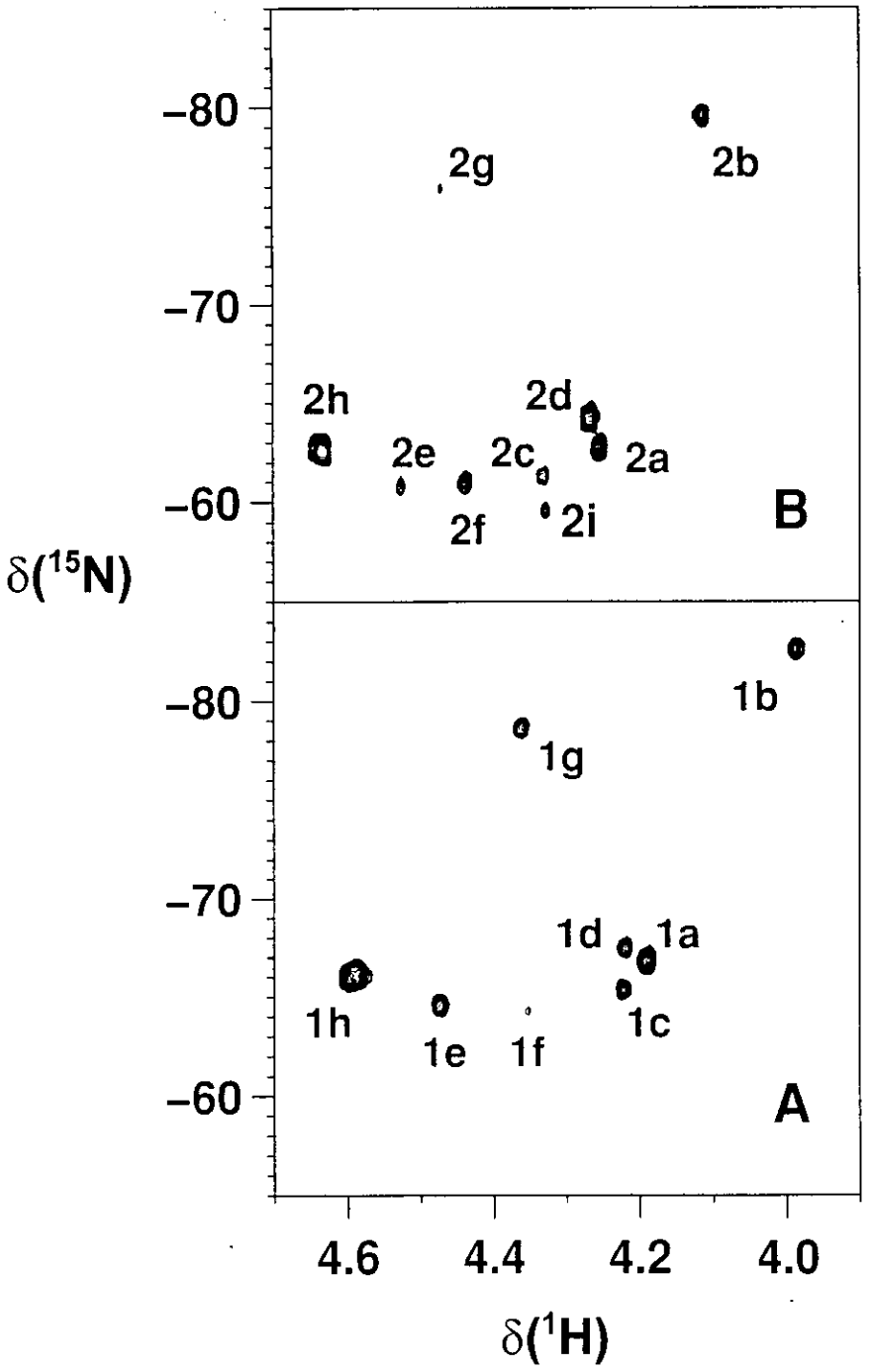

Figure 5.1 2D [^{1}H, ^{15}N] HSQC NMR spectra from reactions of 2 mol equiv. of 5′-GMP (0.1 M $NaClO_4$, 296 K) with (A) ($^{15}NH_3$)-**1**, pH = 6.85, after 40 h and (B) ($^{15}NH_3$)-**2** pH = 6.55, after 20 h. Peak assignments are given in Table 5.1.

reaction, increased in intensity with time, and became the major cross-peak after 24 h. This is assignable to the final bis 5′-GMP product *cis*-[Pt($^{15}NH_3$)(3-picoline)(5′-GMP-*N7*)$_2$]$^{2+}$ (**2h**). An unassigned cross-peak **2i** at 4.33/-59.55 ppm, appeared after 8 h of reaction, but accounted for only a very small amount of the total Pt-NH_3 species present (< 4%), and disappeared after 1 week. The assignments and chemical shifts of all peaks are listed in Table 5.1. The reaction pathway is summarised in Scheme 5.1.

The reaction of the 2-picoline complex **1** with 5′-GMP was much slower in comparison with complex **2**. Only peaks for complex **1** (peak **1a**) (4.19/66.75 ppm) and two monoaqua hydrolysis adducts (peaks **1b** and **1c**) with similar intensity (3.99/-82.61, 4.22/-65.34 ppm, respectively) were observed after two hours at 296 K. The chemical shift distribution of the cross-peaks for the 2-picoline complexes in Figure 5.1A is very similar to that for the 3-picoline complexes in Figure 5.1B, except that all the ^{15}N chemical shifts of the signals in Figure 5.1B are shifted to low frequency by *ca* 3 ppm. However, the relative intensities of the cross-peaks for the intermediates in the reaction of complex **1** with 5′-GMP are different from those for complex **2**. Cross-peaks **1e** at 4.47/-64.51 ppm and **1g** at 4.36/-78.60 ppm are stronger than the peaks **1d** at 4.22/-67.43 ppm and **1f** at 4.35/-64.18 ppm, respectively. Whereas, for complex **2**, cross-peaks **2d** and **2f** are much stronger than **2e** and **2g**. The two cross-peaks **1b** and **1c** for the monoaqua adducts of complex **1** had similar intensities during the reaction. The final bisGMP adduct is formed much more slowly for complex **1** compared to complex **2**. The broad cross-peak (**1h**) for the bisGMP adduct of complex **1** appeared to be composed of two overlapping cross-peaks at 4.59/-65.96 and 4.58/-66.05 ppm. The peak intensity *versus* time profiles (Figure 5.2) allowed similar assignments to be made for the cross-peaks obtained from reactions between complexes **1** and **2** with 5′-GMP (Table 5.1). Cross-peaks **1g**,

Table 5.1 ^{1}H and ^{15}N NMR Pt-NH_3 chemical shifts at 296 K for *cis*-{Pt($^{15}NH_3$)(2-picoline)}$^{2+}$ and *cis*-{Pt($^{15}NH_3$)(3-picoline)}$^{2+}$ complexes.

Compound [a]	Peak*	$\delta(^{1}H)$	$\delta(^{15}N)$ ($^{15}NH_3$ *trans* to)
$[PtCl_2(^{15}NH_3)$(2-picoline)]	**1a**	4.19	-66.75 (Cl)
$[PtCl(^{15}NH_3)$(2-picoline)$(H_2O)]^+$	**1b**	3.99	-82.61 (O)
$[PtCl(^{15}NH_3)$(2-picoline)$(H_2O)]^+$	**1c**	4.23	-65.34 (Cl)
$[PtCl(^{15}NH_3)$(2-picoline)(5′-GMP-*N7*)$]^+$	**1d**	4.22	-67.43 (N)
$[PtCl(^{15}NH_3)$(2-picoline)(5′-GMP-*N7*)$]^+$	**1e**	4.47	-64.51 (Cl)
$[Pt(^{15}NH_3)$(2-picoline)(5′-GMP-*N7*)$(H_2O)]^{2+}$	**1f**	4.35	-64.18 (N)
$[Pt(^{15}NH_3)$(2-picoline)(5′-GMP-*N7*)$(H_2O)]^{2+}$	**1g**	4.36	-78.60 (O)
$[Pt(^{15}NH_3)$(2-picoline)(5′-GMP-*N7*)$_2]^{2+}$	**1h**	4.59	-65.87 (N)
		4.58	-66.15 (N)
$[PtCl_2(^{15}NH_3)$(3-picoline)]	**2a**	4.26	-62.68 (Cl)
$[PtCl(^{15}NH_3)$(3-picoline)$(H_2O)]^+$	**2b**	4.12	-79.62 (O)
$[PtCl(^{15}NH_3)$(3-picoline)$(H_2O)]^+$	**2c**	4.33	-61.31 (Cl)
$[PtCl(^{15}NH_3)$(3-picoline)(5′-GMP-*N7*)$]^+$	**2d**	4.27	-64.21 (N)
$[PtCl(^{15}NH_3)$(3-picoline)(5′-GMP-*N7*)$]^+$	**2e**	4.53	-60.81 (Cl)
$[Pt(^{15}NH_3)$(3-picoline)(5′-GMP-*N7*)$(H_2O)]^{2+}$	**2f**	4.44	-60.93 (N)
$[Pt(^{15}NH_3)$(3-picoline)(5′-GMP-*N7*)$(H_2O)]^{2+}$	**2g**	4.47	-75.92 (O)
$[Pt(^{15}NH_3)$(3-picoline)(5′-GMP-*N7*)$_2]^{2+}$	**2h**	4.63	-62.60 (N)
unassigned	**2i**	4.33	-59.55 (N)

* See Fig. 5.1.

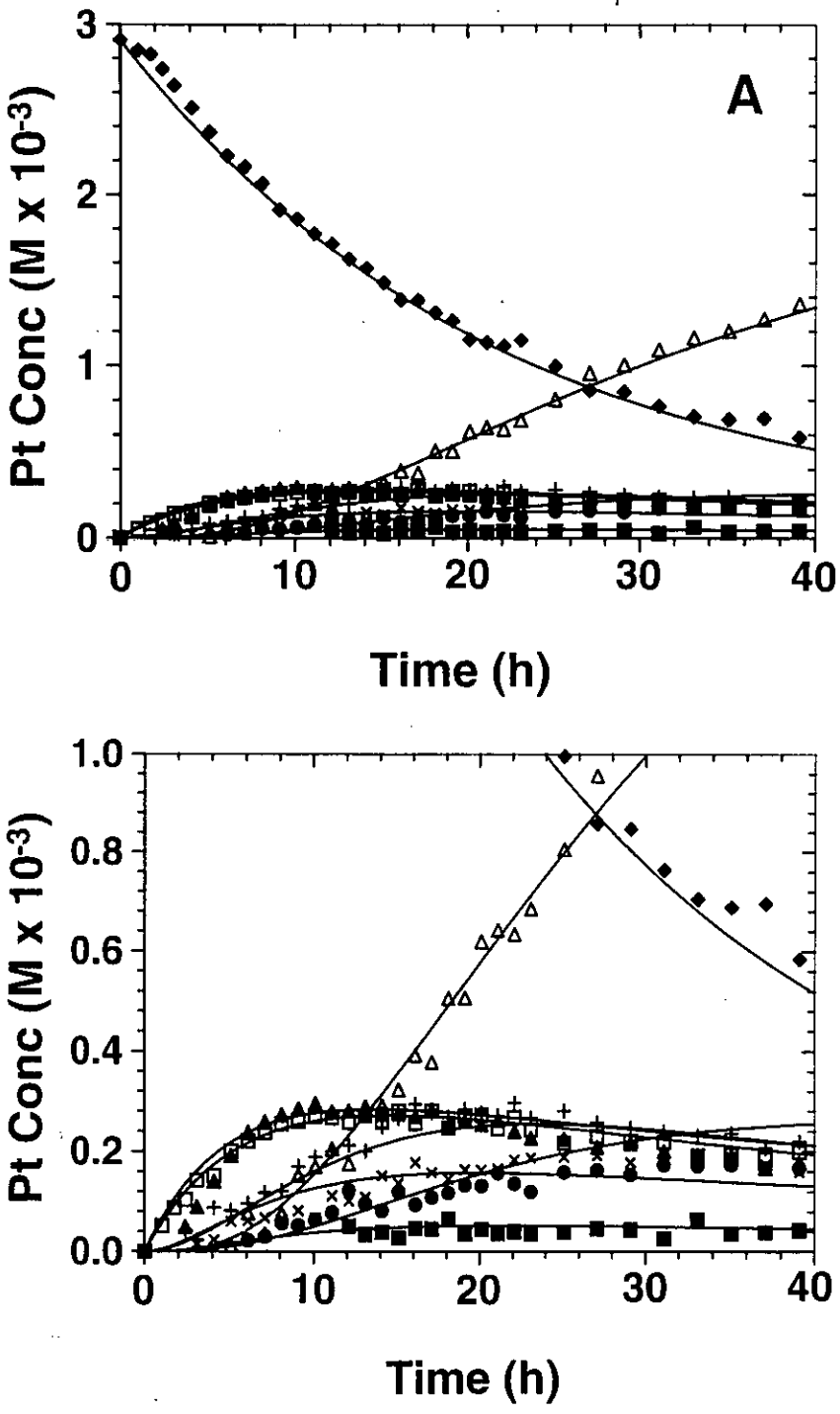

Figure 5.2 Plots of the relative concentrations of species **a** to **h** (based on Pt-NH_3 peak integrals) versus time for the reactions shown in Fig. 5.1. (A) 2-Picoline complex **1**, (B) 3-picoline complex **2**. Peak labels: (**a**) ◆, (**b**) □, (**c**) ▲, (**d**) ×, (**e**) +, (**f**) ■, (**g**) ●, (**h**) Δ. The curves are the computer best fits for the rate constants given in Table 5.2.

Figure 5.2B

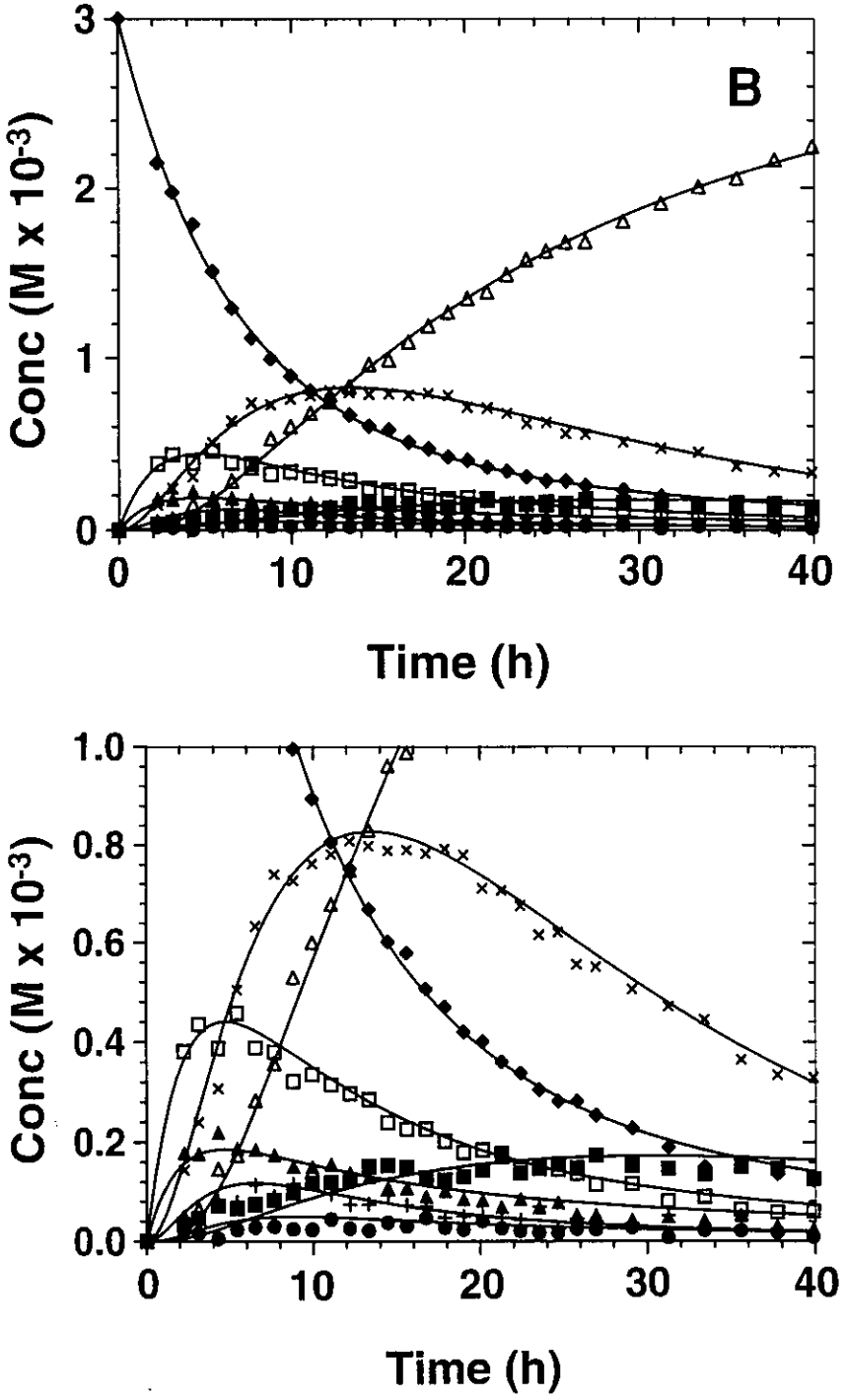

Table 5.2 Rate constants for reactions of *cis*-[$PtCl_2(NH_3)$(picoline)] with 5′-GMP at 296 K (0.1 M $NaClO_4$). The errors represent one standard deviation for fitting.

	Complex		Ratio
Rate constants	2-picoline	3-picoline	$k_{3\text{-pico}} / k_{2\text{-pico}}$
k_1 (s^{-1})	$6.87 (\pm 0.18) \times 10^{-6}$	$2.60 (\pm 0.03) \times 10^{-5}$	4
k_2 (s^{-1})	$5.87 (\pm 0.18) \times 10^{-6}$	$1.17 (\pm 0.03) \times 10^{-5}$	2
k_3 ($M^{-1}\cdot s^{-1}$)	$7.97 (\pm 0.33) \times 10^{-3}$	$1.60 (\pm 0.03) \times 10^{-2}$	2
k_4 ($M^{-1}\cdot s^{-1}$)	$6.67 (\pm 0.37) \times 10^{-3}$	$1.87 (\pm 0.08) \times 10^{-2}$	3
k_5 (s^{-1})	$8.53 (\pm 1.11) \times 10^{-5}$	$1.78 (\pm 0.04) \times 10^{-5}$	0.2
k_6 (s^{-1})	$2.77 (\pm 0.31) \times 10^{-5}$	$1.48 (\pm 0.14) \times 10^{-4}$	5
k_7 ($M^{-1}\cdot s^{-1}$)	$4.2 (\pm 0.6) \times 10^{-2}$	$3.2 (\pm 0.1) \times 10^{-2}$	0.8
k_8 ($M^{-1}\cdot s^{-1}$)	$5.92 (\pm 0.74) \times 10^{-3}$	$6.85 (\pm 0.75) \times 10^{-2}$	12

1f and **1h** were also observed during reaction of the diaqua complex *cis*-[$Pt(^{15}NH_3)$(2-picoline)$(H_2O)_2]^{2+}$ (3 mM) with 5′-GMP (1:2) at 296 K and pH 6.47.

Kinetic fits to the reaction profile in Scheme 5.1 for complexes **1** and **2** are shown in Figures 5.2A and 5.2B, and the rate constants for each step are listed in Table 5.2. Most of the rate constants for the reaction steps of complex **2** with 5′-GMP are more than twice as large as those for complex **1,** except k_5 and k_7. The largest differences are for k_6 and k_8 (substitution of Cl^- *cis* to picoline by H_2O, and then by 5′-GMP in the second stage), which are five and twelve times larger for complex **2**.

Rotation of 5′-GMP and 2-picoline in *cis*-[Pt(2-picoline)(NH_3)(5′-GMP)$_2]^{2+}$

^1H NMR spectra for the reactions between complex **1** or **2** and 5′-GMP (1:2 reaction ratio) at 296 K recorded after 2 hours and 1 week are shown in Fig. 5.3. For complex **1**, after 1 week of reaction, the H8 resonance of free 5′-GMP at 8.19 ppm and the

methyl signal of complex **1** at 3.15 ppm have completely disappeared (Fig. 5.3A). Four major H8 signals were observed in two sets of two singlets between 8.7 and 8.3 ppm, and two methyl-signals appeared at 3.30 and 3.27 ppm. The H1′ signals of bound 5′-GMP were also observed in two sets of two doublets, with vicinal coupling constants ^3J(H1′-H2′) = 4.8, 4.4 and 5.1, 4.9 ± 0.1 Hz. However, for complex **2** after one week of reaction, only two H8 signals at 8.66 and 8.52 ppm were observed together with one methyl signal at 2.37 ppm and two H1′ doublets (^3J(H1′-H2′) = 4.6 and 4.9 ± 0.1 Hz) for bound 5′-GMP (Fig. 5.3B). ^{1}H NMR data for *cis*-[Pt(2-picoline)(NH_3)(5′-GMP)$_2$]$^{2+}$ (**1h**) and *cis*-[Pt(3-picoline)(NH_3)(5′-GMP)$_2$]$^{2+}$ (**2h**) are listed in Table 5.3.

Table 5.3 ^{1}H NMR Chemical shifts and coupling constants (Hz) for bis 5′-GMP adducts of **1** (pH = 6.85) and **2** (pH = 6.55) at 296 K. (Pic = picoline)

Complex	δH8	δCH_3	δH1′	^3J(H1′-H2′)
cis-[$PtCl_2(NH_3)$(2-Pic)] (**1**)		3.15		
[Pt(NH_3)(2-Pic)(5′-GMP)$_2$]$^{2+}$	8.66, 8.63	3.30, 3.27	5.93, 5.92	4.8, 4.4
	8.42, 8.40		5.80, 5.78	5.1, 4.9
cis-[$PtCl_2(NH_3)$(3-Pic)] (**2**)		2.37		
[Pt(NH_3)(3-Pic)(5′-GMP)$_2$]$^{2+}$	8.66, 8.52	2.36	5.93, 5.82	4.6, 4.9

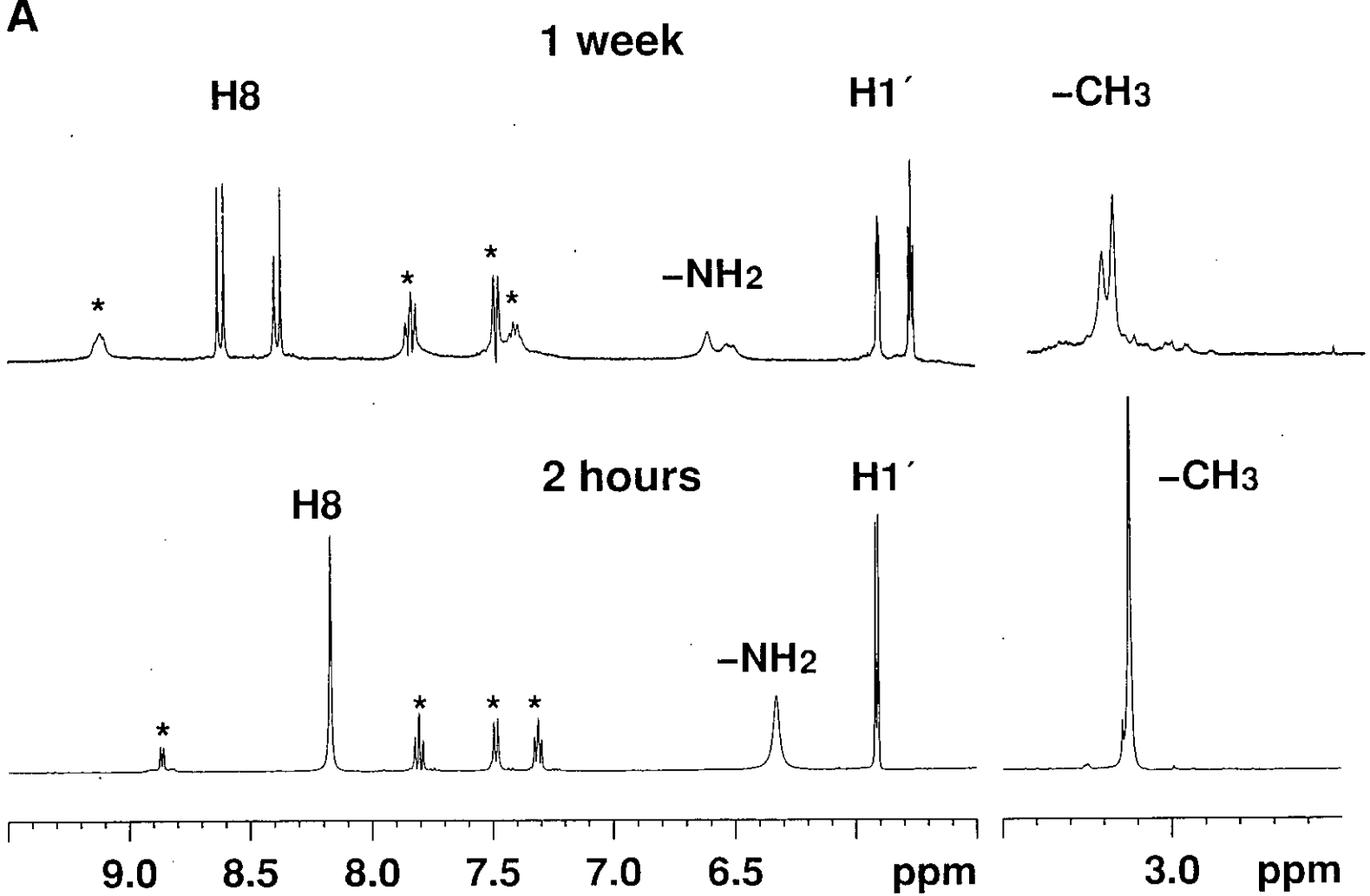

Figure 5.3 ^{1}H NMR spectra recorded after 2 h and 1 week of reactions at 296 K of 5′-GMP (2 mol equiv) with (A) complex **1**, and (B) complex **2**. The peaks labelled * are from the aromatic protons of picoline ligands.

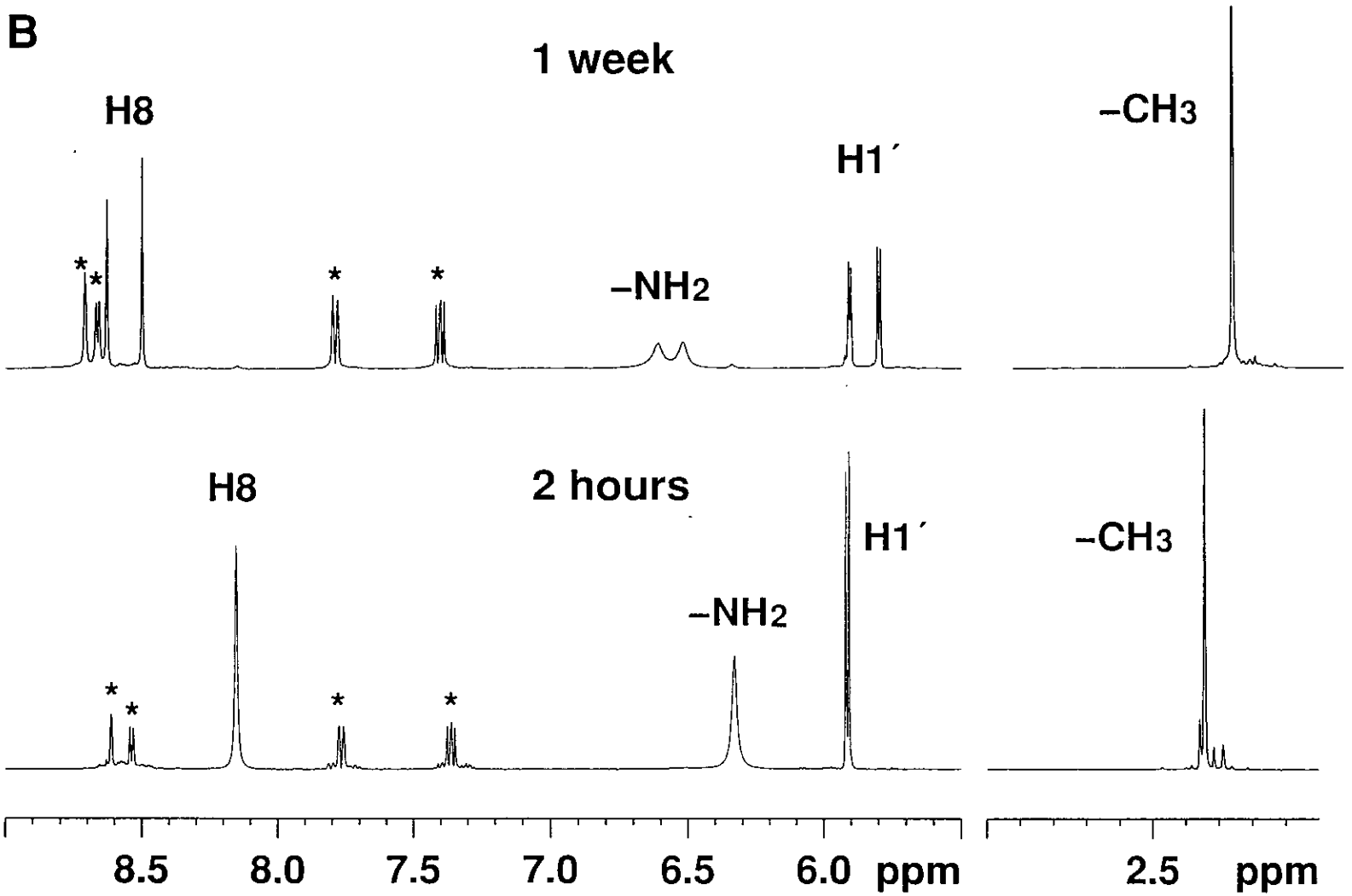
B
1 week
H8
H1´
–CH3
–NH2
2 hours
H8
H1´
–CH3
–NH2
8.5
8.0
7.5
7.0
6.5
6.0
ppm
2.5
ppm

Figure 5.3B

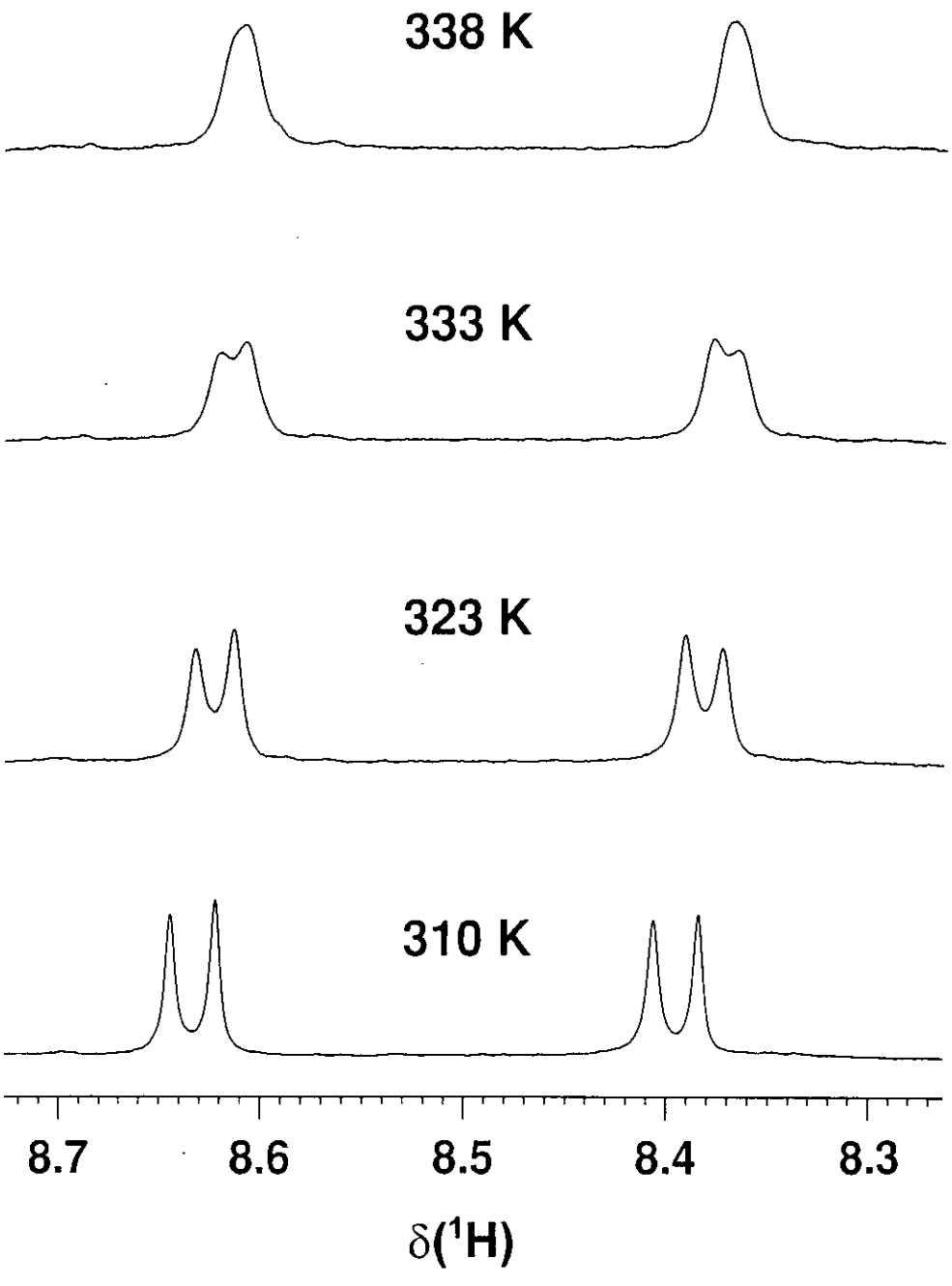

Figure 5.4 The temperature dependence of the H8 ^{1}H NMR signals of *cis*-$[Pt(NH_3)(2\text{-picoline})(5'\text{-GMP})_2]^{2+}$.

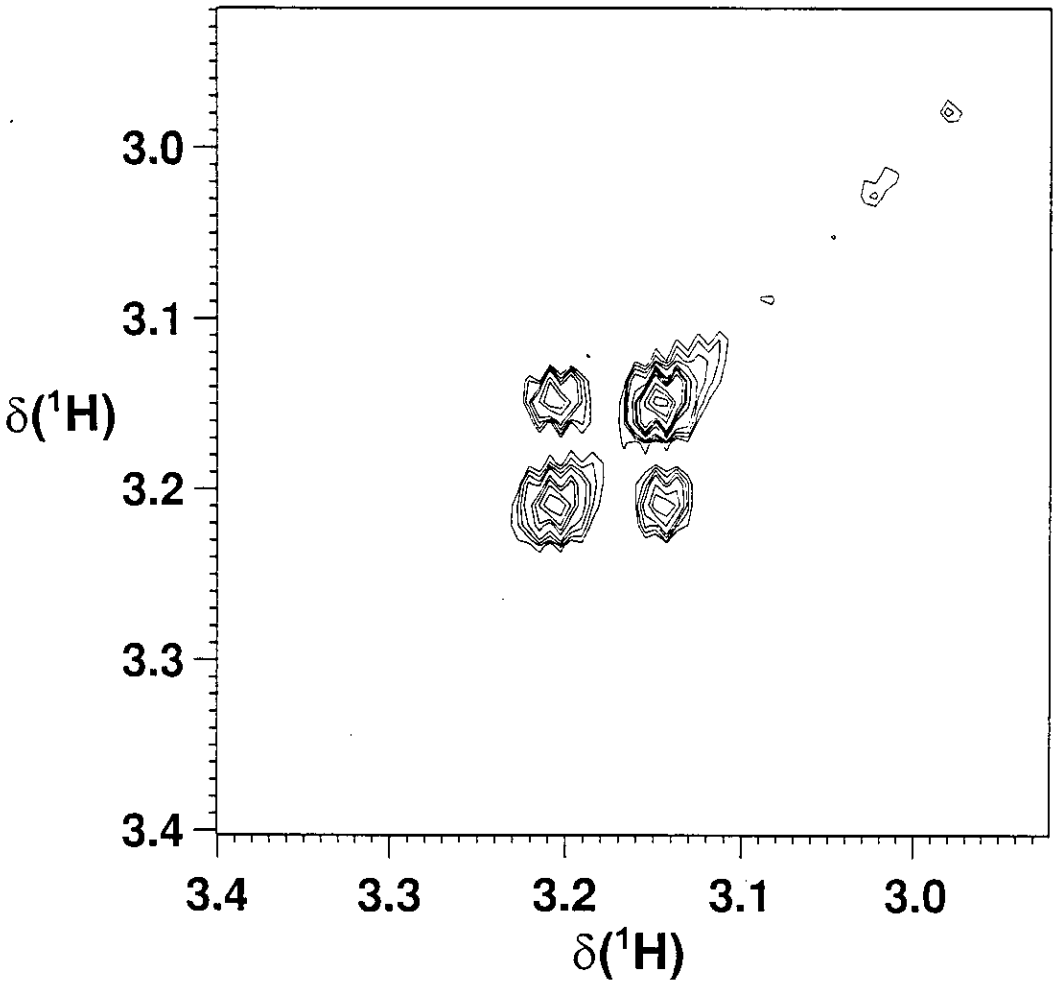

Figure 5.5 2D EXSY spectrum (mixing time = 1 s) for *cis*-[Pt(NH_3)(2-picoline)(5′-GMP)$_2$]$^{2+}$ showing exchange cross-peaks between the two methyl signals, indicative of the slow rotation of coordinated 2-picoline.

The temperature dependence of the H8 signals of $[Pt(2\text{-picoline})(NH_3)(5'\text{-GMP})_2]^{2+}$ is shown in Fig. 5.4. The four H8 singlets coalesced into two singlets when the temperature was raised to 338 K. Based on the coalescence temperature (T_c) and the chemical shift differences ($\Delta\nu$ in Hz) between the two signals in the slow exchange limit, the rate constant k_c and activation free energy $\Delta G^{\ddagger}$ for the exchange process at 338 K were calculated [23]:

$$k_c = 2.22 \cdot \Delta\nu = 25.5 \text{ s}^{-1}$$

$$\Delta G_c^{\ddagger} = 19.14\, T_c\, (10.32 + \log \frac{T_c}{k_c}) \text{ J mol}^{-1} = 73.2 \text{ kJ} \cdot \text{mol}^{-1}$$

At 338 K, the two ^{1}H, ^{15}N cross-peaks which constituted peak **1h** (Fig. 5.1A) for bis-GMP adducts of complex **1** merged into one cross-peak. The two methyl signals at δ 3.30 and 3.27 ppm also became closer when the temperature was raised to over 333 K. Because of the temperature limitation of the NMR probe, the spectrum was recorded at a maximum temperature of 348 K, where no coalescence of the two methyl signals was observed. When the spectra were recorded at 250 MHz, the two methyl signals were observed to coalescence at 343 K, from which similar k_c (25.6 s^{-1}) and $\Delta G^{\ddagger}$ (75.15 kJ • mol^{-1}) values were obtained. A 2D EXSY experiment with a mixing time of 1 s (Fig. 5.5) showed clear exchange cross-peaks between the two methyl signals at 296 K. An average rate constant for the exchange process of 0.62 s^{-1} at this temperature was determined. Interestingly, one of the four H8 signals at 8.42 ppm for the bisGMP adduct of complex **1** became broader when the temperature was below 296 K (Fig. 5.3A), as did one of the -CH_3 signals at 3.30 ppm.

Reactions of complexes 1 and 2 with glutathione (1:1, pH 7)

Reactions of complexes **1** and **2** with GSH were followed by 2D [^{1}H, ^{15}N] HSQC NMR spectroscopy. Spectra recorded after 3.5 h are shown in Fig. 5.6. In both cases, peaks assignable to hydrolysis products (**1b**, **1c** and **2b**, **2c**) were observed before the appearance of peaks for GSH adducts. For complex **2**, cross-peaks from GSH adducts

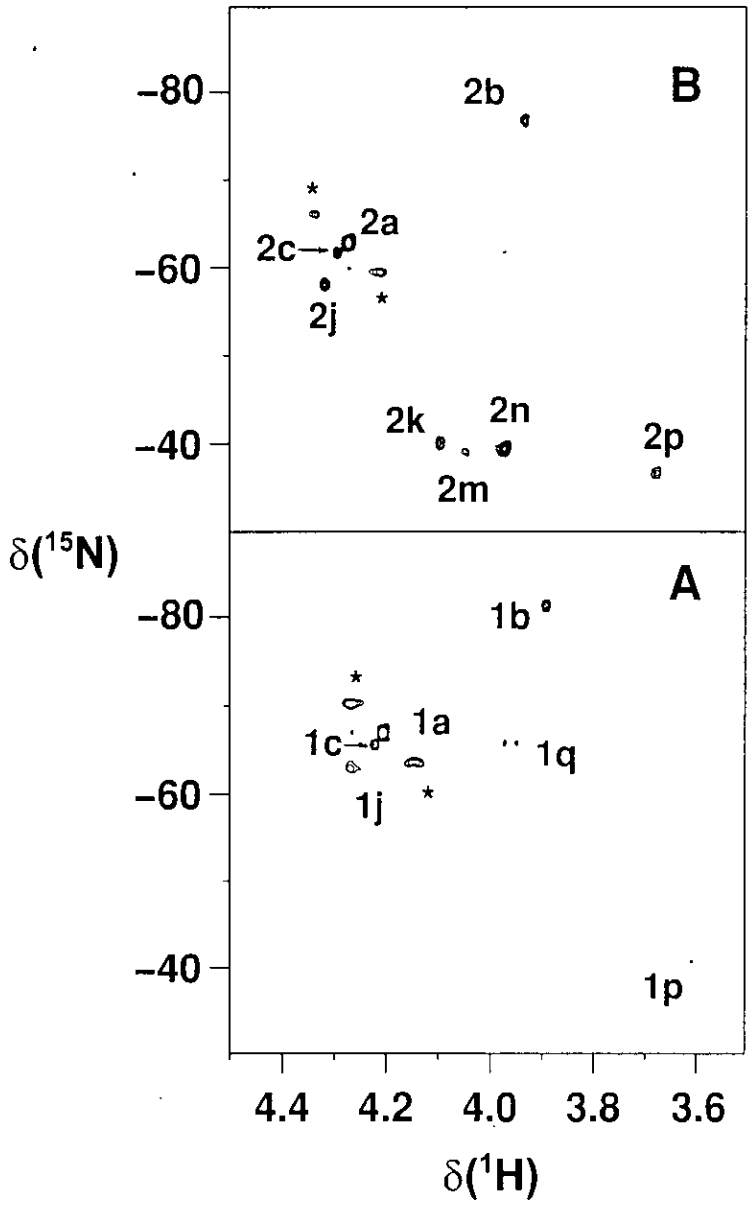

Figure 5.6 Two-dimensional [^{1}H, ^{15}N] HSQC NMR spectra for reactions of GSH (1 mol equiv.) with (A) complex **1,** and (B) complex **2,** recorded at 296 K, pH 7 (100 mM phosphate buffer) after 3.5 h. Peaks (**1a** to **1c,** and **2a** to **2c**) are assigned according to Table 5.1; the others are unassigned. Satellites (^{195}Pt) of peaks **1a** and **2a** are labelled with *. Peaks with ^{15}N chemical shifts near -40 ppm are characteristic of NH_3-Pt *trans* to sulfur.

Table 5.4 ^{1}H and ^{15}N NMR Pt-NH_3 chemical shifts at 296 K for the major peaks observed during the reactions of **1** and **2** with GSH (1:1 molar ratio, pH 7).

Peak [a]	$\delta(^{1}H)$	$\delta(^{15}N)$ ($^{15}NH_3$ *trans* to)
1a	4.21	-66.84 (Cl)
1b	3.89	-81.27 (O)
1c	4.23	-65.49 (Cl)
1j	4.27	-62.64 (N or Cl)
1p	3.60	-40.85 (S)
1q	3.97, 3.95	-65.84, -65.95 (N or Cl)
*	4.29	-62.52 (N or Cl)
*	4.25	-62.89 (N or Cl)
*	3.96	-43.24 (S)
*	4.05	-42.76 (S)
*	3.69	-42.12 (S)
2a	4.27	-62.82 (Cl)
2b	3.93	-76.77 (O)
2c	4.30	-61.74 (Cl)
2j	4.32	-58.14 (N or Cl)
2k	4.10	-40.09 (S)
2m	4.05	-39.01 (S)
2n	3.97	-39.37 (S)
2p	3.68	-36.70 (S)

[a] For peak labels, see Fig. 5.6. Peaks labelled * were not observed in the same spectrum as the other peaks but appeared at later times.

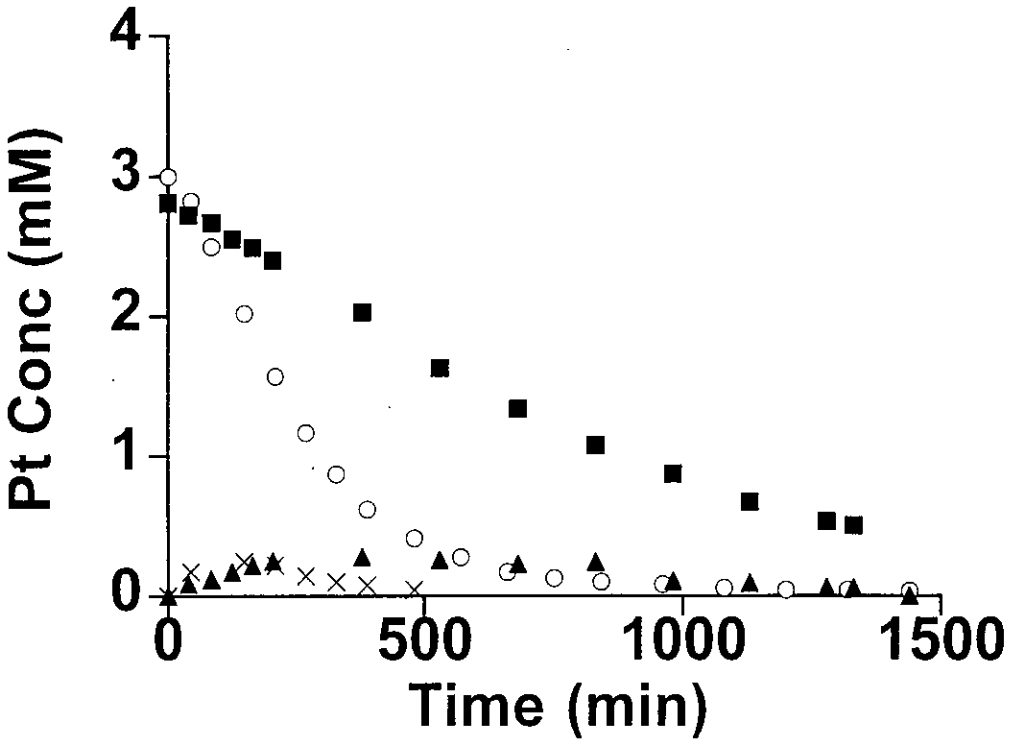

Figure 5.7 Time dependence of the concentrations of the starting complex **1** (■), its monoaquachloro adducts (**1b** + **1c**) (▲), and complex **2** (O), its monoaquachloro adducts (**2b** + **2c**) (×), during reactions with GSH (1:1 molar ratio, pH 7, 296 K).

began to appear after 45 minutes in the $\delta(^{15}N)$ region of -35 to -40 ppm which corresponds to NH_3 *trans* to S, while for complex **1**, new peaks were observed only after 2 h and in the $\delta(^{15}N)$ region of -62 to -67 ppm which corresponds to NH_3 *trans* to N or Cl. Therefore, the first binding site for GS^- is *trans* to 2-picoline for complex **1,** but *cis* to 3-picoline for complex **2**. Due to the complicated nature of the reactions (Table 5.4), no specific assignments for the products of the reactions between complex **1** and **2** and GSH have been made. Time dependences of the concentrations of complexes **1** and **2** and their monoaquachloro adducts during the reactions with GSH are shown in Fig. 5.7. The rate of reaction of complex **2** is about 3 times as fast as that of complex **1**. After two weeks' standing at ambient temperature, yellow precipitates formed in both reactions, and all the signals had disappeared from the 2D [^1H, ^{15}N] HSQC NMR spectra.

Competitive reactions of 1 or 2 with GSH and 5′-GMP

The reaction of complex **1** with GSH in the presence of 5′-GMP (1:2:2) was followed by 2D [^1H, ^{15}N] NMR spectroscopy at 296 K, pH 7 (100 mM phosphate buffer). A spectrum recorded after 14.5 h of reaction is shown in Figure 5.8. Only the peaks for the starting complex **1** (peak **1a**) and hydrolysis products (peaks **1b**, **1c**) were present after 0.5 h. Peak **1q**, which was also observed during the reaction with GSH (Fig. 5.6a), began to appear after 1 h of reaction. The mono-GMP adduct (peak **1e**) began to form after 2.5 h, and the bis-GMP adduct (peak **1h**) was present after 8 h of reaction. Peaks due to both 5′-GMP adducts (**1d**, **1e**, **1f** and **1h**) and GSH adducts (peaks **1q**, **1j**, **1r** and those in dashed box) are present in Fig. 5.8. Due to the complicated nature of GSH reactions, no attempt was made to assign the peaks **1q**, **1j** or those in the region for NH_3-Pt *trans* to S (dashed box, Fig. 5.8). Most of these peaks for GSH adducts were also observed in the reaction of complex **1** with GSH in the absence of 5′-GMP. Peak **1r** has an ^{15}N chemical shift in the region of NH_3-Pt

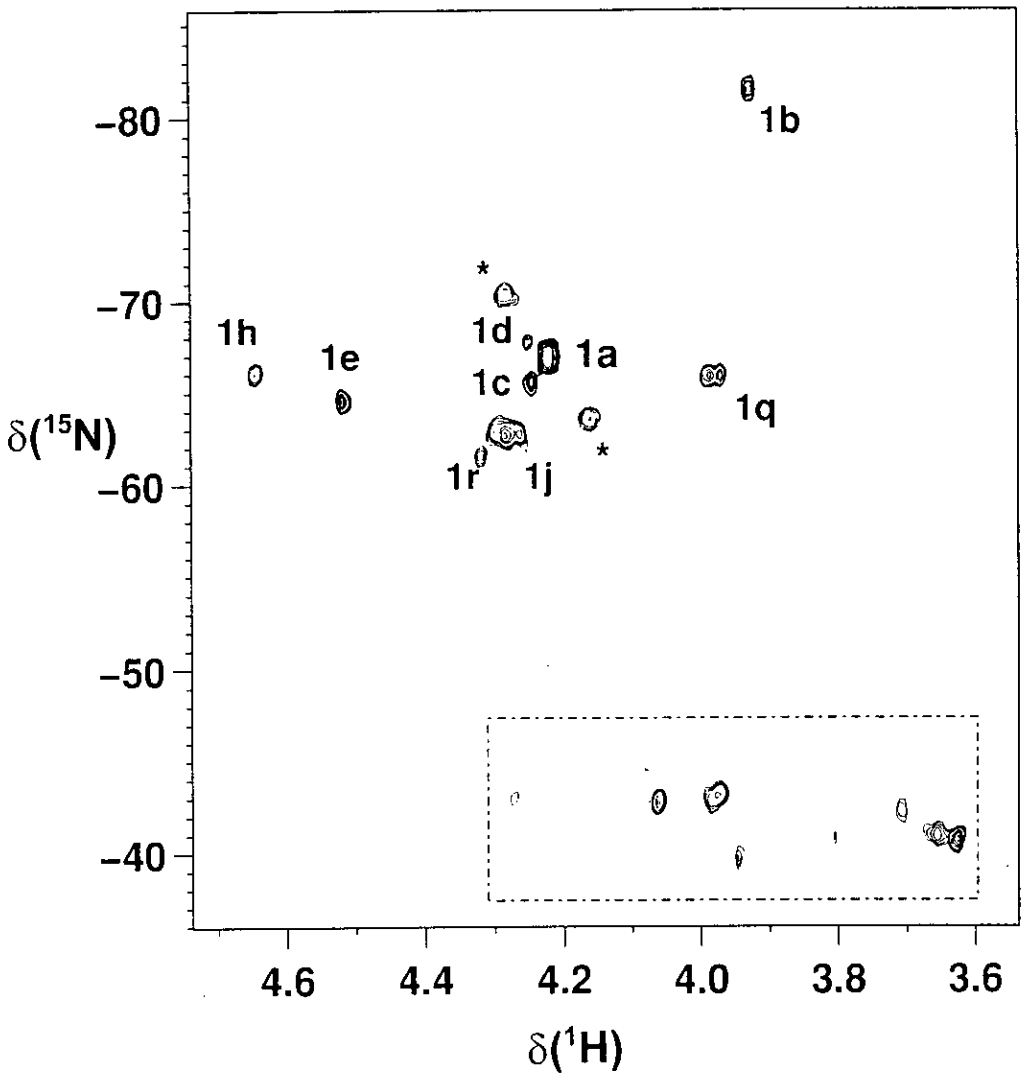

Figure 5.8 2D [^{1}H, ^{15}N] HSQC NMR spectrum for the competitive reaction of GSH and 5′-GMP with complex **1** (molar ratio: 2:2:1) at 296 K, pH 7.0 (100 mM phosphate buffer) recorded after 14.5 h. Peaks of 5′-GMP adducts (**1d**, **1e**, **1h**) and GSH adducts (**1j**, **1q**) are labelled according to those in Table 5.1 and Table 5.4. Satellites of peak **1a** are labelled with *. The peaks in the dashed box are due to the formation of GSH adducts (^{15}N chemical shifts near -40 ppm are characteristic of NH_3-Pt *trans* to sulfur), but no specific assignments were made. Peak **1r** is tentatively assigned to an adduct with one GMP and one GSH ligand in the *cis* position (NH_3-Pt *trans* to N7).

trans to N or Cl, and was not observed in the reactions of **1** with 5′-GMP or with GSH. It can be tentatively assigned to a mixed-ligand adduct containing GMP *trans* to NH_3 and a GS^- ligand. Spectra recorded after 3 days of reaction at 296 K showed that only one major peak (**1h**) in the region of NH_3-Pt *trans* to N or Cl ($\delta^{15}N$: -60 to -70 ppm) together with some other peaks ($\delta^{15}N$: -40 to -45 ppm) in the region of NH_3-Pt *trans* to S. The presence of a strong H8 signal at 8.13 ppm due to free 5′-GMP in 1D spectra recorded after 3 days showed that most of the 5′-GMP was still unreacted at this stage, while signals for free GSH had nearly disappeared. The 2-methyl signal at 3.15 ppm from coordinated 2-picoline had shifted to 2.57 ppm, which implied that the 2-picoline ligand had been mostly displaced. Signals for the bisGMP adduct were only just visible in 1D spectra because of their low intensity and overlap with broad signals. Compared with **1**, the competitive reaction of **2** with GSH and 5′-GMP (1:2:2) was much faster and peaks assignable to GSH adducts were detectable after 0.5 h. Mono and bisGMP products started to appear after 1.5 and 5 h of reaction, respectively. Much less of the bisGMP adduct of complex **2** was formed in the competative reaction with GSH compared to complex **1**.

5.5 Discussion

Cis-[$PtCl_2(NH_3)$(2-picoline)] (**1**) is a new anticancer drug which has a different spectrum of biological activity compared to cisplatin. In particular it is active against cisplatin-resistant cell lines and xenographs.[2,3,4] In order to shed light on the chemical reactivity of **1**, and to elucidate the potential role of steric hindrance,[5] kinetic studies of reactions of complex **1** with 5′-GMP and GSH have been made in comparison to the isomeric 3-picoline complex **2**. By labelling complexes with $^{15}NH_3$, it was possible to determine for the first time the specificity of substitution of the chloride ligands by 5′-GMP and GSH using 2D [^1H, ^{15}N] HSQC NMR spectroscopy. Because of the sensitivity of the ^{15}N chemical shifts to the ligand *trans* to H_3N-Pt, and of ^1H

NH_3 shifts to *cis* effects, it has been possible to resolve peaks for a variety of intermediates in the reactions, detect them at micromolar concentrations, and make reasonable assignments.

Reactions with 5′-GMP

Concentration versus time profiles for reactions of complexes **1** and **2** with 5′-GMP fitted well to the kinetic scheme shown in Scheme 5.1, showing that they are two-step and two stage: initial hydrolysis followed by 5′-GMP substitution to give the 1:1 Pt-5′GMP adduct, and then further hydrolysis and 5′-GMP substitution to give the final product, the bis 5′-GMP complex. For each complex there are two routes to the final product, depending on whether initial substitution is *trans* to picoline or *trans* to NH_3. From the rate constants listed in Table 5.2, the following conclusions can be drawn:

(i) The rates of ligand substitution (Cl^- by H_2O, or H_2O by 5′-GMP) *cis* to picoline (k_1, k_3, k_6, k_8) are 2-12 times slower for the 2-picoline complexes compared to 3-picoline.

(ii) The rates of substitution *trans* to picoline are also slower for the 2-picoline complex (2-3 times slower) except when 5′-GMP is present as the *cis* ligand (compare k_5 and k_7 values for complexes **1** and **2**, Table 5.2). However, it should be noted that the errors for some of the rate constants determined for the second stage of the reaction are rather large on account of the low concentrations of the intermediates.

The relative rates of the first step of the GMP reactions are similar to those we determined previously for hydrolysis of the complexes, and for complex **2** these follow the order expected from the higher *trans* influence of NH_3 (pK_a 9.29) compared to 3-picoline (pK_a 6.0),[24] which is the weaker σ donor. Since 2-picoline has a similar pK_a value (6.1) to that of 3-picoline, the similarity in the hydrolysis

rates for Cl^- *trans* to NH_3 and *trans* to 2-picoline in complex **1** can be attributed to steric hindrance provided by the 2-methyl group. In the X-ray structure of complex **1**, the 2-picoline ligand is almost perpendicular to the Pt square plane (102.7°) and the methyl group is close to Pt ($H_3C\bullet\bullet\bullet Pt$: 3.224 Å).[5]

Such steric hindrance is well known to slow down the rates of ligand substitution reactions in square-planar metal complexes.[25] For example, the rate constants (s^{-1}) for the hydrolysis of *cis*-$[PtCl(L)(PEt_3)_2]$ complexes (the replacement of Cl^- by H_2O) decrease in the order of (L): pyridine (800×10^{-4}) > 2-methylpyridine (2.0×10^{-4}) > 2,6-dimethylpyridine (0.01×10^{-4}).[26] In the latter case the methyl groups block entry of incoming nucleophiles both above and below the square-plane. The steric effect is more prominent in the position *cis* to 2-picoline which is consistent with the CH_3 group being further from the entering and leaving groups in the trigonal bipyramidal transition state if the pyridyl ligand is in the trigonal plane.[26,27] The plane of the 3-picoline ring in complex **2** is tilted by 48.9° with respect to the Pt square plane, and the rates of substitution for (**2**) are determined mainly by the *trans* effect.

The rate of binding of the second 5′-GMP ligand in the position *cis* to picoline is much slower for complex **1** compared with **2**, which gives rise to a long-lived monofunctional adduct for the 2-picoline complex. This may explain the brief report that complex **1** forms DNA cross-links extremely slowly.[7] There appears to be no comparable kinetic data available in the literature for reactions of 5′-GMP with cisplatin. Compared to the rate constants for the second stage of binding of 5′-GMP to $[Pt(NH_3)_2(5'\text{-GMP})(H_2O)]^{2+}$ (298 K, 0.24 M^{-1} s^{-1}),[28] those for complexes **1** and **2** are an order of magnitude smaller. The rates of reactions of aquachloro cisplatin with DNA oligonucleotides[29,30] are also about two orders of magnitude faster in comparison to those for reaction of the chloroaqua species of the picoline complexes **1** and **2** with 5′-GMP.

Rotation of ligands in bis 5′-GMP adducts

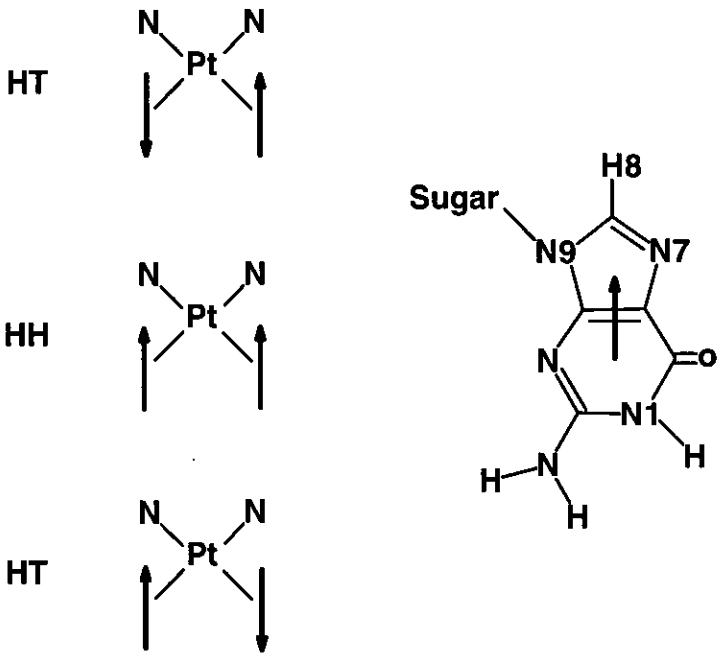

Figure 5.9 Schematic representations of the possible isomers in a C_2-symmetrical *cis*-PtA_2G_2 complex and their interconversion. Arrow represent an N7-bound G, with the head of the arrow denoting H8. (based on Ref. 31)

Restricted rotation about the Pt-N7 bonds can potentially lead to three different bisGMP stereoisomers for square-planar complexes having two *cis* ligands with C_2 local symmetry: two head-to-tail (HT) and one head-to-head (HH) species (Fig. 5.9), with the H8s of 5′-GMP on the opposite side or on the same side of the Pt coordination plane, respectively. Because of the chiral ribose of 5′-GMP, the H/T enantiomers become diastereomers and should be distinguishable by NMR. Each HT is C_2-symmetrical and has one H8 signal, but the HH with two nonequivalent H8s has two H8 signals. So four H8 signals in total are expected for the three stereoisomers. If the *cis*-PtA_2 moiety lacks local C_2 symmetry (e.g., two different A

(A, A′) or an unsymmetrical chelate), four different stereoisomers (two HT and two HH) are possible when there is restricted rotation about the Pt-N7 bonds in bis-GMP complexes.[11] Normally only HT conformations are expected to be thermodynamically favoured and detectable in solution, as is found in most solid-state crystallographic studies.[10,32,33] Each H8 is non-equivalent for both HT stereoisomers,[33,34,35] giving a total of four H8 signals for the HT stereoisomers.[36] For the 2-picoline complex **1**, the 2-methyl group can be on the upper side or the lower side of the platinum plane for each HT stereoisomer, so theoretically eight H8 signals should be observed for the two HT isomers together with four methyl signals (Fig. 5.10) when there is slow rotation (on the NMR timescale) about both the Pt-N7 GMP and Pt-N-picoline bonds. Usually fast rotation of bound GMP about Pt-N7 bond in *cis*-[$PtA_2(GMP)_2$] (where A_2 are two unidentate or one bidentate amine ligands) is expected if the substituents on the two *cis* amine ligands are not very bulky.[34,36] In our NMR experiments, only four H8 signals in two sets of two singlets were

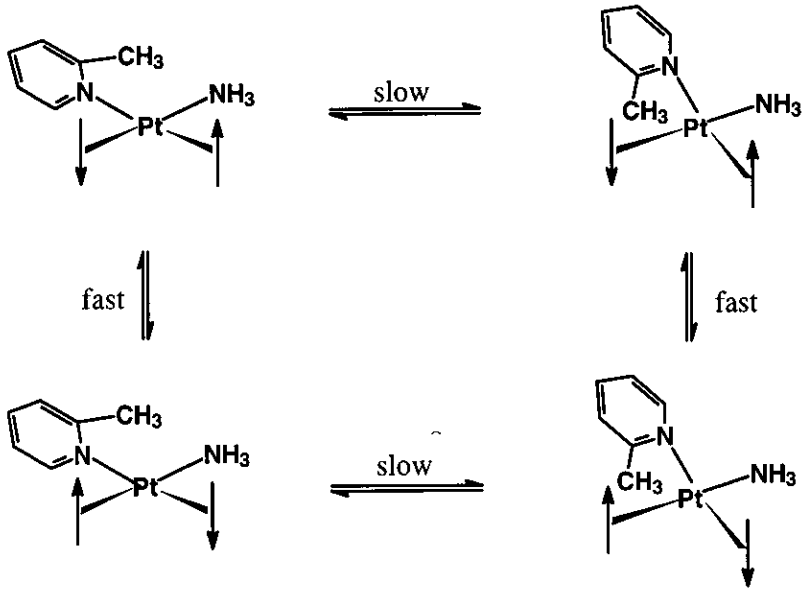

Figure 5.10 Diastereomers of *cis*-[$Pt(^{15}NH_3)$(2-picoline)(5′-GMP-*N7*)$_2$]$^{2+}$. The arrows (↣) represent 5′-GMP molecules, with the head of the arrow denoting H8.

observed for complex **1,** together with two methyl signals. This suggests that rotation of 5′-GMP about the Pt-N7 bond is fast on the NMR timescale but slow about the Pt-N bond for 2-picoline. This slowness of the rotation was evident from the exchange rate (0.62 s^{-1}, 296 K) determined by 2D EXSY spectrum. The activation free energy ($\Delta G^{\ddagger}$) measured from the coalescence temperature of the H8 signals represents the barrier for rotation about the Pt-N-(2-picoline) bond. The coalescence of the two close cross-peaks comprising peak **1h** in the 2D [^{1}H, ^{15}N] HSQC NMR spectrum of the bisGMP adduct of complex **1** at 65°C can also be attributed to faster rotation about the Pt-N-(2-picoline) bond at higher temperature. The broadening of one H8 signal and one -CH_3 signal at low temperature (< 296 K) suggests that one of the bound GMP ligands (probably that *cis* to 2-picoline) in a HT stereoisomer is more affected by the rotation of Pt-N-(2-picoline) than the other. Compared with complex **1**, the rotation of 3-picoline in complex **2** is facile, there being little steric hindrance from the methyl group in this case. Slow rotation about Pt-N-(2-picoline) bonds has been reported previously for *cis*-[Pt(2-picoline)$_2$(Guo)$_2$]$^{2+}$ (Guo = guanosine) at room temperature, whilst the rotation about Pt-N7-Guo was still fast on the NMR time scale.[37]

Hydrogen-bond interactions between ammine hydrogens and O(6) or the 5′-phosphate of GMP can give rise to high-frequency ^{1}H chemical shifts of Pt-NH_3 groups in bisGMP adducts (**1h** and **2h**). Platinum coordination to nucleotides is known to induce a change in the sugar-ring conformation from S-type (C2′-*endo*) to N-type (C3′-*endo*), which changes the H1′–H2′ coupling constant,[38] consistent with the small decrease observed in the present work.

The facile rotation of guanine about the Pt-N7 bond is thought to be important in the binding of cisplatin to DNA. From the results obtained here, several isomers would be expected when complex **1** reacts with G bases of DNA because of the steric

effect of 2-picoline and the non-C_2-symmetrical structure, which is similar to *cis*-$[Pt(NH_3)(C_6H_{11}NH_2)Cl_2]$.[39] These isomers may be stabilized by different H-bonding patterns and have contrasting reactivities. Such studies may allow the further development of strategies for the systematic design of platinum antitumor complexes.

Reactions with GSH

The reactions of cisplatin and related Pt complexes with S-containing nucleophiles usually occur *via* direct substitution without prior aquation,[40] as been observed for substitution of Cl^- by methionine, GSH and metallothionein.[41,42,44] However, in the reactions described here, aqua adducts were the first species observed during reactions of both complexes **1** and **2** with GSH. There could be two reasons for this: (1) reactions of complexes **1** and **2** with GSH do proceed *via* hydrolysis, or (2) because of the steric effect of the picoline ligands, binding of GSH is slowed down and hydrolysis is fast enough to compete with direct substitution. Unfortunately the reactions were too complicated to allow a kinetic analysis to be carried out.

The thiolate sulfur of GSH has a high *trans* effect and this can lead to labilization and release of the ammine ligand in the *trans* position.[43] However, despite an overall loss of general signal intensity, no cross-peak for free $^{15}NH_4^+$ was observed in the 2D spectra, probably because of fast proton exchange with H_2O at pH 7. The yellow solids formed during reactions of thiols with platinum complexes are usually thought to be sulfur-bridged polymers.[43,44,45] From the 2D [^{1}H, ^{15}N] HSQC NMR spectrum (Fig. 5.6), the initial binding site for GSH on complex **1** is in the position *trans* to 2-picoline, and attributable to the steric effect in *cis* position, which is similar to the situation of GMP binding.

No rate constants were determined for the reactions of complexes **1** and **2** with GSH due to their complicated nature, but, the time-dependent plots (Fig. 5.7) showed

that complex **1** reacted much more slowly than complex **2**. The half life ($t_{1/2}$) of complex **1** was about three times longer than that of complex **2**.

Competitive binding of GSH and 5′-GMP

At neutral pH, GMP cannot usually compete with thiols for binding to Pt(II) when both ligands are present at equal concentrations.[17] The kinetic preference of $[Pt(dien)(H_2O)]^{2+}$ at neutral pH is exclusively toward thiols when in competition with 5′-GMP.[17] Complex **1** increases steric crowding in the square-plane and circumvents resistance caused by reactions with glutathione and other cellular thiols, but still maintains the ability to form cytotoxic lesions with DNA.[4] From the experimental results obtained above, the rate of binding of the thiol ligand GSH to complex **1** is greatly slowed down but is still faster than that of 5′-GMP. Substitution of Cl^- by the thiol ligand appeared to proceed *via* prior aquation because of the steric hindrance by 2-methylpyridine ligand. The presence of hydrolysis products in the system provides a pathway for the formation of mono- and bis-GMP adducts which are formed *via* hydrolysis steps. The bisGMP adduct was stable in the presence of free GSH even after 3 days, but was present in only small amounts.

5.6 Conclusion

Labelling of the new anticancer drug *cis*-$[PtCl_2(^{15}NH_3)$(2-picoline)] has allowed detailed insight to be gained into the kinetics and mechanisms of its reactions with 5′-GMP and glutathione. The steric effect of 2-picoline reduces the reactivity of complex **1** towards 5′-GMP compared to its 3-picoline analogue, especially towards substitution in the position *cis* to 2-picoline. The low reactivity of complex **1** towards 5′-GMP may explain why it forms interstrand DNA cross-links much more slowly than cisplatin.[2] Two HT isomers were observed for *cis*-$[Pt(^{15}NH_3)$(2-picoline)(5′-GMP-*N7*)$_2]^{2+}$ due to the slow rotation of 2-picoline and non-C_2-symmetrical

structure. Reactions of GSH with complex **1** were *ca.* three times slower than those with **2**, and appeared to proceed *via* aquated intermediates, with initial binding of GS^- *trans* to 2-picoline for **1** and *trans* to NH_3 for **2**. The bisGMP adduct of complex **1** was able to form in the presence of GSH at neutral pH in a competitive reaction. The steric effect of 2-picoline and asymmetric structure of **1** may give rise to several isomers when it binds to DNA. This, together with its low reactivity towards GSH may play an important role in its high activity against cisplatin-resistant cell lines.

5.7 References

(1) J. Reedijk, *Chem. Commun.*, **1996**, 801.

(2) F. I. Raynaud, F. E. Boxall, P. M. Goddard, M. Valenti, M. Jones, B. A. Murrer, M. Abrams, L. R. Kelland, *Clinical Cancer Res.*, **1997**, *3*, 2063.

(3) J. Holford, S. Y. Sharp, B. A. Murrer, M. Abrams, L. R. Kelland, *British J. Cancer*, **1998**, *77*, 366.

(4) J. Holford, F. Raynaud, B. A. Murrer, K. Grimaldi, J. A. Hartley, M. Abrams, L. R. Kelland, *Anti-Cancer Drug Design*, **1998**, *13*, 1.

(5) Y. Chen, Z. J. Guo, S. Parsons, P. J. Sadler, *Chem. Eur. J.*, **1998**, *4*, 672.

(6) S. E. Miller, D. A. House, *Inorg. Chim. Acta*, **1989**, *161*, 131.

(7) F. Raynaud, F. Boxall, P. Goddard, M. Valenti, M. Jones, B. Murrer, C. Giandomenico, L. Kelland, *Proc. 88th Annual Meeting American Assoc. Cancer Res.*, April 12-16, 1997, San Diego, CA, Vol 38, No. 2085, pp. 311.

(8) Y. Zou, B. Van Houten, N. Farrell, *Biochemistry*, **1993**, *32*, 9632.

(9) A. T. M. Marcelis, J. L. van der Veer, J. C. M. Zwetsloot, J. Reedijk, *Inorg. Chim. Acta*, **1983**, *78*, 195.

(10) Y. Xu, G. Natile, F. P. Intini, L. G. Marzilli, *J. Am. Chem. Soc.* **1990**, *112*, 8177.

(11) D. Kiser, F. P. Intini, Y. Xu, G. Natile, L. G. Marzilli, *Inorg. Chem.* **1994**, *33*, 4149.

(12) A. Eastman, *Chem. -Biol. Interact.* **1987**, *61*, 241.

(13) P. C. Dedon, R. F. Borch, *Biochem. Pharmacol.* **1987**, *36*, 1955.

(14) J. Reedijk, in *Handbook of Metal-Ligand Interactions in Biological Fluids*, ed. G. Berthon, Marcel Dekker Inc., New York, 1995, vol. 2, pp. 967.

(15) T. Ishikawa, F. A.-Osman, *J. Biol. Chem.* **1993**, *268*, 20116.

(16) T. Ishikawa, C.D. Wright, H. Ishizuka, *J. Biol. Chem.*, **1994**, *269*, 29085.

(17) R. N. Bose, S. Moghaddas, E. L. Weaver, E. H. Cox, *Inorg. Chem.*, **1995**, *34*, 5878.

(18) S. J. S. Kerrison, P. J. Sadler, *J. Chem. Soc., Chem. Commun.* **1977**, 861.

(19) M. Piotto, V. Saudek, V. Sklenar, *J. Biomol. NMR*, **1992**, *2*, 661.

(20) J. Stonehouse, G. L. Shaw, J. Keeler, E. D. Laue, *J. Magn. Reson. Ser. A*, **1994**, *107*, 178.

(21) E. W. Abel, T. P. J. Coston, K. G. Orrell, V. Sik, D. Stephenson, *J. Magn. Reson.*, **1986**, *70*, 34.

(22) S. J. Berners-Price, P. J. Sadler, *Coord. Chem. Rev.*, **1996**, *151*, 1.

(23) H. Friebolin, *Basic One- and Two- Dimensional NMR Spectroscopy*, VCH, Weinheim, 1991.

(24) G. Pettit, L. D. Pettit, *IUPAC Stability Constants Database*, IUPAC and Academic Software, Otley, United Kingdom, 1993.

(25) F. Basolo, J. Chatt, H. B. Gray, R. G. Pearson, B. L. Shaw, *J. Chem. Soc.* **1961**, 2207.

(26) D. F. Shriver, P. W. Atkins, C. H. Langford, *Inorganic Chemistry*, second edition, Oxford, 1994, pp. 627.

(27) R. Romeo, D. Minniti, M. Trozzi, *Inorg. Chem.*, **1976**, *15*, 1134.

(28) S. S. Eapen, M. Green, I. M. Ismail, *J. Inorg. Biochem.*, **1985**, *24*, 233.

(29) K.J. Barnham, S. J. Berners-Price, T. A. Frenkiel, U. Frey, P. J. Sadler, *Angew. Chem.*, **1995**, *34*, 1874.

(30) S. J. Berners-Price, K. J. Barnham, U. Frey, P. J. Sadler, *Chem. Eur. J.*, **1996**, *2*, 1283.

(31) S. O. Ano, Z. Kuklenyik, L. G. Marzilli, in "*Cisplatin-Chemistry and Biochemistry of a Leading Anticancer Drug*", edited by B. Lippert, WILEY-VCH, 1999, pp. 250.

(32) B. Lippert, *Prog. Inorg. Chem.*, **1989**, *37*, 1.

(33) M. D. Reily, L. G. Marzilli, *J. Am. Chem. Soc.*, **1986**, *108*, 6785.

(34) R. E. Cramer, P. L. Dahlstrom, *Inorg. Chem.*, **1985**, *24*, 3420.

(35) S. J. Berners-Price, U. Frey, J. D. Ranford, P. J. Sadler, *J. Am. Chem. Soc.*, **1993**, *115*, 8649.

(36) K. Inagaki, F. J. Dijt, E. L. M. Lempers, J. Reedijk, *Inorg. Chem.*, **1988**, *27*, 382.

(37) A. T. M. Marcelis, J. L. Van Der Veer, J. C. M. Zwetsoot, J. Reedijk, *Inorg. Chim. Acta,* **1983**, *78*, 195.

(38) K. Okamoto, V. Behnam, M. T. Phan Viet, M. Polissiou, J. Y. Gauthier, S. Hanessian, T. Theophanides, *Inorg. Chim. Acta*, **1986**, *123*, L3.

(39) J. F. Hartwig, S. J. Lippard, *J. Am. Chem. Soc.*, **1992**, *114*, 5646.

(40) A. J. Repta, D. F. Long, in *Cisplatin Current Status and New Developments*, eds. A. W. Prestayko, S. T. Crooke and S. K. Carter, Academic Press: New York, 1980, pp. 285.

(41) M. I. Djuran, E. L. M. Lempers, J. Reedijk, *Inorg. Chem.*, **1991**, *30*, 2648.

(42) B. J. Corden, *Inorg. Chim. Acta,* **1987**, *137*, 125.

(43) K. J. Barnham, M. I. Djuran, P. del S. Murdoch, J. D. Ranford, P. J. Sadler, *Inorg. Chem.*, **1996**, *35*, 1065.

(44) T. G. Appleton, J. W. Connor, J. R. Hall, P. D. Prenzler, *Inorg. Chem.*, **1989**, *28*, 2030.

(45) B. Odenheimer, W. Wolf, *Inorg. Chim. Acta*, **1982**, *66*, L41.

Chapter 6

Solution Structural Studies of a DNA 14-mer Duplex Possessing a d(GpG) Cisplatin Intrastrand Cross-link

6.1 Abstract

The intrastrand d(GpG) cross-link is the major adduct for cisplatin binding to DNA. I present here NMR solution structural studies of a DNA 14-mer duplex, d(ATACAT*G*G**TACATA)·d(TATGTA*CC*ATGTAT) intrastrand cross-linked at the d(G*pG*) site by *cis*-$\{Pt(NH_3)_2\}^{2+}$. This DNA duplex is longer in length and richer in A-T base pairs compared with the platinated DNA duplexes reported in previously studies. The binding of cisplatin cause the adjacent guanine bases to roll toward each other by 43°, leading to an overall helix bending angle of 47°. The minor groove opposite the platinum binding lesion is widened and flattened with geometric parameters similar to those of A-form DNA. The unwinding of the helix at the platinated site is 26°. The structural differences between the results of the current study and those of other studies are discussed based on the differences of DNA sequence and length.

6.2. Introduction

The complex *cis*-$[PtCl_2(NH_3)_2]$, clinically known as 'cisplatin', is the most widely used antitumor drug.[1] Its antitumor activity is believed to result from covalent binding to DNA and subsequent modification of the structure of DNA. Cisplatin forms many kinds of DNA adducts in cells, including major intrastrand d(GpG) (70%) and d(ApG) (15%) cross-links, where platinum binds to two adjacent guanine residues or an adjacent adenine and guanine.[1] Other minor adducts include 1,3-intrastrand and interstrand cross-links. The major intrastrand crosslink adducts formed at the d(GpG) and d(ApG) sites have been suggested to be responsible for the biological activity of cisplatin, because their presence in cancer patients correlates with a positive response to treatment with the drug.[2] Such lesions have deleterious effects on DNA replication and transcription,[3] and cause mutations.[4] Recent studies show that proteins containing one or more high-mobility group (HMG) domains can

recognise and bind to these intrastrand *cis*-[Pt(NH$_3$)$_2$\{d(GpG)\}] and *cis*-[Pt(NH$_3$)$_2$\{d(ApG)\}] adducts.[5,6,7] The shielding of excision repair caused by binding of the HMG proteins on DNA has been confirmed by *in vitro* and *vivo* experiments.[8,9] Such biological effects are clearly correlated with the structures of the cisplatin-DNA adducts, and it is therefore very important to understand the structural details of these DNA duplex adducts.

Several studies have been reported on the structural distortions of cisplatin-DNA adducts. An X-ray crystal structure of *cis*-[Pt(NH$_3$)$_2$-\{d(GpG-N7(1),N7(2))\}] shows that cisplatin forms bidentate adducts with the two adjacent guanines joined together in a "head-to-head" configuration, with the dihedral angles between the two Gs ranging from 72° to 82°. The deoxyribose rings of the 5′- and 3′-dG nucleotides have C3′-endo (N-type) and the C2′-endo (S-type) pucker, respectively.[10] More recently, the crystal structure of a duplex dodecamer d(5′-CCTCTG*G*TCTCC-3′)·d(5′-GGAGACCAGAGG-3′) (**2**), where G*G* represents the 1,2-intrastrand cisplatin adduct, was solved to a resolution of 2.6 Å.[11,12] The triclinic crystals contained two independent molecules which have similar structures for the platinum-modified duplex. Two different bending angles were observed, one of 39° and the other of 55°. The bend is largely due to a roll of 26° toward the major groove at the G*G* site of the platinum intrastrand cross-link. The binding of the platinum atom to the N7 atoms of adjacent guanine residues, caused the major groove to become compacted and the minor groove widened and flattened. In particular, the Pt atom was displaced from the plane of each guanine base by approximately 1 Å. The overall structure of the cisplatin-modified duplex contains an unusual A-/B-form junction situated just to the 3′ side of the platinum adduct, most likely to be due to crystal packing force. An analysis of the unit cell packing revealed end-to-end and end-to-groove interactions between the platinated duplexes.

The effects of crystal packing are known to influence structures and for this reason there is much interest in solving solution structures of platinated DNA duplexes. NMR spectroscopy has played an important role in structural studies of platinum-DNA adducts. Early attempts to elucidate the solution structure of the cisplatin 1,2-intrastrand cross-link in double-stranded DNA indicated that the duplex formed a kink towards the major groove at the platinum coordination site.[13] With the aid of molecular mechanics and dynamics calculations to build models consistent with observed NMR data, the kink was estimated to be about 60° and the remainder of the helix was in an undistorted B-form. More recently, the NMR structure of a short octameric duplex d(CCTG*G*TCC) was reported.[14] The NOE-restraint refined duplex is unwound (~-21°) and kinked (~58°) towards the major groove at the G*G* site, and the minor groove is significantly widened. In order to detect the structural consequences of the major cisplatin adduct over at least one turn of DNA duplex and compare differences between the solution and solid state structures, the solution structure of a platinated DNA duplex dodecamer, with the same DNA sequence used in X-ray crystal structure studies d(CCTCTG*G*TCTCC), was recently reported from the group of Lippard.[15] Although the unwinding and flattening of the minor groove opposite the platinum adduct is similar in both the solution and crystal structures, some of the features are more exaggerated in the solution structure compared with the X-ray crystal structure. The *cis*-[$Pt(NH_3)_2$-{d(GpG-N7(1),N7(2))}] lesion causes the adjacent guanine bases to roll toward one another by 49°, leading to an overall helix bend angle of 78°. This deformation is especially noteworthy for the solution structure, because the DNA sugar puckers are primarily those of B-form DNA. Unwinding of the helix at the site of platination is 25° and the Pt atom is displaced from each base plane by ~0.8 Å. The greater helix deformation may have been prevented in the crystal structure due to helix packing interactions at the site of platination. Of total 12 possible imino resonances, only that from G6* was

not observed indicating fast exchange with H_2O and disruption of base pairing at 5′-G*, as reported for other studies.[14] The imino protons for terminal bases can only be observed at low temperature without any NOEs to other protons. Using a nitroxide spin-labeled platinum complex *cis*-[Pt(NH_3)(4-aminoTEMPO)Cl], the same group also determined the NMR solution structure of an undecamer DNA duplex d(CTCTCG*G*TCTC). The structure was determined from conventional NOE studies of the reduced, diamagnetic undecamer and long-range (10-20 Å) electron-proton restraints from the paramagnetic duplex.[16] Refinements of the structure with either conventional interproton restraints or a combination of the electron-proton and interproton restraints afforded the same local but different global structures. Significant similarity was found for the later structure to the tertiary structure of a cisplatin-modified dodecamer duplex solved by X-ray crystallography, although their bending angles determined by the programme CURVES are quite different.[11]

Comparing the results of previous studies, differences appear to show between the solution structures of the cisplatin d(G*pG*) cross-linked DNA duplexes depending on the methods used to solve the structures, and, more importantly, on the sequence and length of DNA duplex used for the study. A rearrangement from an intrastrand to a more stable interstrand cross-link was observed in the study of d(CCTG*G*TCC), while this was not observed for the dodecamer d(CCTCTG*G*TCTCC).[14,15] The differences observed in the studies were attributed to the short length and instability of the duplex, which is responsible for the reactivity of its strained Pt-N7 bonds.

The 14-mer DNA duplex, d(ATACATG*G*TACATA), has been used in kinetic studies of DNA platination.[17] Remarkably long-lived monofunctional adducts, which could have important biological significance, were observed during the course of the formation of the GpG bifunctional adducts. The sequence of this DNA 14-mer is more rich in AT base pairs compared with the other reported DNA sequences used in

structural studies of DNA intrastrand platination. In duplex DNA, major and minor grooves provide the topology and there are sequence-dependent variations in the patterns of hydrogen bonding with relatively significant variations in the minor groove. Features which vary according to DNA sequence range from relatively gross changes in bending, to effects of groove width, and finally to local variations in the disposition of contact points with bound ligand. Usually DNA or RNA duplexes rich in AT base pairs exhibit slightly different structural characteristics compared with those rich in GC base pairs.[18] Knowledge about sequence-dependent variations in platinated DNA duplex geometry may be essential to protein recognition. Besides the sequence, the length of d(G*pG*) platinated DNA duplex may also have an important influence on the structure. To my knowledge, the length of the DNA used in this study (14-mer), which is over one turn, is the longest used in the structural studies of interactions between cisplatin and DNA.

In this work, the solution structure of the platinated DNA 14-mer duplex has been determined by NMR spectroscopy and restrained Molecular Dynamics (rMD). The observed structural features are compared to those reports previously for crystal and NMR-derived platinated DNA structures, and the results are discussed.

5′ d(A_1 T_2 A_3 C_4 A_5 T_6 G_7 $G_8$$T_9$ $A_{10}$$C_{11}$$A_{12}$$T_{13}$$A_{14}$) I

I + II = III

3′ d($T_{28}$$A_{27}$$T_{26}$$G_{25}$$T_{24}$$A_{23}$$C_{22}$$C_{21}$$A_{20}$$T_{19}$$G_{18}$$T_{17}$$A_{16}$$T_{15}$) II

6.3. Experimental

Materials

cis-[$PtCl_2(^{15}NH_3)_2$] and *cis*-[$Pt(^{15}NH_3)_2(H_2O)_2]^{2+}$ were prepared as previously described.[19] The sodium salts of HPLC-purified 14-mer oligonucleotides d(ATACATG*G*TACATA) (strand **I**) and its complement strand d(TATGTACCATGTAT) (strand **II**) were supplied by Oswel (Southampton, U. K.).

Platination of single strand I with *cis*-$[Pt(^{15}NH_3)_2(H_2O)_2]^{2+}$

The platinated DNA adduct (**I***) of the GG 14-mer single strand **I** was prepared by reaction of 0.1 mM GG single strand **I** with 1.2 mole equiv. of prepared *cis*-$[Pt(^{15}NH_3)_2(H_2O)_2]^{2+}$ in water at 298 K in the dark. The reaction was monitored by HPLC using a Nucleosil C_8 300 Å stainless steel column. After a total of one week of incubation, the reaction was judged to be complete and the separation was carried out using Biocad perfusion chromatography with a Poros RV Column (100 mm × 4.5 mm). Operating conditions: mobile phase ammonium acetate 5mM, 50 % acetonitrile (gradient: 5% acetonitrile for 5 mins; from 5 min to 19 min 5% to 25%, from 19 min to 22 min 25%), flow rate 1 ml·min^{-1}, 298 K. The retention time of unplatinated single strand was 7.7 min compared with the platinated adduct of 14.9 min. The platinated adduct was collected and freeze-dried to remove the volatile salts. The final yield of platinated single strand was less than 50%. The purity of the separated G*G* adduct was checked by both HPLC, 1D ^{1}H and 2D [^{1}H, ^{15}N] HSQC NMR spectroscopy. The method development for HPLC separation was carried out with the assistance of Dr. P. del. S. Murdoch.

Preparation of Platinated DNA 14-mer Duplex

The NMR sample was prepared by adding one mole equivalent amount of the complementary CC strand **II** to the purified platinated GG strand **I** to give a final platinated DNA duplex concentration of 0.9 mM in 100 mM $NaClO_4$ and 90% H_2O/10% D_2O. The concentrations of the DNA single strands **I** and **II** were measured by UV spectroscopy (extinction coefficients at 260 nm for GG strand: 149 $M^{-1}cm^{-1}$; CC strand: 137.2 $M^{-1}cm^{-1}$). The precise ratio of the two strands was also monitored by 1D ^{1}H-NMR spectra. The platinated DNA duplex (**III***) was annealed by heating briefly to 343 K followed by slow cooling of the solution to room

temperature. The extent of duplex formation was verified by the 1D ^{1}H-NMR and 2D [^{1}H, ^{15}N] HSQC NMR spectra. The pH of the solution was raised from 4.3 to 6.2 using 0.5 M NaOH solution. Dioxane (3.767 ppm, 25 °C) was added as an internal reference for ^{1}H NMR. The D_2O sample was prepared by freeze-drying the DNA sample twice from 99.9% D_2O and finally dissolving it in 99.9% D_2O to afford a concentration of 0.9 mM DNA duplex.

NMR Data Acquisition and Analysis

One-dimensional (1D) ^{1}H and two-dimensional (2D) NOESY and DQF-COSY NMR spectra were acquired both at 500 MHz on a Bruker DMX500 NMR spectrometer using a TBI [^{1}H, ^{13}C, X] probe-head equipped with a z-field gradient coil, and at 600 MHz on a Varian ^{Unity}INOVA spectrometer using a triple resonance probe-head [^{1}H, ^{13}C, ^{15}N] equipped with z-field gradients. 500 MHz 2D NOESY experiments on exchangeable imino protons were carried out at 5 °C using a 90% H_2O/10% D_2O sample. Data were acquired over a ^{1}H spectral width of 21 ppm (10.5 kHz) into 4096 data points with 64 transients for each of 512 t_1 increments (TPPI). The mixing times were 150 and 300 ms, and the recycle delay was 2.0 s. The solvent signal is on resonance and water suppression was achieved by using the WATERGATE[20] pulse sequence prior to data collection. One-dimensional (1D) NMR spectra were acquired with 128 transients into 32 K data points over a spectral width of 10.5 kHz using a double pulsed field gradient spin echo pulse sequence.[21] Other acquisition parameters were: relaxation delay, 1.8 s; dummy scans, 4; solvent selective pulse length, 1.954 ms. Data were apodized using a line broadening function of 0.5 Hz prior to Fourier transformation into 32 K data points. Chemical shifts were internally referenced to dioxane calibrated at different temperatures according to the expression: $\delta = 3.8415 - (0.25 \times 10^{-3} \times T/K)$.

High resolution 600 MHz 2D NOESY data sets were acquired at 5 °C using the 99.9% D_2O sample with 40 transients acquired over a ^1H spectral width of 9 ppm (5.4 kHz) into 4096 data points for each of 2×256 t_1 increments (States). The mixing times were 150 and 300 ms and the recycle relay was 3.5 s. The 512 data increments were zero filled to 1024 points and apodized using a $\pi/2.5$ shifted sine-squared function before Fourier transformation. Automatic baseline corrections were carried out in both dimensions. 600 MHz 2D DQF-COSY spectrum was acquired at the same temperature (5 °C) with 96 transients for each of 2×512 t_1 increments (States) over a spectral width of 10 ppm (6.0 kHz). Water suppression was achieved by presaturation using a 1.5 s pulse during the pre-acquisition delay.

Two-dimensional (2D) [^1H, ^{15}N] HSQC NMR data sets were acquired on the 500 MHz at a calibrated probe temperature of 25 °C. All data acquisitions were carried out using 8 transients into 1024 data points over a ^1H (F2) spectral width of 2 kHz (4 ppm, centred at the water resonance) for each of 128 t_1 increments (TPPI), and over a ^{15}N (F1) spectral width of 1.52 kHz (30 ppm, centred at -75 ppm). A GARP decoupling scheme, centred at ^{15}N chemical shift of -75 ppm, was applied during the acquisition time. A relaxation delay of 2.0 s was used for all experiments. Coherence pathways were selected *via* the use of z-field gradients,[22] and the ^1H solvent resonance was eliminated as part of this procedure. Data were zero-filled to 1024 data points in both dimensions prior to apodization with Gaussian weighting functions and Fourier transformation. Data were referenced internally (^1H) to dioxane at 3.767 ppm and externally (^{15}N) to the ^{15}N resonance of $^{15}NH_4Cl$ at 0 ppm. A post-acquisition filter was applied at the solvent signal position to remove the residual solvent resonance. Typically 2D [^1H, ^{15}N] HSQC spectra were acquired over a 33 minute period.

All spectra were processed using XWIN-NMR version 1.3 (Bruker U. K. Ltd.). Processed data were imported into the TRIAD NMR module of Sybyl (version

6.3, Tripos Inc.) for data reduction. NOESY data were assigned for the platinated-DNA 14-mer duplex using well established assignment strategies for right-handed B-form DNA.[23,24] DQF-COSY data were used to confirm the assignments of 2′ and 2″H resonances of sugar rings.

Generation of Experimental Restraints

Initial structures for canonical A- and B-DNA conformations were generated using the Sybyl 6.3 software. The atom charges for DNA were calculated using the Pullman method.[25] The backbone charges were reduced to 0.5 to implicitly incorporate counter-ion effects. The *cis*-diammineplatinum(II) residue was docked onto the N7 atoms of G7* and G8*. The bond lengths and angles of docked *cis*-diammineplatinum(II) residue were set according to the crystal structure data with the chloride ligands removed.[11] Charges for the *cis*-diammineplatinum(II) residue and the bound guanine bases were modified according to a molecular mechanics calculation by Herman et al.[13] The platinated A- and B-DNA structures were energy-minimized, and subsequently used as starting structures in the restrained molecular dynamics calculations.

2D NOE intensities were measured using peak-picking in NMR Triad module of Sybyl 6.3. Final intensities were obtained by averaging corresponding cross-peaks on both sides of the diagonal. Proton-proton distances were calculated from 2D NOE cross-peak intensities using the complete relaxation matrix approach implemented in the program MARDIGRAS[26] repeated with randomly assigned correlation times τ_c (2, 3, 4 ns) and noise levels (0.002, 0.003, 0.004). An isotropic tumbling motion was assumed for the molecule, with an overall correlation time of 2.0 ns.[27] MARDIGRAS calculations were carried out on both A- and B-form starting structures from NOESY data acquired at two different mixing times (150, 300 ms). A final distance restraint set was pooled using Windows 95 EXCEL from all the results calculated by

MARDIGRAS.[28] The distances involving exchangeable protons were calculated quantitatively by classifying the intensity of NOE cross-peaks as strong, medium and weak using a single set of intensities acquired with 150 ms mixing time.

Deoxyribose sugar puckers were deduced for those sugar rings displaying clearly resolved DQF-COSY cross-peaks between 2′, 2″H and 1′H using the programs SPHINX and LINSHA.[29] A six component spin-system (H1', H2', H2", H3', H4' and P) was used for all simulations with strong coupling only between geminal protons (H2' and H2"). The conformations of the sugar rings were estimated by matching the experimental coupling constants to values calculated assuming a two-state model with rapid N-S interconversion for the sugar pucker, which reflects the dynamics of sugar rings.[30] Coupling constants and resonance linewidths were systematically varied until the best match between simulated and experimental data was observed. Simulations were compared for cross-peaks from both sides of the diagonal. Other simulation variables such as digital resolution, acquisition time and window functions were also set to match. This analysis yielded five torsion angle restraints per sugar residue for the subsequent rMD structure refinement. The torsion angle restraints were inputted manually according to the simulation results.

In addition to the NMR-derived sugar torsion angles and interproton distances, hydrogen bond distances and angles were also included in the restraint data set to maintain Watson-Crick hydrogen bonding during the simulations. These restraints were taken from crystallographic data. Target distances between proton donor and acceptor in G·C base pairs were set to 2.81 Å ≤ d(GO6, CN4) ≤ 3.01 Å, 2.84 Å ≤ d(GN1, CN3) ≤ 3.05 Å, and 2.76 Å ≤ d(GN2, CO2) ≤ 2.96 Å; for A·T base pair, lower and upper limits were 2.72 Å ≤ d(AN1, TN3) ≤ 2.92 Å and 2.85 Å ≤ d(AN6, TO4) ≤ 3.05 Å.[31] The force constants for Watson-Crick hydrogen bonding distance restraints were always lower than that for experimental NOE distance restraints throughout the simulations.

Overall, the restraint set consisted of 120 torsion angle restraints, 665 distance restraints and an additional 76 restraints (distance and angle) defining the Watson-Crick hydrogen bonds of the DNA duplex. The angles of the *cis*-$\{Pt(NH_3)_2\}^{2+}$ residue was also defined so as to maintain square-planar geometry.

Restrained Molecular Dynamics

The Molecular Dynamics module in Sybyl 6.3 enables energy refinements on structures to be performed using NMR-derived distance and torsion angle restraints. Restraint energy violations are calculated for each distance restraints using a flat-well potential, where the lower and the upper bounds derived from MARDIGRAS define the size of the flat-well width. The force constants ($kcal \cdot mol^{-1} \cdot Å^{-2}$) for NOE distance restraints were defined according to the difference between the calculated upper and lower bounds from MARDIGRAS: below 1 Å (20), 1 to 2 Å (15), 2 to 3 Å (10), 3 to 5 Å (5), 5 to 10 Å (1), over 10 Å (0). All the calculations were carried out on a Silicon Graphics Indigo2 workstation.

Different rMD strategies were applied to platinated A-form and B-form starting DNA structures. For B-DNA, all the rMD runs were kept at the same temperature of 300 K. While for A-DNA, a strategy similar to simulated annealing techniques for proteins (elevated temperature with high force-constants) was used to overcome energy barriers associated with larger conformational changes.[32] Typical molecular dynamics simulations were carried out *in vacuo* with a time step of 1 fs. Snapshots were taken every 100 fs. All atoms within 30 Å radius were included in non-bonded interactions, and the non-bonded pair list was updated every 25 steps. The Tripos force field was used in all the calculations. The snapshots from the last 3-5 ps of the rMD trajectory were averaged and energy-minimized with restraints to remove averaging artifacts. During all restrained energy minimization, force constants were the same as those employed during the final rMD equilibrium period.

The structures were energy-minimized by steepest descent first, followed by 200 steps of Powell minimization.

The NMR experiments and final structural calculations were carried out with the assistance of Dr. J. A. Parkinson.

pH Measurements

These were made using a Corning 145 pH meter equipped with an Aldrich micro-combination electrode calibrated with Aldrich buffer solutions of pH 4, 7 and 10. Values of pH were adjusted with 1 M $HClO_4$ or NaOH as appropriate.

6.4. Results

Preparation of purified G*G* platinated single strand and DNA duplex Platinated G*G* single strand **I*** was prepared by incubation of GG single strand **I** (0.1 mM) with 1.2 molar equivalents of *cis*-$[Pt(^{15}NH_3)_2(H_2O)_2]^{2+}$ at 25 °C. After one week, the reaction was judged to reach equilibrium and the separation of platinated single strand **I*** was carried out by HPLC. Figure 6.1 (A, B) shows HPLC chromatograms corresponding to the samples before and after HPLC separation. The separated samples of the free and platinated single strand were re-injected into HPLC using the elution conditions reported before.[33] From the retention time, the two separated peaks are confirmed to be free and G*G* platinated single strand. The purified platinated single strand **I*** and double strand **III***, which was prepared by annealing with complementary CC strand **II**, were also checked by 2D [^{1}H, ^{15}N] HSQC NMR and spectra are shown in Figure 6.2. In both cases, two cross-peaks were observed for platinated single strand (δ ^{1}H/^{15}N, 4.58/-65.19, 4.51/-66.49) and double strand (δ ^{1}H/^{15}N, 4.43/-70.45, 4.20/-70.26). Comparing the spectra with reported shifts for the same adducts,[33] these two pairs of cross-peaks correspond to the platinated G*G* 14-mer single strand and platinated DNA duplex (Figure 6.2A and 6.2B, respectively).

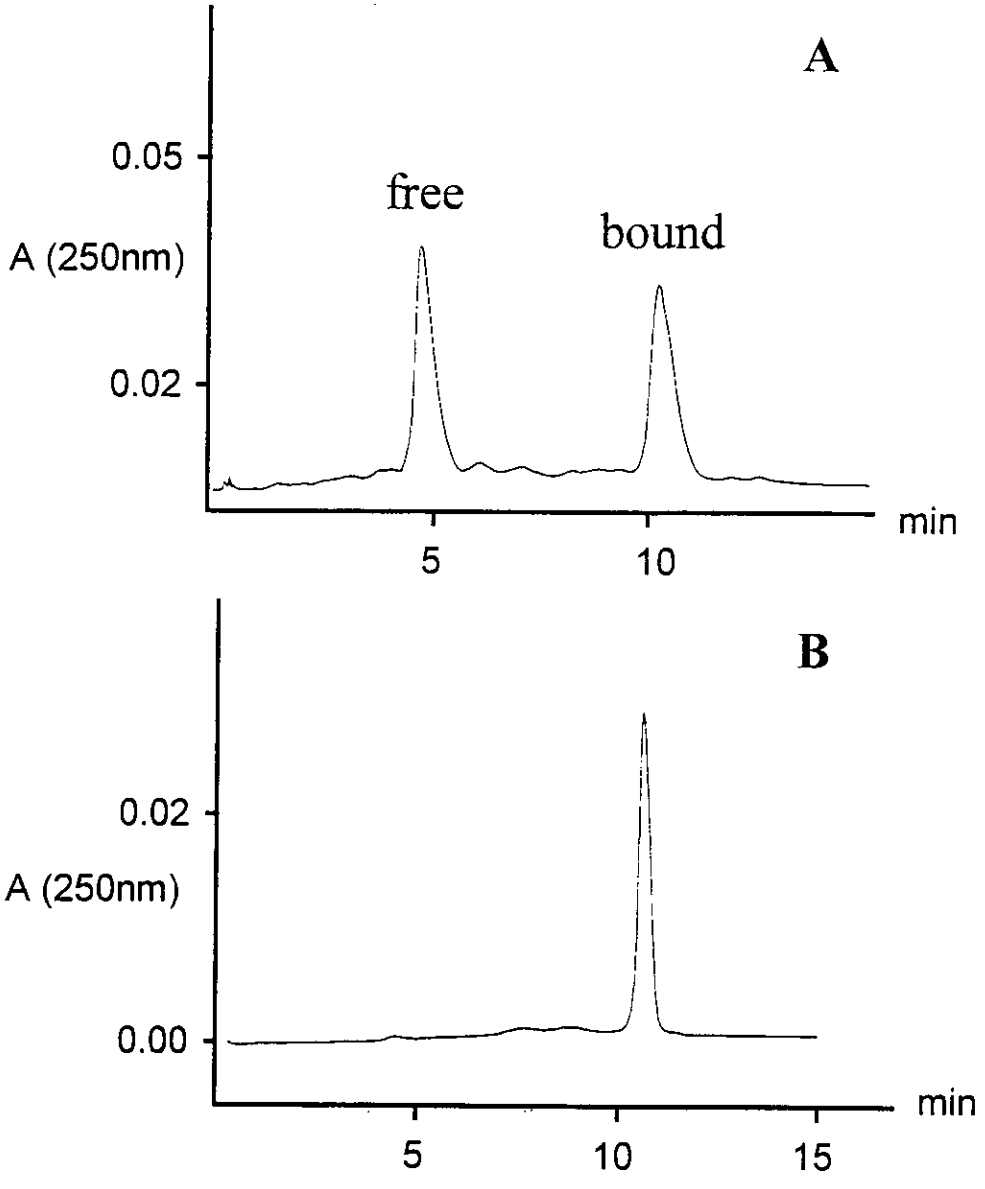

Figure 6.1 HPLC chromatograms for the reaction of *cis*-$[Pt(NH_3)_2(H_2O)_2]^{2+}$ with DNA 14-mer single strand **I** (100 μM, 1:1.2 molar ratio, 298K). (A) one week after incubation; (B) re-injection of purified sample corresponding to "bound" fraction in A, the unplatinated single strand with retention time *ca.* 7 min has disappeared.

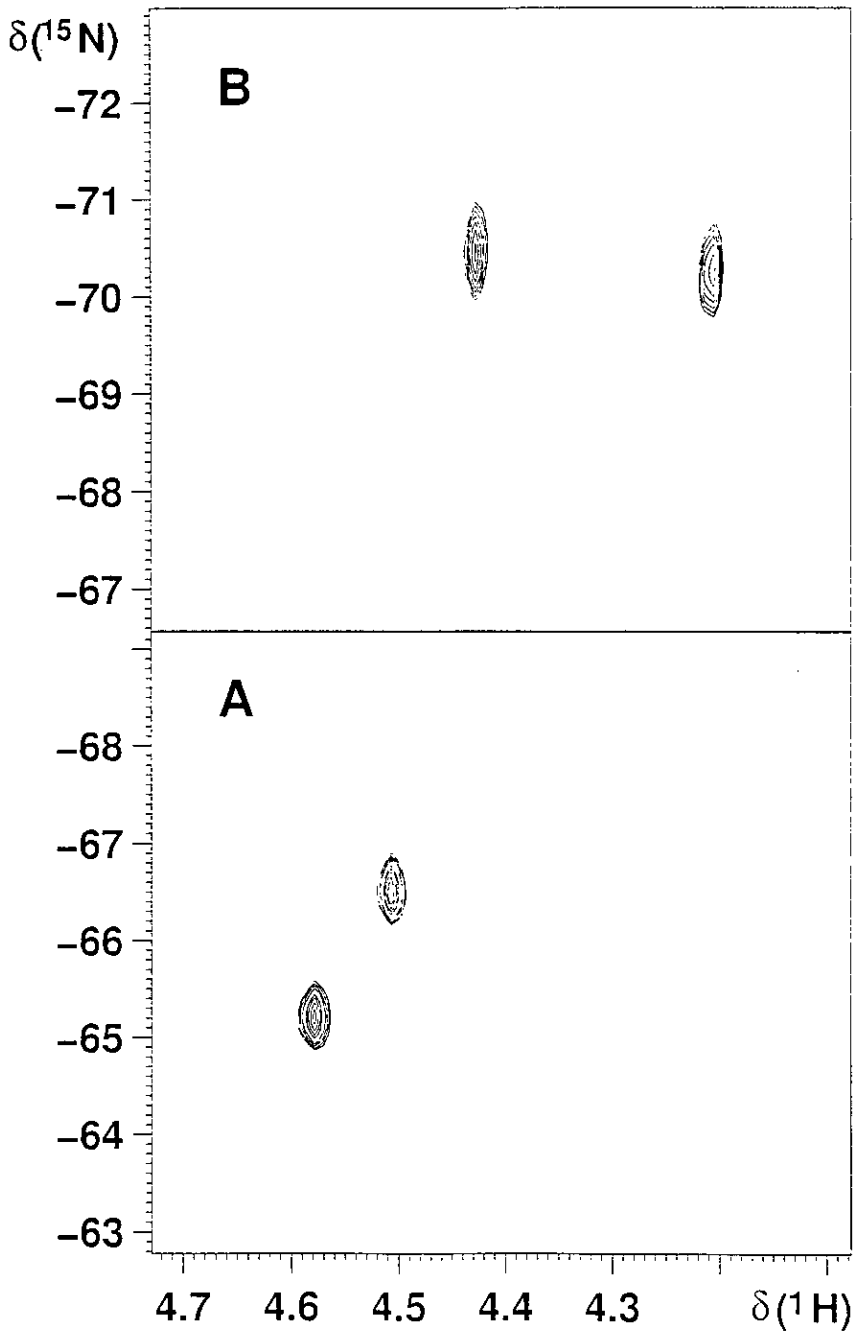

Figure 6.2 2D [^{1}H, ^{15}N] NMR spectra recorded at 298 K of (A) the HPLC purified platinated G*G* 14-mer single strand **I***; (B) platinated 14-mer DNA duplex **III*** formed by annealing the purified G*G* single strand **I*** with its complementary CC strand **II** (0.1 M $NaClO_4$, pH 6.0, 9 mM phosphate buffer, 90% H_2O/10% D_2O). Only one pair of cross-peaks was observed in each spectrum which suggests that the purity of the platinated single strand and duplex samples is high.

NMR Spectroscopy of Platinated 14-mer DNA duplex Assignments of the base and sugar protons were made through analysis of the 150 and 300 ms NOESY spectra using established methods.[24,29] Contour plots of the H8/H6/H2-to-H1′ region of the 300 ms NOESY spectrum are shown in Figure 6.3. The H6/H8 resonances of the 5′-terminal residues (A1 and T15 for strands **I** and **II** respectively) are NOE connected only to the H1′ of their own sugars and therefore only one cross-peak is exhibited for each. These NOEs were used as starting points for the sequential assignment of both strands. The sequential connectivities from *n*H8/H6 to *n*H1′ and from *n*H1′ to (*n*+1)H8/H6 for A1 to A14 in the platinated (top) strand **I*** and for T15 to T28 in the complementary (bottom) strand **II** were all identified and are shown in Figures 6.3A and 6.3B. The assignment walks are fundamentally consistent with right-handed duplex DNA. The H8 signals of the two platinated bases G7* (8.64 ppm) and G8* (8.08 ppm) are downfield (high frequency) shifted from their normal positions (G7: 7.75 ppm; G8: 7.56 ppm)[34] for a free B-DNA duplex. Strong NOE connectivities were observed between these two protons, which is similar to the previously reported NMR studies of DNA duplexes platinated at G*G* sites by cisplatin.[14,15] NOESY spectra recorded at different temperatures were used to clarify assignments for some of the overlapped cross-peaks. Besides H8/H6 to H1′ cross-peaks, relatively weak NOE signals were observed for most of the adenosine H2 protons (except A10 and A20) to interstrand, intra- and inter-nucleotide H1′ sugar protons. Strong intranucleotide NOEs were observed between cytosine H6 to H5 protons, which also show internucleotide NOE connectivities to H8 of nearby 5′-adenosine.

An analogous NOESY walk between the base and sugar protons was used to assign H3′, H2′ and H2′′ protons. A significantly high-field shifted resonance was observed for T6 H2′ (from 1.92 ppm[34] to 1.37 ppm). A contour plot of the H2′/H2′′/thymidine Me-to-aromatic region from the 300 ms NOESY spectrum is

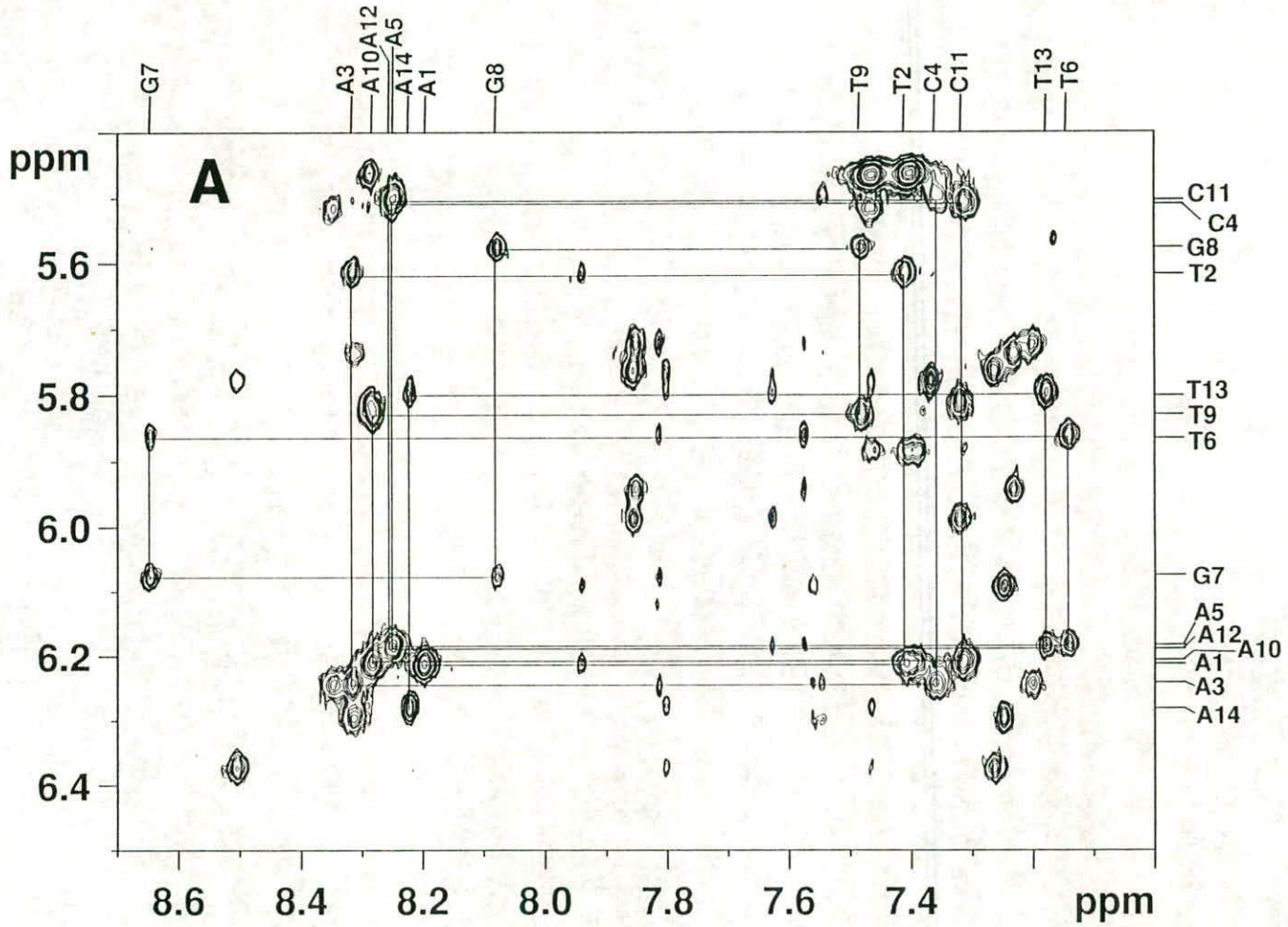

Figure 6.3 Contour plots of the 2D NOESY spectrum (300 ms mixing time, 99.9% D2O, 278 K) of **III*** showing the aromatic H8/H6/H2 to H1′/H5 region. The sequential NOESY walks are shown in (A) for the platinated G*G* top strand **I*** and (B) for the unplatinated CC bottom strand **II** present in duplex **III***.

Figure 6.3B

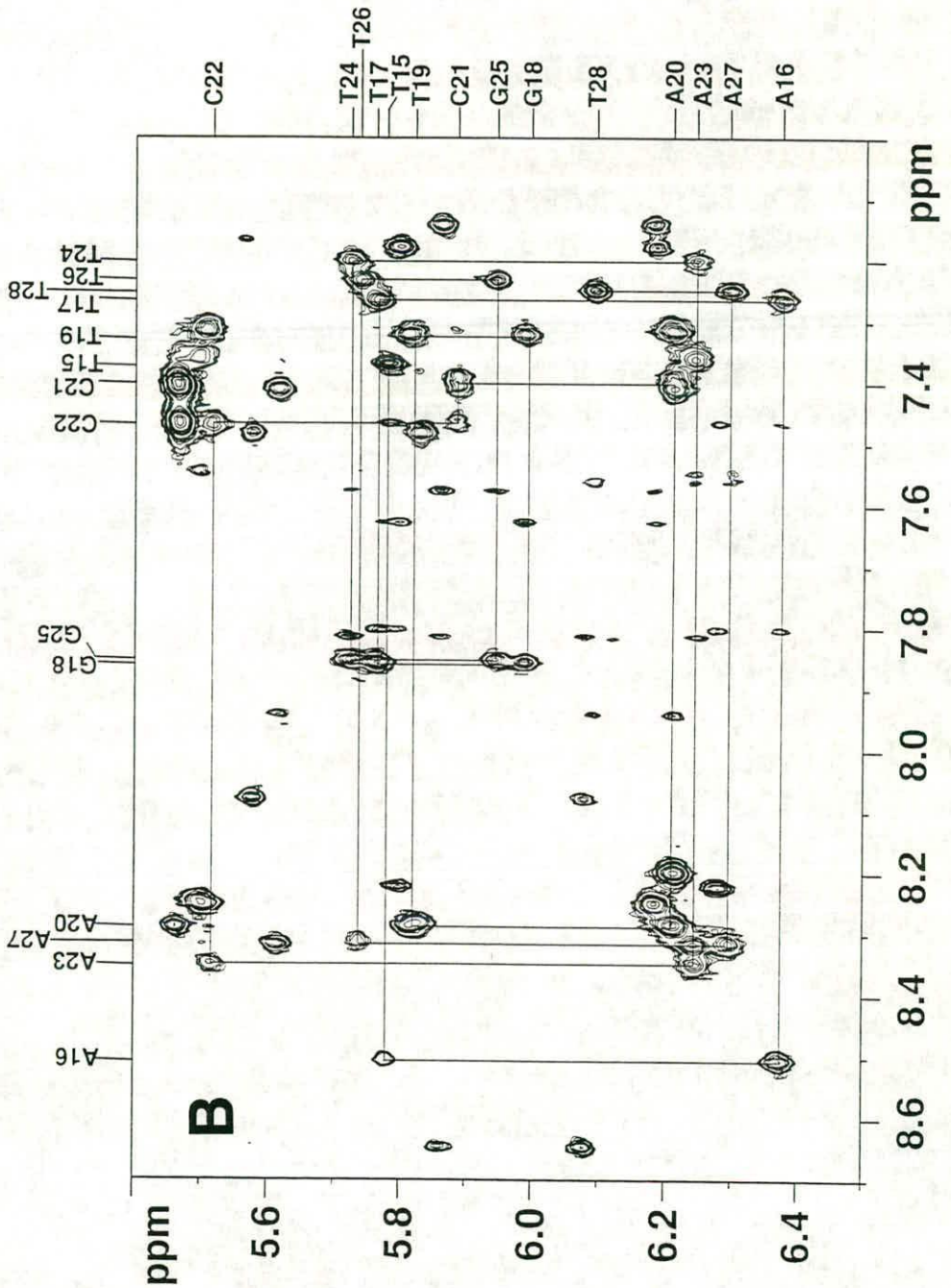
C22
T24
T26
T17
T15
T19
C21
G25
G18
T28
A20
A23
A27
A16
B
ppm
5.6
5.8
6.0
6.2
6.4
8.6
8.4
8.2
8.0
7.8
7.6
7.4
ppm

shown in Figure 6.4. A combination of NOESY and DQF-COSY data were used to complete and confirm the assignments of the sugar protons including the H4′ and some of the H5′/H5′′ protons. The chemical shifts of the assigned non-exchangeable protons are listed in Table 6.1.

Assignments for important exchangeable protons for the platinated 14-mer DNA duplex were made through analysis of the 150 ms NOESY spectra recorded in 90% H_2O/10% D_2O at 5 °C. The imino-to-imino contour plot region is shown in Figure 6.5. The assignment of these protons was achieved *via* a chain of connectivities involving Watson-Crick hydrogen bonding, only interrupted at the G7* site. The resonances for the imino protons of the pairs A1-T28, T2-A27, T13-A16 and A14-T14 present at the 5′ and 3′ ends were missing. The imino proton of G7* was assigned by comparing 1D ^{1}H NMR spectra recorded at different temperatures (Figure 6.6). On lowering the temperature, an imino proton signal at 13.49 ppm gradually increased in intensity and became clearly visible at 5 °C, but no NOE connectivities were observable between this proton and other imino protons in Figure 6.5. The assignments for imino proton resonances were further confirmed by cross-peaks from thymidine imino protons to adenosine H2 protons within A·T base pairs and guanosine imino protons to cytidine H4 amino protons within G·C base pairs. It is interesting to note that the NOE connectivities remain intact between G7* 1-NH and C22 4-NH_2 (both the hydrogen-bonded amino proton in the G·C base pair and the non-hydrogen-bonded amino proton), but relatively weaker than the NOE between G8* NH and C21 4-NH_2. Similarly, strong NOEs were observed between the imino protons of G18 and G25 and 4-NH_2 of C11 and C4, respectively. Both the imino proton chemical shifts of G7* (13.49 ppm) and G8* (13.06 ppm) appear downfield shifted compared with G18 (12.46 ppm) and G25 (12.42 ppm). This is also true for the imino protons of T6 (13.96 ppm) and T9 (13.80 ppm). The chemical shifts for the exchangeable protons are listed in Table 6.1.

Table 6.1 ^{1}H chemical shift assignments (ppm) for the DNA 14-mer duplex **III*** in 0.1 M $NaClO_4$ at pH 6.2 and 278 K.

base	H6/H8 [a]	H5/CH_3/H2 [b]	H1′	H2′/H2″	H3′	H4′	H5′/H5″	GH1/TH3	CH4b/H4f [c]
A1	8.20	7.94	6.21	2.69/2.85	4.87	4.27	3.81		
T2	7.41	1.37	5.61	2.20/2.48	4.91	4.23	4.12		
A3	8.31	7.54	6.24	2.73/2.90	5.06	4.46			
C4	7.36	5.29	5.50	2.12/2.39	4.84	4.23*			8.12/6.59
A5	8.25	7.58	6.18	2.63/2.83					
T6	7.14	1.41	5.86	1.37/2.37	4.79	4.29	4.11/4.06	13.96	
G7	8.64		6.08	2.50/2.72	5.09	4.23	4.15/4.07	13.50	
G8	8.08		5.58	2.23/2.55	4.64	4.18	4.08	13.06	
T9	7.48	1.31	5.83	2.27/2.63	4.91	4.24		13.80	
A10	8.28		6.21	2.67/2.90	5.03	4.41			
C11	7.32	5.30	5.51	2.05/2.37*	4.84	4.19			8.17/6.63
A12	8.28	7.63	6.18	2.59/2.84					
T13	7.18	1.48	5.80	1.90/2.27	4.81	4.11	4.11/4.08		
A14	8.22	7.47	6.28	2.67/2.43	4.70	4.20			

base	H6/H8 [a]	H5/CH_3/H2 [b]	H1′	H2′/H2″	H3′	H4′	H5′/H5″	GH1/TH3	CH4b/H4f [c]
T15	7.37	1.56	5.78	1.85/2.25	4.68	4.02	3.65		
A16	8.50	7.80	6.37	2.88/3.05	5.05	4.47	4.14/4.05		
T17	7.27	1.42	5.77	2.22/2.50	4.90	4.27		13.39	
G18	7.85		5.99	2.63/2.78	4.94	4.41	4.23/4.19	12.46	
T19	7.32	1.42	5.81	2.22/2.56	4.91			13.53	
A20	8.29		6.21	2.62/2.83		4.38			
C21	7.40	5.46	5.88	1.97/2.36	4.73	4.09*	4.28		8.39/6.92
C22	7.47	5.47	5.52	2.02/2.36	4.79	4.06*	3.93		7.87/6.80
A23	8.34	7.81	6.24	2.77/2.93	5.02	4.37			
T24	7.20	1.38	5.73	2.17/2.45	4.89	4.21		13.36	
G25	7.85		5.94	2.61/2.76	4.95	4.39	4.21/4.14	12.42	
T26	7.25	1.45	5.74	2.06/2.45	4.88	4.21		13.55	
A27	8.31	7.56	6.29	2.74/2.90		4.42			
T28	7.25	1.48	6.09	2.14	4.52	4.02	4.31/4.08		

[a] H6: TH6 or CH6; H8: AH8 or GH8. [b]H5: CH5; CH_3: TCH_3; H2: AH2. [c]CH4b is the cytosine amino proton involved in H-bonding in the CG base pair. CH4f is the non-hydrogen-bonded amino proton.

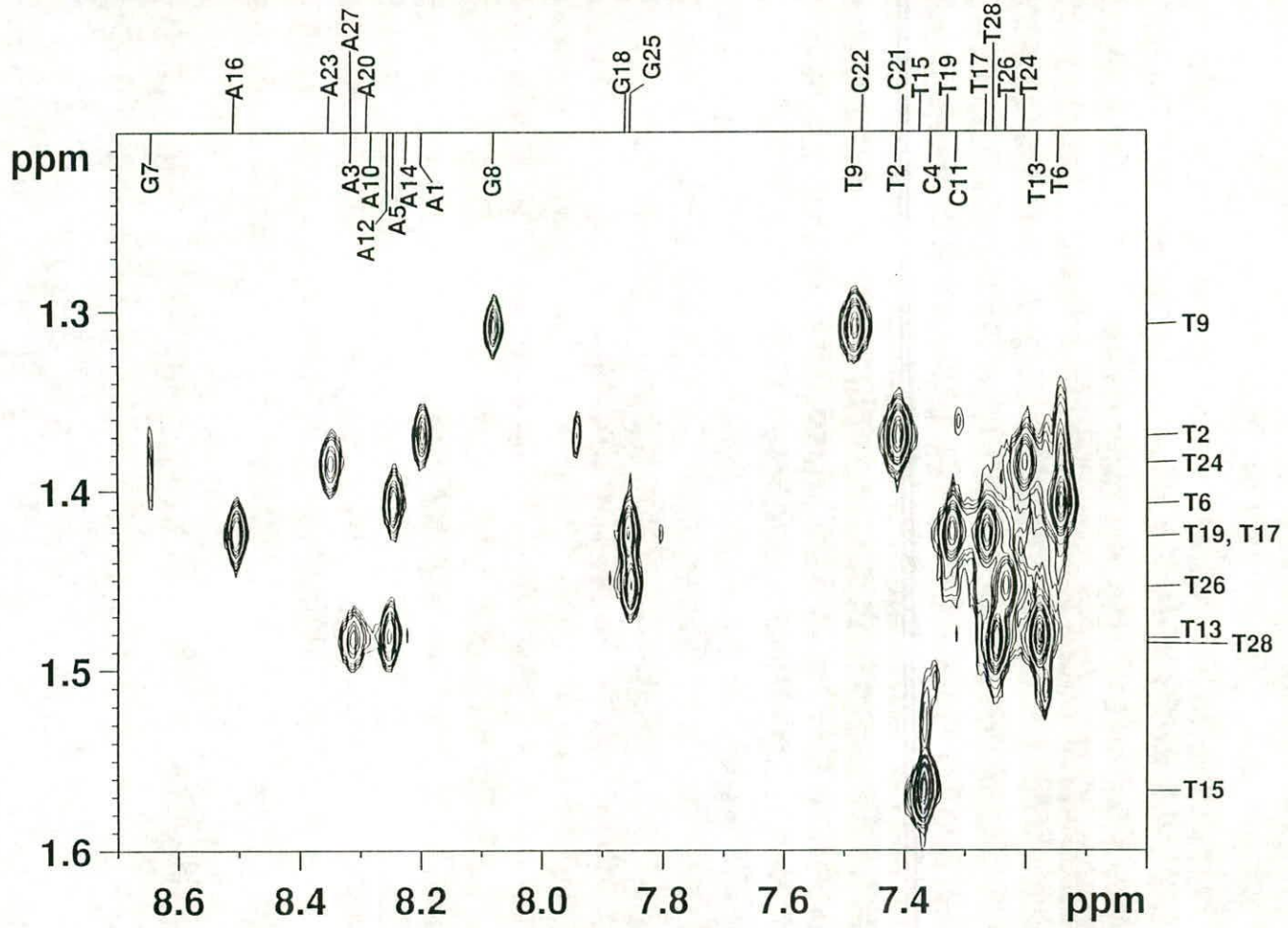

Figure 6.4 A contour plot of 300 ms NOESY spectrum of DNA duplex **III*** at 278 K showing the H2´/H2´´/thymidine Me-to-aromatic region NOE connectivities.

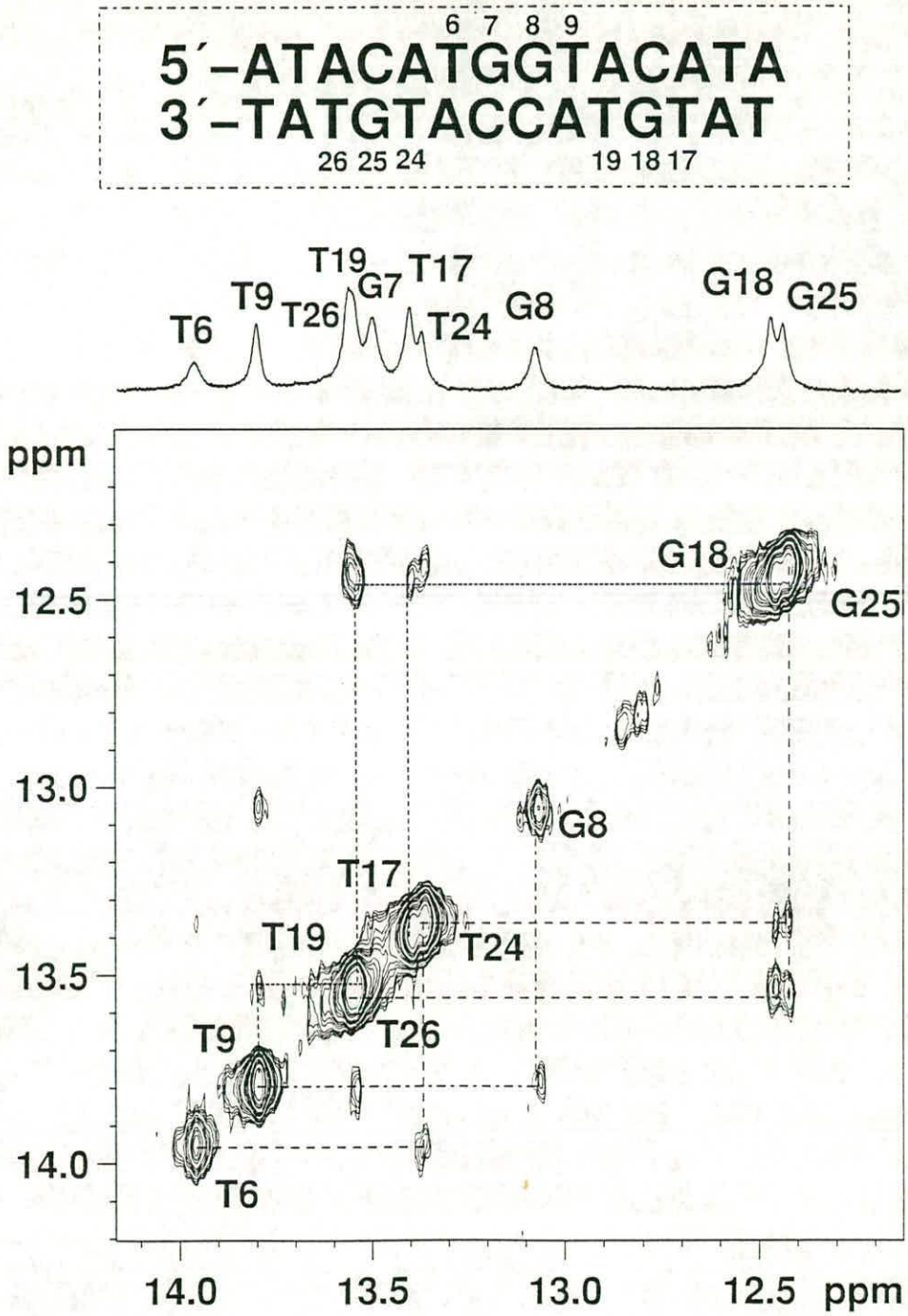

Figure 6.5 A contour plot of the 150 ms NOESY spectrum of DNA duplex **III*** recorded in 90% H_2O/10% D_2O at 278 K showing the imino-to-imino region. A sequential walk was made between the imino protons involved in Watson-Crick hydrogen bonding in the platinated 14-mer DNA duplex, which is only interrupted at G7* site. The imino protons of the two base-pairs at each of the 5′ and 3′ ends are not observed. The 1D ^1H spectrum of the same region is plotted on the top.

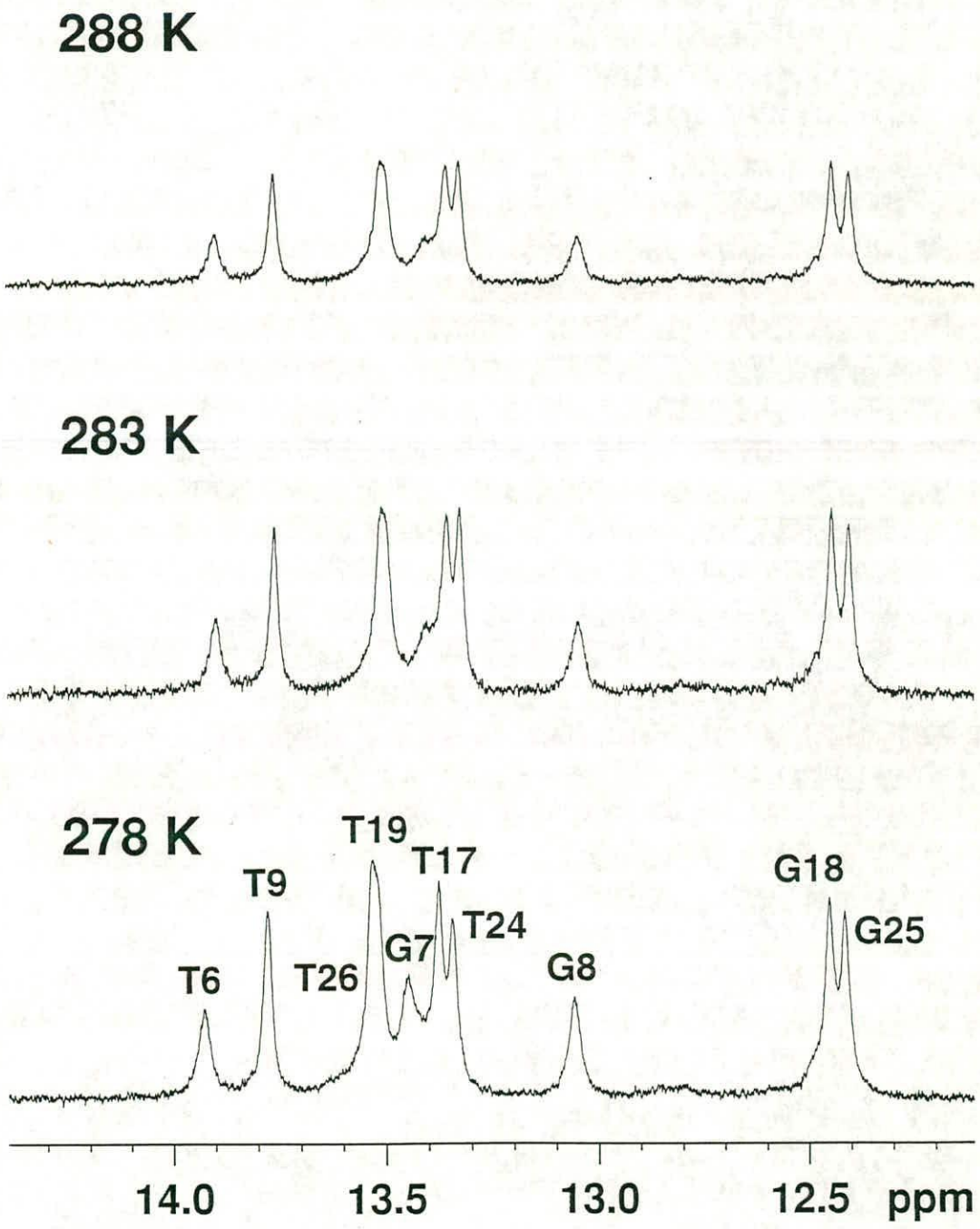

Figure 6.6 Temperature dependent 1D ^{1}H spectrum of DNA duplex **III*** in the imino proton region showing the appearance of G7* imino proton at low temperature. Assignments are indicated on the top of the peaks.

The intensity of the strong intra-nucleotide G7* H8-H3′ NOE cross-peak compared with that of the modest G8* H8-H3′ NOE cross-peak suggests that the deoxyribose rings of the G7* and G8* nucleotides are of the N-type (C3′-endo) and S-type (C2′-endo) conformations, respectively. From the 2D DQF-COSY data, it is clear that the coupling patterns of H1′-to-H2′/H2′′ of G7 and A14 are different to the other nucleotides. By using SPHINX and LINSHA programs to simulate the DQF-COSY cross-peak patterns, the proton homonuclear $^3J_{1'2'}$, $^3J_{1'2''}$, $^3J_{2'3'}$, $^3J_{2''3'}$, and $^3J_{2'2''}$ coupling constants were extracted. To obtain pseudorotational parameters, which describe the geometry of the sugar moiety, experimental *J* coupling constants were compared with theoretical values using a graphical method. A two-state model with rapid *N-S* interconversion was assumed to match experimental values. Figure 6.7 shows the final simulated DQF-COSY cross-peaks compared with the actual cross-peaks in spectra. From the result, only G7* and 3′-end A14 in strand **I*** are predominantly C3′-endo conformations, while the others, including T6 and G8 are all in C2′-endo or related C3′-exo conformations.

All together 574 and 662 NOE cross-peak integrals were measured from the NOESY spectra at mixing times of 150 ms and 300 ms respectively.

Structure Determination of Cisplatin-Modified DNA 14-mer Duplex. Both the energy-minimized B- and A-form DNA duplexes modified by cisplatin were used as starting models for rMD calculations (Figure 6.8). Starting from energy-minimized B-DNA, the force constants for the distance restraints were gradually increased to a final value of 20 kcal·mol^{-1}·Å^{-2} in the first three rMD runs (20 ps each). The system was strongly coupled to a heat bath and kept at 300 K. The initial velocity for rMD was assigned to a Boltzmann default value. After the final constraints were set up, a long rMD run (100 ps) was performed. Coordinates of the final 5 ps of the dynamics trajectory were averaged and subjected to 200 cycles of Powell minimization to

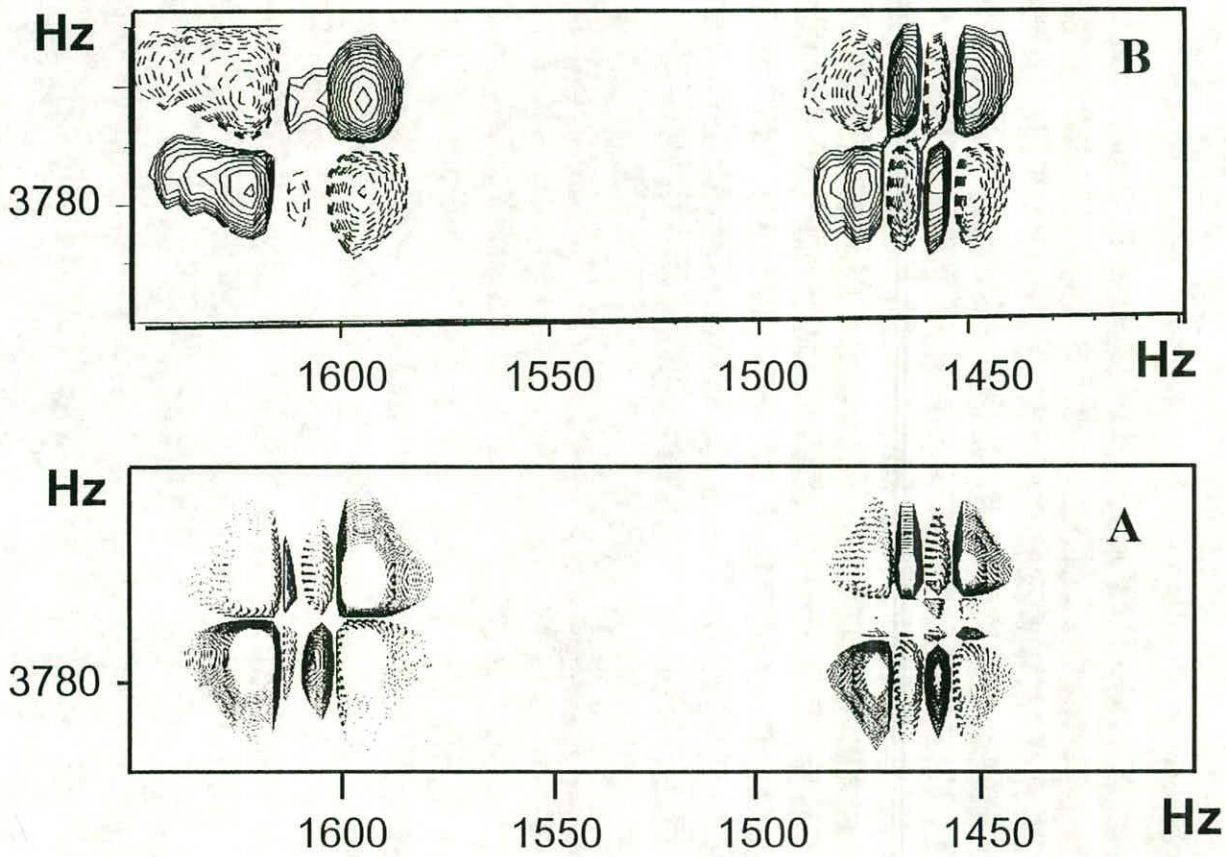

Figure 6.7 Simulated (A) and observed (B) cross-peaks for A14 H1´-to-H2´ and H2´´in 2D DQF-COSY spectra of DNA duplex **III***. The simulation was carried out using SPHINX and LINSHA programs, The simulation indicates the presence of only the C3´-endo conformation for A14 deoxyribose.

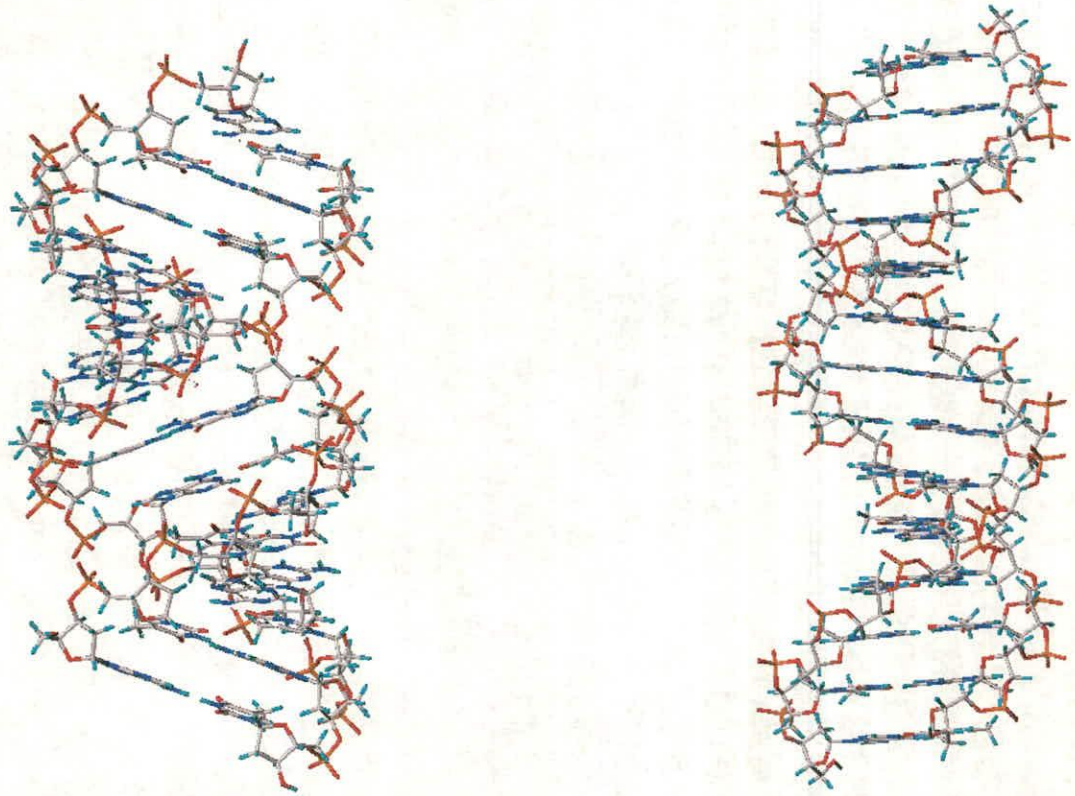

A-form **B-form**

Figure 6.8 Standard A- and B-form 14-mer DNA duplexes built in Sybyl 6.3 and used as starting models for structural calculations. Colour code: C (white), H (cyan), N (blue), O (red), P (orange).

achieve a single coordinate set expected to reflect the averaged conformational characteristics. The structure obtained after this calculation is called B-1.

With energy-minimized A-DNA as the starting structure, the system had to be brought up to high temperature utilising high force constants in order to pass over energy barriers to achieve successful convergence. Initially the temperature was set to 100 K, with the model being gradually heated to 900 K. The force constant was increased with temperature and finally reached 100 kcal·mol^{-1}·Å^{-2} at 900 K. After a 10 ps rMD run at 900 K, the system was slowly cooled down to 300 K in 5 ps steps and the force constant was reduced to 20 kcal·mol^{-1}·Å^{-2}. The slow cooling process can avoid the system being trapped in local energy minima. Large conformational changes were observed during the rMD run at 900 K. A further 30 ps rMD run was carried out at 300 K and the coordinates for the last 3ps of the rMD trajectory were averaged. The average was subsequently subjected to restrained energy minimization. The structure obtained at the end of this procedure is called A-1. Comparing A-1 and B-1, the two structures exhibited an average root-mean-square deviation (RMSD) of 1.5 Å for best-fit backbone of the central base-pairs or 2.0 Å for heavy atoms (all atoms except for hydrogen), which means a convergence has been achieved from starting A- and B-form standard duplex (RMSD for heavy atoms, 6.7 Å). Due to the limited amount of experimental NMR data directly related to the backbone geometry, the two ends of this distorted DNA duplex are relatively flexible during the rMD runs, which affects the whole backbone RMSD value.

To cover more conformational space, a series of short molecular dynamics runs (20 ps each) were carried out with randomly assigned initial atom velocities for both A-1 and B-1 structures (five each). The final 3 ps (31) structures of each run were averaged and restrained-minimized. This resulted in families of structures with very similar energy and similar overall geometry. Average atom RMSDs for five structures of B-form DNA family were between 0.85 to 1.26 Å, and for A-form DNA

family is between 0.50 to 0.71 Å. The structures in each of the two sets were further averaged and restrained-minimized to extract the average features of each set. This gives two subfinal structures, rMD-A and rMD-B. These two structures exhibited an average RMSD of 1.3 Å for best fit backbone or 1.8 Å for heavy atoms. The coordinates of all ten structures from the two sets were superimposed, averaged and restrained-minimized to achieve a single final structure which is called rMD-final, as shown in Figure 6.9. The RMSD values between rMD-A, rMD-B and rMD-final are listed in Table 6.2.

Table 6.2 RMSD values (Å) calculated from structures of rMD-A, rMD-B and rMD-final.

RMSD	rMD-A	rMD-B	rMD-final	Average-RMSD
rMD-A[a]		1.3	0.9	1.1
rMD-B[a]	1.3		1.1	1.2
rMD-final[a]	0.9	1.1		1.0
rMD-A[b]		1.8	1.0	1.4
rMD-B[b]	1.8		1.1	1.5
rMD-final[b]	1.0	1.1		1.1

[a] RMSD of best-fit backbone; [b] RMSD of heavy atoms (all the atoms except protons).

Structure of the Platinated 14-mer DNA Duplex.

The sharp 1D ^{1}H NMR signals of the Pt-DNA sample **III***, together with the single set of detectable proton resonances in the 2D NOESY spectra, suggest that the duplex exists predominantly as a single structure in solution on the NMR time scale. The detection of a nearly complete set of sequential connectivities for the base H8/H6 to sugar H1′, H2′/H2′′ and H3′ provides evidence for a stable right-handed double-helical structure, with all bases orientated in an anti-conformation.

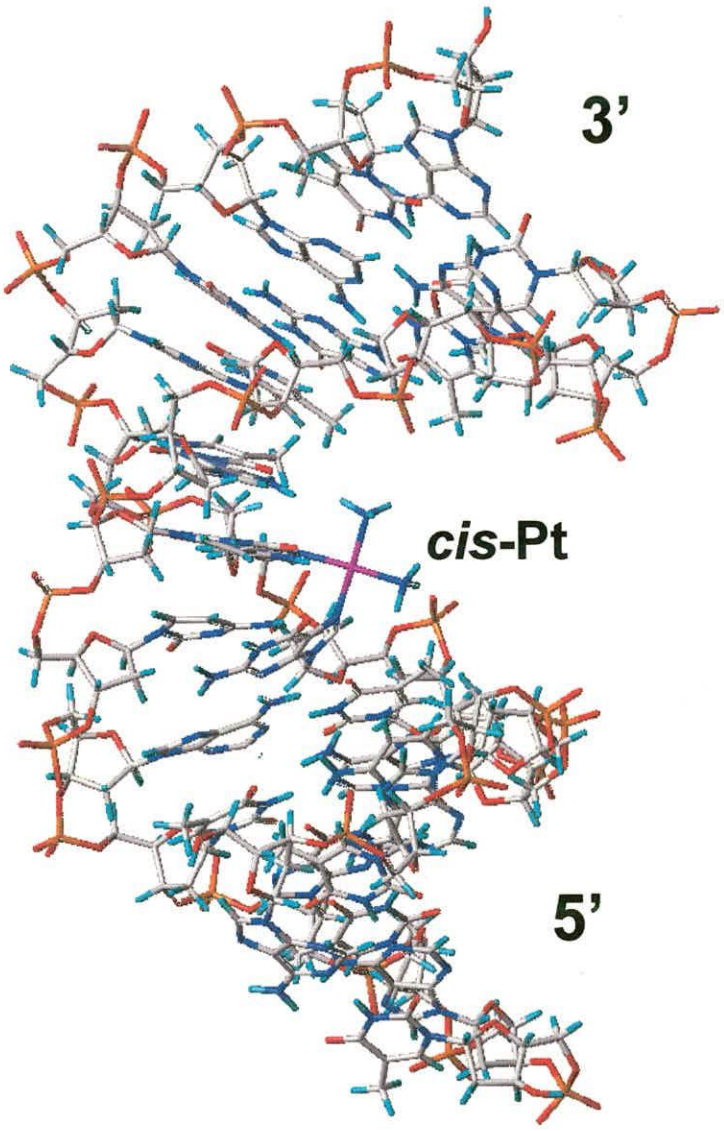

Figure 6.9 A capped stick model of the rMD calculated 14-mer DNA duplex **III***, where the G_7*G_8* site is modified by *cis*-$\{Pt(NH_3)_2\}^{2+}$. Colour code: C (white), H (cyan), N (blue), O (red), P (orange), Pt (purple).

The NOE constraints used in the structure calculation proved to be sufficient to reach the final converged structure from either A- or B-form starting models. The final calculated structure of platinated 14-mer DNA duplex is quite distorted compared to standard A- or B-form models, but it is still primarily a B-form structure according to sugar puckers and phosphate-phosphate distances (6.28 Å). Only the G7* and A14 deoxyribose rings of the final calculated structure have C3´-endo sugar puckers, consistent with the 2D NOESY and DQF COSY data. The other sugar puckers are all S-type, with either a C2´-endo or the related C3´-exo conformation.

The program CURVES 5.2 was used to calculate the helical base-base and base-step parameters which describe the duplex. Those parameters are defined according to the EMBO workshop on DNA curvature and bending.[35] The binding of *cis*-diammineplatinum(II) to the N7 atoms of the adjacent guanine bases G7* and G8* causes a roll of 43° toward the major groove, resulting in a global bend of the duplex of 23.6°. This calculated bending angle is much smaller than the overall appearance of the structure. The global helix axis, as determined in the CURVES program, passes through the center of the duplex at the 5´ end but through the base pairs in the 3´ end, shown in Figure 6.10. It has been shown that the bending angle obtained from CURVES has a large associated error due to the difficulty of making such rigorous calculations for the distorted structures.[11,16] A manual method was used to measure the bend angle of helix axis, and the final value was 47°. The bending point of the helix axis is located at T9 on the 3´ side of G7*G8*, rather than at the platinated G7*-G8* base step. The roll and the geometric distortion at the G7*-G8* base step are consistent with the 2D NOESY data, which shows an intense cross-peak between G7*H8 and G8*H8 protons.

An expanded view of the structure at the platinum-binding site is shown in Figure 6.11. The two guanosine residues coordinate to the N7 atoms of G7*G8* in a head-to-head configuration. The H-bonding of 5´-G7*·C22 base pair is most affected

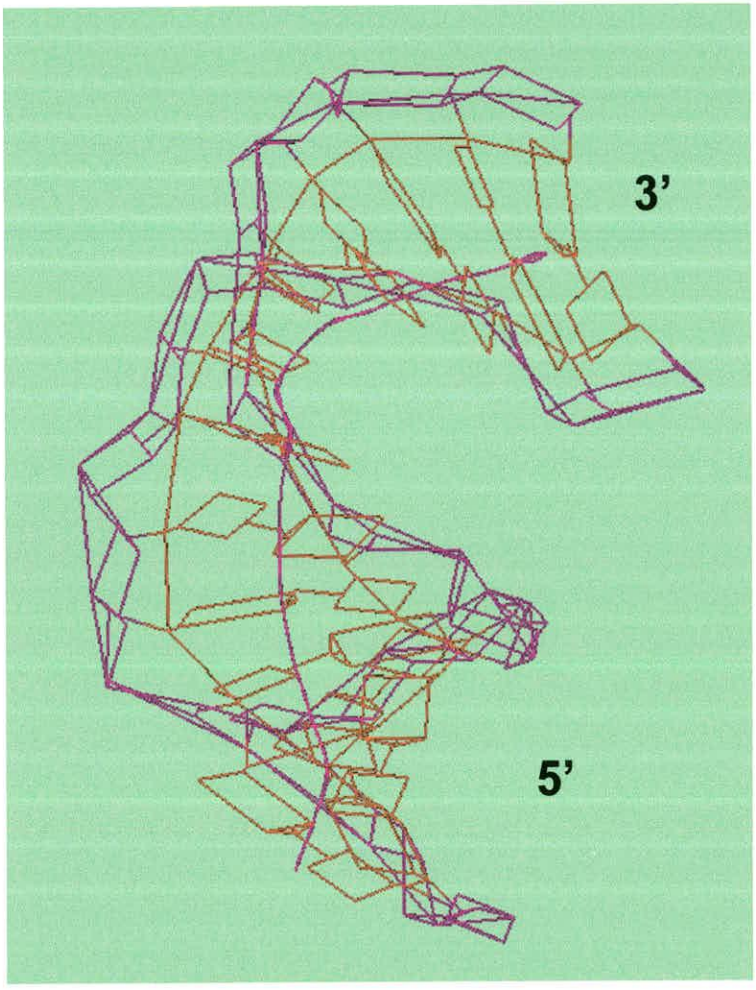

Figure 6.10 Helical axes calculated by the program CURVES for the final structure.

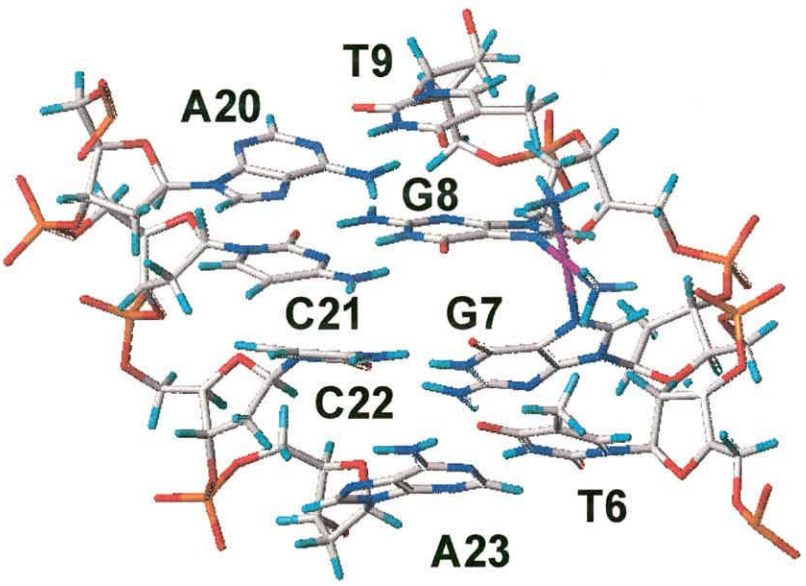

Figure 6.11 Extended view of the central four base pairs $T_6G^*_7G^*_8T_9/A_{23}C_{22}C_{21}A_{20}$ of the platinated 14-mer DNA duplex **III***. The duplex is unwound and the base pairs are destacked at the G*G* site. Colour code: C (white), H (cyan), N (blue), O (red), P (orange), Pt (purple).

and consistent with the weak NOE cross-peaks between G7* 1-NH and C22 4-NH_2. The Pt atom is displaced from the planes of the coordinated guanine bases by 0.8 Å (5′G) and 0.3 Å (3′G). The purine ring of G7* does not stack with G8*, neither does the pyrimidine ring of A23 with C22 in strand **II**, but the cytosine residues which pair with G7* and G8* still stack on one another. The distortions caused by the platinum lesion also include a large positive stretch and buckle at the G7*-C22 base pair and significant opening and stagger at the G8*-C21 base pair.

In the 2D NOESY spectrum, both the chemical shifts of G7* H8 (8.64 ppm) and G8* H8 (8.08 ppm) are very much low field shifted from the normal chemical shift region of guanosine H8 (7.8 ppm),[34] and the H8 chemical shift of 5′-G7* is more downfield shifted than that of 3′-G8*. This is consistent with the R-conformation, which is usually observed for G*G* intrastrand platinated DNA duplexes.[36] In the final structure, the G8* H8 proton remains underneath the imidazole ring of the G7* base, therefore sensing the ring-current shielding effect of the G7* base. This and the inductive effect of platinum binding causes the chemical shift of 5′-G* H8 to be more downfield shifted than that of 3′-G* H8. The T6 deoxyribose is also affected by the platinum crosslink at the G7*G8* site, which induces characteristic chemical shift changes for T6 H1′ (from 5.71 to 5.86 ppm) and H2′ (from 1.92 to 1.37 ppm), compared with unplatinated, normal DNA duplex with the same sequence. Similar shifts for the H1′ and H2′ of 5′-deoxyribose are observed in the other reported structural analyses of intrastrand cross-linked DNA duplexes.[14,15,37] It indicates that T6 H2′ is located in the shielding zone of the G7* purine ring.

The minor groove opposite the site of platination is widened and shallow compared with normal B-form DNA which has an average width of 6.0 Å and a depth of 8.2 Å.[38] It is opened from 8 to 11 Å over the region of G7* to A10, with a depth ranging from 3.9 to 1.3 Å. Both the width and shallowness of minor groove

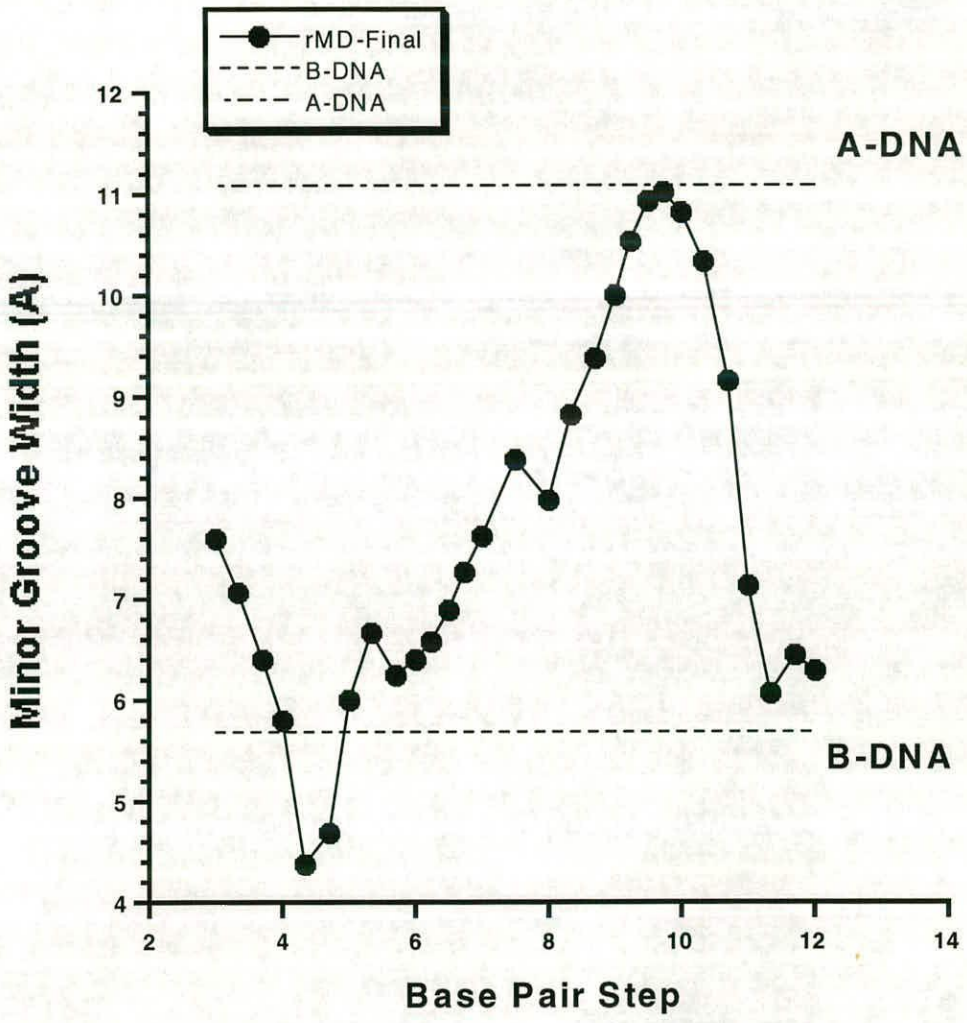

Figure 6.12 Graphic plots of the variation of the minor groove width with the base pair step. The minor groove width of standard A- and B-forms of DNA are plotted with dashed lines for comparison. (•) for the platinated 14-mer DNA duplex.

reach their biggest values at the T9-A10 step. The variation of minor groove width with the base pair step is graphically depicted in Figure 6.12. The platinated DNA structure shows significant unwinding by approximately 26° twist. All the structural data are listed in Table 6.3, and compared with other published results.

Table 6.3 Major structural parameters for G*G* platinated DNA structures.[39]

DNA	14-mer (**1**)	12-mer (**2**)[11]	12-mer (**3**)[15]	11-mer (**4**)[16]
Method	NMR[a]	X-ray[a]	NMR[a]	NMR[b]
DNA form	primarily B	A/B junction	primarily B	primarily B
Minor groove width(Å)	8.0-11.0	9.5-11.0	9.4-12.5	9.0-12.0
depth (Å)	1.3	3.0	1.4	2.1
P-P distance (Å)	6.3	5.5	6.9	6.8
Roll at G*G* bases (°)	43	26	49	59
Pt atom displacement	0.8 Å, 5′	1.3 Å, 5′	0.8 Å, 5′	0.5 Å, 5′
from guanine ring	0.3 Å, 3′	0.8 Å, 3′	0.8 Å, 3′	0.65 Å, 3′
Average helix twist (°)	26	32	25	26
DNA bend (°)	~47	39 and 55[c]	78	~81
Sequence[d]	**5′-ATACATGGTACATA** **3′-TATGTACCATGTAT** **(14mer)**	**5′-CCTCTGGTCTCC** **3′-GGAGACCAGAGG** **(12mer)**		**5′-CTCTCGGTCTC** **3′-GAGAGCCAGAG** **(11-mer)**

[a] *cis*-[$Pt(NH_3)_2Cl_2$] adduct. [b] Spin-labelled compound *cis*-[$Pt(NH_3)$(4-amino-TEMPO)ClI] was used in this study. [c] Two independent molecules. [d] The same sequence was used in structural studies of DNA 12-mer by X-ray (**2**) and NMR (**3**).

6.5. Discussion

Structures determined *via* rMD have two major determinants: the experimental restraints and the force field applied. The role of the force field is to provide an energetically feasible structural framework for the molecule as the rMD

protocol is utilised to search conformational space for a structure most consistent with the experimental constraints.[40] The results of these studies have shown that a successful convergence to the final structure has been achieved from the starting standard A- and B-form DNA duplexes (RMSD, 6.7 Å). The heavy atom RMSD value is reduced to 1.8 Å between rMD-A and rMD-B.

Due to the lack of long distance constraints (>5 Å) from 2D NOESY data and flexible nature of this highly distorted structure, the two ends of this platinated DNA duplex are distorted and less well defined, which affects the final RMSD value. The superimposed 10 structures calculated from A-1 and B-1 with randomly assigned initial atom velocities (five each) are shown in Figure 6.13. The flexibility of the 5′ and 3′-ends can be clearly seen. During the rMD runs, the bending angle of the duplex fluctuated with time and the longer molecular dynamics (100 ps) runs proved to be very important for defining this highly distorted duplex. The fluctuation of this DNA duplex during the rMD runs also reflects the possible existence of multiple exchanging conformations in solution and rapid internal motions, which affects the time-averaged NOE distance constraints.

Compared with the two ends, the conformation of central four base pairs is very well defined in all the final rMD runs. When the cisplatin was replaced by another anticancer active complex *cis*-[$PtCl_2(NH_3)$(2-picoline)] in the reaction with 14-mer DNA duplex, which is reported in Chapter 7, it was surprising to find that little rearrangement of the conformations for those base pairs was needed to satisfy all the NOE connectivities between the 2-picoline ligand and nearby T6 and G7* protons as well as the ring current effect of pyridine on the chemical shift of T6 H2′ (see Figure 7.8 in Chapter 7). This is impossible if the *cis*-$\{Pt(NH_3)$(2-picoline)$\}^{2+}$ is docked onto the reported 12-mer G*G* platinated DNA structures (**2** and **3**), although the sequences of the central four base pairs TG*G*T are the same.

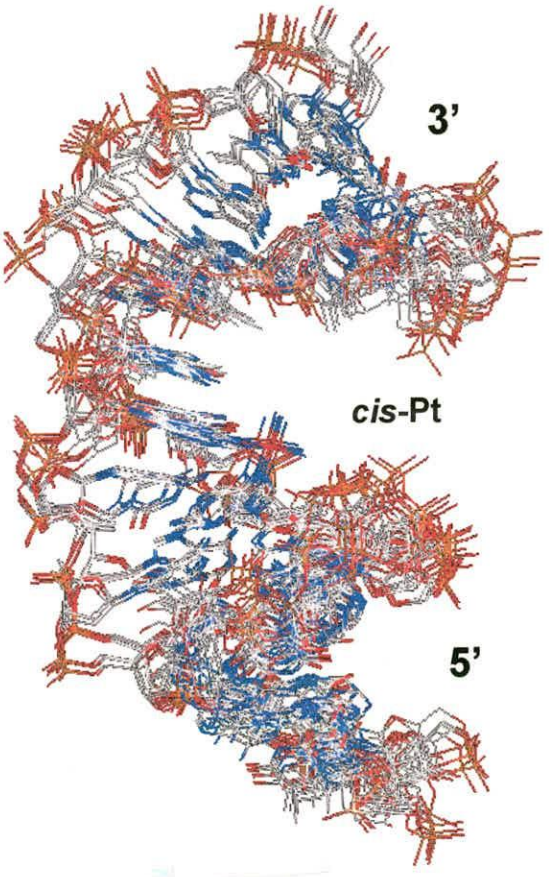

Figure 6. 13 Superimposed 10 structures calculated from A-1 and B-1 with randomly assigned initial atom velocities (five each), showing the flexibility of the 5′ and 3′-ends. Colour code: C (white), N (blue), O (red), P (orange), Pt (purple).

The major structural difference between structure **1** and previously reported structures (**2**, **3**, **4** in Table 6.3) of intrastrand platinated DNA duplex is the bending position of the duplex. In structure **1**, both the widest and most shallow position of the minor groove occurs at the T9 site, resulting in the 3′ side of the 14-mer DNA duplex being much more bent towards the major groove. This contrasts to the previous reports, in which the widest positions of the minor groove occurs on the 5′ side of the X-G* (X: T or C) base step and in consequence the 5′ side of the duplex is more bent towards the major groove.[12,15,16] This structural difference could be due to the different sequences chosen for the studies. The sequence of the 14-mer DNA duplex is richer in A·T base pairs compared with all the previously reported Pt-DNA structures. It has only one G·C base pair on each side of G7*G8*, separated by two A·T base pairs. The data from CURVES analysis shows that both the G7*-G8* step and T9-A10 step have large positive rolls, which causes the helix to bend towards the major groove. The large positive roll on the G7*-G8* step is due to the binding of cisplatin, while the positive roll on T9-A10 is a feature reported to be typical for pyrimidine-purine steps including C-A (= T-G), T-A, or less frequently C-G.[18,41] This extra T-A step, adjacent to G*G* on the 3′ side, is unique in this 14-mer DNA duplex. Bending of DNA is sequence-dependent. Pyrimidine-purine steps have a tendency toward positive roll bending because of the relatively limited overlap between base pairs, but in a given setting, not every pyrimidine-purine step is necessarily bent. It is analogous to a flexible hinge which can only bend under proper stress. Previous studies have shown that there are positions where a C-A step or a T-G step exists but is not bent.[41] In the 14-mer DNA duplex, there are two hinges on either side of the G7*G8* platination site, e.g. 5′ side T6-G7* and 3′ side T9-A10 steps which can both cause roll bending. The final structural analysis reveals that the most bent position occurs at G8*-T9-A10 steps, which causes the 3′ side of the DNA to bend towards the major groove. In the other reported Pt-DNA structures (**2, 3, 4** in

Tables 6.3), there is only one hinge (T-G* or C-G*) on the 5′ side of G*G*. The positive roll on both T·G* (or C·G*) and G*·G* steps causes the 5′-side of the DNA duplex to bend towards the major groove and the opposite minor groove to open. This sequence-dependent differential bending of G*G* intrastrand cross-linked DNA could have important implications for the recognition of DNA-binding proteins. Besides the sequence, the length of the current 14-mer DNA duplex might also have some influence on the bending position. It has been reported that short DNA sequences can destabilize the binding of cisplatin, causing migration from intrastrand to interstrand cross-links.[14,15]

Recent X-ray crystal structure studies of HMG domain A protein complex with cisplatin-modified DNA has shown that HMG1-A binds to the widened minor groove of G*G* platinated DNA duplex and protein binding extends exclusively to the 3′ side of the platinated strand.[42] Both domains (A and B) of HMG1 protein bind preferentially to DNA having A/T flanking sequences, with slightly different base pair preference.[43] HMG1-A binds much more tightly than HMG1-B to any of the platinated DNAs, having typically a 10- to 100-fold lower K_d value. The more flexible A-T base pairs flanking the platinum lesion would facilitate further bending of the DNA duplex caused by HMG protein binding. The tighter binding of HMG1-A is also accompanied by a much more distinct flanking sequence specificity, with the 3′-flanking nucleotide of G*G* determining the sequence preference. The slightly different binding abilities of the two domains in a full-length protein suggests a mechanism for sequence recognition.[39]

The bending angle (47°) of this platinated DNA 14-mer duplex **III*** is less than those of the reported for the solution structures of **3** (78°)[15] and **4** (81°)[16], but close to that of a reported 8-mer (58°)[14] and X-ray crystal structure of a platinated 12-mer (39° and 55°)[12]. From the previous reports and this study, it is difficult to calculate rigorously the bending angle of a highly distorted DNA structure with the

programme CURVES and use it to compare with other structures. The overall shape of the platinated DNA 14-mer duplex **III*** is very similar to that of the reported X-ray crystal structure (**2**) and structure (**4**) determined by combining long-range electron-proton and short-range interproton distance restraints. For comparison, the bending angles analysed by gel mobility assays which reflect macroscopic duplex shape are between 32-34° and the bending angle of platinated DNA in HMG1-A-DNA complex is 61°.[44,42]

In all the previously reported NMR structural studies of intrastrand G*G* cross-linked DNA duplex,[14,15,16] the imino proton of the 5′-G* is not observable even at low temperature. This is because of the distortion of 5′ G*·C base pair by the G*G* bischelate, which causes fast exchange of 5′-G* H1 proton with water. But for the platinated DNA 14-mer duplex **III***, the intensity of the 5′-G7* imino proton resonance was quite strong at low temperature and showed clear NOE connectivities with the opposite C22 4-NH_2 (both the hydrogen-bonded and non-hydrogen-bonded proton). This implies that the Watson-Crick base-pair between G7 and C22 still remains, although the hydrogen-bonding is much weaker compared with the other G·C base pairs. This observation is consistent with the calculated final structure. The different bending position in our structure (at T9-A10 step, 3′ side of G7*G8*) compared with the other reported structures (at T-G* or C-G* step) causes the hydrogen-bonding of G7*-C22 to be relatively less distorted. No NOE connectivities were found between the imino proton of G7* and the nearby T6 and G8* bases, which suggests that the base-stacking is disordered at the G7*G8* site. The absence of Watson-Crick base-paired imino protons at both ends of the DNA duplex indicates flexibility at the two ends, which is a common feature of DNA NMR studies.

6.6. Conclusion

By combining NMR spectroscopy and restrained Molecular Dynamics, a successfully converged structure of G*G* platinated DNA 14-mer duplex has been obtained. The platinum atom is coordinated to the N7 positions of adjacent guanines. The binding of cisplatin causes the DNA duplex to be bent towards the major groove and unwind. The minor groove opposite the platinated site is significantly widened. The final refined structure is a distorted B-form DNA. The major structural difference between this platinated 14-mer DNA duplex and the other previous studies is the bending position of the DNA. The 14-mer DNA duplex **III*** is bent at the 3′ side of G*G* (T9 position), which causes the 3′ side of DNA duplex to be much more bent towards the major groove, while the other reported DNA structures are all bent at the other side of G*G* and the 5′ side of the DNA is more bent towards the major groove. The structural difference is most likely due to the different DNA sequence chosen in the studies. Platinated DNA duplexes with different structural characteristics, for example either with the 3′ side or 5′ side of the platination lesion more bent, may be recognized differently by DNA-binding proteins.

6.7. References

[1] J. Reedijk, *Chem. Commun.*, **1996**, 801.

[2] E. Reed, R. F. Ozols, R. Tarone, S. H. Yuspa, M. C. Poirier, *Proc. Natl. Acad. Sci. U. S. A.* **1987**, *84*, 5024.

[3] Y. Corda, M. -F. Anin, M. Leng, D. Job, *Biochemistry*, **1992**, *31*, 1904.

[4] L. J. N. Bradley, K. J. Yarema, S. J. Lippard, J. M. Essigmann, *Biochemistry*, **1993**, *32*, 982.

[5] C. S. Chow, C. M. Barnes, S. J. Lippard, *Biochemistry*, **1995**, *33*, 2954.

[6] U. -T. Ohndorf, J. P. Whitehead, N. L. Raju, S. J. Lippard, *Biochemistry*, **1997**, *36*, 14807.

[7] E. E. Trimmer, D. B. Zamble, S. J. Lippard, J. M. Essigmann, *Biochemistry*, **1998**, *37*, 352.

[8] D. B. Zamble, D. Mu, J. T. Reardon, A. Sancar, S. J. Lippard, *Biochemistry*, **35**, 10004.

[9] J.-C. Huang, D. B. Zamble, J. T. Reardon, S. J. Lippard, A. Sancar, *Proc. Natl. Acad. Sci. U.S.A.*, **1994**, *91*, 10394.

[10] S. E. Sherman, D. Gibson, A. H. -J. Wang, S. J. Lippard, *Science*, **1988**, *230*, 412.

[11] P. M. Takahara, C. A. Frederick, S. J. Lippard, *J. Am. Chem. Soc.*, **1996**, *118*, 12309.

[12] P. M. Takahara, A. C. Rosenzweig, C. A. Frederick, S. J. Lippard, *Nature*, **1995**, *377*, 649.

[13] F. Herman, J. Kozelka, V. Stoven, E. Guittet, J. -P. Girault, T. Huynh-Dinh, J. Igolen, J.-Y. Lallemand, J. -C. Chottard, *Eur. J. Biochem.* **1990**, *194*, 119.

[14] D. Yang, S. S. G. E. van Boom, J. Reedijk, J. H. van Boom, A. H. -J. Wang, *Biochemistry*, **1995**, *34*, 12912.

[15] A. Gelasco, S. J. Lippard, *Biochemistry*, **1998**, *37*, 9230.

[16] Shari U. Dunham, Stephen U. Dunham, C. J. Turner, S. J. Lippard, *J. Am. Chem. Soc.* **1998**, *120*, 5395.

[17] S. J. Berners-Price, K. J. Barnham, U. Frey, P. J. Sadler, *Chem. Eur. J.* **1996**, *2*, 1283.

[18] M. Tonelli, E. Ragg, A. M. Bianucci, K. Lesiak, T. L. James, *Biochemistry*, **1998**, *37*, 11745.

[19] a) S. J. S. Kerrison, P. J. Sadler, *J. Chem. Soc. Chem. Commun.* **1977**, 861; b) S. J. Berners-Price, A. Corazza, Z. Guo, K. J. Barnham, P. J. Sadler, Y. Ohyama, M. Leng, D. Locker, *Eur. J. Biochem.*, **1997**, *243*, 782.

[20] M. Piotto, V. Saudek, V. Sklenar, *J. Biomol. NMR*, **1992**, *2*, 661.

[21] T. -L. Hwang, A. J. Shaka, *J. Magn. Reson. Series A*, **1995**, *112*, 275.

[22] J. Stonehouse, G. L. Shaw, J. Keeler, E. D. Laue, *J. Magn. Reson. Series A*, **1994**, *107*, 178.

[23] S. S. Wijmenga, M. M. W. Mooren, C. W. Hilbers, in "*NMR of Macromolecules, A Practical Approach*" (G. C. K. Roberts, Ed.) pp 217-288, Oxford University Presss, New York.

[24] K. Wüthrich, in "*NMR of Proteins and Nucleic Acids*", John Wiley & Sons, New York, **1986**.

[25] H. Berthod, A. Pullman, *J. Chem. Phys.*, **1965**, *62*, 942.

[26] B. A. Borgias, T. L. James, *J. Magn. Reson.* **1990**, *87*, 475.

[27] A. Mujeeb, S. M. Kerwin, W. Egan, G. L. Kenyon, T. L. James, *Biochemistry*, **1992**, *31*, 9325.

[28] B. A. Borgias, T. L. James, *J. Magn. Reson.* **1990**, *87*, 475.

[29] a) H. Widmer, K. Wüthrich, *Journ. Magn. Reson.*, **1987**, *74*, 316-336; b) H. Widmer, K. Wüthrich, *J. Magn. Reson.*, **1986**, *70*, 270.

[30] U. Schmitz, G. Zon, T. L. James, *Biochemistry*, **1990**, *29*, 2357.

[31] W. Saenger, *Principles of Nucleic Acid Structure,* Springer, New York.

[32] U. Schmitz, T. L. James, *Methods Enzymol.*, **1995**, *261*, 3.

[33] F. Reeder, Z. Guo, P. del S. Murdoch, A. Corazza, T. W. Hambley, S. J. Berners-Price, J.-C. Chottard, P. J. Sadler, *Eur. J. Biochem.* **1997**, *249*, 370.

[34] S. J. Berners-Price, J. A. Parkinson, P. J. Sadler, unpublished data.

[35] R. E. Dickerson, *J. Biomol. Struct. Dyn.* **1989**, *6*, 627.

[36] J. Kozelka, M.-H. Fouchet, J.-C. Chottard, *Eur. J. Biochem.* **1992**, *205*, 895.

[37] M.-H. Fouchet, E. Guittet, J. A. H. Cognet, J. Kozelka, C. Gauthier, M. L. Bret, K. Zimmermanm, J.-C. Chottard. *J. Biol. Inorg. Chem.* **1997**, *2*, 83.

[38] S. Neidle, in "*DNA Structure and Recognition*", Oxford Univ. Press, Oxford, **1994**.

[39] A. Gelasco, S. J. Lippard, in "*Topics in Biological Inorganic Chemistry*", (M. J. Clarke and P. J. Sadler, Eds.), Springer-Verlag, Berlin, 1999, Vol. 1, 1-43.

[40] A. Mujeeb, S. M. Kerwin, W. Egan, G. L. Kenyon, T. L. James, *Biochemistry*, **1992**, *31*, 9325

[41] R. E. Dickerson, *Nucleic Acids Res.* **1998**, *26*, 1906.

[42] U. -M. Ohndorf, M. A. Rould, Q. He, C. O. Pabo, S. J. Lippard, *Nature*, **1999**, *399*, 708.

[43] S. U. Dunham, S. J. Lippard, *Biochemistry*, **1997**, *35*, 11428.

[44] S. F. Bellon, S. J. Lippard, *Biophys. Chem.* **1990**, *35*, 179.

Chapter 7

New Platinum Anticancer Drug Forms

Highly Stereoselective Adduct with Duplex DNA

7.1 Abstract

The new anticancer drug *cis*-[$PtCl_2(NH_3)$(2-picoline)] (**1**) forms a highly stereoselective GG intrastrand bischelate with a 14-mer DNA duplex (2-picoline *cis* to 5′G and 2-methyl group pointing to the major groove). This is in contrast with the reactions between complex **1** and d(GpG) or a 14mer single strand, in which four stereoisomers were observed in each of the cases, with the 2-picoline ligand in the position either *cis* to 5′G or 3′G and the rotation about the Pt-N picoline bond. From NMR data and molecular modelling, several factors are found to contribute this high stereoselectivity: favourable steric interactions between the 2-picoline ring and the nearby nucleotides, hydrogen-bonding between the NH_3 ligand and O6 of G8, and together with van der Waals interactions between the 2-picoline CH_3 and the CH_3 of nearby T6. In addition, kinetic factors may also play a role. The result of these studies provides a structural basis for optimising the design of the substituted pyridine ligand as a way of controlling the rate of formation, stability of GG-intrastrand crosslinks and DNA duplex sequence selectivity of platination. The highly stereoselective formation and stability of this adduct could play an important role in the unique anticancer activity of **1**, especially for the activity against cisplatin-resistant cell lines.

7.2 Introduction

Much attention is currently focused on the design of new generations of platinum anticancer complexes which circumvent cisplatin resistance. Such resistance often involves the recognition of platinated DNA adducts by proteins and enzymes in the nucleotide excision-repair, mismatch repair and post-replication repair systems in cells.[1] Recent study shows that the carrier ligands of Pt anticancer agents, including oxaliplatin and JM216, appear to play an important role in determining their efficacy against tumours with both intrinsic and acquired resistance to cisplatin.[2] Both the mismatch repair and post-replication repair pathways have

shown carrier ligand specificity. The use of chiral ligand in DWA2114R provides the interesting observation that the *R*-isomer is not toxic while the *S*-isomer is,[3] which suggests different interactions that occur following DNA binding. It is therefore vital to understand how ligand design influences the nature of platinated DNA lesions.

A complex with high activity against cisplatin-resistant cell lines is the 2-picoline (2-Pic, 2-methylpyridine) complex *cis*-[$PtCl_2(NH_3)$(2-Pic)] **1** (ZD0473).[4,5] As described in Chapter 4 and 5, the steric effect of 2-picoline plays an important role in determining the rates of hydrolysis and substitution reactions with the nucleotide 5′-GMP.[6,7] Due to slow rotation about the Pt-N 2-picoline bond (0.62 s^{-1}, 296 K), together with the non-C_2-symmetrical structure of complex **1**, four isomers of the bis(GMP) adduct are possible, and these are formed in equal amounts.[7]

In all previous reports of the stereoselective formation of platinated GG adducts by unsymmetrically substituted cisplatin derivatives (general formula *cis*-[$PtCl_2$(LL′)]),[8,9] the selectivity has been low and with the orientation of NH_3 *cis* to 5′G preferred. In the case of *cis*-[$PtCl_2(NH_3)(C_6H_{11}NH_2)$], a metabolite of the orally-active Pt(IV) drug JM216, the most abundant platinated G*G* stereoisomer (isomer ratio 2:1) has the cyclohexylamine ligand directed towards the 3′G of both calf thymus DNA and shorter single strand 12-mer oligonucleotides.[10] This preference was attributed partly to Pt-NH_3 H-bonding with the 5′-phosphate, which was a structural feature identified as being important in the major cisplatin adducts with DNA. Opposite selectivity was observed in the platination of the dinucleoside mono-phosphate d(GpG), which contains no 5′-phosphate.[10] The same ratio (2:1) and preference of orientational isomers (NH_3 *cis* to 5′G) have also been observed for an 11-mer DNA duplex platinated at G*G* with *cis*-{$Pt(NH_3)$(4-aminoTEMPO)}$^{2+}$, which has a spin-labelled ligand.[11]

In dramatic contrast, the reactions of **1** with the 14mer DNA duplex **III** give predominantly a single stereoisomer, whereas relatively little stereoselectivity is

observed for reactions with d(GpG) or the 14-mer single strand **I**. The structural basis for this unusually high stereoselectivity has been revealed by NMR studies and molecular modelling in this report.

5′ d(A_1 T_2 A_3 C_4 A_5 T_6 G_7 G_8 T_9 $A_{10}$$C_{11}$$A_{12}$$T_{13}$$A_{14}$) I

I + II = III

3′ d($T_{28}$$A_{27}$$T_{26}$$G_{25}$$T_{24}$$A_{23}$$C_{22}$$C_{21}$$A_{20}$$T_{19}$$G_{18}$$T_{17}$$A_{16}$$T_{15}$) II

7.3. Experimental

2-Picoline was purchased from Aldrich. The sodium salts of 14-mer oligonucleotides were prepared by Oswel (Southampton, U. K.). *Cis*-[$PtCl_2(^{15}NH_3)$(2-Pic)] **1** was prepared from *cis*-[$PtCl_2(^{15}NH_3)_2$] by the procedure described in Chapter 4.[12]

The concentrations of GG 14mer single strand and its complementary CC strand were determined by UV according to their ε values at 260 nm (GG strand: 149 $M^{-1}cm^{-1}$; CC strand: 137.2 $M^{-1}cm^{-1}$). The DNA 14-mer duplex **III** was annealed by slow cooling the solution containing equivalent of GG and CC 14mer single strands from 70 °C. The reaction of **1** with **III** was conducted at a 1:1 molar ratio (1 mM) in 90% H_2O/10% D_2O (0.5 ml). Samples contained 0.1 M $NaClO_4$ to maintain a constant ionic strength. Phosphate buffer (9 mM) was used in the reactions to maintain the pH at 6.0. For experiments in D_2O, the sample was freeze-dried twice from 99.9% D_2O and finally dissolved in 99.9% D_2O.

NMR spectra were acquired, as previously described,[6,7] on both Bruker DMX500 and Varian ^{Unity}INOVA600 NMR spectrometers operating at ^1H resonance frequencies of 500.13 and 599.842 MHz respectively. 2D ^1H NOESY data sets were acquired for both the 90% H_2O/10% D_2O sample and the 99.9% D_2O sample using a 200 ms mixing time at 278 K. 2D DQFCOSY data were acquired only on the 99.9% D_2O sample.

Measurements of pH were made using a Corning 145 pH meter equipped with an Aldrich micro combination electrode calibrated with Aldrich buffer solutions of pH 4, 7 and 10.

Molecular modelling was carried out using Sybyl version 6.3 (Tripos Inc.). DNA duplex structures were based on an energy minimised model of a cisplatin-DNA duplex with the same sequence calculated from NMR data (Chapter 6). The X-ray crystal structure coordinates of **1**[6] were used to construct the fragment $\{Pt(NH_3)(2\text{-Pic})\}^{2+}$ for docking onto the G*G* site of DNA 14mer duplex. Distances (2.0 Å) between G*N*7 and Pt were based on the crystal coordinates of the 12-mer DNA duplex-cisplatin adduct.[13] Four different models reflecting the possible geometry of the final DNA adduct were built. Inter-proton distance constraints were built into each model based on an assessment of the distances calculated from the NOE data. Distance bounds were set for strong, medium and weak NOEs in the ranges 2.5-4.5 Å, 3.0-5.0 Å and 4.0-5.0 Å, respectively, with force constants of 20 kcal mol^{-1} $Å^{-2}$ each. A total of 8 identifiable NOE distance constraints between the 2-picoline ring and the DNA duplex were incorporated into the models. Substructures of each model (T_6G_7*G_8*T_9 + $\{Pt(NH_3)(2\text{-Pic})\}^{2+}$) were subjected to 200 steps conjugate gradient energy minimisation to allow each model to satisfy the distance constraints. The molecular modelling was done with Dr. J. A. Parkinson.

7.4 Results and Discussion

Reactions of complex **1** with both d(GpG) and 14-mer single strand **I** at a 1:1 molar ratio (1 mM, pH 6.0, 9 mM phosphate, 100 mM $NaClO_4$, 90% H_2O/10% D_2O, 298 K) were followed by 1D ^1H and 2D [^1H, ^{15}N] HSQC NMR spectroscopy. In each case the GG chelate finally gave rise to four cross-peaks of similar intensities corresponding to similar populations of the four possible stereoisomers (Figure. 7.1A): 2-picoline orientated towards 5′G or 3′G, and slow rotation about Pt-N(2-Pic)

bond. The chemical shifts ($^1H/^{15}N$) for the adducts of d(G*pG*) were 4.61/-65.68, 4.57/-65.73, 4.48/-65.63 and 4.46/-65.31 (relative intensities: 2:2:3:3), and for the adducts of **I*** were 4.84/-65.12, 4.82/-65.03, 4.69/-65.12 and 4.65/-65.25 (partially overlapped with water, relative intensities: *ca.* 2:2:3:3). When the temperature was increased, the two pairs of $^1H/^{15}N$ cross-peaks for the d(G*pG*) adducts began to merge into two (Figure. 7.1B), as observed for the bis(GMP) adducts because of the faster rotation of Pt-N(2-Pic) bond at higher temperature.[7]

The reaction of **1** with duplex **III** at a 1:1 molar ratio was studied under the same conditions, and followed in the same way. A 2D HSQC spectrum recorded after 15 hours of reaction is shown in Figure 7.2A, in which the peak of one of the monoaqua hydrolysis species (peak b, δ $^1H/^{15}N$: 4.16/-84.57, H_2O *trans* to NH_3) is much stronger (1.7:1) than the other one (peak c, δ $^1H/^{15}N$: 4.31/-65.02, H_2O *trans* to 2-Pic), in contrast to the two monoaqua species observed with similar intensity during the hydrolysis experiment in Chapter 4 and reactions with 5′-GMP in Chapter 5.[6] After one week, one major cross-peak was observed (Figure 7.2B, δ $^1H/^{15}N$: 4.51/-67.46) which accounted for 90% of the total quantity of platinated adducts. In the 1D ^1H spectrum, peaks for the H6 (8.88 ppm) and 2-methyl (3.15 ppm) protons of the 2-Pic ligand of unreacted **1** were replaced by two new signals at 9.205 and 3.19 ppm, respectively (Figure 7.3). A feature of the new 2-picoline signals was their broadness relative to free **1**, due to the 2-picoline complex taking on the T_2 relaxation characteristics of a macromolecule *via* irreversible binding to DNA. New NMR resonances were also observed outside the usual windows expected for both aromatic and methyl protons of DNA (peaks at 8.55, 1.16, 0.43 ppm). These signals enabled further assignments to be made.

The use of NMR methods was explored to determine the structure around the platination site of the major adduct even though the NMR spectra were complicated

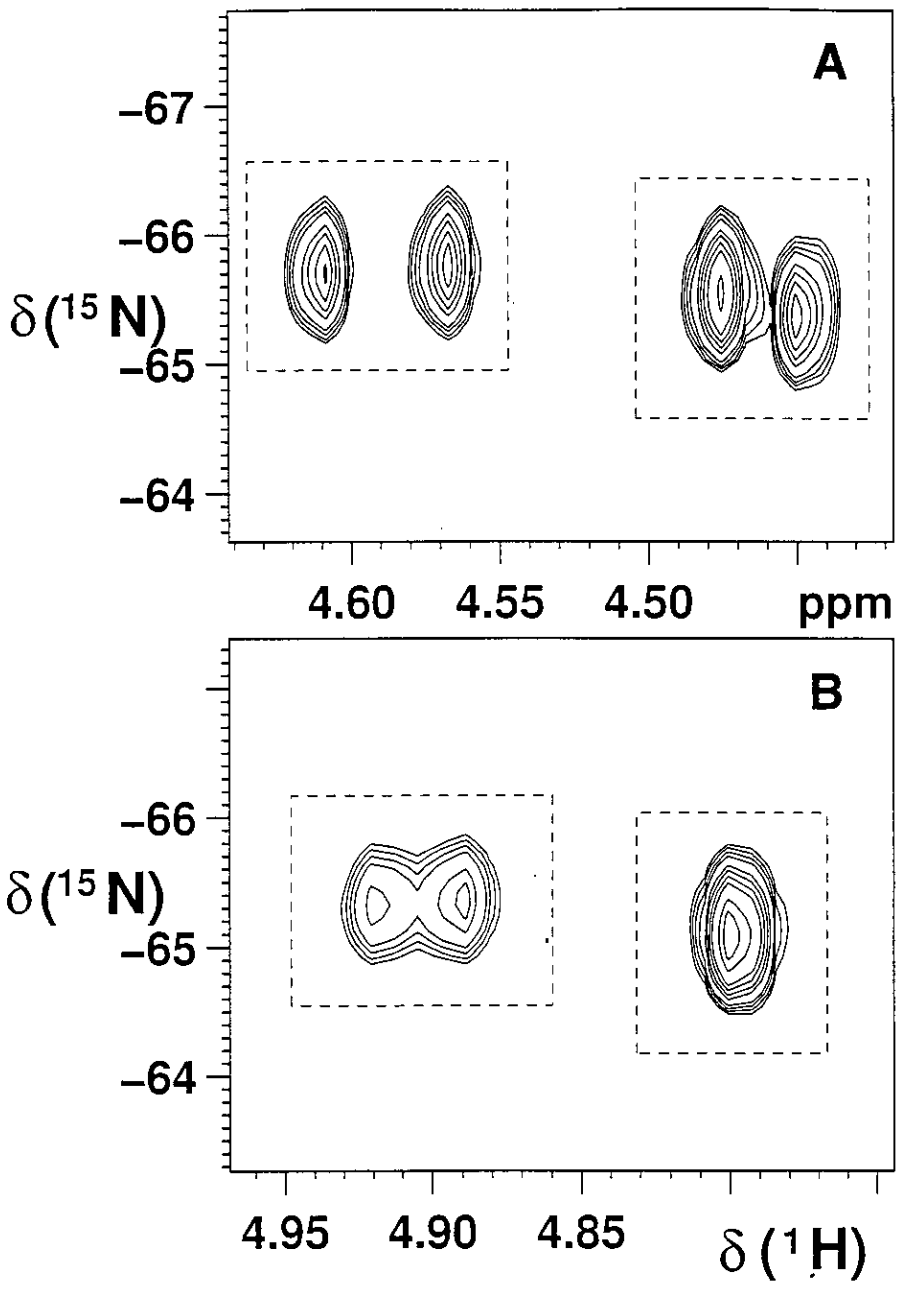

Figure 7.1 The 2D [^{1}H, ^{15}N] HSQC NMR spectrum recorded after 1 week of reaction of *cis*-[$PtCl_2(^{15}NH_3)$(2-Pic)] **1** with d(GpG) dimer at (A) 298 K (1 mM, 1:1 molar ratio, 100 mM $NaClO_4$, pH 6.0, 9 mM phosphate buffer, 90% H_2O/10% D_2O). The two pairs of peaks are shown in two dotted boxes and their relative intensities are 2:2:3:3 (from left to right). (B) 338 K, one pair of peaks becomes closer and the other pair has merged.

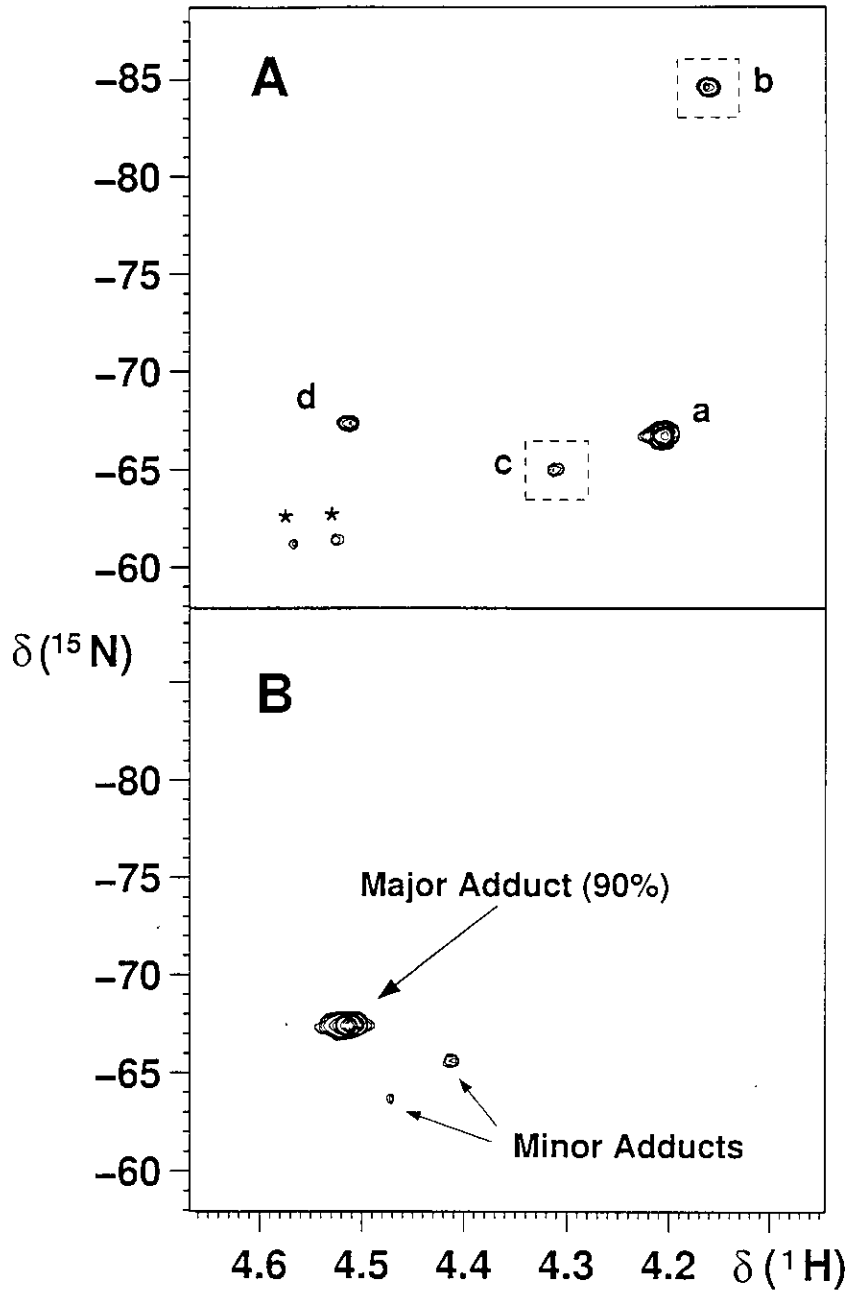

Figure 7.2 The 2D [^{1}H, ^{15}N] HSQC NMR spectrum of reaction of *cis*-[$PtCl_2(^{15}NH_3)$(2-Pic)] **1** (1 mol equiv.) with 14-mer DNA duplex **III** at 298 K (1 mM, 100 mM $NaClO_4$, pH 6.0, 9 mM phosphate buffer, 90% H_2O/10% D_2O) recorded after (A) 15 hours. Peak assignments: **a** is the starting complex **1**; **b** and **c** are the two monoaqua species (in dashed boxes for intensity comparison with those in hydrolysis experiment in Chapter 4); **d** is the final major adduct; those intermediates unassigned are labelled as *. (B) Recorded after 1 week. The integral percentages of the major peak and the two minor peaks are indicated.

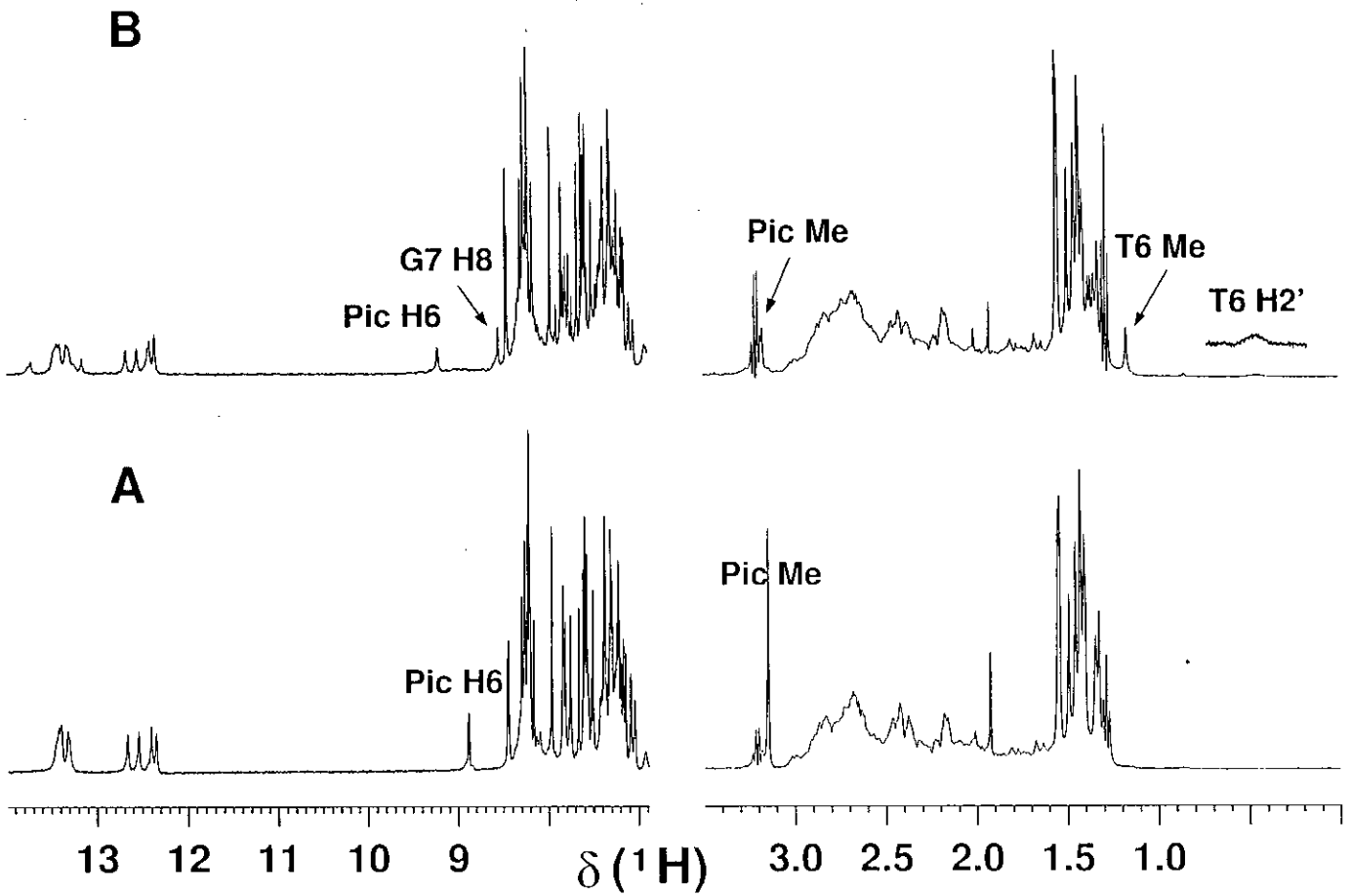

Figure 7.3 ^{1}H NMR spectrum recorded after (A) 0.5 h and (B) 1 week of reaction of *cis*-[$PtCl_2(^{15}NH_3)$(2-Pic)] **1** (1 mol equiv.) with 14-mer DNA duplex **2** at 298 K for the same sample in Fig. 7.2. The assignments of peaks in (B) are listed in Table 7.1. Broad peak for T6 H2′ at 0.43 ppm is scaled up on top.

Table 7.1 Assignments of key ^{1}H resonances for the G*G* chelate of duplex **III** with *cis*-{Pt($^{15}NH_3$)(2-Pic)}$^{2+}$.

Assignment (2-Pic)	δ	Assignment (DNA)	δ
H6	9.20	T6 CH_3	1.16
H5	7.67	T6 H1′	5.82
H4	8.18	T6 H2′	0.43
H3	7.59	T6 H2′′	1.91
2-CH_3	3.19	T6 H3′	4.69
		T6 H4′	4.00
		G7 H8	8.55
		G8 H8	8.18

Table 7.2 Key NOE signals observed between 2-picoline and DNA protons after platination of DNA duplex **III** with the platinum anticancer drug **1**. The corresponding distances in the four models are listed for comparison. Distances over 5 Å are beyond the limit for NOEs, and are labelled (-).

NOE Observed	Distances (Å) in Models			
1.....III	**3a**	**3b**	**3c**	**3d**
H6.....G7 H8	4.45	3.47	5.70(-)	5.15(-)
H6.....T6 H3′	4.88	4.53	7.21(-)	7.06(-)
H6.... T6 H2′′	4.98	4.50	7.08(-)	7.02(-)
H6.....T6 H2′	3.33	3.52	5.57(-)	5.88(-)
H5.....T6 H2′	3.78	3.85	7.86(-)	8.09(-)
CH_3.....T6 CH_3	8.22(-)	4.03	9.07(-)	5.31(-)
H3.....T6 CH_3	7.26(-)	2.73	9.66(-)	7.35(-)
H4.....T6 CH_3	5.42(-)	4.70	9.02(-)	9.15(-)

by the presence of peaks for the minor adducts and free duplex **III**. A ^{1}H 2D NOESY NMR spectrum (mixing time 200 ms) was acquired for the same sample and compared to that for the cisplatin GG bischelated adduct of the same DNA duplex (Chapter 6). The key ^{1}H NMR assignments derived from these data are listed in Table 7.1. They are based on the following observations: a clear strong NOE between G7 H8 and G8 H8 with chemical shifts similar to those observed for the cisplatin-DNA adduct of DNA duplex which indicates bischelate at G_7G_8 site by $\{Pt(NH_3)(2\text{-Pic})\}^{2+}$ (Figure 7.4),[14] an NOE between 2-picoline H6 and G7 H8, a cross-peak between a resonance in the usual H2′/ H2′′ region and a resonance at 0.42 ppm assignable to T6 H2′ (which is significantly low-frequency-shifted compared to that for DNA platinated by cisplatin, 1.37 ppm for duplex **III**, c.f. 1.40 ppm for a reported 12-mer duplex[14]), a strong cross-peak between 2-picoline CH_3 and T6 CH_3 which also showed NOEs to T6 H1′and T6 H2′. The assignments of resonances for T6 were further confirmed by the NOE observed between T6 H2′ and G7 H8. Figure 7.5 shows slices taken through the NOESY data at the chemical shifts of T6 CH_3, T6 H2′ and 2-picoline H6. Key assignments of NOEs around the platination site are listed in Table 7.2. Confirmation of assignments for the 2-picoline ring protons were made from a ^{1}H 2D DQFCOSY NMR spectrum, shown in Figure 7.6.

Four molecular models of the GG adduct of duplex **III** were built by docking $\{Pt(NH_3)(2\text{-Pic})\}^{2+}$ onto the $G_7^*G_8^*$ site of the 14-mer DNA duplex **III**. The structure of the latter was based on that of the cisplatin adduct in Chapter 6. The models differed as follows (Figure 7.7): 2-picoline *trans* to G8 (3′-G) with the 2-methyl group orientated either towards the phosphate backbone **(Methyl-Out)** (**3a**) or towards the centre of the major groove **(Methyl-In)** (**3b**); 2-picoline *trans* to 5′-G also with either **Methyl-Out** (**3c**) or **Methyl-In** (**3d**) orientations. Distance restraints were applied to each case, based on the NOE data shown in Table 7.2, and the models minimised in the region of the bischelate site in order to satisfy the data. Of

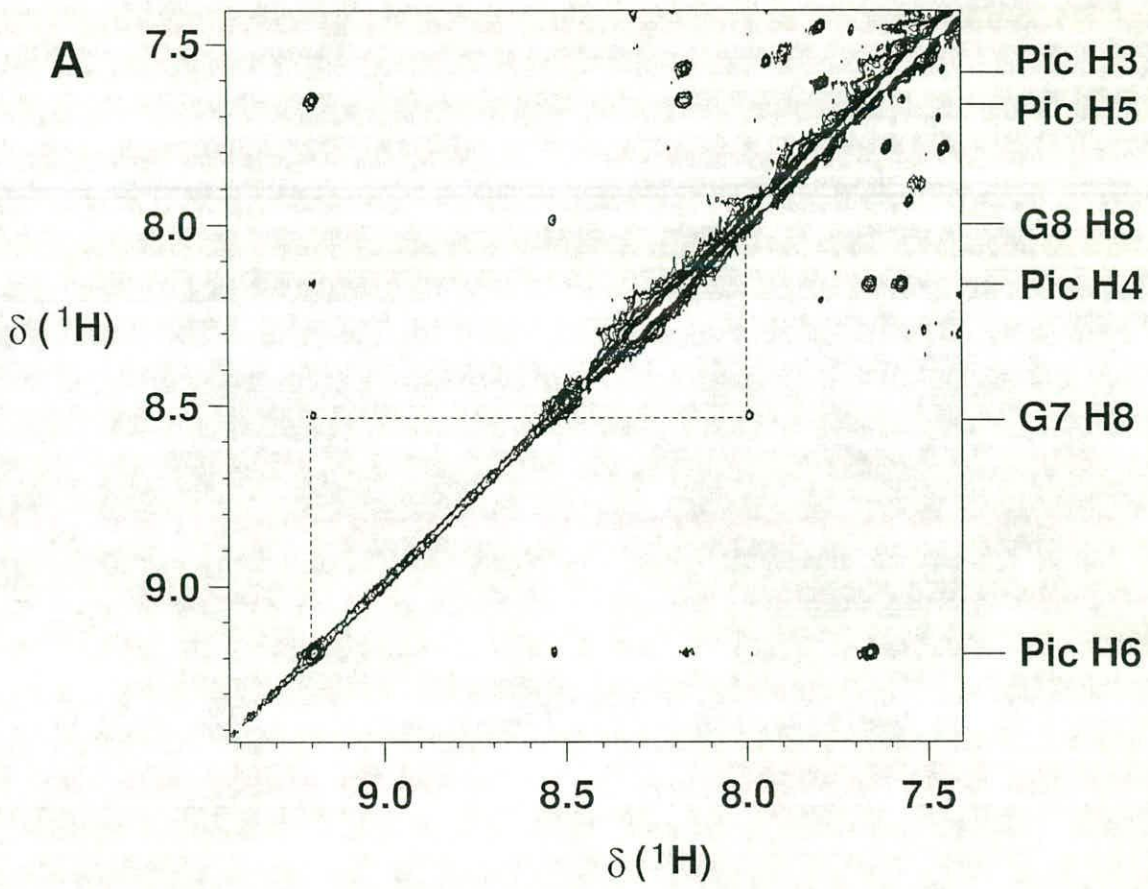

Figure 7.4 Expansion of the aromatic region of the 200 ms 2D NOESY NMR spectrum for the same sample of platinated DNA duplex as used for Fig. 7.2 in 99.9% D_2O. Assignments are shown on the right-hand side (Pic refers to the 2-methylpyridine ligand), and the dashed line shows the connectivity from Pic-H6 to G7 H8 and G7 H8 to G8 H8.

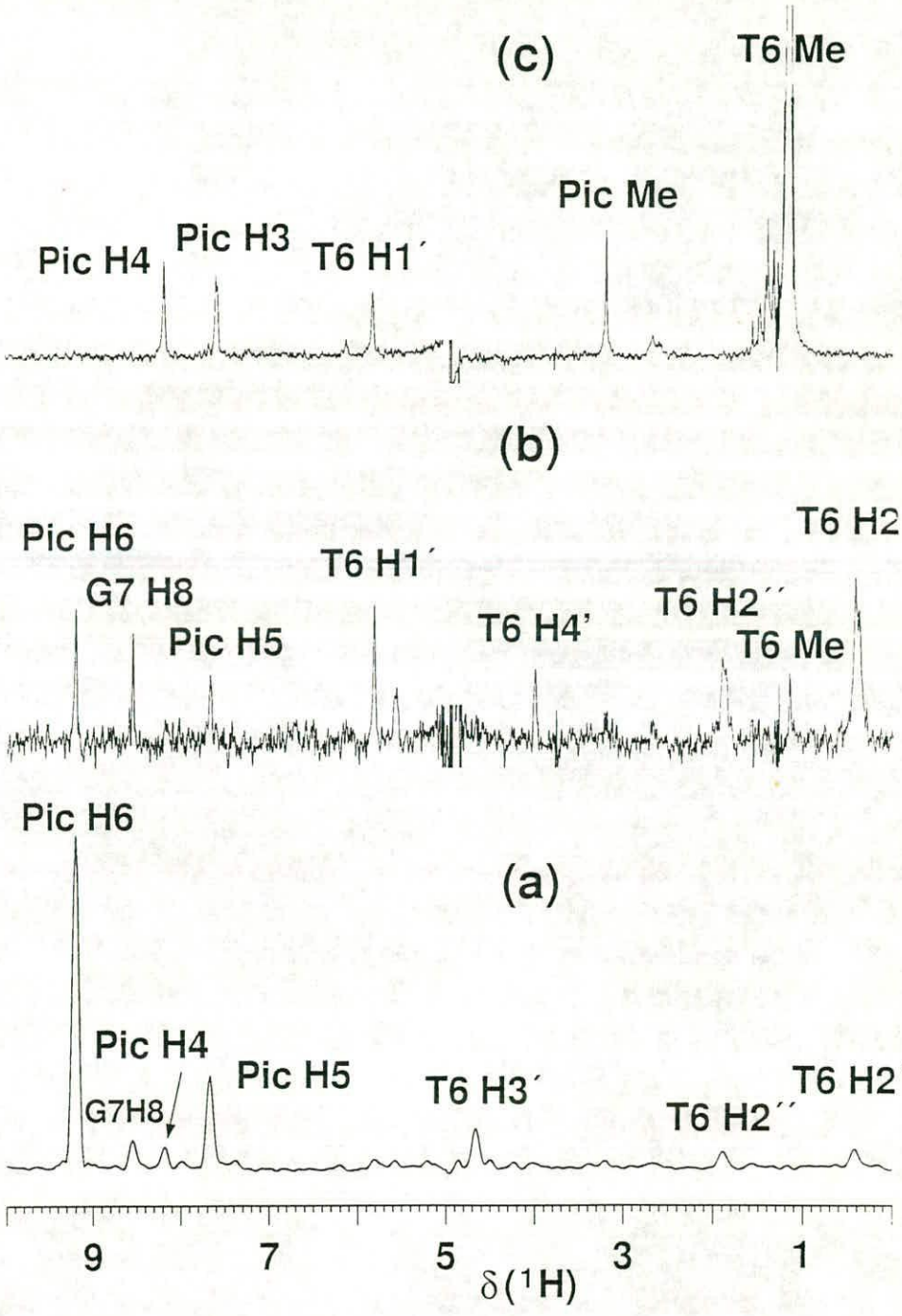

Figure 7.5 Slices taken through the 2D NOESY spectrum at the chemical shifts of (a) 2-picoline H6, (b) T6 H2´ and (c) T6 CH_3, showing NOE connectivities to other protons. Detailed peak assignments and NOE information are listed in Tables 7.1 and 7.2, respectively.

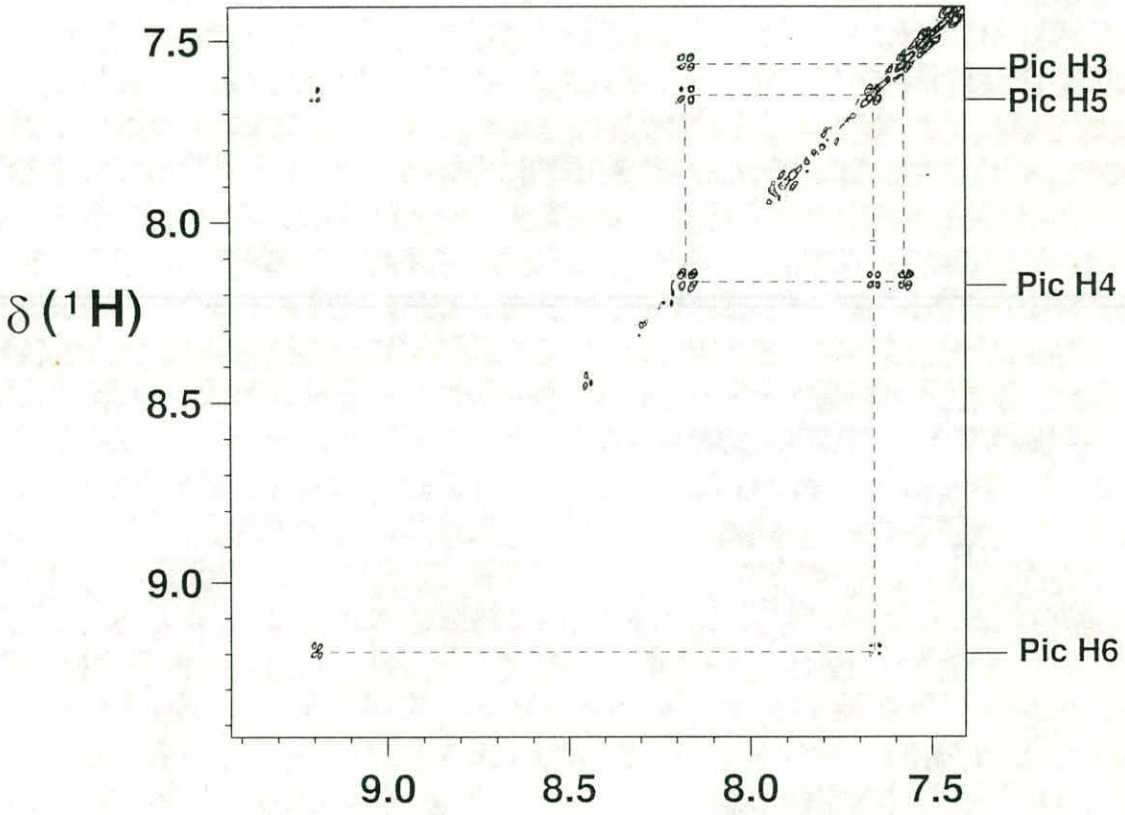

Figure 7.6 2D DQFCOSY NMR spectrum for the same sample as Fig. 7.2 in 99.9% D_2O. The assignments of protons on picoline ring are shown on the right-hand side (Pic refers to the 2-methylpyridine ligand), and the dashed lines show connectivities between Pic-H6, H5, H4 and H3.

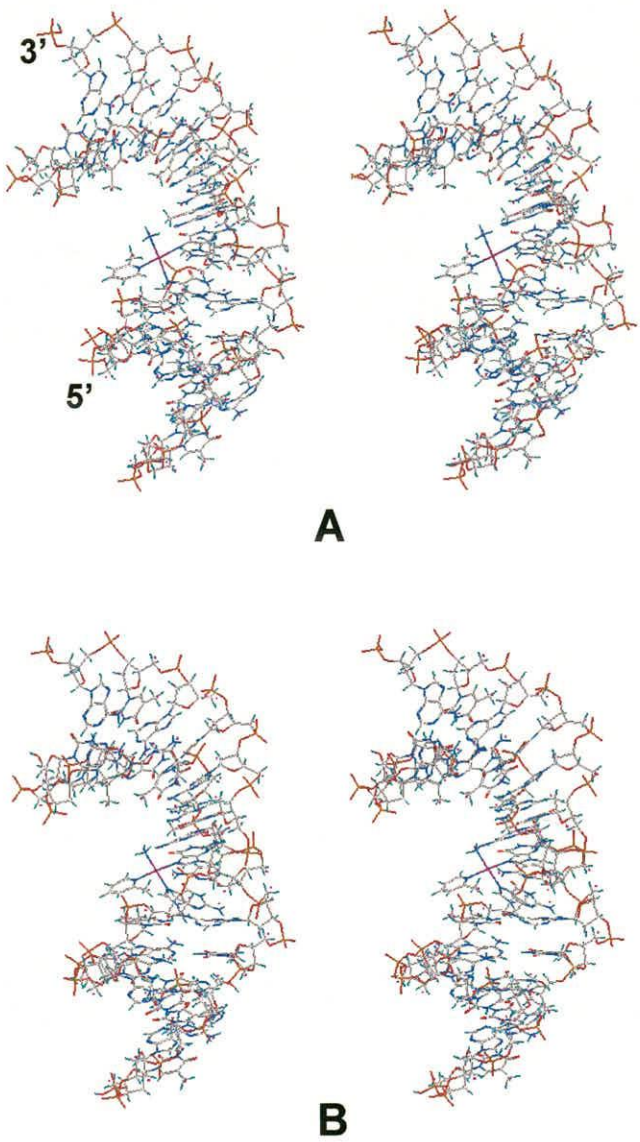

Figure 7.7 Stereoview of four molecular models for the G*G* adduct of duplex **III**: 2-picoline *trans* to G8 (3′-G) with the 2-methyl group orientated either (A) towards the phosphate backbone (**Methyl-Out**) or (B) towards the centre of the major groove (**Methyl-In**); 2-picoline *trans* to 5′-G also with either (C) **Methyl-Out** or (D) **Methyl-In** orientations.

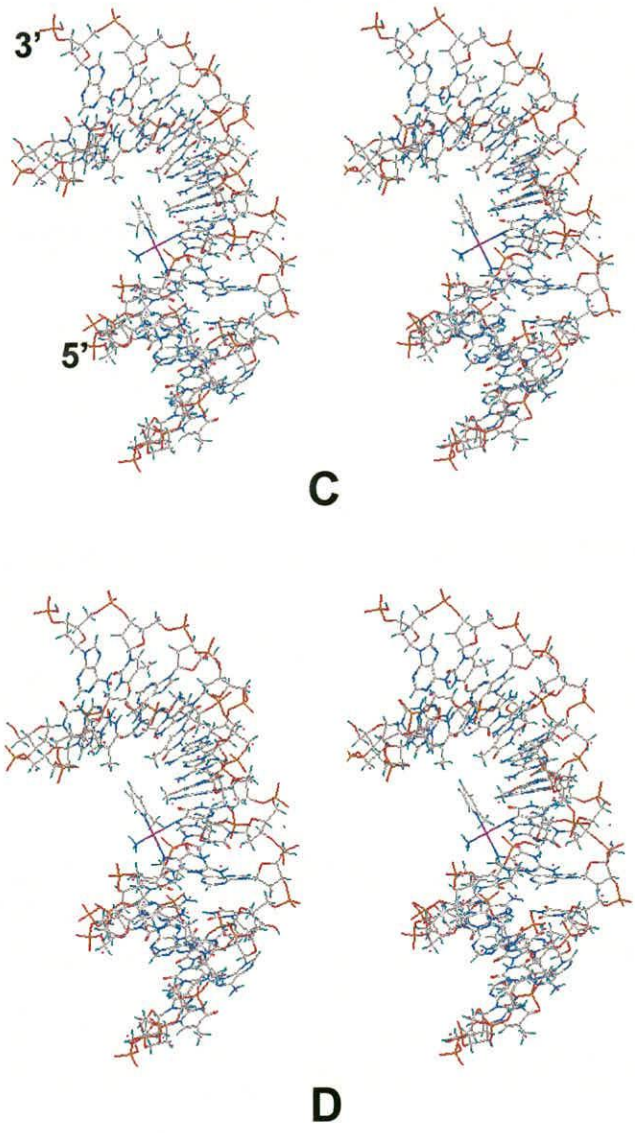

Figure 7.7 (C) and (D)

the 4 models, only that with 2-picoline *trans* to 3′-G with the **Methyl-In** orientation (model **3b**) satisfied all of the observed NOE constraints, as shown in Table 7.2 and Figure 7.8. The first notable feature of model **3b** is that the picoline ring fits perfectly into the major groove of the DNA duplex and lies along the phosphate backbone, as shown in Figure 7.8A. Models **3c** and **3d**, in which the 2-picoline is *trans* to 5′-G with **Methyl-Out** or **Methyl-In,** have the 2-picoline ring in an almost perpendicular orientation with respect to the planes of the nearby nucleotide bases (Fig. 7.7). This steric clash causes models **3c** and **3d** to be far less stable than those with 2-picoline *trans* to 3′-G. The other notable feature is the orientation of the 2-picoline ring, which lies almost perpendicular to the Pt square plane (angle 100°), as in the crystal structure of **1** (103°).[6] Model **3b** satisfies several other features of the NMR data. As shown in Table 7.1, the T6 H2′ resonance at 0.44 ppm is significantly low-frequency-shifted from its normal position for a G*G* DNA duplex/cisplatin adduct (usually near 1.39 ppm). It can be seen in **Figure 7.8B**, that T6 H2′ for molecule **3b** lies directly beneath, and within 3 Å of, the centre of the 2-picoline ring. This is consistent with strong aromatic ring current shielding effects.[15,16] The ^{1}H chemical shift of the NH_3 signal of the platinated duplex is shifted to high frequency by 0.4 ppm compared with that for **1** itself. This is consistent with the presence of hydrogen-bonding in model **3b** between the NH_3 of $\{Pt(NH_3)(2\text{-Pic})\}^{2+}$ and O6 of DNA residue G8. Additional stabilisation of complex **3b** may arise from van der Waals contact between the 2-picoline 2-methyl group and the T6 methyl of DNA (C···C: 3.78 Å).[17] This contact is not observed in the **Methyl-Out** model **3a** (closest distance between 2-CH_3 and T9 CH_3: 5.13 Å) and appears to be important in distinguishing between the **Methyl-In** and **Methyl-Out** models.

In the case of *cis*-$[PtCl_2(NH_3)(C_6H_{11}NH_2)]$ and *cis*-$\{Pt(NH_3)(4\text{-aminoTEMPO})\}^{2+}$, the preferred orientational isomers are NH_3 *cis* to the 5′-nucleotide.[10,11] This is probably because the bulky groups in those two complexes are

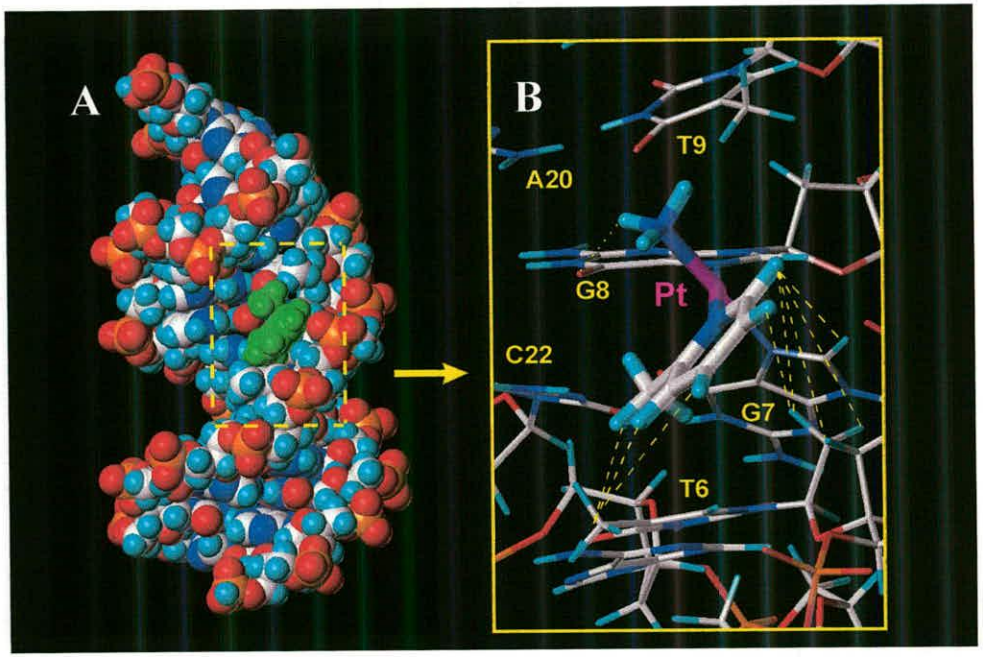

Figure 7.8 (A) Space-filling model of *cis*-{Pt(NH_3)(2-Pic)}-d(ATACAT**G***G*TACATA)·d(TATGTACCATGTAT), with *cis*-{Pt(NH_3)(2-Pic)}$^{2+}$ shown in green. The perfect fit and alignment of the 2-picoline ligand along the major groove can be seen. (B) Close-up view of the Pt binding site showing NOE connectivities (yellow dashed lines, listed in Table 7.2) between 2-picoline and DNA. H-bonding between Pt-NH_3 and O6 of G8 is shown as a yellow dotted line. Colour code: C (white), H (cyan), N (blue), O (red), P (orange), Pt (purple).

Scheme 7.1 Pathways for reactions of anticancer complex **1** with DNA duplex **III** (only G7 and G8 are shown). Charges on complexes are not shown. A possible preferred route to the major GG adduct with 2-picoline *cis* to 5′-G is indicated by bold arrows.

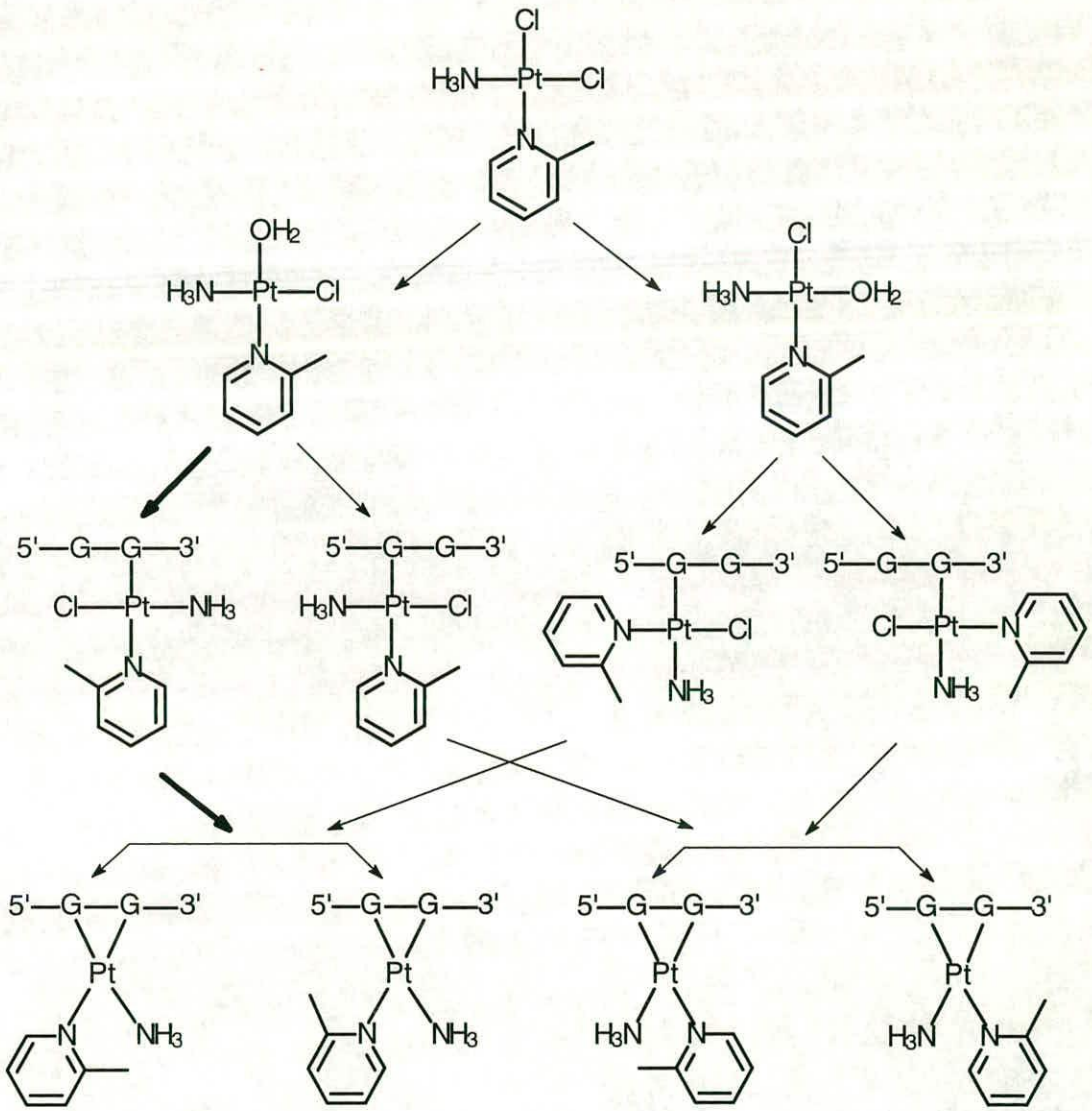

(3a: Methyl-Out) **(3b: Methyl-In)** **(3c: Methyl-Out)** **(3d: Methyl-In)**

further away from Pt atom compared with **1**, and both of the ligands $C_6H_{11}NH_2$ and 4-aminoTEMPO are relatively flexible so that they could easily fit into the distorted DNA duplex structure. The H-bonding between Pt-NH_3 and 5′-phosphate instead of steric effect in the two complexes therefore appears to be more significant in determining the preference for orientational isomers. Considering the sequence-dependent structures of G*G* platinated DNA duplexes discussed in Chapter 6, either the 5′- or 3′-side of the DNA can be more bent towards the major groove. It is also possible that the preference for orientation of a bulky group (*cis*- to 5′ or 3′-G) in platinated DNA duplexes is sequence-dependent.

Preliminary kinetic studies of the reaction of complex **1** with duplex **III** show that the monoaqua species with 2-picoline *trans* to water reacts faster with DNA (Fig. 7.2A), from comparing the hydrolysis rates of the two chloride ligands in complex **1**.[6] Therefore monofunctional adducts with G*N*7 *trans* to 2-picoline are formed in preference to those with NH_3 *trans* to G*N*7 (Scheme 7.1), which is probably due to unfavourable steric interactions when 2-picoline is *cis* to G*N*7. This contrasts with the formation of monofunctional adducts of *cis*- and *trans*-$[PtCl(NH_3)_2(4\text{-Me-Py})]^+$ where the methyl substituent is further away from the coordination plane,[18] and emphasises further the important role played by the 2-methyl group of **1** which is close to Pt. Monofunctional 3′G platinated adducts of DNA duplexes with cisplatin usually form faster and ring-close faster than 5′G monofunctional adducts.[19] If this is also the case for adducts of **1**, then this, together with the preference for substitution *trans* to 2-picoline, would explain why the bifunctional adduct with 2-picoline *cis* to 5′G is the preferred product.

Studies have shown that the anticancer active complex, *cis*-$[PtCl(NH_3)_2(4\text{-Me-Py})]^+$, forms monofunctional adduct with DNA duplex and destabilise the DNA significantly.[18] The base pairs located on the 5′ side of the oligonucleotide, beyond the platinum lesion site, are disrupted in order to accommodate the pyridine ring. The

presence of bulky aromatic amine ligand, such as methyl-pyridine and N-Me-2-diazapyrenium,[20] is apparently important for the anticancer activity of these monofunctional platinum complexes. The monofunctional adducts formed during the reaction of complex **1** with DNA duplex can also play a role in its anticancer activity.

7.5 Conclusion

This work has shown that a number of factors appear to drive the high stereoselectivity in reactions of the anticancer drug *cis*-[$PtCl_2(NH_3)$(2-Pic)] with DNA duplex **III**. These include: unfavourable steric interactions between the 2-picoline ring and the nearby nucleotide bases in models **3c** and **3d**, favourable hydrogen-bonding between the NH_3 ligand and O6 of G8 in model **3b**, and together with van der Waals interactions between the 2-picoline CH_3 and the CH_3 of nearby T6, which is absent in model **3a**. Both thermodynamic and kinetic factors seem to favour the formation of complex **3b**. The high stability of **3b** may be important in determining the lack of cross-resistance between **1** and cisplatin. Such a lesion may be recognised differently from cisplatin-DNA adducts by the excision repair systems in cells.[3,21]

7.6 References

[1] R. P. Perez, *Eur. J. Cancer* **1998**, *34*, 1535.

[2] S. G. Chaney, *8th International Symposium on Platinum and Other Metal Coordination Compounds in Cancer Chemotherapy*, Mar. 28-31, 1999, Oxford, UK, meeting abstract, 4.O1.

[3] T. Matsumoto, K. Endoch, K. Akamatsu, K. Kamisango, H. Mitsui, K. Koizumi, K. Morikawa, M. Koizumi, T. Matsuno, *Br. J. Cancer* **1991**, *64*, 41.

[4] F. I. Raynaud, F. E. Boxall, P. M. Goddard, M. Valenti, M. Jones, B. A. Murrer, M. Abrams, L. R. Kelland, *Clin. Cancer Res.* **1997**, *3*, 2063.

[5] J. Holford, S. Y. Sharp, B. A. Murrer, M. Abrams, L. R. Kelland, *Br. J. Cancer* **1998**, *77*, 366.

[6] Y. Chen, Z. Guo, S. J. Parsons, P. J. Sadler, *Chem. Eur. J.* **1998**, *4*, 672.

[7] Y. Chen, Z. Guo, J. A. Parkinson, P. J. Sadler, *J. Chem. Soc. Dalton Trans.* **1998**, 3577.

[8] T. W. Hambley, *Coord. Chem. Rev.* **1997**, *166*, 181.

[9] M. J. Bloemink, R. J. Heetebrij, K. Inagaki, Y. Kidani, J. Reedijk, *Inorg. Chem.* **1992**, *31*, 4656.

[10] J. F. Hartwig, S. J. Lippard, *J. Am. Chem. Soc.* **1992**, *114*, 5646.

[11] S. U. Dunham, S. U. Dunham, C. J. Turner, S. J. Lippard, *J. Am. Chem. Soc.* **1998**, *120*, 5395.

[12] S. J. Barton, K. J. Barnham, A. Habtemariam, P. J. Sadler, R. E. Sue, *Inorg. Chim. Acta* **1998**, *273*, 8.

[13] P. M. Takahara, C. A. Frederick, S. J. Lippard, *J. Am. Chem. Soc.* **1996**, *118*, 12309.

[14] A. Gelasco, S. J. Lippard, *Biochemistry* **1998**, *37*, 9230.

[15] C. Giessner-Prettre, B. Pullman, *Biochem. Biophys. Res. Commun.* **1976**, *70*, 578.

[16] J. A. Parkinson, S. E. Ebrahimi, J. H. McKie, K. T. Douglas, *Biochemistry* **1994**, *33*, 8442.

[17] A. H. Krotz, L. Y. Kuo, T. P. Shields, J. K. Barton, *J. Am. Chem. Soc.* **1993**, *115*, 3877.

[18] C. Bauer, T. Peleg-Shulman, D. Gibson, A. H.-J Wang, *Eur. J. Biochem.* **1998**, *256*, 253.

[19] F. Reeder, Z. Guo, P. del S. Murdoch, A. Corazza, T. W. Hambley, S. J. Berners-Price, J.-C. Chottard, P. J. Sadler, *Eur. J. Biochem.* **1997**, *249*, 370.

[20] D. Payet, F. Gaucheron, M. Sip, M. Leng, *Nucleic Acids Res.* **1993**, *21*, 5846.

[21] E. Cvitkovic, *Br. J. Cancer* **1998**, *77*, 8.

Conferences Attended

1) European COST programme D1/92/0002 meeting, Leiden, Netherlands, April, 1997. (oral presentation)
2) 31st University of Scotland Inorganic Club Conference (USIC), University of Edinburgh, September, 1997. (poster presentation)
3) European COST programme D8 meeting, Leiden, Netherlands, June, 1998. (oral presentation)
4) 32st USIC Conference, University of Strathclyde, Glasgow, September, 1998. (poster presentation)
5) European COST programme D8 meeting, Oxford, U. K., March, 1999. (oral presentation)
6) 8th International Symposium on Platinum and other Metal Coordination Compounds in Cancer Chemotherapy, Oxford, U. K., March, 1999. (oral presentation)
7) 14th International Meeting on NMR Spectroscopy, Edinburgh, U. K., July, 1999.
8) Workshop-Structural chemistry and biology: the interference between NMR, X-ray and modelling, Edinburgh, July, 1999. (oral presentation)
9) 33st USIC conference, University of Heriot-Watt, Edinburgh, September, 1999. (oral presentation)

Courses Attended

1) Practical Training Course on "*Chemistry of Metals in Biological Systems*", Université Catholique de Louvain, Louvain-la-Neuve, Belgium, May 14-24, 1997. (poster presentation)
2) BRUKER AVANCE/XWIN-NMR Course, Coventry, 10-14 February, 1997.
3) Course on "Metals in Medicine", Prof. Peter. J. Sadler, 1998.
4) Graduate course on Modern NMR Spectroscopy, January, 1998.

5) Courses on computer applications: UNIX (I, II, III), WINDOWS (Powerpoint, Excel), Visual Basic, HTML (for writing webpage).

6) Postgraduate lecture course on Coordination Chemistry, Department of Chemistry, University of Edinburgh, 1998.

7) Weekly Inorganic Section Seminars during the terms, 1996-1999.